THERMOELASTOPLASTIC AND CREEP ANALYSIS OF THICK-WALLED CYLINDERS

Abbas Loghman

B.Sc. Sharif University of Tech. Tehran-Iran

M.Sc. Amirkabir University of Tech. Tehran-Iran

Department of Mechanical Engineering

The University of Adelaide

South Australia 5005

Submitted for the degree of Doctor of Philosophy, 10th of October 1995

Contents

List of Figures

List of Tables

ABSTRACT

Time-independent thermoelastoplastic and time-dependent creep stress and damage analysis of thick-walled cylinders have been investigated using incremental theory of plasticity in conjunction with improved material elastoplastic and creep constitutive models. The results are validated experimentally and numerically.

For time-independent thermoelastoplastic analysis thick-walled cylinders of SUS 304 stainless steel have been selected. The material's loading and unloading properties including the Bauschinger effect factor (BEF) are obtained experimentally and represented mathematically as continuous functions of effective plastic strain. The material's model and the BEF have been incorporated in an analytical-numerical model to predict the cylinder's plastic and residual stresses as well as the critical pressures of direct and reverse yielding. The analytical-numerical models for the prediction of critical inner pressure, plastic stress distributions and the subsequent residual stresses of thick-walled cylinders are validated experimentally. Several experiments are carried out on thick-walled cylindrical test specimens in which internal hydraulic pressure has been increased and the outer surface deformations are measured by the strain gauges.

Subsequently the load has been released and the residual strains are again measured at the outer surface of the cylinder. These experimental measured values are compared with the predicted values of the analytical-numerical model and, in most cases, the model predictions are accurate.

For time-dependent creep stress and creep damage analysis, thick-walled tubes of $\frac{1}{2}Cr, \frac{1}{2}Mo, \frac{1}{4}V$ ferritic steel have been considered. Improved material creep and rupture properties are obtained from the available literature. A numerical model has been developed for the computation of creep stresses and strains and the creep damages in a thick-walled tube which is subjected to an internal pressure and a thermal gradient. The model predicts histories of stresses and strains as well as the damage history during the life of the tube due to variation in stresses with time and through-thickness variations. The creep damage accumulation is based on the Robinson's linear life fraction damage rule which has been incorporated in a non-linear time-dependent stress analysis. Following the stress histories the damages are calculated and cumulatively summed during the life of the tube. From the effective stress histories a reference time has been identified when the effective stress distributions become uniform throughout the tube wall. Effect of internal pressure on this reference time is investigated. The accuracy of the results has been examined by comparing the theoretically predicted creep curves and the numerically followed curves. Deviation of the followed paths from the predicted paths is small.

STATEMENT OF ORIGINALITY

This work contains no material which has been accepted for the award of any other degree or diploma in any university or other tertiary institution and, to the best of my knowledge and belief, contains no material previously published or written by another person, except where due reference has been made in the text.

I give consent to this copy of my thesis, when deposited in the University Library, being available for loan and photocopying.

Abbas Loghman

ACKNOWLEDGMENTS

I would like to thank Dr. M.A. Wahab for supervision of this research project. I am grateful to him for his patience and advice.

I wish to express my sincere appreciation for the enthusiastic support and suggestions of the academic members and the fellow post graduate students of the Department of Mechanical Engineering.

Thanks to all the staff in the Mechanical Engineering Department who contributed in some way to this work. In particular, my thanks to Herwig Bode and the Instrumentation section and the Engineering workshops for their excellent technical support and advice.

Financial support of the Iranian Government is acknowledged with thanks.

NOTATION

a,b	Inside, outside radii
BEF	Bauschinger effect factor
E	Modulus of elasticity
P_a, P_b	Inner, outer pressures
P_i, P_o	Dimensionless inner, outer pressure
P_{crit}	Critical pressure
r	Radius
r_c	Elastic plastic interface radius
S_r, S_θ, S_z	Dimensionless stress components
S_r^e, S_θ^e, S_z^e	Dimensionless elastic stress components
S_r^p, S_θ^p, S_z^p	Dimensionless plastic stress components
S_r^r, S_θ^r, S_z^r	Dimensionless residual stress components
T_a, T_b	Inner, outer temperatures
α	Linear coefficient of thermal expansion
β	Radii ratio (b/a)
ΔP	Increment of pressure load

ΔT	Temperature gradient
$\Delta\varepsilon_e^c$	Effective creep strain increment
$\Delta\varepsilon_r^c, \Delta\varepsilon_\theta^c, \Delta\varepsilon_z^c$	Creep strain increments
$\Delta\varepsilon_r^p, \Delta\varepsilon_\theta^p, \Delta\varepsilon_z^p$	Plastic strains increment
$\Delta\epsilon_p$	Effective plastic strain increment
$\epsilon_r, \epsilon_\theta, \epsilon_z$	Dimensionless strains
$\epsilon_r^p, \epsilon_\theta^p, \epsilon_z^p$	Dimensionless plastic strains
$\varepsilon_r, \varepsilon_\theta, \varepsilon_z$	Strain components
$\varepsilon_r^c, \varepsilon_\theta^c, \varepsilon_z^c$	Creep strains
$\varepsilon_r^p, \varepsilon_\theta^p, \varepsilon_z^p$	Plastic strain components
$\dot{\varepsilon}_e^c$	Effective creep strain rate
$\dot{\varepsilon}_r^c, \dot{\varepsilon}_\theta^c, \dot{\varepsilon}_z^c$	Creep strain rates
Θ	Dimensionless temperature gradient
ν	Poisson's ratio
ρ	Dimensionless radius
ρ_c	Dimensionless elastic-plastic interface radius
σ_e	Effective stress
σ_0, ε_0	Yield stress, Yield strain
$\sigma_r, \sigma_\theta, \sigma_z$	Stress components
$\sigma_r^c, \sigma_\theta^c, \sigma_z^c$	Creep stress components

Subscript

a	Inner

b	Outer
c	Elastic-plastic interface
e	Effective
r, θ, z	Cylindrical coordinates

Superscript

e	Elastic
c	Creep
p	Plastic
r	Residual

Chapter 1

INTRODUCTION

1.1 General Introduction

The application of high-pressure technology in high temperature environment has undergone a tremendous growth in the areas of oil, chemical, power generation and in defence industries. All of these industries use pressure vessels, piping systems and thick-walled cylinders and in general, failures that arise in their systems are always catastrophic. Therefore, there is a strong need for studies relating to non-linear deformations of these systems due to high pressure in the presence of high temperature environment. Experimental modeling with careful analytical and numerical research is necessary to investigate the non-linear response of these systems in order to develop reliable procedures for the safe design against catastrophic failures. Time-independent non-linear deformation analysis of thick-walled cylinders will provide information concerning the through-thickness yielding characteristics of thick-walled vessels. This is

important when intentional-yielding introduces beneficial residual stresses into the vessel wall and improves the performance characteristics of the operating systems.

As a thick-walled cylinder is pressurized, the bore material, which is the most highly stressed portion of the cylinder, begins to yield. The yield surface begins to propagate through the thickness of the vessel until it reaches the outer surface. When more and more of the cylinder material is entering the plastic regime, the bore material begins to strain harden. If the yielded cylinder is unloaded, the compressive residual stresses will be developed at the inner surface of the cylinder. Highly compressive residual stresses can cause reverse yielding to take place at the inner surface of the cylinder. An important ingredient of the non-linear and residual stress analysis is the material constitutive model. Metals initially overstrained in tension have a significantly lower elastic limit in compression (Bauschinger phenomenon). This phenomenon must be considered in the material model for a more realistic prediction of residual stresses and the onset of reverse yielding. It is also necessary to know the stress and strain histories during overloading to calculate the subsequent residual stresses. There is however considerable disagreement among solutions obtained by different investigators for the residual stress distribution in the cylinder (for example, Koiter (1953), Bland (1956), Franklin and Morrison (1960), Parker and Andrasic (1981), Chen (1986), Rees (1987a), Stacey and Webster (1988)). All the solutions presented by these investigators are obtained with some simplifications in the geometry constraints, material models, yielding criteria and the associated plastic flow rules. Determination of the residual stress distribution is

important in the fracture analysis and the fatigue life estimation of thick-walled cylindrical pressure vessels (for example, Hussain et al. (1980), Throop and Reemsnyder (1982), Parker et al. (1983), Pu and Chen (1983), Findley and Reed (1983), Koh and Stephens (1991), Rees (1987a, 1991a, 1991b), Perl and Arone (1994a,1994b) and Seshadri (1994)). Therefore, an accurate prediction of residual stresses by using a realistic material model including the Bauschinger phenomenon and a more realistic geometrical constraint can have a significant contribution to improve the fracture analysis of thick-walled cylinders.

In the presence of a high-temperature, non-linear deformation of cylinder becomes a time-dependent process known as creep. Creep mechanism causes micro-structural damages such as dislocation movement, cavity formation and spacing. The history of creep stresses and the consequent creep damages of thick-walled tubes are extremely important in the life assessment and for the routine inspection of high-temperature high-pressure tubes to avoid unexpected failures. The development of reliable procedures for design and prediction of remaining life of thick-walled tubes that operate at creep ranges has been an activity of considerable research interest because of relevance to plant safety and reliability (for example, Simonen and Jaske (1985), Seshadri (1988), Cohn (1990), Jaske (1990), Viswanathan et al. (1994), Ibarra and Konet (1995), Nogata and Takahashi (1995) and Jaske (1995)). Realistic tube-life predictions are essential to economical design, inspection strategy and tube retirement evaluations.

A major difficulty in the design of tube life or remaining tube life is that the rate of creep damage changes during the life of the tube due to time-dependency of stresses and variation in stresses through the tube wall thickness. While in-service examinations of these components can provide useful information about material condition, greater understanding of the component's non-linear deformation behaviour is essential before the information obtained from the inspection procedures can be used to provide accurate predictions of future component performance. Furthermore, if an improved damage model can be predicted for the vessel then the component examinations and inspections can be scheduled in a selective manner.

One of the ingredients of a time-dependent non-linear stress and damage analysis is the material's constitutive model. A constitutive model for the prediction of long-term creep behaviour of low alloy steels from a relatively short term data has been introduced by Evans et al. (1984). The model known as "the Theta (Θ) projection" has been adopted internationally (for example, Parker (1985), Maruyama and Oikawa (1987), Maruyama et al. (1990) and Zamrik (1990)). The model accurately predicts the material behaviour and the changes in the shapes of the creep curves with changing stress and temperature. However, due to the complex mathematical representation of the proposed material model, application of the model in practical problems is not yet well developed.

The aim of this project is to develop, improve and validate the analytical-numerical

models for a more realistic prediction of the time-independent and time-dependent non-linear response of thick-walled cylinders subjected to an internal pressure and thermal gradients by using a detail incremental deformation analysis and the improved material properties in elastic, plastic and creep regimes. The outcome of this study will be specially valuable to thermal power generating industries, pipe lines and in defence research where efficient and safe design of pressure vessels and cylinders are crucial.

1.2 Problem Definition

A thick-walled cylinder of strain-hardening material has been considered in this study. Loading of the cylinder is assumed to consist of a temperature gradient and a monotonically increasing internal pressure . The cylinder ends are assumed to be closed for the case of time-independent elastoplastic and subsequent residual stress analysis and are assumed to be open for the case of time-dependent creep stress and damage analysis. The material's strain-hardening properties and the Bauschinger phenomenon will be considered for a more realistic prediction of plastic stresses and the consequent residual stresses and the onset of reverse yielding. The material's time-dependent properties are considered as full creep curves up to rupture defined by the theta projection concept. Other assumptions used in the analysis are as follows:

1. For both time-dependent and time-independent non-linear analysis, von Mises criterion and its associated flow rule is adopted

2. The material is assumed to be incompressible in the plastic and creep regimes

3. A generalized plane strain case is considered in which the strain in the axial direction is constant (ε_z=constant). This assumption is a more realistic constraint than the plane strain for a closed ended cylinder because the cylinder is permitted to expand in the axial direction while surfaces normal to the longitudinal axis remain plane during deformation.

4. None of the plastic and creep strain increments are assumed to be zero and all the three-dimensional plastic and creep strain components are considered in the analysis.

5. The temperature gradient is constant and the heat flow is assumed to be outward.

Details of the material properties used in both time-dependent and time-independent analysis are introduced below.

1.3 Material Consideration

Material's time-independent constitutive model and the Bauschinger effect factor as well as the time-dependent creep properties and the creep rupture criterion used in this investigation are introduced here in this section.

1.3.1 Material Time-Independent Constitutive Model

The material for time-independent thermoelastoplastic deformation and the subsequent residual stress analysis is selected as SUS 304 stainless steel. This material is commonly used in high pressure and high temperature environment. In this investigation the material non-linear properties are obtained experimentally. A large number of test specimens have been loaded up to a specific strain beyond the elastic limit and then reverse loaded down to zero strain by using a computer controlled testing machine. The stress-strain diagram of the material during loading up to 0.75% overstrain and unloading down to zero strain obtained from the experiment is shown in Figure 1.1.

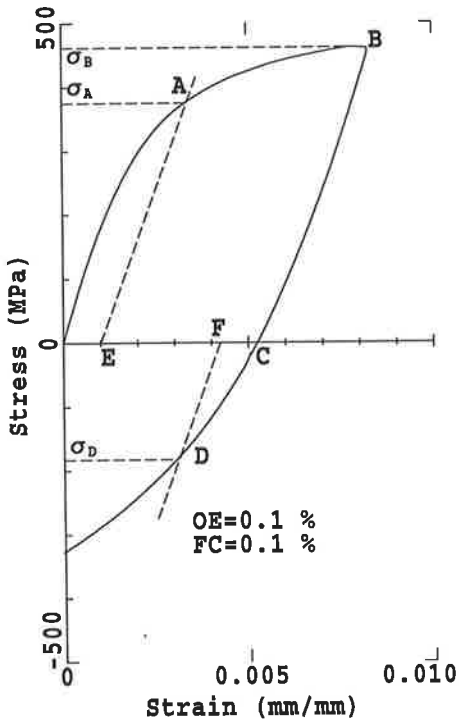

Figure 1.1: Experimental loading-unloading stress-strain curve obtained for SUS 304

Using the material's data file in conjunction with a curve fitting software the strain-hardening is mathematically represented by the following constitutive equation:

$$\sigma_e = 232.68187 + 689.01541(\varepsilon_p)^{0.21842186} \tag{1.1}$$

where σ_e and ε_p are the effective stress and effective plastic strain respectively. The material high-temperature properties and constitutive models are selected from the experimental results of Niitsu and Ikegami (1990).

Effect of the amount of overstraining on reverse yielding is also investigated experimentally in this work and represented by the Bauschinger effect factor.

1.3.2 The Bauschinger Effect Factor (BEF)

Metals initially overstrained in tension have a significantly lower elastic limit in compression. This is known as the Bauschinger phenomenon. By definition, the Bauschinger effect factor (BEF) for a specimen initially overstrained in tension is the ratio of the compressive yield stress upon reverse yielding to the initial yield stress in tension. If σ_A is the initial yield stress in tension and σ_D is the yield stress in reversed direction of loading as shown in Figure 1.1, then the BEF is

$$BEF = \frac{\sigma_D}{\sigma_A} \tag{1.2}$$

The definition of Bauschinger effect factor has been modified by Milligan et al. (1966) to take into account the strain hardening as follows:

$$BEF = \frac{\sigma_D}{\sigma_B} \tag{1.3}$$

where σ_B is the subsequent yield stress.

In this work the BEF is obtained experimentally based on the above modified definition of Milligan. Determination of yield point in tension and compression is based on the ASTM standard procedure of "offset method". In this work 0.1% offset is used to obtain the material's yield strength. From the experimental data of each specific overstraining condition the respective BEF is calculated from equation (1.3). Elastic strains have been subtracted from the total overstrains to give the plastic strains. A functional relationship between the BEF and the percentage amount of plastic strain has been established by using a curve fitting software as follows:

$$BEF = 1.0170029 + 0.36592732(\varepsilon_p\%) - 0.0025343135(\varepsilon_p\%)^3 - 0.97738304(\varepsilon_p\%)^{0.5} \tag{1.4}$$

where $\varepsilon_p\%$ is the percent plastic overstrain. The experimental BEF and its approximated function are compared in Figure 1.2.

1.3.3 Material Time-Dependent Creep Properties

The material considered in this study for the time-dependent creep stress and creep damage analysis is composed of $\frac{1}{2}Cr, \frac{1}{2}Mo, \frac{1}{4}V$ ferritic steel. This composition is widely used in electricity generating power plant for high-pressure and high-temperature components. The material creep and fracture properties are obtained from the experimental results of Evans et al. (1984). The strain-time behaviour of the material has been

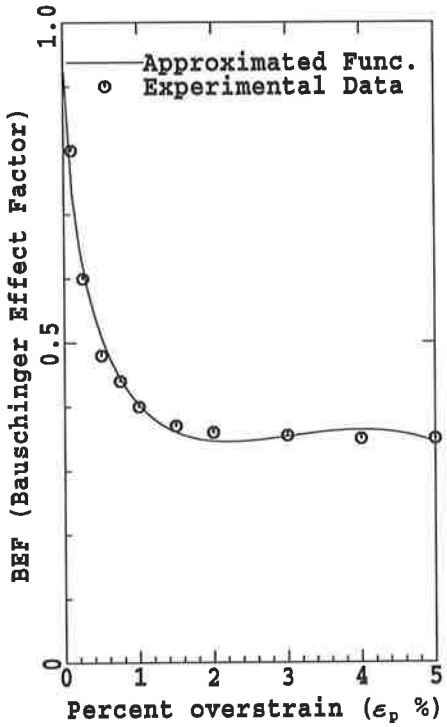

Figure 1.2: Comparison of the experimentally obtained Bauschinger effect factor and the approximated function for SUS 304

described by Evans et al. (1984) by introducing the theta projection concept as follows:

$$\varepsilon = \Theta_1(1 - e^{-\Theta_2 t}) + \Theta_3(e^{\Theta_4 t} - 1) \tag{1.5}$$

where ε and t are creep strain and time respectively. Variables $\Theta_1, \Theta_2, \Theta_3$ and Θ_4 are dependent on stress and temperature and are mathematically represented as follows:

$$Log_{10}\Theta_i = a_i + b_i T + c_i \sigma + d_i \sigma T \qquad i = 1, 2, 3, 4 \tag{1.6}$$

where σ and T are stress and temperature and the coefficients a_i, b_i, c_i and d_i are material constants. For this particular material these constants are obtained experimentally by Evans et al. (1984) and written in Table 1.1.

Table 1.1: Constant coefficients of material constitutive equation.

Parameter	a	b	c	d
Θ_1	-0.8736*10^1	+0.4604*10^{-2}	-0.4489*10^{-1}	+0.6814*10^{-4}
Θ_2	-0.2346*10^{-2}	+0.2225*10^{-1}	+0.2195*10^{-1}	-0.1951*10^{-4}
Θ_3	-0.1869*10^1	-0.2034*10^{-2}	-0.5497*10^{-1}	+0.7990*10^{-4}
Θ_4	-0.1643*10^2	+0.9149*10^{-2}	-0.4723*10^{-1}	+0.7139*10^{-4}

Based on this tabulated data, units of time, temperature and stress are seconds, ^{0}K and MPa respectively. Evans & Wilshire (1985) showed that strain-time behaviour of the material could be represented accurately using equation (1.5). The full creep curves predicted by equation (1.5) for $\frac{1}{2}Cr, \frac{1}{2}Mo, \frac{1}{4}V$ ferritic steel are shown in Figure 1.3.

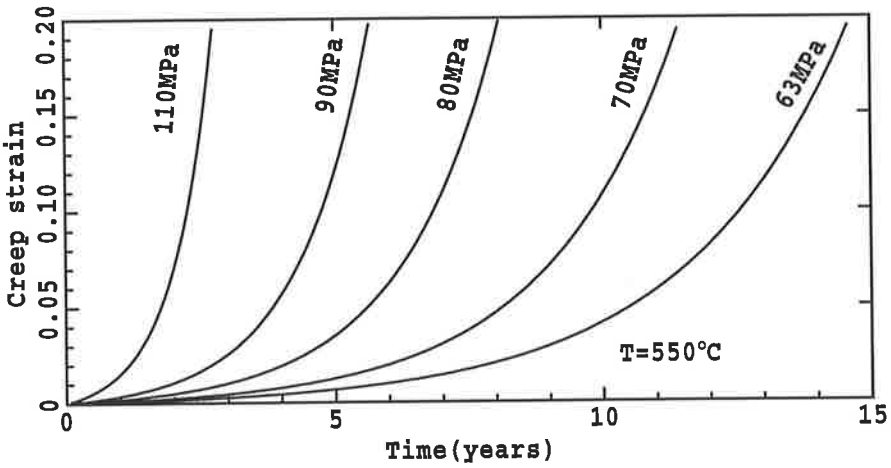

Figure 1.3: Creep curves predicted by the Θ projection for $\frac{1}{2}Cr, \frac{1}{2}Mo, \frac{1}{4}V$ ferritic steel.

A creep failure criterion which can either be the rupture strain (ε_f) or rupture time (t_r) is necessary for the creep damage estimation and the remaining life assessment of high-pressure high-temperature tubes and is described below.

1.3.4 Creep Failure Criterion

For any creep curve a failure criterion may be defined by specifying either the rupture time or rupture strain. It has been shown by Evans and Wilshire (1985) that the material fracture strains (ε_f) can be represented as a function of temperature and stress as

$$\varepsilon_f = a_5 + b_5 T + c_5 \sigma + d_5 \sigma T \tag{1.7}$$

The coefficients in this equation for the $\frac{1}{2}Cr, \frac{1}{2}Mo, \frac{1}{4}V$ steel are shown in Table 1.2.

Table 1.2: Constant coefficients of material rupture constitutive model.

Parameter	a_5	b_5	c_5	d_5
ε_f	-0.1123*10^{1}	+0.1517*10^{-2}	+0.5473*10^{-3}	-0.4721*10^{-6}

On this basis, equations (1.5) and (1.6) can be used to construct a predicted creep curve at any stress and temperature. The relevant rupture life is then defined as the time taken to reach the appropriate failure strain as given by equation (1.7). In this case equation (1.5) may be rewritten in terms of fracture strain and fracture time as:

$$\Theta_1(1 - e^{-\Theta_2 t_r}) + \Theta_3(e^{\Theta_4 t_r} - 1) - \varepsilon_f = 0 \tag{1.8}$$

where t_r is the rupture time and ε_f is the fracture strain. Based on the data shown in Table 1.2 the rupture times of $\frac{1}{2}Cr, \frac{1}{2}Mo, \frac{1}{4}V$ ferritic steel are calculated for a wide range of stress levels and temperatures using equation (1.8). Results are illustrated in Figure 1.4.

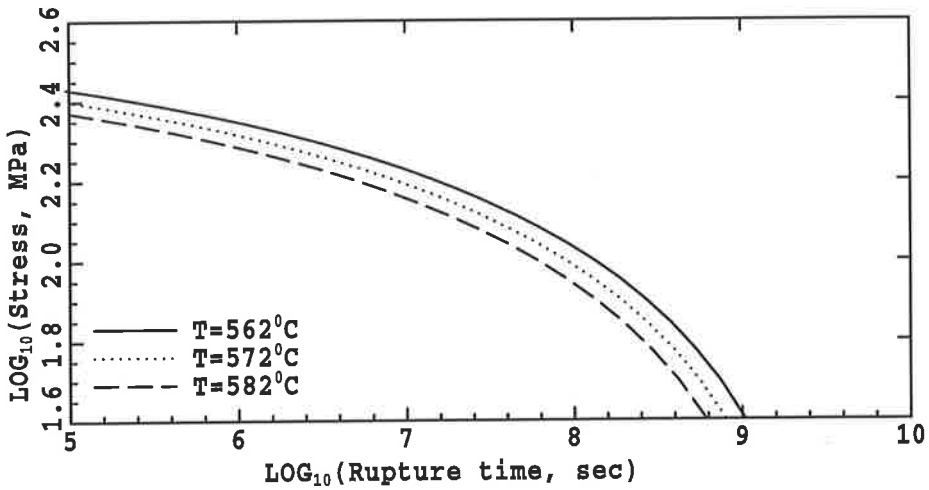

Figure 1.4: Calculated rupture time data for $\frac{1}{2}Cr, \frac{1}{2}Mo, \frac{1}{4}V$ ferritic steel

1.4 Scope of the Thesis

A review of the classical and recently published research work on the non-linear deformation analysis of thick-walled cylinders is discussed in Chapter 2. Effect of the material constitutive model, boundary and end conditions, yielding criterion, temperature and time on the non-linear stress distribution of thick-walled cylinders are reviewed in Chapter 1. Theoretical improvement and a general numerical procedure suggested

for the calculation of the accumulated plastic and creep strains in a loaded thick-walled cylinder are introduced in Chapter 3. Step by step numerical procedure to calculate the non-linear plastic stresses and the consequent residual stresses as well as the time-dependent creep stress and creep damages are introduced in Chapter 4. Experimental set up and specifications of the cylindrical test specimens and procedures are described in Chapter 5. In Chapter 5 the developed analytical-numerical procedure is justified by comparing the model predicted deformations and the experimentally measured values by the strain gauges. The results obtained in this investigation are discussed and interpreted in Chapter 6. A conclusion is derived and a recommendation for the future work is described in Chapter 7 followed by appendices and references. A list of publication generated from this research work is cited at the end of the thesis.

Chapter 2

LITERATURE REVIEW

2.1 Introduction

A considerable amount of work has been done on the problem of time-dependent and time-independent non-linear stress analysis of thick-walled cylinders under internal pressure, with and without the effect of temperature gradients. There are also many closed form solutions available in the literature which are obtained by simplifying the geometry, boundary and end conditions, material constitutive equations and the yielding criterion. This review is divided into two major categories one of which deals with the time-independent elastoplastic deformations and the subsequent residual stresses while the other considers time-dependent creep deformations of thick-walled cylinders.

2.2 Time-Independent Elastoplastic Deformation

Many solutions have been put forward from time to time for the elastoplastic and the consequent residual stress distribution in a thick-walled cylinder subjected to an internal pressure sufficient to cause yielding at the cylinder wall. The first classical solution to this problem was presented by Nadai (1931).

Nadai (1931) considered a thick-walled cylinder under internal pressure assuming that the stresses are independent of deformation. He assumed a zero strain in the axial direction and that the sum of the three total strain components in the radial, tangential and axial directions is equal to zero to satisfy the material incompressibility condition. With these assumption Nadai established expressions for the radial, tangential and axial stresses in a fully plastic cylinder in the following form:

$$\begin{aligned} \sigma_r &= \frac{-2\sigma_0}{\sqrt{3}} ln\frac{b}{r} \\ \sigma_\theta &= \frac{2\sigma_0}{\sqrt{3}}(1 - ln\frac{b}{r}) \\ \sigma_z &= \frac{-2\sigma_0}{\sqrt{3}}(\frac{1}{2} - ln\frac{b}{r}) \end{aligned} \tag{2.1}$$

where σ_r, σ_θ and σ_z are plastic stresses, σ_0 is the yield stress, b is the outer radius and r is the radius. In the case of a partially plastic cylinder, Nadai assumed that the cylinder is composed of a fully plastic and a perfectly elastic cylinder. Therefore, parametric equations of stresses in a fully plastic vessel in conjunction with a fully elastic solution were used to obtain the stress distribution in a partially plastic cylinder. Parameters were obtained using boundary conditions at the inner and outer surfaces

and the condition of continuity at the elastic-plastic interface. For the unloading case of a plastically deformed cylinder under internal pressure Nadai subtracted an elastic stress distribution with the same internal pressure from the plastic stress distributions and obtained an estimate of residual stress distribution in the cylinder wall. Solution presented by Nadai was approximate because the stresses were assumed to be independent of plastic strains. The material's hardening effect and the Bauschinger effect phenomenon were also neglected.

Another solution to the problem of elastoplastic stress distribution in a thick-walled cylinder was obtained by Cook(1934) assuming a constant shear stress throughout the plastic material. Based on the hypothesis of Tresca, in which a constant value of the maximum shear stress was assumed to exist throughout a plastic material in a state of plastic flow, Cook (1934) assumed that a constant shear stress existed over the plastic region of a partially plastic cylinder. This shear stress was assumed to be equal to the shear stress observed during plastic yielding in uniaxial tension which means:

$$\sigma_\theta - \sigma_r = \sigma_0. \tag{2.2}$$

Cook described a theoretical and experimental study of the stress distribution across the walls of thick cylinders of mild steel under internal pressure and overstrained condition. Based on the above assumption Cook calculated the possible internal pressure which produces overstrain throughout the wall thickness. However, the results of cook are not significant because the assumption of constant shear stress during plastic flow is only correct for a perfectly plastic material (constant σ_0) and neglects the hardening

effect.

The overstraining of cylinders by internal pressure was investigated by Manning (1945). He assumed that the axial stress is of magnitude lying between the radial and hoop stress components, then the maximum shear stress depended on these two principal stress components (σ_θ and σ_r) as follows:

$$\sigma_\theta - \sigma_r = 2\tau_{max} \tag{2.3}$$

where τ_{max} is the maximum shear stress. Furthermore, he assumed that the area of cross section of the cylinder does not change during elastic-plastic deformation which is equivalent to the material's incompressibility condition in both elastic and plastic region. With these assumptions the distributions of radial and tangential stress components were obtained and the axial stress component was neglected. The assumption of incompressibility in both, elastic and plastic regimes made by Manning is permissible when the plastic strain component is large compared with elastic strain component and the cylinder is in a fully plastic condition.

Combined effect of elastic and plastic strain components on the stress distribution in thick-walled cylinders was investigated by Hill et al. (1947). Hill et al. (1947) developed the theory of the deformation of material under combined stresses in which both elastic and plastic components of strain were involved. The relationship between stress and strain was represented on a plane diagram which was graphically used to evaluate the elastic and plastic components of strain. They applied the theory to the defor-

mation of a long thick tube under internal pressure with zero longitudinal extension. They showed that while plastic flow is constrained by surrounding elastic material, the correct stress distribution of the thick tube can be obtained by considering the elastic part of the total strain in the material flowing plastically. In the particular case of a thick tube an error of up to 60% resulted in the determination of the longitudinal stress on the assumption of zero elastic strain in the plastic region. All the above solutions to the elastoplastic stress distribution in thick-walled cylinders were independent of the cylinder ends condition. However, effect of the ends condition on the stresses and progress of plastic zone were introduced by Hill (1950) .

Hill (1950) considered elastic and elastoplastic deformation of tubes under internal pressure. He derived expressions for the elastic stresses in tubes. Hill considered three possible cases: plane strain, open and closed end condition. Using the elastic stresses Hill obtained the critical internal pressures of cylinders using both Tresca and von Mises yielding criteria. Hill showed that all cylinders with various end conditions have the same critical pressure, according to Tresca's criterion. The critical pressure based on Tresca's criterion was obtained as follows:

$$P_{crit} = \frac{1}{2}\sigma_0(1 - \frac{a^2}{b^2}) \tag{2.4}$$

where P_{crit} is the critical pressure, a and b are the inner and outer radii respectively. Hill pointed out that if von Mises criterion is adopted, the cylinders end condition affects the critical pressure. Using the von Mises criterion, the critical pressures of

cylinders were obtained for the three possible cases as follows:.

$$\begin{aligned} P_{crit} &= \frac{\sigma_0}{\sqrt{3}}(1-\frac{a^2}{b^2}) && (closed-end) \\ P_{crit} &= \frac{\sigma_0}{\sqrt{3}}(1-\frac{a^2}{b^2})/\sqrt{(1+\frac{a^4}{3b^4})} && (open-end) \\ P_{crit} &= \frac{\sigma_0}{\sqrt{3}}(1-\frac{a^2}{b^2})/\sqrt{(1+(1-2\nu)\frac{a^4}{3b^4})} && (plane-strain) \end{aligned} \tag{2.5}$$

It was indicated that the tube with open ends yields at the lowest pressure. The critical pressures for the closed-end and plane-strain conditions differ by less than three per cent. Assuming a perfectly plastic material Hill established a closed form solution for radial and tangential stress components expressed in the following form:

$$\begin{aligned} \frac{\sigma_r}{\sigma_0} &= -0.5 - ln(\frac{r_c}{r}) + \frac{r_c^2}{2b^2} && (a < r < r_c) \\ \frac{\sigma_\theta}{\sigma_0} &= +0.5 - ln(\frac{r_c}{r}) + \frac{r_c^2}{2b^2} && (a < r < r_c) \end{aligned} \tag{2.6}$$

where r_c is the elastic-plastic interface. Hill, for the first time used an incremental relationship (Reuss incremental stress-strain relationship) to obtain axial stresses while his solution for the radial and tangential stress components (equation (2.6)) were independent of plastic strains. Effect of the incremental stress-strain law and the total plastic stress-strain law on the elastoplastic stress distribution of thick-walled cylinders were considered by Hodge and White (1950).

Hodge and White (1950) considered an infinitely long hollow cylinder under internal pressure. Stresses were obtained for a perfectly plastic material according to the Prandtl-Reuss incremental stress-strain law and the Hencky deformation law (total strain theory). In both cases the von Mises yield condition was used. It was shown

that the two theories yield substantially to close results for this particular problem. Although Hodge and White used the von Mises criterion to obtain the solution for the stress components but the effect of axial stress on von Mises criterion was neglected. In fact the von Mises condition was reduced to a relationship between the radial and tangential stress components in both cases to obtain the solution.

A review of many solutions available in the literature for the stress distribution in a thick tube subjected to an internal pressure was presented by Allen et al. (1951). Total strain solutions with the Hencky-Mises flow condition as well as incremental strain solutions were reviewed. They presented a new total strain solution making fewer assumption and developed into a form suitable for practical application. Their analysis assumed that the strain at any stage depends only on the stress system and not on how that stress system is reached. The search for simple practical solution was continued by Steele (1952)

In a search for assumptions leading to a simplified theory for design purposes all the previous theories for partially plastic thick-walled cylinders under internal pressure were reviewed by Steele (1952). Steele concluded that the solutions using incremental theory vary a small amount from those solved by total strain theory. However, the Hencky total strain theory was preferred because of the mathematical convenience. Based on the comparison, a theory was presented by Steele to include the Hencky stress-strain relations and Tresca's criterion in conjunction with the Ludwik's shear

stress-strain diagram of a linear hardening type as shown in Figure 2.1.

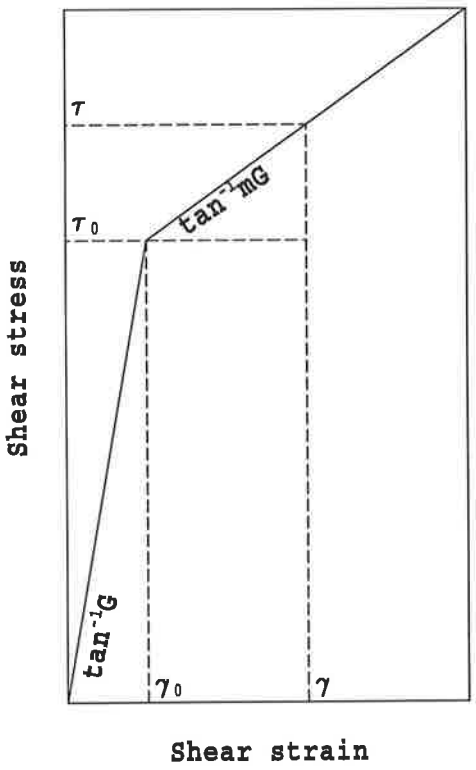

Figure 2.1: Ludwik's linear strain-hardening diagram (Steele (1952)).

The Hencky total strain theory was rewritten as follows:

$$\begin{aligned}
\varepsilon_r &= \frac{1}{E}[\sigma_r - \nu(\sigma_z + \sigma_\theta)] + \lambda[\sigma_r - \frac{1}{2}(\sigma_z + \sigma_\theta)] \\
\varepsilon_\theta &= \frac{1}{E}[\sigma_\theta - \nu(\sigma_z + \sigma_r)] + \lambda[\sigma_\theta - \frac{1}{2}(\sigma_z + \sigma_r)] \\
\varepsilon_z &= \frac{1}{E}[\sigma_z - \nu(\sigma_\theta + \sigma_r)] + \lambda[\sigma_z - \frac{1}{2}(\sigma_r + \sigma_\theta)]
\end{aligned} \tag{2.7}$$

where λ was called plastic flow function. The Ludwik's linear shear stress-strain hardening relationship incorporated in Tresca's criterion was written as follows:

$$\sigma_\theta - \sigma_r = 2f(\gamma) \tag{2.8}$$

where γ is the maximum shear strain which was linearly related to the shear stress as follows:

$$\tau = \tau_0 + mG(\gamma - \gamma_0) \tag{2.9}$$

where τ_0 and γ_0 are the shear stress and strain at yield, G is the shear modulus and mG is the slope of the linear strain hardening as shown in Figure 2.1. Material was assumed incompressible in both elastic and plastic regimes. Closed form solutions were presented for the stresses and strains the value of which could be obtained for specific applied pressures.

There are several review of the elastoplastic stress analysis of thick-walled cylinders in the literature one of which is of Koiter (1953). Koiter (1953) discussed the solutions to the problem of stress distribution in an elastoplastic thick-walled tube which had been presented by Hill (1950), Hodge and White (1950), Allen and Sopwith (1951), and by Steele (1952). These solutions differed in the yield criterion and the plastic stress-strain relations which they assumed. Koiter adopted the Tresca yield criterion and its associated flow rule. Koiter determined the stresses in radial, tangential and axial directions (σ_r, σ_θ and σ_z) for a tube of non-hardening material in both elastic and plastic regions. He showed that his solutions agreed well with the few available solutions based on the Mises yield criterion and the associated flow rule except for the axial stress and strain. However, as the axial stress and strain were very small compared to the radial and tangentialstressesand strains, Koiter concluded that the differences were of minor practical importance.

Effect of temperature on stress distribution which was neglected by previous investigators was first considered by Whalley (1956). Whalley (1956) considered elastic and plastic behaviour of thick-walled cylinders of perfectly plastic material subjected to internal and external pressures and a temperature distribution across the cylinder wall. He established equations for critical pressure in a thick-walled cylinder with closed ends under pressure and thermal loading using Tresca's criterion. In a vessel subjected to both pressure and thermal stresses he assumed that the thermal stresses are not sufficiently high relative to the pressure stresses and the axial stress never becomes a major or minor principal stress. With these assumptions Tresca's criterion became independent of axial stress and the equilibrium equation was also independent of axial stress. Therefore, a closed form solution for the radial and tangential stress components was established. Whalley obtained the residual stresses by subtracting an elastic solution from the above closed form solution. He concluded that the onset of yielding, the plastic flow and the residual stresses are affected by thermal stresses. The axial stress was not obtained and the effect of hardening was not considered by Whalley.

Bland (1956), using Tresca's criterion, established stress and displacement equations for a tube of linear strain-hardening material subjected to pressure and steady state heat flow. His analysis is the only closed form solution available in the literature for a work-hardening material. The material hardening was given as a linear function of

effective stress and effective plastic strain as follows:

$$\sigma_e = \sigma_0(1 + \eta\varepsilon_p) \tag{2.10}$$

where σ_e and ε_p, the effective stress and the effective plastic strain were given based on Tresca's criterion in the following form.

$$\sigma_e = \sigma_\theta - \sigma_r \tag{2.11}$$

$$\varepsilon_p = \frac{2}{\sqrt{3}}\varepsilon_\theta^p \tag{2.12}$$

The closed form solution presented by Bland was based on the linear strain-hardening material rather than a perfectly plastic model of previous investigators. Residual stresses in a closed end tube were given for elastic unloading by subtracting the elastic stress obtained from the imposed pressure and temperature from the elastoplastic stress system. However the Bauschinger effect was not considered by Bland. There are a number of investigators who used the shear stress-strain data to predict the non-linear behaviour of thick-walled cylinders (Crossland et al. (1959)).

The strength and non-linear behaviour of thick-walled steel cylinders subjected to an internal pressure were investigated in a number of publications by Crossland et al. (1955, 1958, 1959). The complete theoretical non-linear behaviour of the cylinder was computed from shear stress-strain data obtained from torsion tests and was shown to be in close agreement with the experimental results. Using the shear stress-strain data in non-linear analysis was not followed by other investigators because theories of plasticity attempted to predict the non-linear behaviour of a member from the uniaxial

tension test results.

Although conditions for the start of the plastic yielding in thick-walled cylinders has generally been considered by many investigators but the combined effect of temperature and pressure on the start of yielding has rarely been considered by researchers.

Derington (1962), using Tresca's criterion, described the onset of yielding in thick-walled cylinders subjected to pressure and thermal gradients with open and closed end conditions. Derington showed that when combined pressure and thermal loads are exerted, yielding may start everywhere according to loading conditions. He also showed that yielding is not always due to radial and tangential stress components, and that there are loading combinations in which the axial stress becomes a minor or major principal stress. In this case, even with Tresca's criterion the elastoplastic analysis becomes history dependent and the problem must be solved numerically.

Sidebottom et al. (1975) used a total-strain, incompressible, analytical solution to predict load-strain relations for thick-walled cylinders as the loads were increased from zero to the bursting pressure. Loading function represented by a finite number of straight lines and the material was assumed to obey the von Mises yield condition and its associated flow rule. Unloading of thick-walled cylinders that had been plastically deformed were also investigated by Sidebottom et al. (1976). The predicted residual-stress distributions and deformations of the unloaded cylinder were obtained by superposition of the previous solution and the unloading solution, provided that the

stress-strain diagram for unloading and reverse loading of tension specimens represents the loading function for unloading. The Bauschinger effect was not considered in Side-bottom work. The solution for the residual stress distribution without considering the Bauschinger effect is not a realistic one particularly when significant amount of plastic strains has been developed in the cylinder wall.

There are also a few closed-form solutions and simulation for residual stress distribution in thick-walled cylinders available in the literature. Hussain et al. (1980) showed that an active thermal load can be used to produce thermal stresses equivalent to residual stresses. In fact, they realized that there were many similarities between residual stress distributions and the thermal stress distributions (due to a steady state outward flow of heat). For example, residual tangential and axial stresses were compressive at the inside surface of the cylinder and were tensile at the outer surface which were similar to thermal stresses. Residual radial stresses were zero at the inside and outside surfaces and were compressive throughout the thickness which were the same as radial thermal stresses. They obtained a thermal gradient which could produce thermal stresses equivalent to residual stresses of an autofrettaged cylinder. The Bauschinger effect was neglected in this simulation and therefore the simulation was correct only for small amount of overstrained condition.

Chen (1986) presented a closed form solution for the residual stress distribution in a cylinder of high strength steel. He proposed a theoretical constitutive material model

for high strength steel in which he used a perfectly plastic loading condition and a linear hardening unloading function including the Bauschinger effect. The material was assumed to obey Tresca's yield criterion and its associated flow rule for both loading and unloading conditions. In the case of reverse yielding the Tresca's criterion was written in the following form:

$$\sigma_\theta - \sigma_r = f\sigma_0 \tag{2.13}$$

where f was the Bauschinger effect factor. Using this material model and following the procedures in Bland's (1956) work, Chen obtained a closed form solution and calculated residual stresses and strains in the reverse yielding zone as well as in the elastic zone. Results of Chen showed that the magnitude of the compressive residual stresses at the inner surface of the cylinder were significantly decreased when reverse yielding took place in the vessel. Therefore, the advantage of the compressive residual stresses will be significantly decreased if reverse yielding occurs in the cylinder. Closed form solution of Chen for residual stresses including the Bauschinger effect was significant, however, he simplified the material model into a perfectly plastic loading condition and therefore neglected the hardening effect on residual stresses.

Rees (1987a), using von Mises criterion, considered closed-end cylinders of hardening and non-hardening material subjected to an internal pressure. He assumed that the axial plastic strain is zero, and radial and tangential plastic strain increments are equal in magnitude but opposite in sign. With this assumption the effective plastic strain

increment was reduced to a function of tangential plastic strain increment as follows:

$$\Delta\varepsilon_e^p = \frac{2}{\sqrt{3}}\Delta\varepsilon_\theta^p \tag{2.14}$$

He also assumed that the axial stress is the average of the radial and hoop stresses. With this assumption the von Mises yield condition was reduced to a relation between the radial and hoop stress components as follows:

$$\sigma_\theta - \sigma_r = \frac{2}{\sqrt{3}}\sigma_0 \tag{2.15}$$

With these assumptions the history dependent problem of elastic-plastic stress analysis was reduced to a numerical integration using uniaxial stress-strain data. Using the above analysis Rees compared the residual stress distribution from the above mentioned two different material models and showed that the residual stresses were affected by the strain hardening and that the hardening model was more realistic.

An investigation into the prediction of the deformation and the residual hoop stress distribution in autofrettaged thick-walled tubing of high-strength low-alloy steel with a diameter ratio of 2.07 was presented by Stacey et al. (1988). Analytical and numerical estimates were compared with the experimental measurements. Using Tresca's criterion in conjunction with a perfectly plastic material model, a closed form solution, similar to Hill (1950) was obtained for radial and hoop stress components. A solution was also obtained by using the simplified von Mises yield criterion ($\sigma_\theta - \sigma_r = \frac{2}{\sqrt{3}}\sigma_0 = 1.155\sigma_0$). Stacey concluded that the closed form solution obtained with Tresca's criterion remain valid for the von Mises criterion, provided that σ_0 is replaced by 1.155 σ_0.

2.2.1 Conclusion (Time-Independent Analysis)

All the solutions presented for the non-linear time-independent stress analysis and the subsequent residual stresses in thick-walled cylinders are obtained with some kind of simplifications in geometry, material model, yielding criterion and the associated plastic flow rules. The plane strain case has been considered in all the solutions available in the literature. This implies that the total strain in axial direction must be zero ($\varepsilon_z = 0$). On the other hand, the cylinder is not permitted to expand in axial direction. Deformations and stresses in the radial and tangential directions are affected by imposing this constraint because of the relationship between the longitudinal and lateral deformations defined by Poisson's ratio and its contribution in the three dimensional stress-strain relationship. In a more realistic approach, the cylinder can have deformation in axial direction while planes normal to the axial direction remain plane. A generalized plane strain case in which the total strain in axial direction is a constant ($\varepsilon_z = constant$), is a more realistic approach for the closed ended cylinders. Many solutions have also ignored the material strain hardening effect and instead they have used a perfectly plastic material model or a kind of linear hardening model. Using the material's hardening effect exactly the same as obtained from the experiment can significantly improve the analytical-numerical results. Another important material property is that the metals initially overstrained in tension have a significantly lower elastic limit in compression (Bauschinger phenomenon). This phenomenon must be considered in the material model for a more realistic prediction of residual stresses and the start of reverse yielding in thick-walled cylinders resulted from unloading of the

overstrained vessel. Although it is understood that the material reverse yielding point depends on the amount of accumulated plastic strain during overloading, but this is not yet fully incorporated into the available material models. The conventional kinematic hardening material models exhibit the Bauschinger effect phenomenon but the reverse yielding points in these models are defined with the assumption that the total elastic range ($2\sigma_0$) remains constant irrespective of the amount of prior plastic strain. Although finite element methods and softwares have used the material non-linearities in the non-linear stress analysis, but the material models considering the Bauschinger effect phenomenon are limited to the conventional models in the available softwares. The ANSYS finite element program (version 5.0) provides seven options to characterize different types of material behaviours; two of which exhibit the Bauschinger phenomenon. These are bi-linear kinematic hardening model designated by BKIN and multi-linear kinematic hardening model designated by MKIN both of which are defined based on the conventional assumption that the total elastic range ($2\sigma_0$) remains constant irrespective of the amount of prior plastic strain and the material's actual behaviour during reverse loading. This study incorporates the material model in a manner which considers the Bauschinger effect phenomenon as a function of the amount of irreversible effective plastic strain rather than the conventional models. This is a more realistic material model and will significantly improve the accuracy of the solution particularly the residual stresses and the reverse yielding predictions.

2.2.2 Objective 1

Following the above conclusion the specific objectives of the non-linear time-independent analysis are defined as follows:

- Improvement of the analytical-numerical model for the prediction of non-linear stresses by considering a realistic geometrical constraint for the case of a closed ended thick-walled cylinders (generalized plane strain).

- Using the material strain hardening as obtained from the experiment for the loading function of the non-linear analysis without any simplification to improve the accuracy of the results of plastic stresses and deformations.

- Improvement of the analytical-numerical model for prediction of residual stresses as well as the onset of reverse yielding by considering the material Bauschinger effect factor. The material's Bauschinger effect factor is obtained experimentally and is represented as a continuous function of the amount of irreversible plastic strains during overstraining rather than the conventional kinematical model in which the reverse yield point is related to the forward yield point.

- Experimental verification of the analytical-numerical model for the prediction of critical pressures, plastic stresses and the subsequent residual stresses.

2.3 Time-Dependent Creep Deformation of Tubes

Thick-walled tubes are often used in high-pressure high-temperature environment. The most important influence of high-temperature is to bring in the factor of time which must be considered in the tube's stress and deformation analysis. One of the important ingredients of a time-dependent structural stress and deformation analysis is the material's behaviour and its constitutive model. Therefore, some of the important material creep constitutive models and creep-rupture properties are also considered in this review.

The first major step toward the analysis of stress and deformation of structures working at high temperatures was taken by Bailey (1929) and Norton (1929). They introduced a uniaxial relationship between creep strain rate ($\dot{\varepsilon}$) and stress (σ) in the following form:

$$\dot{\varepsilon} = A\sigma^n \tag{2.16}$$

where A and n are temperature dependent constants. This equation was suggested by Bailey and Norton to replace Hook's law in analyzing the stresses and strains in loaded bodies. The major problem was that the relation was a uniaxial state of creep while in practical problems the situation was multi-axial.

The above uniaxial equation (Eq. (2.16)) was later generalized to the multi-axial state of creep by Bailey (1935). The major objective was to offer a basis for solving the creep problems under multi-axial system of stress in a form that was linked directly

with the case of simple creep tension test. General relationships were suggested by Bailey for creep in the direction of principal stresses such that for simple tension they were reduced to uniaxial creep equation (2.16). For example, the creep strain rate in the principal direction of X (i.e. $\dot{\varepsilon}_X$) was represented by

$$\dot{\varepsilon}_X = \frac{A}{2}[\frac{1}{2}(\sigma_X - \sigma_Y)^2 + \frac{1}{2}(\sigma_Z - \sigma_X)^2 + \frac{1}{2}(\sigma_Y - \sigma_Z)^2]^m[(\sigma_X - \sigma_Y)^{n-2m} - (\sigma_Z - \sigma_X)^{n-2m}] \tag{2.17}$$

where A, m and n are temperature dependent material constants and σ_X, σ_Y and σ_Z are principal stresses. For simple tension ($\sigma_Z = 0$, $\sigma_Y = 0$) the above equation was reduced to $\dot{\varepsilon}_X = A\sigma_X^n$ which is the same as equation (2.16). Experimental data were obtained from the creep deformation of lead tubes under combined internal pressure and axial torsion to verify the suggested model. The model was complex and approximate and the experimental data were interpreted based on the uniform tangential and axial stresses for thin tubes.

In another attempt, to interpret the creep deformation of tubes with the uniaxial creep deformation, an experimental study of creep in tubular pressure vessel was performed by Norton (1939). He carried out experiments on the tangential and longitudinal creep under internal pressure and high temperature in steel tubes such as boiler tubes. He compared with the creep properties of uniaxial tensile specimens of the same type of steel at the same temperature and under a stress equal to the tangential stress in the tube. Norton concluded that the creep strain rate in the tangential direction is about half of the uniaxial tensile specimens and the axial creep strain rate is negligible. No

specific formula or model was suggested in this work to relate the uniaxial data and multi-axial deformation.

Previous work of Bailey (1935) had indicated a theoretical basis (equation (2.17)) that metals under combined stresses had a lower rate of creep deformation than when under a pure tensile stress of the same magnitude. However, some experimental work had shown close agreement between the flow under tensile conditions and the flow under combined stresses. It was, therefore, desired to make more careful creep tests on tubes to investigate the relationship between the multi-axial and uniaxial creep deformation. Norton (1941) conducted creep tests on tubular specimens and indicated that the longitudinal creep deformation of the tubes is substantially zero and the tangential creep deformation rate is approximately the same as the creep in the tensile specimen with a stress equivalent to the tangential stress in the tube. There was no time-dependent analysis of stress and strain in this work and the conclusion was based on experimental results only.

In another attempt, to relate the creep deformation of tubes with the uniaxial creep deformation, Soderberg (1941) used the theory of yielding and the concepts of "intensity of strain" and "intensity of stress" introduced by Hencky (1933). Soderberg (1941) related the principal creep strain rates in a three-dimensional stress system with the creep strain rate of a tensile creep specimen in the following form:

$$\begin{aligned}
\dot{\varepsilon}_1 &= \frac{\dot{\varepsilon}}{s}[\sigma_1 - \frac{1}{2}(\sigma_2 + \sigma_3)] \\
\dot{\varepsilon}_2 &= \frac{\dot{\varepsilon}}{s}[\sigma_2 - \frac{1}{2}(\sigma_3 + \sigma_1)] \\
\dot{\varepsilon}_3 &= \frac{\dot{\varepsilon}}{s}[\sigma_3 - \frac{1}{2}(\sigma_1 + \sigma_2)]
\end{aligned} \tag{2.18}$$

where, $\dot{\varepsilon}_1$, $\dot{\varepsilon}_2$ and $\dot{\varepsilon}_3$ are the rate of principal creep strains, σ_1, σ_2 and σ_3 are the principal stresses, s is the intensity of stress and $\dot{\varepsilon}$ is the rate of the intensity of strain. The intensity terms were defined as follows:

$$\begin{aligned}
\dot{\varepsilon} &= \frac{\sqrt{2}}{3}\sqrt{(\varepsilon_1 - \varepsilon_2)^2 + (\varepsilon_2 - \varepsilon_3)^2 + (\varepsilon_3 - \varepsilon_1)^2} \\
s &= \frac{1}{\sqrt{2}}\sqrt{(\sigma_1 - \sigma_2)^2 - (\sigma_2 - \sigma_3)^2 - (\sigma_3 - \sigma_1)^2}
\end{aligned} \tag{2.19}$$

Soderberg (1941) applied the above theory to a thin tube under internal pressure with the assumption that the creep curves approach straight lines (constant strain rate) with a minimum slope which depended on the stress. Soderberg concluded that the tangential creep strain rate is $\sqrt{3}/2$ times the creep rate of a uniaxial creep tensile test. Finally he stated that the analysis of creep of a thick-walled tube is a matter of considerable difficulty. He showed that the postulates of creep did not conflict with those of stationary plastic flow. In fact, Soderberg modified the available plasticity theory (Hencky deformation theory) in a manner which was suitable to use in a rate dependent analysis and used this concept in an stationary analysis of thin tubes.

Later, Norton and Soderberg (1942) modified the solution to include the thick-walled

tube by introducing a deviation factor in the following form:

$$f = [1 - (\frac{t}{2R)^2}]^2 \tag{2.20}$$

where t is the tube thickness and R is the mean radius. This factor was multiplied by the intensity of stress of a thin tube to give the intensity of stress at the mean radius of a thick-walled tube. The deviation factor, f, was obtained with these assumptions that the creep rate varies as the nth power of the stress intensity ($\dot{\varepsilon} = A\sigma^n$) and that the radial displacement varies inversely with radius and the tangential creep rate varies inversely with the square of the radius.

So far, all the above investigators have considered the case of thin tubes or they have modified the thin tube formula to include the thick-walled tube. Furthermore, they have all considered the steady state creep (secondary creep regime) in their stress analysis which is evident from the strain rate equation ($\dot{\varepsilon} = A\sigma^n$) which has been adopted by all of them.

The first non-steady creep stress analysis of thick-walled cylinders was given by Coffin et al. (1949). They evaluated the stresses and creep strains at a particular time resulting from loading a thick-walled cylinder under constant internal pressure and a constant elevated temperature throughout the thickness. It was assumed that in the creep test, time (t), temperature (T) and strain (ε^*) are independent variables represented by the following function:

$$\sigma^* = f(\varepsilon^*, t, T) \tag{2.21}$$

where σ^* and ε^* were called effective stress and effective strain defined in the following form:

$$\begin{aligned} \sigma^* &= \sigma_\theta - \sigma_r \\ \varepsilon^* &= \varepsilon_\theta - \varepsilon_r \end{aligned} \tag{2.22}$$

in which σ_θ and σ_r were tangential and radial stresses and ε_θ and ε_r were tangential and radial strains. Only primary creep characteristic of a given material was taken into account. A family of conventional creep curves of strain versus time at constant stress were re-plotted by Coffin as stress-strain curves for a given time (isochronous curves). The procedure for plotting the isochronous curves is schematically shown in Figure 2.2.

Coffin assumed that during small time intervals these isochronous curves represent the effective stress and effective strain relationship and solved the problem similar to a plasticity problem. Result of stress distributions after 25hr, 100hr and 1000hr were reported by Coffin. Although the distribution of stresses were reported for short periods of time, but it was shown that the stresses were redistributed and changed with time.

It was understood that the stress and deformation of tubes working at creep ranges are time-dependent, but the design of tubes was based on the maximum tangential creep stress obtained from an stationary analysis.

Bailey (1951a) considered several principal matters which should be taken into account

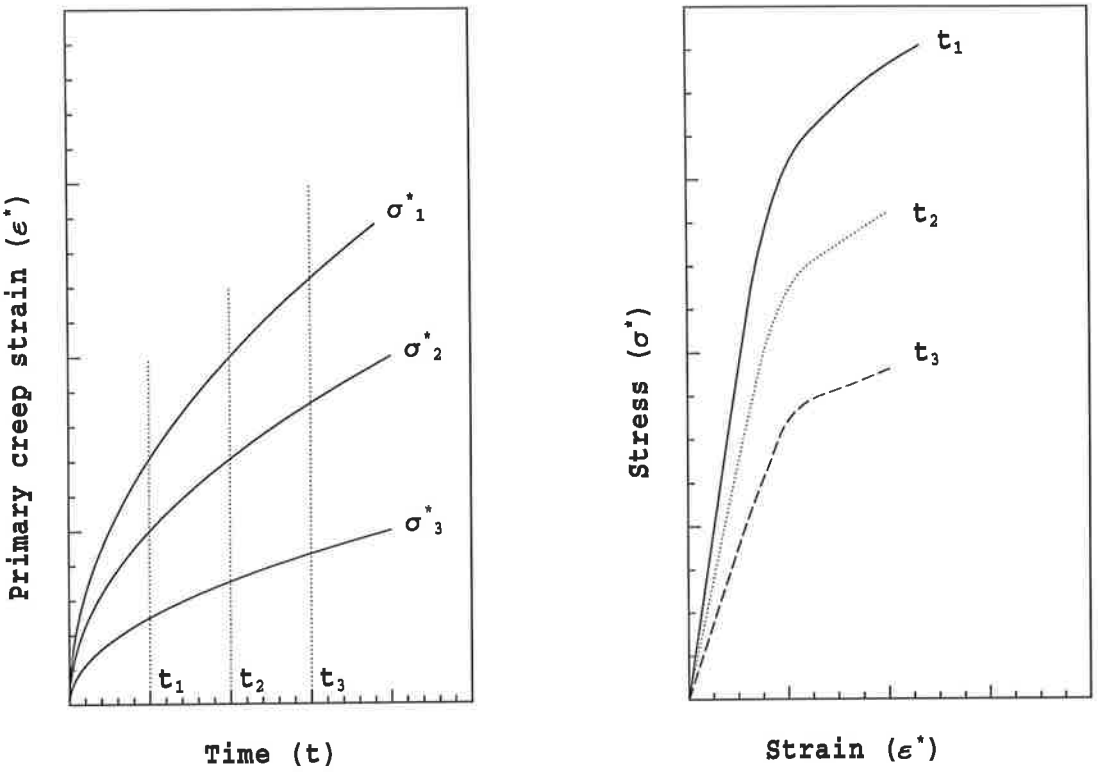

(a) (b)

Figure 2.2: (a) Primary creep strain; (b) Schematic figure of isochronous curves

in steam piping design for high pressure and high temperature. Principles such as stress redistribution as a result of creep and the creep strain allowable for design and the design temperature were generally discussed. Creep test results for $Mo - V$ steel for high stress level and high temperatures from $630°C$ to $700°C$ were reported by Bailey (1951a). He selected temperature as ordinate and logarithm of time to attain creep strains of 0.001, 0.002 and 0.003 as abscissa and showed a linear relationship between temperature and the logarithm of time as illustrated in Figure 2.3.

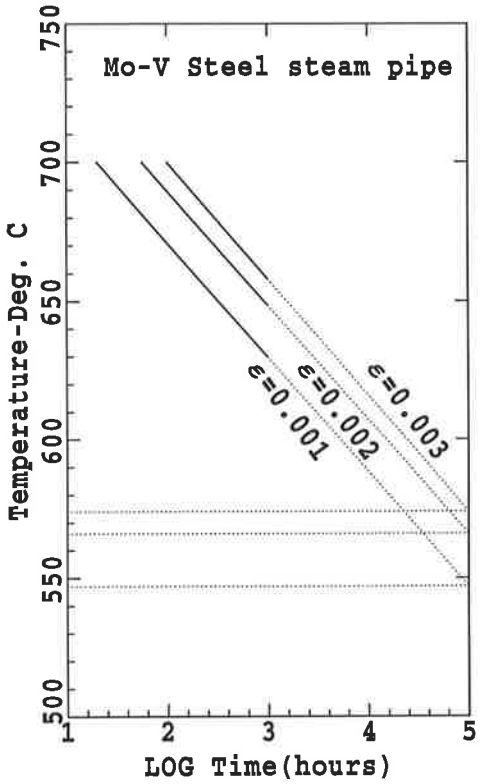

Figure 2.3: Creep test results on Mo-V steel steam pipe for stresses of 3 Ton per square inch (45.6 MPa).

These lines were extended to a time of 100,000 hours to give the extrapolated value of design temperatures. In order to obtain the design temperature for a tube, stress distribution and creep of tubes under internal pressure were investigated in a separate paper by Bailey (1951-b). He derived expressions for the principal stresses in a thick-walled tube provided that a single stage of creep were applied across the tube wall and that the creep strains were sufficient to ignore elastic strains. He used the previously defined formula for the creep strain rate in three principal directions (equation (2.16)) and obtained a relationship for the design temperature of the tube which was related

to the internal pressure.

It was not feasible to run experiment for a long time duration at operating condition (temperature and stress) of a steam tube to introduce a design life for the tube after which the tube would be retired. Therefore, for the first time Bailey carried out experiments at very high temperatures (accelerated creep test) and applied stress to attain a certain amount of accumulated strain and linearly extrapolated a design temperature and life.

The concept of linear relationship between temperature and the logarithm of time to achieve a certain creep strain introduced by Bailey (1951a) was later developed by Larson and Miller (1952). They established a time-temperature relationship for rupture and creep stresses. They showed that the lines of logarithm of time-to-rupture versus (1/T) converge to a constant value for different constant stresses.They introduced the Larson-Miller parameter (P_{LM} which was the product of temperature (T) and a function containing logarithm of time-to-rupture (t_R) as follows:

$$P_{LM}(\sigma) = T(C + log_{10}t_R) \tag{2.23}$$

Larson and Miller selected $C = 20$ for most materials in the above equation. They showed that the parameter depends only on stress and introduced the Larson-Miller parameter curves. Larson-Miller parameter is used extensively in structural creep rupture analysis. Many investigators questioned the use of $C = 20$ for all materials and therefore other parameters were proposed. Manson and Haferd (1953) plotted logarithm of time-to-rupture as a function of temperature and showed that for different

stress levels all the lines converge to a point which is material dependent. They introduced a parameter which was somewhat more general than Larson-Miller parameter for each material. Finally Manson (1963) introduced a generalized parameter from which Larson-Miller and Manson-Haferd parameters could be obtained.

The concept of design life and rupture life were already introduced by Bailey (1951-b) and Larson and Miller (1952). The expenditure of life when temperature or stress varies with time was first considered by Robinson et al. (1952). Robinson calculated the factor of safety of a structural member with reference to a stated life for the system operating under stress and at high temperature and the stress or temperature varies moderately according to some definite pattern. The formula presented is based on the assumption that the expenditure of each particular fraction of the life span at elevated temperature is independent of and without influence upon the expenditure of all other fraction of life to rupture and thus can be accumulated to give the total expenditure of life. To facilitate the calculation of this quantity, the expenditure of life (E)was defined as follows:

$$E = \sum_{i=1}^{n} \frac{t_i}{L_i} = \frac{t_1}{L_1} + \frac{t_2}{L_2} + \frac{t_3}{L_3} + ... \tag{2.24}$$

in which t_i and L_i are time and the time-to-rupture at any particular condition of stress and temperature. The concept of damage was not introduced at that time but later this rule became famous as the Robinson's life fraction damage rule.

The concept of expenditure of life did not draw attention until the life assessment of

fossil fueled power stations became an active area of research in mid 1980's. However, the analysis of thick-walled tube was continued by approximate analytical techniques the most important of which was the reference stress method.

Schulte (1960) observed that in a creep solution of beams there were points in the cross section at which the stress did not change as the solution progressed from initial elastic to stationary solution at constant bending moment. This constant stress was called reference stress. By running a creep test at this constant stress Schulte was able to predict the beam deflections. Basically, the idea of the method was that a given structure could be analyzed with data obtained from a single creep test at its reference stress.

Marriott and Leckie (1964) observed that there are points in components undergoing transient creep at which the stress does not change with time. In a pressurized thick cylinder this point was called "skeletal point" which is shown in Figure 2.4 (point A). However they did not use this skeletal point in any particular analysis.

A method for establishing the reference stress was suggested by Mackenzie (1968) provided that the material obey a power creep law of the following form:

$$\dot{\varepsilon} = B\sigma^n \tag{2.25}$$

The steady state solution for the stresses using the above creep law in particular structures such as beams and thick walled cylinders were known, the reference stresses were obtained by comparing the stationary solution with the elastic solution. Using the

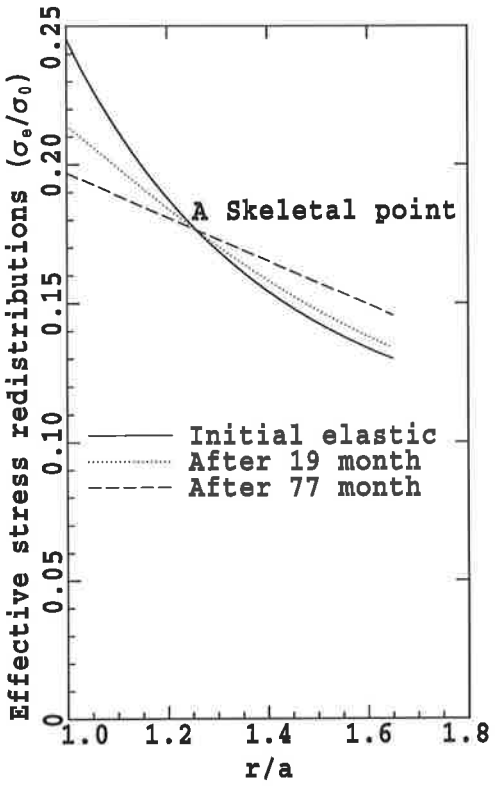

Figure 2.4: Effective stress redistribution from the initial elastic to stationary creep

reference stress (σ_{ref}) and the corresponding strain rate ($\dot{\varepsilon}_{ref}$), the power law equation was rewritten by Mackenzie in terms of σ_{ref} and $\dot{\varepsilon}_0$ as follows:

$$\frac{\dot{\varepsilon}_1}{\dot{\varepsilon}_{ref}} = (\frac{\sigma_1}{\sigma_{ref}})^n \tag{2.26}$$

Mackenzie applied the above equation and the stress-strain rate equations (Eqs. (2.18)) to a number of structures including the thick-walled cylinder and obtained an estimate of their deformation rate in terms of reference parameters. The tangential creep strain rate at the outer ($\dot{\varepsilon}_{\theta o}$) and inner ($\dot{\varepsilon}_{\theta i}$) surfaces of the cylinder were given in terms of

$\dot{\varepsilon}_{ref}$ as follows:

$$\begin{aligned} \dot{\varepsilon}_{\theta i} &= 1.5\frac{\lambda\dot{\varepsilon}_{ref}\beta^2}{(\beta^2-1)} \\ \dot{\varepsilon}_{\theta o} &= 1.5\frac{\lambda\dot{\varepsilon}_{ref}}{(\beta^2-1)} \end{aligned} \tag{2.27}$$

where β is the radii ratio (R_o/R_i) and λ is a parameter which depends on β. Variations of λ versus β were given on a graph which could be used to obtain the tangential creep strain rates of different cylinders.

The creep problems of pressurized cylinders and spheres with a negative temperature gradient in the radial direction were analyzed by Sim (1973). A reference temperature was defined for the vessel. Knowing the reference stress and also the reference temperature, it was shown that the stationary state radial displacement of the vessel wall was approximately proportional to the creep strain which occurs in a tensile specimen loaded by a stress equal to the reference stress and at a temperature equal to the reference temperature of the vessel. Consequently the creep displacement of cylinders and spheres under internal pressure with a negative temperature gradient in the radial direction may be predicted if the creep strain-time behaviour of a material specimen loaded at the reference stress and reference temperature is known.

Kraus (1980) presented the stationary creep stress distribution in a thick-walled cylinder. It was assumed that the creep strain rate in axial direction is zero and that the radial and tangential creep strain rates are equal in magnitudes and opposite in signs. For the stationary state the effective creep strain rate and the effective creep stress

were related by the Bailey-Norton uniaxial relation for steady creep as; $\dot{\varepsilon} = A\sigma^n$. In a comparison of the stationary solution with the elastic solution Kraus showed that when n was set to unity the elastic solution was resulted. He concluded that this was consistent with the elastic analogy introduced by Hoff (1956). He also concluded that redistribution has occurred for the stresses from their initial elastic to their final stationary distribution. To see how the initial elastic stress state redistributed into the stationary state, Kraus showed that the non-stationary stress analysis is a statically indeterminate problem and cannot be done in closed form. The non-stationary stress analysis gives the history of stresses and strains which are important and necessary in the damage analysis and the life assessment of thick-walled tubes.

A computational method for predicting the life of tubes used in petrochemical heater service has been introduced by Simonen et al. (1985). The model uses conventional numerical approaches to solve finite element models of two dimensional creep problems. The Larson-Miller parameter is used to represent stress rupture data for tube material. This paper also addresses the practical difficulties of applying such models to real service conditions and real commercial alloys. The result given in this paper shows that the maximum damage occurs near the mid-wall of the tube (heater tube with an inward flow of heat) while there is no damage in the outer surface of the tube even when the tube approaching the end of its service

In view of practical difficulties in using the above model, Seshadri (1988) introduced

an analytical method in which upper-bound estimates of creep deformations and creep damages of fired heater tubes are obtained using a linear elastic analysis. The method is based on the concept of the elastic-core developed by Bree (1967) and O'Donnell et al. (1974), and evaluations of time-dependent inelastic effects can be carried out by using linear elastic calculations. However the effect of stress redistribution is ignored by using an average value of the upper limit hoop stresses at the inside and outside tube wall as a conservative value of the effective hoop stress for the whole thickness.

Traditional life prediction methods involve the calculation of stress using the mean diameter equation based upon the design pressure. The computed stress is then used to calculate the life of the tube (API recommended practice (1978)). This approach is simple but the results are not reliable due to ignoring the stress redistributions. Although it is well understood that the stresses in general and the hoop stress in particular are changed with time in a thick-walled tube operating at high temperature, but the mean diameter formula for calculating hoop stress is still used in estimating the remaining life of high-energy piping system (Seshadri (1988) and Ripley et al. (1995)). A better estimate of the remaining life was introduced by Cohn (1990) using the equivalent stress formulas rather than the mean diameter formula.

Cohn (1990) used several equivalent stress formulas for the life assessment of high-energy piping system. These systems are subjected to multi-axial state of stress, but creep rate and stress rupture data are based on uniaxial load tests. Several combined

stress equations or equivalent stresses have been postulated by Hayhurst (1972), Brown et al. (1982) and Huddlestone (1985). These equivalent stresses together with the available time-dependent design stress values for Cr-Mo steels were used to predict time to rupture of these components. In fact, design or applicable stresses were converted in time in hours. In this method, total life was computed and the past operating life was subtracted from the computed total life to obtain an estimate of the remaining life. Cohn concluded that the prediction of rupture life is complicated in a multi-axial state of stress due to stress redistributions and variation of stresses with time. He suggested that a more accurate prediction can be obtained using an incremental life exhaustion procedure.

Current remaining life assessment of the creep exposed components is based on the accelerated post-exposure creep rupture tests of the service exposed material, Tolksdorf (1995). Accelerated creep tests are carried out at service stress (iso-stress tests) but at higher temperatures so that extrapolation to the service temperature gives an estimate of the remaining useful creep life of the component as shown in Figure 2.5.

Accelerated tests at higher stress and the service temperature (isothermal tests) or tests at both higher stress and higher temperature have also been commonly used for the remaining life evaluations (Tolksdorf (1995)). In these methods sufficient material for the manufacture of several miniature test specimens has to be removed from the component which means that these methods are destructive and more importantly the

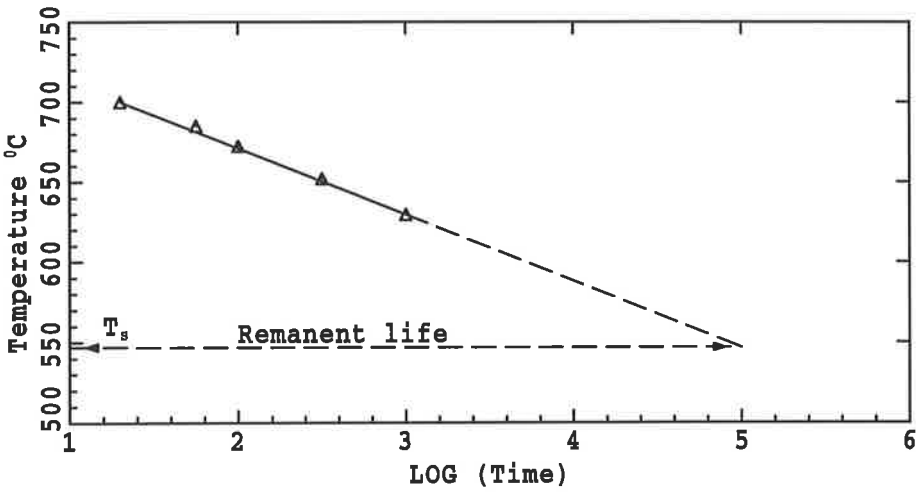

Figure 2.5: Accelerated post-exposure stress-rupture test data at higher temperatures and the service stress are extrapolated to the service temperature to obtain an estimate of the remaining life.

test specimens are not necessary representative of the bulk of material or the mostly damaged material.

Recent creep damage evaluations are based on the in-service inspection methods, visual and non-destructive examinations, surface hardening, surface metallography and replication to assess the micro-structural changes, Nogata and Takahashi (1995). However, the information obtained from the in-service inspection may not necessary be representative of the bulk of material. Furthermore, current surface assessment methods neither provide a quantitative estimate of the damage nor give any information about the damage gradients.

While in-service testing and non-destructive examinations of thick-walled tubes can provide useful information about material condition, greater understanding of the component non-linear time-dependent stress and damage behaviour is essential before the information obtained from the inspection procedures can be used to provide predictions of future component performance. In fact, the first step in all these methodologies must be a detailed creep stress and damage analysis of the component. If an improved damage model can be predicted for the vessel then the component examinations and inspections can be scheduled in a selective manner. A complete creep deformation and creep damage analysis must consider the incremental deformation and life exhaustion. As the stress relaxes from the initial elastic state to the present condition, the calculated damage and life exhaustion are cumulated in incremental periods at the applicable stress.

An important ingredient of the non-stationary stress and damage analysis is the material constitutive model and rupture properties. The accuracy of life predictions is currently limited by the wide variation in short-term available materials data. The use of parametric techniques such as larson-Miller procedure allows data extrapolation of only three times as the longest rupture life according to ASTM standards.

A potential solution to the problem of data description and long-term extrapolation was obtained by Evans et al. (1982) introducing the "Theta (Θ) projection" concept.

The theta projection concept considers the creep strain to be the sum of a primary or decaying and a tertiary or accelerating creep strain rate components as follows:

$$\varepsilon = \Theta_1(1 - e^{-\Theta_2 t}) + \Theta_3(e^{\Theta_4 t} - 1) \tag{2.28}$$

The theta projection concept has been successfully applied to $\frac{1}{2}Cr, \frac{1}{2}Mo, \frac{1}{4}V$ ferritic steel which is the selected material in this investigation. However, due to the complex mathematical representation of the proposed material model, application of the model in practical problems is not yet well developed.

2.3.1 Conclusion (Time-dependent Analysis)

Creep is an important damage mechanisms to be considered for the life assessment of power plants high-pressure high-temperature piping systems. Creep damage and the life exhaustion analysis of thick-walled tubes is not yet well developed due to the combined effect of loading, time and temperature. A major difficulty in the damage analysis of thick-walled tubes and the consequent life exhaustion of these components is that the stresses are changed with time and redistributed across the wall thickness of the tubes. For an accurate analysis of damage and life exhaustion, the history of stresses is necessary and therefore a non-stationary creep stress analysis is inevitable. As the stresses change with time from their initial elastic state to the present condition, the increments of damage and life exhaustion must be calculated and cumulated in incremental periods of time at the applied stresses.

2.3.2 Objective 2

According to the above conclusion the main objective of the time-dependent stress analysis is itemized as follows:

- Introducing a non-stationary creep stress analysis of thick-walled tubes by using an improved long-term material creep constitutive model defined by the theta projection concept which can significantly improve the long-term prediction of stress and deformation histories.

- Incorporating the Robinson's linear life fraction damage rule, which has been adopted by the ASME Code (Case N47), into the above non-stationary analysis to predict the creep damages across the thickness of the tube as well as its variation with time (damage histories).

- Using the damage histories and the material's rupture properties to evaluate the remaining life of the component.

- Verification of the analytical-numerical procedure.

Chapter 3

THEORETICAL ANALYSIS

3.1 Introduction

In the elastic range strains are linearly related to the stresses by Hooke's law. In the plastic and creep regimes the stress-strain relationship is generally non-linear. An important distinction between the elastic and plastic stress-strain relations is that in the elastic range the strains are uniquely determined by the stresses using Hooke's law, but in the plastic and creep regimes the strains are not uniquely determined by the stresses and depend on the complete loading history (path dependent) or on how the state of stress is reached.

Because of this history dependence of the plastic and creep strains, it is necessary to compute either the differentials or the increments of plastic and creep strains throughout the loading history and then obtain the total plastic or creep strains by integration

or summation. To determine the actual magnitude of the plastic or creep strain increments in a multi-axial state of stress and strain, the non-linear incremental stress-strain relationships are employed. In these relationships, increments of plastic or creep strains are related to the multi-axial state of stress and the loading history. It is difficult to follow the loading path in the stress space of a multi-axial state of stress condition. Therefore an effective stress and an effective plastic or creep strain increment are defined in order to facilitate the use of material's uniaxial property in a multi-axial state of stress and strain. In this Chapter non-linear plastic and creep deformation of thick-walled cylinders are being formulated and general procedures for the solution are suggested. However, details of the proposed analytical-numerical procedures and their experimental verification will be discussed in the next two Chapters.

3.2 Formulation of Thermoelastoplastic Problem in Thick-Walled Cylinders

A thick-walled cylinder which is loaded with an internal pressure and a thermal gradient is considered. For each element of the cylinder the equilibrium of forces and compatibility of displacements must be satisfied regardless of the elastic-plastic or creep situation. However, stresses and strains are influenced by plasticity or creep through the stress-strain relationship in which plastic or creep strains are considered. In a thick-walled cylinder containing high internal pressure the middle section of the vessel is the most susceptible to failure area as it has been shown by many investigators

(Crossland et al. (1958), Roach and Priddy (1994)). Therefore a cylindrical element at the middle section of the cylinder is shown in Figure 3.1 and has been considered for the analysis.

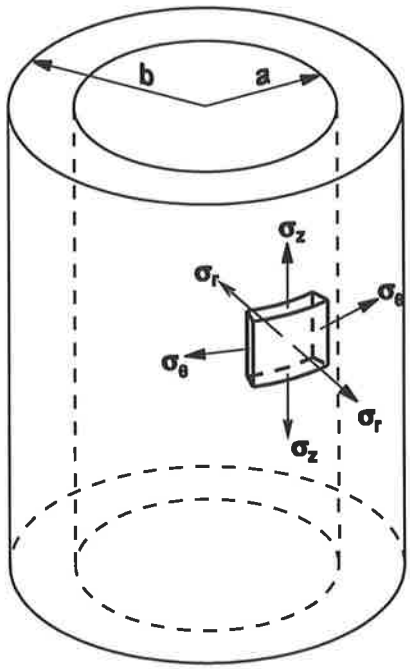

Figure 3.1: Location of a cylindrical element at the mid-center of the cylinder

The equation of equilibrium and compatibility for such an element are written in the following form:

Equilibrium:

$$\frac{d\sigma_r}{dr} + \frac{\sigma_r - \sigma_\theta}{r} = 0 \tag{3.1}$$

Compatibility:

$$\frac{d\varepsilon_\theta}{dr} + \frac{\varepsilon_\theta - \varepsilon_r}{r} = 0 \tag{3.2}$$

where σ_r and σ_θ are radial and tangential stresses and ε_r and ε_θ are radial and tangential strains.

The stress-strain relations depend on plasticity and creep. In the general case it is adopted in solid mechanics that the total strain is the sum of elastic, plastic, creep and thermal strain components as follows:

$$\varepsilon_{ij} = \varepsilon^e_{ij} + \varepsilon^p_{ij} + \varepsilon^c_{ij} + \alpha T \delta_{ij} \tag{3.3}$$

where the superscripts 'e', 'p' and 'c' refer to the elastic, plastic and creep strain respectively. The coefficient of linear thermal expansion is represented by α, T is the temperature change and δ_{ij} is the Kronecker delta. In cylindrical coordinate this equation is rewritten as follows:

$$\begin{aligned}
\varepsilon_r &= \frac{1}{E}[\sigma_r - \nu(\sigma_\theta + \sigma_z)] + \varepsilon^p_r + \varepsilon^c_r + \alpha T \\
\varepsilon_\theta &= \frac{1}{E}[\sigma_\theta - \nu(\sigma_z + \sigma_r)] + \varepsilon^p_\theta + \varepsilon^c_\theta + \alpha T \\
\varepsilon_z &= \frac{1}{E}[\sigma_z - \nu(\sigma_r + \sigma_\theta)] + \varepsilon^p_z + \varepsilon^c_z + \alpha T
\end{aligned} \tag{3.4}$$

where ε_r, ε_θ and ε_z are total strains, ε^p_r, ε^p_θ and ε^p_z are total plastic strains, ε^c_r, ε^c_θ and ε^c_z are time-dependent creep strains, σ_r, σ_θ and σ_z are normal stresses, E is the material's modulus of elasticity and ν is the Poisson's ratio. In this section the thermoelasto-plastic deformation of thick-walled cylinders will be considered and therefore the creep strains will be ignored. Therefore the stress-strain relation in this case is rewritten from the equation (3.4) as follows:

$$\begin{aligned}
\varepsilon_r &= \frac{1}{E}[\sigma_r - \nu(\sigma_\theta + \sigma_z)] + \varepsilon_r^p + \alpha T \\
\varepsilon_\theta &= \frac{1}{E}[\sigma_\theta - \nu(\sigma_z + \sigma_r)] + \varepsilon_\theta^p + \alpha T \\
\varepsilon_z &= \frac{1}{E}[\sigma_z - \nu(\sigma_r + \sigma_\theta)] + \varepsilon_z^p + \alpha T
\end{aligned} \tag{3.5}$$

Effect of the creep strains will be considered in the next section which is devoted to time-dependent creep stress and damage analysis of thick-walled tubes.

A major difficulty in the above stress-strain relationship is the history dependency of the total plastic strains, $\varepsilon_r^p, \varepsilon_\theta^p$ and ε_z^p. If the cylinder develops some plastic region as a result of high internal pressure or any other loading condition, then the total plastic strains must be calculated in the plastic region of the vessel. Therefore, it is necessary to introduce the incremental stress-strain relationship or plastic flow rule which facilitates the computation of plastic strain increments. These increments can be integrated along the loading path to give the total accumulated plastic strains.

3.2.1 Plastic Flow Rule

The total plastic strains in equation (3.5) depend on the loading history, therefore they can be calculated by integration or by summation of the plastic strain increments throughout the loading history. If the load is applied during a large number of loading steps, then the total plastic strains $\varepsilon_r^p, \varepsilon_\theta^p$ and ε_z^p can be obtained by summation of the plastic strain increments in the following form:

$$\begin{aligned} \varepsilon_r^p &= \sum_{i=1}^{n} \Delta\varepsilon_{r,i}^p \\ \varepsilon_\theta^p &= \sum_{i=1}^{n} \Delta\varepsilon_{\theta,i}^p \\ \varepsilon_z^p &= \sum_{i=1}^{n} \Delta\varepsilon_{z,i}^p \end{aligned} \tag{3.6}$$

where $\Delta\varepsilon_r^p$, $\Delta\varepsilon_\theta^p$ and $\Delta\varepsilon_z^p$ are radial, tangential and axial plastic strain increments and the subscript i represents the loading step. To determine the plastic strain increments in equation (3.6) the incremental plastic stress-strain relationship is necessary. From the theory of plasticity, the incremental stress-strain relationship depends on the yield criterion. On the other hand a yield criterion is associated with an incremental stress-strain relationship which is usually called its associated flow rule. The material yield criterion and its associated flow rule will be employed for calculation of plastic strain increments. The material selected in this time-independent non-linear analysis is stainless steel SUS 304. The material strength can be best described by the von Mises yield criterion. Therefore, the von Mises yield criterion and its associated flow rule are selected and introduced here. The yield criterion determines the stress level at which yielding will take place. In multi-axial state of stress, a function containing the individual stresses which can be interpreted as the effective stress is a measure of plastic yielding. The von Mises effective stress in a multi-axial stress state of a cylinder is written as follows:

$$\sigma_e = \frac{1}{\sqrt{2}}[(\sigma_r - \sigma_\theta)^2 + (\sigma_\theta - \sigma_z)^2 + (\sigma_z - \sigma_r)^2]^{\frac{1}{2}} \tag{3.7}$$

where σ_e is the von Mises effective stress. According to the von Mises criterion yielding starts when the effective stress is equal to the material's yield stress (σ_0) as follows:

$$\sigma_e = \sigma_0 \tag{3.8}$$

Then the von Mises yield criterion may be written in the following form:

$$(\sigma_r - \sigma_\theta)^2 + (\sigma_\theta - \sigma_z)^2 + (\sigma_z - \sigma_r)^2 = 2\sigma_0^2 \tag{3.9}$$

The associated flow rule of the von Mises criterion is known as Prandtl-Reuss equations. The Prandtl-Reuss equations relate the increments of plastic strain to the loading history and the state of stress. In this case, the Prandtl-Reuss equations are written in terms of radial and tangential plastic strain increments, $\Delta\varepsilon_r^p$ and $\Delta\varepsilon_\theta^p$ as follows:

$$\begin{aligned} \Delta\varepsilon_r^p &= \frac{\Delta\varepsilon_p}{\sigma_e}[\sigma_r - \frac{1}{2}(\sigma_\theta + \sigma_z)] \\ \Delta\varepsilon_\theta^p &= \frac{\Delta\varepsilon_p}{\sigma_e}[\sigma_\theta - \frac{1}{2}(\sigma_z + \sigma_r)] \end{aligned} \tag{3.10}$$

where $\Delta\varepsilon_p$ is the effective plastic strain increment and will be defined later in this section. The fraction $\Delta\varepsilon_p/\sigma_e$ in equation (3.10) is the history dependent part of non-linear stress-strain relationship. The axial plastic strain increment can be written in terms of radial and tangential plastic strain increments by using the material incompressibility condition in plastic regime. Although in elastic regime the material's incompressibility is not an acceptable assumption, but in the plastic regime metals are more or less incompressible. Therefore, the plastic strain increment in the axial direction may be obtained from the incompressibility condition as follows:

$$\Delta\varepsilon_z^p = -(\Delta\varepsilon_r^p + \Delta\varepsilon_\theta^p) \tag{3.11}$$

The effective plastic strain increment in equation (3.10) is defined in the following form:

$$\Delta\varepsilon_p = \frac{\sqrt{2}}{3}[(\Delta\varepsilon_r^p - \Delta\varepsilon_\theta^p)^2 + (\Delta\varepsilon_\theta^p - \Delta\varepsilon_z^p)^2 + (\Delta\varepsilon_z^p - \Delta\varepsilon_r^p)^2]^{\frac{1}{2}}. \tag{3.12}$$

The effective stress and the effective plastic strain increment in a multi-axial state of stress and strain will facilitate to reduce the history dependent part of the non-linear stress-strain relationship ($\Delta\varepsilon_p/\sigma_e$) to the history of a uniaxial loading. A functional relationship between the effective stress and the effective plastic strain increment can be written in the following form:

$$\begin{aligned} \sigma_e &= H(\varepsilon_p) \\ \varepsilon_p &= \int d\varepsilon_p \end{aligned} \tag{3.13}$$

where H is the material's hardening function. This functional relationship given by equations (3.13) can be obtained from the uniaxial tensile stress-strain data plotted in Figure 3.2. The uniaxial stress-strain data obtained from experiment is based on the stress and total strain. In order to find the functional relationship represented by equation (3.13), it is necessary to convert the stress-strain data into a new format based on the stress and plastic strain. Therefore, in this investigation a computer program is written which transforms the material's data file obtained from the experiments, into a new data file based on the effective stress and effective plastic strain. In fact the computer program subtracts the elastic strain from the total strain to obtain the effective plastic strain. The new formatted data file is then used as an input of a curve fitting software to find the best continuous function representing the new data file. The best function representing the effective stress and effective plastic strain relationship is

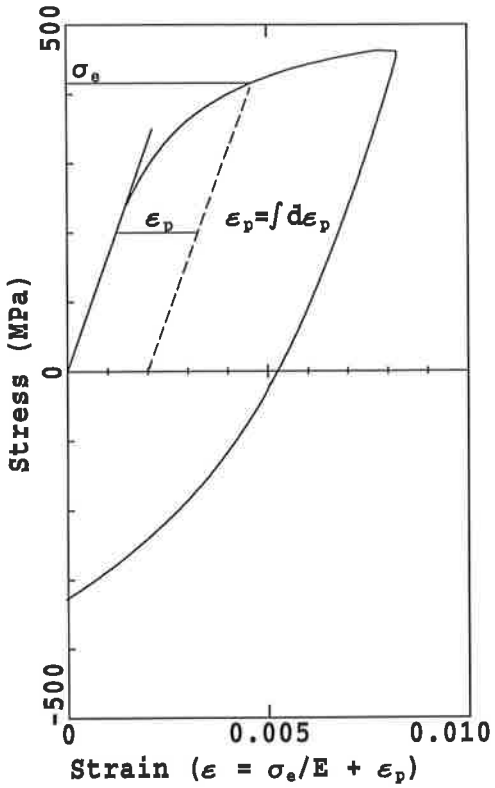

Figure 3.2: The material stress-strain curve obtained by experiment.

obtained as follows:

$$\sigma_e = 232.68187 + 689.01541(\varepsilon_p)^{0.21842186} \tag{3.14}$$

A plot of the new data file represented by the above equation is shown in Figure 3.3. So far the equations of equilibrium, compatibility and stress-strain as well as incremental stress-strain relations and their relationship to the loading history are introduced. To obtain a solution for the non-linear plastic stresses and strains the above mentioned equations plus the boundary and end conditions must be satisfied.

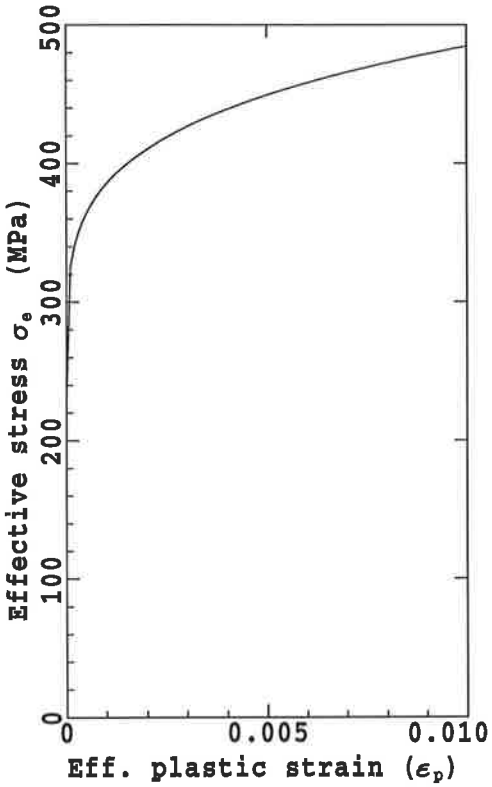

Figure 3.3: Relation between effective stress and effective plastic strain.

3.2.2 Boundary and End Conditions

It is assumed that the cylinder ends are closed which is also consistent with the experimental model incorporated in this study. It is also assumed that the internal pressure of the cylinder is P_a and there is no external pressure present on the cylinder outer surfaces. However, for the generality of the analytical-numerical model an outer pressure, P_b is supposed to exist at the outer surface of the cylinder. It will be set to zero whenever there is no outer pressure acting on the surface. The radial stress at the inner

and outer surfaces of the cylinder must be equal to the compressive stress of internal and external pressures. Therefore the boundary conditions at the internal and external surfaces of the cylinder are written in the following form:

$$\begin{aligned} \sigma_r &= -P_a \qquad at \quad r = a \\ \sigma_r &= -P_b \qquad at \quad r = b \end{aligned} \tag{3.15}$$

where a and b are the inner and outer radii of the cylinder and the negative sign is for the compressive stresses.

For a closed end cylinder the integration of axial stress σ_z over the cross-sectional area must be equal to the longitudinal force caused by the internal pressure. The longitudinal force generated by an internal pressure P_a in a cylinder with the inner radius of a is $F = P_a \pi a^2$. Therefore the end condition is mathematically expressed as follows:

$$\int_a^b \sigma_z dA = P_a \pi a^2 \tag{3.16}$$

Before presenting a solution to the non-linear stresses and strains in the cylinder it is convenient to summarize the above governing equations and the boundary and end conditions and then set off for a solution.

3.2.3 Summary of the Governing Equations

All the above governing equations which must be satisfied for the plastic stresses and strains in a thick-walled cylinder are summarized here as follows:

Equilibrium:

$$\frac{d\sigma_r}{dr} + \frac{\sigma_r - \sigma_\theta}{r} = 0 \tag{3.17}$$

Compatibility:

$$\frac{d\varepsilon_\theta}{dr} + \frac{\varepsilon_\theta - \varepsilon_r}{r} = 0 \tag{3.18}$$

Stress-strain:

$$\begin{aligned} \varepsilon_r &= \frac{1}{E}[\sigma_r - \nu(\sigma_\theta + \sigma_z)] + \varepsilon_r^p + \alpha T \\ \varepsilon_\theta &= \frac{1}{E}[\sigma_\theta - \nu(\sigma_z + \sigma_r)] + \varepsilon_\theta^p + \alpha T \\ \varepsilon_z &= \frac{1}{E}[\sigma_z - \nu(\sigma_r + \sigma_\theta)] + \varepsilon_z^p + \alpha T \end{aligned} \tag{3.19}$$

Total plastic strains:

$$\begin{aligned} \varepsilon_r^p &= \sum_{i=1}^{n} \Delta\varepsilon_{r,i}^p \\ \varepsilon_\theta^p &= \sum_{i=1}^{n} \Delta\varepsilon_{\theta,i}^p \\ \varepsilon_z^p &= \sum_{i=1}^{n} \Delta\varepsilon_{z,i}^p \end{aligned} \tag{3.20}$$

Yield criterion:

$$(\sigma_r - \sigma_\theta)^2 + (\sigma_\theta - \sigma_z)^2 + (\sigma_z - \sigma_r)^2 = 2\sigma_0^2 \tag{3.21}$$

Incremental stress-strain relations:

$$\begin{aligned} \Delta\varepsilon_r^p &= \frac{\Delta\varepsilon_p}{\sigma_e}[\sigma_r - \frac{1}{2}(\sigma_\theta + \sigma_z)] \\ \Delta\varepsilon_\theta^p &= \frac{\Delta\varepsilon_p}{\sigma_e}[\sigma_\theta - \frac{1}{2}(\sigma_z + \sigma_r)] \end{aligned} \tag{3.22}$$

Incompressibility:

$$\Delta\varepsilon_z^p = -(\Delta\varepsilon_r^p + \Delta\varepsilon_\theta^p) \tag{3.23}$$

Effective stress and effective Plastic strain increment:

$$\sigma_e = \frac{1}{\sqrt{2}}[(\sigma_r - \sigma_\theta)^2 + (\sigma_\theta - \sigma_z)^2 + (\sigma_z - \sigma_r)^2]^{\frac{1}{2}} \tag{3.24}$$

$$\Delta\varepsilon_p = \frac{\sqrt{2}}{3}[(\Delta\varepsilon_r^p - \Delta\varepsilon_\theta^p)^2 + (\Delta\varepsilon_\theta^p - \Delta\varepsilon_z^p)^2 + (\Delta\varepsilon_z^p - \Delta\varepsilon_r^p)^2]^{\frac{1}{2}}. \tag{3.25}$$

Material hardening function:

$$\sigma_e = 232.68187 + 689.01541(\varepsilon_p)^{0.21842186} \tag{3.26}$$

Boundary condition:

$$\begin{aligned} \sigma_r &= -P_a \qquad at \quad r = a \\ \sigma_r &= -P_b \qquad at \quad r = b \end{aligned} \tag{3.27}$$

end condition:

$$\int_a^b \sigma_z dA = P_a \pi a^2 \tag{3.28}$$

There is no closed form solution for the set of equations of equilibrium, compatibility and stress-strain (Eqs. (3.17), (3.18) and (3.19)) with the above boundary (Eq. (3.27)) and end conditions (Eq. 3.28)) to obtain stresses and strains. Stresses are functions of total plastic strains in equation (3.19). The total plastic strains are the sum of plastic strain increments, equation (3.20). The plastic strain increments are again depended on the stresses and history of loading defined by equation (3.22) which is the incremental stress-strain relationship and the associated flow rule of von Mises yield criterion

(equation (3.21)). Loading history is obtained from the material's uniaxial stress-strain data and mathematically represented by equation (3.26). To obtain a solution for the stresses and plastic strains, a successive elastic approximation method has been developed. The method will be simplified as the functional relationships between stresses and total plastic strains are derived.

3.2.4 Successive Elastic Approximation Method

A successive elastic approximation method for this particular problem has been developed as follows. The load is applied in a large number of increments. For the first increment of load, a distribution is assumed for the plastic strain increments in radial and tangential directions, $\Delta\varepsilon_r^p$ and $\Delta\varepsilon_\theta^p$. At this initial loading step the total plastic strains ε_r^p, ε_θ^p and ε_z^p are zero. The set of equations of equilibrium (3.17), compatibility (3.18) and stress-strain (3.19) can now be solved like an ordinary elasticity problem, and a first approximation can be obtained for the stresses and total strains. At the same time, using the assumed values of plastic strain increments, an effective plastic strain increment $\Delta\varepsilon_p$ is computed from equation (3.25). From the material's hardening function (equation (3.26)) the corresponding value of effective stress σ_e can be determined. This is shown graphically in Figure 3.4. At initial loading step the total effective plastic strain, ε_p is equal to the effective plastic strain increment. Now a new approximation can be obtained for the individual plastic strain increments using equation (3.22). Using these new plastic strain increments, equations (3.17), (3.18) and

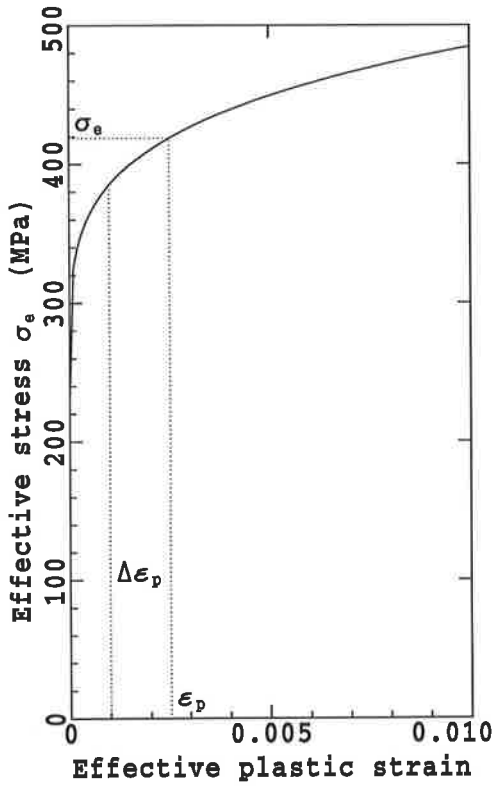

Figure 3.4: Determination of effective stress from the effective plastic strain.

(3.19) are solved again as a new updated elastic problem. A second, and presumably better, approximation is obtained for the stresses and total strains. At the same time, using these last values of the plastic strain increments, a new approximation can be computed for the effective plastic strain increment $\Delta\varepsilon_p$ from equation (3.25). Using this value of $\Delta\varepsilon_p$, a new value is obtained for σ_e from the materials hardening function shown in Figure 3.4. New approximations are now obtained for the plastic strain increments $\Delta\varepsilon_r^p$ and $\Delta\varepsilon_\theta^p$ using the Prandtl-Reuss equations (3.22). The process is continued until convergence is obtained. The flow diagram for the calculation of plastic strain increments is illustrated in Figure 3.5.

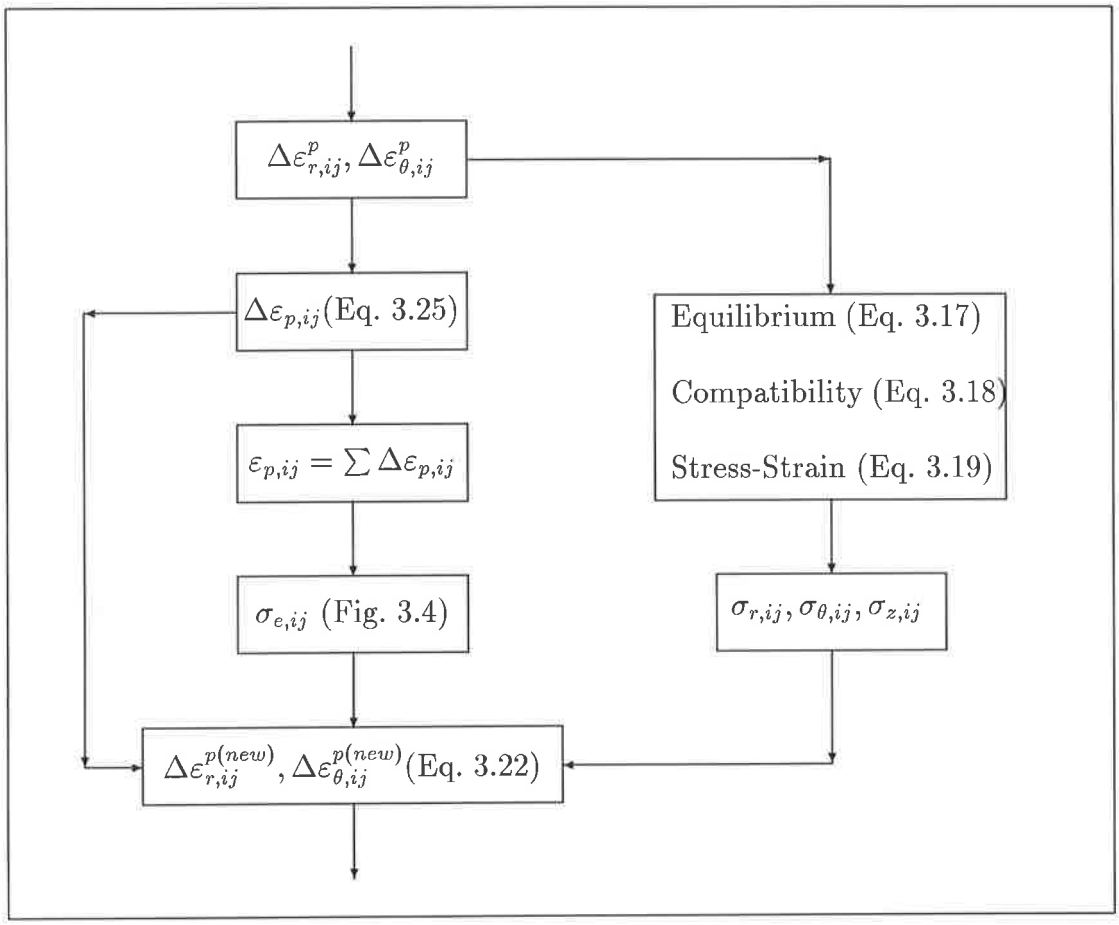

Figure 3.5: Flow diagram for the computation of plastic strain increments.

In the above flow diagram the subscript i denotes the ith loading step and j denotes the jth layer across the thickness of the cylinder. In this manner the solution is obtained for the first increment of loading. For the next increment of load an exactly similar calculation is performed except that ε^p_r, ε^p_θ and ε^p_z are no longer zero but are equal to the known values of $\Delta\varepsilon^p_r$, $\Delta\varepsilon^p_\theta$ and $\Delta\varepsilon^p_z$ obtained for the first increment of loading. The complete stress and strain history can thus be obtained when the complete load is applied.

This successive approximation method can be simplified by deriving the functional relationship between the stresses and the plastic strains as will be shown in the next section.

3.2.5 Derivation of Thermoelastoplastic Stresses

The set of equations of equilibrium (equation (3.17)), compatibility (equation(3.18)) and stress-strain (equation(3.19)) are solved simultaneously for the stresses to obtain the functional relationship between the stresses and the total plastic strains. From the third equation of the stress-strain relationship (equation (3.19)), the axial stress σ_z is substituted into the first two relations of equation (3.19). Then ε_r and ε_θ are substituted into the compatibility equation (3.18). The result is a differential relation between radial and tangential stress components which can be solved in conjunction with the equilibrium equation (3.17). The procedure is indicated below. The third equation of stress-strain relationship equation (3.19) is rewritten in the following form:

$$E\varepsilon_z = [\sigma_z - \nu(\sigma_r + \sigma_\theta)] + E\varepsilon_z^p + E\alpha T \tag{3.29}$$

Then the axial stress σ_z from the above equation may be derived in terms of the other two stress components, σ_r and σ_θ as follows:

$$\sigma_z = E\varepsilon_z + \nu(\sigma_r + \sigma_\theta) + E(\varepsilon_r^p + \varepsilon_\theta^p) - E\alpha T \tag{3.30}$$

Substituting σ_z which is in terms of σ_r and σ_θ into the first and second relations of equation (3.19) gives the following relations for the radial and tangential total strains,

ε_θ and ε_r as:

$$\begin{aligned}\varepsilon_r &= \frac{1+\nu}{E}[(1-\nu)\sigma_r - \nu\sigma_\theta] + (1+\nu)\alpha T - \nu\varepsilon_z + [(1-\nu)\varepsilon_r^p - \nu\varepsilon_\theta^p] \\ \varepsilon_\theta &= \frac{1+\nu}{E}[(1-\nu)\sigma_\theta - \nu\sigma_r] + (1+\nu)\alpha T - \nu\varepsilon_z + [(1-\nu)\varepsilon_\theta^p - \nu\varepsilon_r^p] \end{aligned} \quad (3.31)$$

Now, four variables of σ_r, σ_θ, ε_r and ε_θ can be obtained in terms of the total plastic strains using four equations of equilibrium (3.17), compatibility (3.18) and equations (3.31). In this way, the following two equations are obtained by differentiating the second relation of equations (3.31) with respect to r and subtractions of both equations (3.31),

$$\frac{d\varepsilon_\theta}{dr} = \frac{1+\nu}{E}[(1-\nu)\frac{d\sigma_\theta}{dr} - \nu\frac{d\sigma_r}{dr}] + (1+\nu)\alpha\frac{dT}{dr} + [(1-\nu)\frac{d\varepsilon_\theta^p}{dr} - \nu\frac{d\varepsilon_r^p}{dr}] \quad (3.32)$$

and

$$\frac{\varepsilon_\theta - \varepsilon_r}{r} = \frac{1+\nu}{E}(\frac{\sigma_\theta - \sigma_r}{r}) + \frac{\varepsilon_\theta^p - \varepsilon_r^p}{r} \quad (3.33)$$

The above two equations are obtained in terms of the radial and tangential stresses (σ_r and σ_θ) and the total plastic strains. Substituting equations (3.32) and (3.33) into the compatibility equation (3.18) results in a differential equation which is a relationship between the σ_r and σ_θ and the total plastic strains written as follows:

$$\frac{d}{dr}(\sigma_\theta + \sigma_r) = -\frac{E\alpha}{1-\nu}\frac{dT}{dr} - \frac{E}{1-\nu^2}[(1-\nu)\frac{d\varepsilon_\theta^p}{dr} - \nu\frac{d\varepsilon_r^p}{dr} + \frac{\varepsilon_\theta^p - \varepsilon_r^p}{r}] \quad (3.34)$$

The above equation and the equation of equilibrium may be solved simultaneously for the radial and tangential stresses, σ_r and σ_θ. In this way, by integrating equation (3.34), the sum of the radial and tangential stress components is obtained as follows:

$$\sigma_\theta + \sigma_r = -\frac{E\alpha T}{1-\nu} - \frac{E}{1-\nu^2}[(1-\nu)\varepsilon_\theta^p - \nu\varepsilon_r^p + \int_a^r \frac{\varepsilon_\theta^p - \varepsilon_r^p}{r}dr] + C_1 \quad (3.35)$$

where C_1 is an integration constant. The functional relationship between stresses and plastic strains may be obtained by using equation (3.34) and the equation of equilibrium (3.17). The equilibrium equation is rewritten in the following form.

$$\sigma_\theta = \sigma_r + r\frac{d\sigma_r}{dr} \tag{3.36}$$

Substituting σ_θ from equation (3.36) into equation (3.35) results in the following differential equation which must be solved for the radial stress (σ_r).

$$\frac{d\sigma_r}{dr} + \frac{2\sigma_r}{r} = K(r) \tag{3.37}$$

in which,

$$K(r) = -\frac{E\alpha T}{(1-\nu)r} - \frac{E}{1-\nu^2}[(1-\nu)\frac{\varepsilon_\theta^p}{r} - \nu\frac{\varepsilon_r^p}{r} + \frac{1}{r}\int_a^r \frac{\varepsilon_\theta^p - \varepsilon_r^p}{r}dr] + \frac{C_1}{r} \tag{3.38}$$

The above differential equation (3.37) can be solved for the radial stress (σ_r) using the following procedure. Writing σ_r as the product of two homogeneous (λ) and non-homogeneous (ζ) components, then $\sigma_r = \lambda.\zeta$, and differentiating both sides with respect to r gives

$$\frac{d\sigma_r}{dr} = \zeta\frac{d\lambda}{dr} + \lambda\frac{d\zeta}{dr} \tag{3.39}$$

Equation (3.37) can now be written in the following form

$$\lambda\frac{d\zeta}{dr} + \zeta(\frac{d\lambda}{dr} + \frac{2}{r}\lambda) = K(r) \tag{3.40}$$

Setting the coefficient of ζ equal to zero, the above differential equation may be written in terms of λ and ζ in the following form as:

$$\frac{d\lambda}{dr} + \frac{2}{r}\lambda = 0 \tag{3.41}$$

$$\lambda \frac{d\zeta}{dr} = K(r) \tag{3.42}$$

Since $\lambda = A_1/r^2$ satisfies the equation (3.41) a solution for ζ may be obtained by integration of equation (3.42) as

$$\begin{aligned}\zeta &= \frac{1}{A_1}\{\frac{-E\alpha}{1-\nu}\int_a^r Trdr - \frac{E}{1-\nu^2}[(1-\nu)\int_a^r r\varepsilon_\theta^p dr - \nu\int_a^r r\varepsilon_r^p dr \\ &+ \int_a^r r\int_a^r \frac{\varepsilon_\theta^p - \varepsilon_r^p}{r}drdr] + \frac{C_1}{2}(r^2-a^2)\} + A_2\end{aligned} \tag{3.43}$$

Substituting for λ and ζ into $\sigma_r = \lambda.\zeta$ and introducing $C_2 = A_1A_2$ the radial stress can be expressed as follows:

$$\begin{aligned}\sigma_r &= \frac{-E\alpha}{(1-\nu)r^2}\int_a^r Trdr - \frac{E}{(1-\nu^2)r^2}[(1-\nu)\int_a^r r\varepsilon_\theta^p dr - \nu\int_a^r r\varepsilon_r^p dr \\ &+ \int_a^r r\int_a^r \frac{\varepsilon_\theta^p - \varepsilon_r^p}{r}drdr] + \frac{C_1}{2}(1-\frac{a^2}{r^2})\} + \frac{C_2}{r^2}\end{aligned} \tag{3.44}$$

The double integral in the above equation is simplified by using integration by parts:

$$\int_a^r r\int_a^r \frac{\varepsilon_\theta^p - \varepsilon_r^p}{r}drdr = \frac{r^2}{2}\int_a^r \frac{\varepsilon_\theta^p - \varepsilon_r^p}{r}dr - \frac{1}{2}\int_a^r(\varepsilon_\theta^p - \varepsilon_r^p)rdr \tag{3.45}$$

Inserting the simplified integral from equation (3.45) into equation (3.44) the result for σ_r and then σ_θ are as follows:

$$\begin{aligned}\sigma_r &= \frac{-E\alpha}{(1-\nu)r^2}\int_a^r Trdr - \frac{E}{2(1-\nu^2)r^2}[(1-2\nu)(\int_a^r r\varepsilon_\theta^p dr + \int_a^r r\varepsilon_r^p dr) \\ &+ r^2(\int_a^r \frac{\varepsilon_\theta^p - \varepsilon_r^p}{r}dr] + \frac{C_1}{2}(1-\frac{a^2}{r^2})\} + \frac{C_2}{r^2} \\ \sigma_\theta &= \frac{E\alpha}{(1-\nu)r^2}\int_a^r Trdr - \frac{E\alpha T}{1-\nu} + \frac{E}{2(1-\nu^2)r^2}[(1-2\nu)\int_a^r r(\varepsilon_\theta^p + \varepsilon_r^p)dr \\ &- r^2\int_a^r \frac{\varepsilon_\theta^p - \varepsilon_r^p}{r}dr] - \frac{E}{1-\nu^2}[(1-\nu)\varepsilon_\theta^p - \nu\varepsilon_r^p] + \frac{C_1}{2}(1+\frac{a^2}{r^2})\} - \frac{C_2}{r^2}\end{aligned} \tag{3.46}$$

Constants C_1 and C_2 in the above relations are obtained using the boundary condition equations (3.27), the results are as follows:

$$\begin{aligned} C_1 &= \frac{2E\alpha}{(1-\nu)(b^2-a^2)}\int_a^b Trdr + \frac{E}{(1-\nu^2)(b^2-a^2)}[(1-2\nu)\int_a^b(\varepsilon_\theta^p+\varepsilon_r^p)rdr \\ &\quad +b^2\int_a^b\frac{\varepsilon_\theta^p-\varepsilon_r^p}{r}dr] + \frac{2P_a a^2}{b^2-a^2} - \frac{2P_b b^2}{b^2-a^2} \\ C_2 &= -P_a a^2 \end{aligned} \tag{3.47}$$

Substituting C_1 and C_2 from equations (3.47) into equations (3.46) the radial and tangential components of stress are expressed as follows:

$$\begin{aligned} \sigma_r &= \frac{-E\alpha}{(1-\nu)r^2}\int_a^r Trdr - \frac{E}{2(1-\nu^2)r^2}[(1-2\nu)(\int_a^r r\varepsilon_\theta^p dr + \int_a^r r\varepsilon_r^p dr) \\ &\quad +r^2\int_a^r\frac{\varepsilon_\theta^p-\varepsilon_r^p}{r}dr] + \frac{E}{2(1-\nu^2)(b^2-a^2)}[(1-2\nu)\int_a^b(\varepsilon_\theta^p+\varepsilon_r^p)rdr \\ &\quad +b^2\int_a^b\frac{\varepsilon_\theta^p-\varepsilon_r^p}{r}dr](1-\frac{a^2}{r^2}) + [\frac{E\alpha}{(1-\nu)(b^2-a^2)}\int_a^b Trdr](1-\frac{a^2}{r^2}) \\ &\quad +\frac{P_a a^2}{b^2-a^2}(1-\frac{b^2}{r^2}) - \frac{P_b b^2}{b^2-a^2}(1-\frac{a^2}{r^2}) \end{aligned} \tag{3.48}$$

$$\begin{aligned} \sigma_\theta &= \frac{E\alpha}{(1-\nu)r^2}\int_a^r Trdr - \frac{E\alpha T}{1-\nu} \\ &\quad +\frac{E}{2(1-\nu^2)r^2}[(1-2\nu)\int_a^r r(\varepsilon_\theta^p+\varepsilon_r^p)dr - r^2\int_a^r\frac{\varepsilon_\theta^p-\varepsilon_r^p}{r}dr] \\ &\quad -\frac{E}{1-\nu^2}[(1-\nu)\varepsilon_\theta^p-\nu\varepsilon_r^p] + \frac{E}{2(1-\nu^2)(b^2-a^2)}[(1-2\nu)\int_a^b(\varepsilon_\theta^p+\varepsilon_r^p)rdr \\ &\quad +b^2\int_a^b\frac{\varepsilon_\theta^p-\varepsilon_r^p}{r}dr](1+\frac{a^2}{r^2}) + [\frac{E\alpha}{(1-\nu)(b^2-a^2)}\int_a^b Trdr](1+\frac{a^2}{r^2}) \\ &\quad +\frac{P_a a^2}{b^2-a^2}(1+\frac{b^2}{r^2}) - \frac{P_b b^2}{b^2-a^2}(1+\frac{a^2}{r^2}) \end{aligned} \tag{3.49}$$

The axial stress (σ_z) must satisfy the equation (3.30) derived from the stress-strain relationship as well as the end condition equation (3.28). These equations are rewritten

here as follows:

$$\sigma_z = E\varepsilon_z + \nu(\sigma_r + \sigma_\theta) + E(\varepsilon_r^p + \varepsilon_\theta^p) - E\alpha T \tag{3.50}$$

$$\int_a^b \sigma_z dA = P_a \pi a^2 \tag{3.51}$$

It is necessary to point out that the axial strain in equation (3.50) is not zero but it has been assumed zero by all the previous investigators. Since all the surfaces normal to the cylinder longitudinal axis remain plane, the most accurate and reasonable assumption is to consider a constant axial strain rather than zero (plane strain). It is also validated by the experiment performed in this investigation; and that the assumption of zero axial strain (plane-strain) is not accurate. Therefore a constant axial strain (generalized plane-strain) is assumed in this investigation. Substituting σ_z from equation (3.50) into the end condition equation (3.51) and integrating across the wall from the inner to the outer surface of the cylinder and considering the generalized plane strain case, (ε_z =constant), the following relation is obtained for the constant value of ε_z as,

$$\begin{aligned} E\varepsilon_z &= \frac{2E\alpha}{b^2-a^2}\int_a^b Trdr - \frac{2\nu}{b^2-a^2}\int_a^b(\sigma_\theta+\sigma_r)rdr \\ &\quad -\frac{2E}{b^2-a^2}\int_a^b(\varepsilon_\theta^p+\varepsilon_r^p)rdr + \frac{P_a a^2}{b^2-a^2} \end{aligned} \tag{3.52}$$

Substituting this constant value, which also depends on the internal pressure, from equation (3.52) into equation (3.30) the expression for the axial stress is obtained as:

$$\begin{aligned} \sigma_z &= \frac{-E\alpha T}{1-\nu} + \frac{2E\alpha}{(1-\nu)(b^2-a^2)}\int_a^b Trdr \\ &\quad -\frac{\nu E}{1-\nu^2}[(1-\nu)\varepsilon_\theta^p - \nu\varepsilon_r^p + \int_a^r \frac{\varepsilon_\theta^p - \varepsilon_r^p}{r}dr] \\ &\quad +\frac{\nu E}{(1-\nu^2)(b^2-a^2)}[(1-2\nu)\int_a^r(\varepsilon_\theta^p+\varepsilon_r^p)rdr + b^2\int_a^b \frac{\varepsilon_\theta^p-\varepsilon_r^p}{r}dr] \\ &\quad -\frac{2E}{b^2-a^2}\int_a^b(\varepsilon_\theta^p+\varepsilon_r^p)rdr + E(\varepsilon_\theta^p+\varepsilon_r^p) + \frac{P_a a^2}{b^2-a^2} \end{aligned} \tag{3.53}$$

Equations (3.48), (3.49) and (3.53) describe the general stress distribution for any internal and external pressures and any arbitrary axi-symmetric temperature distribution. Assuming a steady state outward flow of heat through the cylindrical wall, the differential equation for temperature distribution is given by

$$\frac{d^2T}{dr^2} + \frac{1}{r}\frac{dT}{dr} = 0 \tag{3.54}$$

If temperature at the inner and outer surfaces of the cylinder are designated by T_a and T_b respectively, then the thermal boundary conditions can be written as follows:

$$\begin{aligned} T &= T_a \qquad at \quad r = a \\ T &= T_b \qquad at \quad r = b \end{aligned} \tag{3.55}$$

Solving the differential equation (3.54) with the above thermal boundary conditions the temperature distribution is obtained as follows:

$$T = ln\frac{a}{b}(T_a ln\frac{b}{r} - T_b ln\frac{a}{r}) \tag{3.56}$$

Substituting the above temperature distribution into the expressions obtained for the stresses, equations (3.48), (3.49) and (3.53), the following solution for the radial, tangential and axial stresses is obtained.

$$\begin{aligned} \sigma_r = \; & \frac{E\alpha(T_a - T_b)}{2(1-\nu)(b^2-a^2)ln\frac{b}{a}}[\frac{a^2b^2}{r^2}ln\frac{b}{a} + b^2 ln\frac{r}{b} - a^2 ln\frac{r}{a}] \\ & - \frac{E}{2(1-\nu^2)r^2}[(1-2\nu)(\int_a^r r\varepsilon_\theta^p dr + \int_a^r r\varepsilon_r^p dr) + r^2(\int_a^r \frac{\varepsilon_\theta^p - \varepsilon_r^p}{r}dr] \\ & + \frac{E}{2(1-\nu^2)(b^2-a^2)}[(1-2\nu)\int_a^b (\varepsilon_\theta^p + \varepsilon_r^p)rdr + b^2\int_a^b \frac{\varepsilon_\theta^p - \varepsilon_r^p}{r}dr](1 - \frac{a^2}{r^2}) \\ & + \frac{P_a a^2}{b^2-a^2}(1 - \frac{b^2}{r^2}) - \frac{P_b b^2}{b^2-a^2}(1 - \frac{a^2}{r^2}) \end{aligned} \tag{3.57}$$

$$\sigma_\theta = \frac{E\alpha(T_a - T_b)}{2(1-\nu)(b^2-a^2)ln\frac{b}{a}}[-\frac{a^2b^2}{r^2}ln\frac{b}{a} + b^2ln\frac{r}{b} - a^2ln\frac{r}{a} + (b^2-a^2)]$$
$$+\frac{E}{2(1-\nu^2)r^2}[(1-2\nu)\int_a^r r(\varepsilon_\theta^p + \varepsilon_r^p)dr - r^2\int_a^r \frac{\varepsilon_\theta^p - \varepsilon_r^p}{r}dr -$$
$$2r^2((1-\nu)\varepsilon_\theta^p - \nu\varepsilon_r^p)] + \frac{E}{2(1-\nu^2)(b^2-a^2)}[(1-2\nu)\int_a^b(\varepsilon_\theta^p + \varepsilon_r^p)rdr$$
$$+b^2\int_a^b \frac{\varepsilon_\theta^p - \varepsilon_r^p}{r}dr](1+\frac{a^2}{r^2}) + \frac{P_a a^2}{b^2-a^2}(1+\frac{b^2}{r^2}) - \frac{P_b b^2}{b^2-a^2}(1+\frac{a^2}{r^2}) \quad (3.58)$$

$$\sigma_z = \frac{E\alpha(T_a - T_b)}{2(1-\nu)(b^2-a^2)ln\frac{b}{a}}[2b^2ln\frac{r}{b} - 2a^2ln\frac{r}{a} + (b^2-a^2)]$$
$$-\frac{\nu E}{1-\nu^2}[(1-\nu)\varepsilon_\theta^p - \nu\varepsilon_r^p + \int_a^r \frac{\varepsilon_\theta^p - \varepsilon_r^p}{r}dr] + \frac{\nu E}{(1-\nu^2)(b^2-a^2)}[$$
$$(1-2\nu)\int_a^b(\varepsilon_\theta^p + \varepsilon_r^p)rdr + b^2\int_a^b \frac{\varepsilon_\theta^p - \varepsilon_r^p}{r}dr] - \frac{2E}{b^2-a^2}\int_a^b(\varepsilon_\theta^p + \varepsilon_r^p)rdr$$
$$-\frac{E}{b^2-a^2}[2\int_a^b(\varepsilon_\theta^p + \varepsilon_r^p)rdr - (b^2-a^2)(\varepsilon_\theta^p + \varepsilon_r^p)] + \frac{P_a a^2}{b^2-a^2} \quad (3.59)$$

The functional relationship between stresses and total plastic strains are established in equations. (3.57), (3.58) and (3.59). Then the suggested numerical procedure for calculating plastic strain increments can be simplified as shown in the following flow diagram.

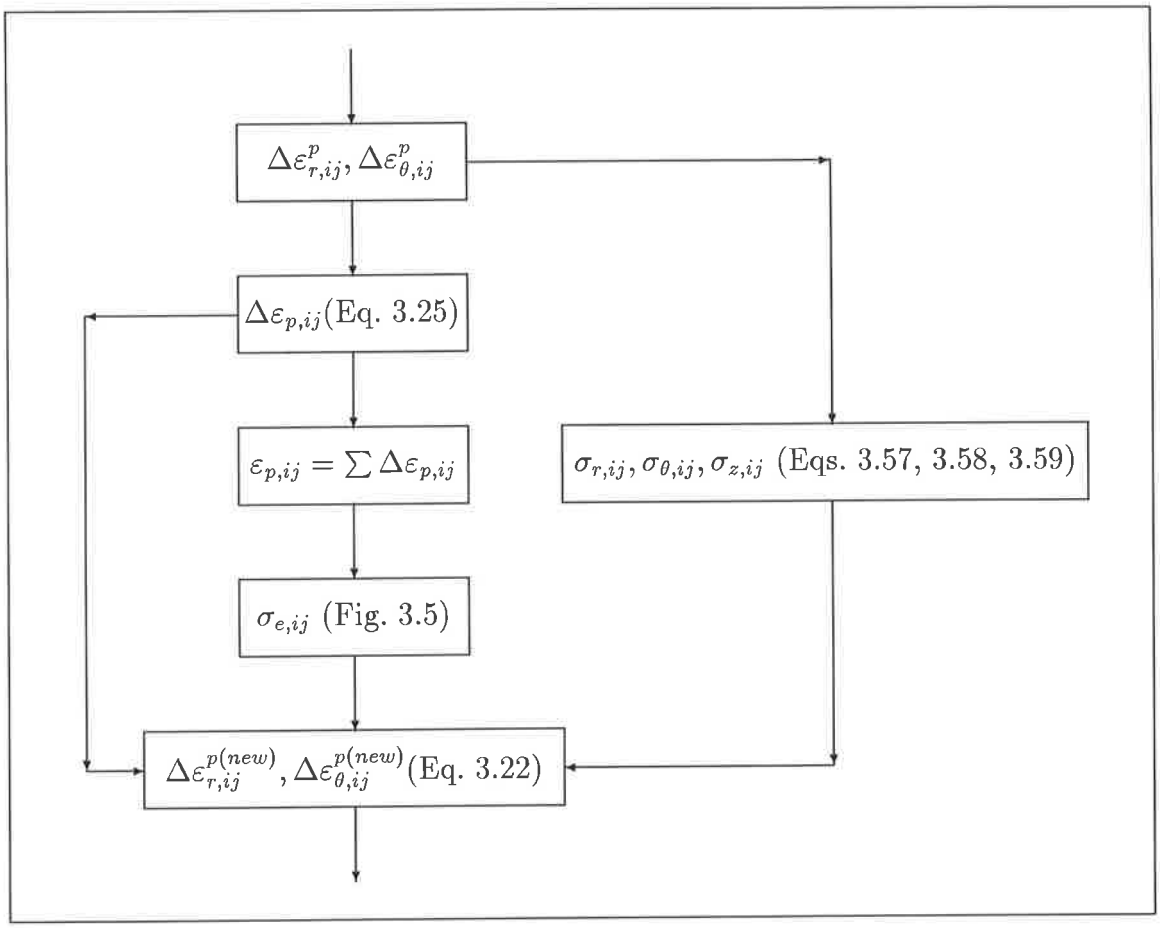

Figure 3.6: Simplified flow diagram for the computation of plastic strain increments.

The above solution for the stresses depends on the dimensions of the cylinder. It is useful to introduce a dimensionless solution for the stress functions which can be used for any cylinder. The dimensionless solution is derived in the next section.

3.2.6 Dimensionless solution

For a general solution it is convenient to introduce the following sets of dimensionless quantities S_r, S_θ, S_z, Θ, P_i, P_o, ρ, ϵ_r, ϵ_θ, ϵ_z and ε_0, such that

$$S_r = \sigma_r/\sigma_0 \qquad S_\theta = \sigma_\theta/\sigma_0 \qquad S_z = \sigma_z/\sigma_0 \qquad \Theta = (E\alpha\Delta T)/(1-\nu)\sigma_0$$

$$P_i = P_a/\sigma_0 \qquad P_o = P_b/\sigma_0 \qquad \rho = r/a \qquad \beta = b/a$$

$$\epsilon_r = \varepsilon_r/\varepsilon_0 \qquad \epsilon_\theta = \varepsilon_\theta/\varepsilon_0 \qquad \epsilon_z = \varepsilon_z/\varepsilon_0 \qquad \varepsilon_0 = \sigma_0/E$$

where S_r, S_θ and S_z are dimensionless stresses, Θ is the dimensionless temperature gradient, P_i and P_o are dimensionless internal and external pressures, ρ is the dimensionless radius, ϵ_r, ϵ_θ and ϵ_z are dimensionless strains, σ_0 is the material's yield stress and ε_0 is the yield strain.

If both sides of equations (3.57), (3.58) and (3.59) are divided by σ_0 and the above defined dimensionless quantities are incorporated into the resulted equations, then the following dimensionless results for the radial, tangential and axial stresses are obtained.

$$\begin{aligned} S_r = {} & \frac{\Theta}{2(\beta^2-1)ln\beta}[\frac{\beta^2}{\rho^2}ln\beta + \beta^2 ln\frac{\rho}{\beta} - ln\rho] + \frac{P_i}{\beta^2-1}(1-\frac{\beta^2}{\rho^2}) \\ & -\frac{P_o\beta^2}{\beta^2-1}(1-\frac{1}{\rho^2}) - \frac{1}{2(1-\nu^2)\rho^2}[(1-2\nu)\int_1^\rho(\epsilon_\theta^p+\epsilon_r^p)\rho d\rho \\ & +\rho^2\int_1^\rho\frac{\epsilon_\theta^p-\epsilon_r^p}{\rho}d\rho] + \frac{1}{2(1-\nu^2)(\beta^2-1)}[(1-2\nu)\int_1^\beta(\epsilon_\theta^p+\epsilon_r^p)\rho d\rho \\ & +\beta^2\int_1^\beta\frac{\epsilon_\theta^p-\epsilon_r^p}{\rho}d\rho](1-\frac{1}{\rho^2}) \end{aligned} \tag{3.60}$$

$$\begin{aligned} S_\theta = {} & \frac{\Theta}{2(\beta^2-1)ln\beta}[-\frac{\beta^2}{\rho^2}ln\beta + \beta^2 ln\frac{\rho}{\beta} - ln\rho + \beta^2 - 1] + \frac{P_i}{\beta^2-1}(1+\frac{\beta^2}{\rho^2}) \\ & -\frac{P_o\beta^2}{\beta^2-1}(1+\frac{1}{\rho^2}) + \frac{1}{2(1-\nu^2)(\beta^2-1}[(1-2\nu)\int_1^\beta(\epsilon_\theta^p+\epsilon_r^p)\rho d\rho \\ & +\beta^2\int_1^\beta\frac{\epsilon_\theta^p-\epsilon_r^p}{\rho}d\rho](1+\frac{1}{\rho^2}) - \frac{1}{2(1-\nu^2)\rho^2}[(1-2\nu)\int_1^\rho(\epsilon_\theta^p+\epsilon_r^p)\rho d\rho \\ & +\rho^2\int_1^\rho\frac{\epsilon_\theta^p-\epsilon_r^p}{\rho}d\rho - 2\rho^2((1-\nu)\epsilon_\theta^p - \nu\epsilon_r^p)] \end{aligned} \tag{3.61}$$

$$
\begin{aligned}
S_z &= \frac{\Theta}{2(\beta^2-1)ln\beta}[+2\beta^2 ln\frac{\rho}{\beta} - 2ln\rho + \beta^2 - 1] + \frac{P_i}{\beta^2-1} \\
&+\frac{\nu}{(1-\nu^2)(\beta^2-1}[(1-2\nu)\int_1^\beta(\epsilon_\theta^p+\epsilon_r^p)\rho d\rho + \beta^2\int_1^\beta\frac{\epsilon_\theta^p-\epsilon_r^p}{\rho}d\rho] \\
&+\frac{\nu}{1-\nu^2}[\int_1^\beta\frac{\epsilon_\theta^p-\epsilon_r^p}{\rho}d\rho + (1-\nu)\epsilon_\theta^p - \nu\epsilon_r^p] + \\
&\frac{1}{\beta^2-1}[2\int_1^\beta(\epsilon_\theta^p+\epsilon_r^p)\rho d\rho - (\beta^2-1)(\epsilon_\theta^p+\epsilon_r^p)] \qquad (3.62)
\end{aligned}
$$

It is obvious from the above equations that the stresses are functions of total plastic strains which are non-linear and history dependent. It is convenient to define the history dependent part of the stresses in separate functions of $U(\rho,\beta,\varepsilon_r^p,\varepsilon_\theta^p)$, $V(\rho,\beta,\varepsilon_r^p,\varepsilon_\theta^p)$ and $W(\rho,\beta,\varepsilon_r^p,\varepsilon_\theta^p)$ which are the history dependent part of radial (S_r), tangential (S_θ) and axial (S_z) stresses respectively. Then, equations (3.60) to (3.62) can be represented in terms of the following history dependent and non-history dependent functions.

History dependent functions:

$$
\begin{aligned}
U(\rho,\beta,\varepsilon_r^p,\varepsilon_\theta^p) &= -\frac{1}{2(1-\nu^2)\rho^2}[(1-2\nu)\int_1^\rho(\epsilon_\theta^p+\epsilon_r^p)\rho d\rho + \rho^2\int_1^\rho\frac{\epsilon_\theta^p-\epsilon_r^p}{\rho}d\rho] \\
&+\frac{1}{2(1-\nu^2)(\beta^2-1)}[(1-2\nu)\int_1^\beta(\epsilon_\theta^p+\epsilon_r^p)\rho d\rho \\
&+\beta^2\int_1^\beta\frac{\epsilon_\theta^p-\epsilon_r^p}{\rho}d\rho](1-\frac{1}{\rho^2}) \\
V(\rho,\beta,\varepsilon_r^p,\varepsilon_\theta^p) &= \frac{1}{2(1-\nu^2)(\beta^2-1)}[(1-2\nu)\int_1^\beta(\epsilon_\theta^p+\epsilon_r^p)\rho d\rho + \\
&\beta^2\int_1^\beta\frac{\epsilon_\theta^p-\epsilon_r^p}{\rho}d\rho](1+\frac{1}{\rho^2}) - \frac{1}{2(1-\nu^2)\rho^2}[(1-2\nu)\int_1^\rho(\epsilon_\theta^p+\epsilon_r^p)\rho d\rho \\
&+\rho^2\int_1^\rho\frac{\epsilon_\theta^p-\epsilon_r^p}{\rho}d\rho - 2\rho^2((1-\nu)\epsilon_\theta^p - \nu\epsilon_r^p)] \\
W(\rho,\beta,\varepsilon_r^p,\varepsilon_\theta^p) &= \frac{\nu}{(1-\nu^2)(\beta^2-1}[(1-2\nu)\int_1^\beta(\epsilon_\theta^p+\epsilon_r^p)\rho d\rho \\
&+\beta^2\int_1^\beta\frac{\epsilon_\theta^p-\epsilon_r^p}{\rho}d\rho] + \frac{\nu}{1-\nu^2}[\int_1^\beta\frac{\epsilon_\theta^p-\epsilon_r^p}{\rho}d\rho \\
&+(1-\nu)\epsilon_\theta^p - \nu\epsilon_r^p] + \frac{1}{\beta^2-1}[2\int_1^\beta(\epsilon_\theta^p+\epsilon_r^p)\rho d\rho - (\beta^2-1)(\epsilon_\theta^p+\epsilon_r^p)]
\end{aligned}
$$

Non-history dependent functions:

$$
\begin{aligned}
F(\rho,\beta,\Theta,P_o) &= \frac{\Theta}{2(\beta^2-1)ln\beta}[\frac{\beta^2}{\rho^2}ln\beta+\beta^2ln\frac{\rho}{\beta}-ln\rho]+\frac{P_o\beta^2}{\beta^2-1}(1-\frac{1}{\rho^2}) \\
G(\rho,\beta) &= \frac{1}{\beta^2-1}(1-\frac{\beta^2}{\rho^2}) \\
H(\rho,\beta,\Theta,P_o) &= \frac{\Theta}{2(\beta^2-1)ln\beta}[-\frac{\beta^2}{\rho^2}ln\beta+\beta^2ln\frac{\rho}{\beta}-ln\rho+\beta^2-1]+\frac{P_o\beta^2}{\beta^2-1}(1+\frac{1}{\rho^2}) \\
R(\rho,\beta) &= \frac{1}{\beta^2-1}(1+\frac{\beta^2}{\rho^2}) \\
M(\rho,\beta,\Theta) &= \frac{\Theta}{2(\beta^2-1)ln\beta}[+2\beta^2ln\frac{\rho}{\beta}-2ln\rho+\beta^2-1] \\
N(\beta) &= \frac{1}{\beta^2-1}
\end{aligned}
$$

The non-history dependent functions are a combination of mechanical stresses due to internal pressure and thermal stresses due to thermal gradient. Therefore, the general solution for the non-linear radial, tangential and axial stresses may be rewritten in terms of the above defined functions as follows:

$$
\begin{aligned}
S_r^p &= U(\rho,\beta,\varepsilon_r^p,\varepsilon_\theta^p)+F(\rho,\beta,\Theta,P_o)+G(\rho,\beta)P_i \\
S_\theta^p &= V(\rho,\beta,\varepsilon_r^p,\varepsilon_\theta^p)+H(\rho,\beta,\Theta,P_o)+R(\rho,\beta)P_i \\
S_z^p &= W(\rho,\beta,\varepsilon_r^p,\varepsilon_\theta^p)+M(\rho,\beta,\Theta)+N(\beta)P_i
\end{aligned} \tag{3.63}
$$

where superscript p denotes the plastic solution. The above non-dimensional results for the stresses are used in the previous developed numerical model for the stresses which will be discussed in the next Chapter, devoted to the numerical analysis.

If a cylinder, which has developed plastic strains, is unloaded from the loads which

have caused plastic flow over part of the cylinder, residual stresses will result.

3.2.7 Residual Stress

To increase the maximum pressure that a cylinder can contain, it is a common practice to produce a compressive residual tangential stress near the bore by autofrettage treatment of the cylinder prior to use. As a thick-walled cylinder is pressurized, the bore material, which is the most highly stressed portion of the cylinder, begins to yield. The yield surface begins to propagate through the thickness of the vessel until it reaches the outer surface. If at any stage of elastic-plastic deformation of the cylinder the internal pressure is released, then there will be a residual stress distributions throughout the thickness of the vessel. This is known as the autofrettage process.

The reason for such a residual stress distribution is that the plastic region of the cylinder has developed irreversible plastic strains and can not return back to its original configuration, while the elastic portion of the cylinder is trying to return back to its original condition. The action of the elastic region is counteracted by the plastic region. On the other hand, the plastic region will be compressed by the elastic region until a self-equilibrium condition is reached throughout the thickness of the cylinder. Developing a compressive region at the inside wall of a cylinder is useful to protect the vessel against the fatigue crack growth at the highly stressed inside region of the cylinder. The other important point is that the material located at the plastic portion

of the cylinder has a much higher elastic limit than the material located at the elastic region because of the material's hardening effect. Therefore, it is not only the compressive region at the inside wall of the cylinder which is beneficial, but also the higher elastic limit of the inside material which has taken advantage of the material's strain-hardening effect is another important privilege of the overstraining process. Therefore, this kind of residual stresses can significantly improve the performance characteristics of thick-walled cylinders.

The advantage of the compressive residual stresses will be decreased if reverse yielding occurs in the cylinder (Chen (1986)). For metals, the stress-strain curve in a simple compression test is usually identical with that in a simple tension test. But, if the material is first loaded in tension and develop plastic strain and then unloaded and reverse loaded in compression, the stress-strain curve of the material in compression has a significantly lower yield point than the curve that would be obtained directly from a simple compression test without prior tension loading. This is known as the Bauschinger effect phenomenon. An actual unloading behaviour of the material including the Bauschinger effect factor must be considered for an accurate prediction of reverse yielding and the residual stresses in the cylinder. In this investigation the material's Bauschinger effect factor incorporated in the analysis is obtained experimentally and this has already been discussed in previous Chapter.

The determination of residual stresses is important in the analysis of fracture, and in

fatigue life estimation of thick-walled cylinders. Consider a cylinder which has developed plastic strains as a result of an internal pressure of P_a and a thermal gradient of ΔT and the residual stresses are to be determined upon the release of load. It is obvious that, if the unloaded cylinder is loaded again with the same internal pressure and thermal gradient, it will return back to its configuration right before unloading because this loading-unloading is within the yield surface and is reversible and path independent. On the other hand, if the residual stresses are added to an elastic stress system due to P_a and ΔT, it will result in the plastic stress distribution before unloading. This can be mathematically represented in the following non-dimensional form:

$$\begin{aligned} S_r^p &= S_r^r + S_r^e \\ S_\theta^p &= S_\theta^r + S_\theta^e \\ S_z^p &= S_z^r + S_z^e \end{aligned} \tag{3.64}$$

where S_r^p, S_θ^p and S_z^p are initial plastic stresses, S_r^r, S_θ^r and S_z^r are residual stresses and S_r^e, S_θ^e and S_z^e are elastic stresses. Residual stresses can be written in terms of the elastic and plastic stresses as follows:

$$\begin{aligned} S_r^r &= S_r^p - S_r^e \\ S_\theta^r &= S_\theta^p - S_\theta^e \\ S_z^r &= S_z^p - S_z^e \end{aligned} \tag{3.65}$$

This formulation is correct as long as yielding in the reverse direction does not occur. Since reverse yielding has a negative effect on the cylinder performances, it is important to obtain the condition in which reverse yielding may occur. Therefore in this

investigation the condition for reverse yielding is investigated. The reverse yielding is predicted using the von Mises yielding criterion including the Bauschinger effect factor. In dimensionless form the condition is written as follows:

$$(S_r^r - S_\theta^r)^2 + (S_\theta^r - S_z^r)^2 + (S_z^r - S_r^r)^2 = 2(BEF)^2 \tag{3.66}$$

where BEF is the Bauschinger effect factor. There are significant differences between the results of residual stress distribution with considering the Bauschinger effect and ignoring it. Therefore, neglecting the actual loading and unloading behaviour of the material results in an inaccurate distribution for the residual stresses. The significance of the results are discussed in Chapter 6.

The actual material's loading and unloading properties and the Bauschinger effect factor of the material are obtained experimentally in this investigation. The experimental results are represented by the following function using a curve fitting software and selecting the best possible curve as it has already been discussed in Chapter 1.

$$BEF = 1.0170029 + 0.36592732(\%\varepsilon_p) - 0.0025343135(\%\varepsilon_p)^3 - 0.97738304(\%\varepsilon_p)^{0.5} \tag{3.67}$$

where $\%\varepsilon_p$ is percent overstrain.

Equations (3.65), (3.66) and (3.67) are incorporated in the analytical-numerical model introduced by the flow diagram of Figure 3.6 in order to obtain an accurate prediction of residual stresses and the onset of reverse yielding in thick-walled cylinders. Step-by-step procedure for computation of plastic and residual stresses and the onset of reverse

yielding and their experimental verification are discussed in Chapter 4 and 5. However, before introducing the details of the procedure it is necessary to establish the loading condition which will cause plastic flow to occur in the cylinder wall. This critical loading condition may be established by using expressions for the elastic stresses and the yielding criterion. If the history dependent functions of $U(\rho, \beta, \varepsilon_r^p, \varepsilon_\theta^p)$, $V(\rho, \beta, \varepsilon_r^p, \varepsilon_\theta^p)$ and $W(\rho, \beta, \varepsilon_r^p, \varepsilon_\theta^p)$ are ignored in the general equation (3.63) , then elastic stresses can be written as follows:

$$\begin{aligned} S_r^e &= F(\rho, \beta, \Theta, P_o) + G(\rho, \beta) P_i \\ S_\theta^e &= H(\rho, \beta, \Theta, P_o) + R(\rho, \beta) P_i \\ S_z^e &= M(\rho, \beta, \Theta) + N(\beta) P_i \end{aligned} \tag{3.68}$$

where superscript e stands for the elastic solution. It is obvious that the elastic stresses are functions of dimensionless variables ρ, β, Θ, P_o and P_i. Effects of these variables on the critical condition are investigated.

3.2.8 Critical Condition

When pressure and thermal loads are both present in the cylinder, any combination of these loads may cause yielding to take place in the cylinder wall. The loading condition in which yielding starts in the cylinder thickness is called the critical condition. When yielding starts at a point the von Mises condition must be satisfied at that point. The

dimensionless form of the von Mises criterion is written as follows:

$$(S_r^e - S_\theta^e)^2 + (S_\theta^e - S_z^e)^2 + (S_z^e - S_r^e)^2 = 2 \tag{3.69}$$

Substituting expressions for the elastic stresses from equation (3.68) into equation (3.69) the following equation for the critical condition is obtained.

$$A(\rho,\beta)P_i^2 + B(\rho,\beta,\Theta,P_o)P_i + C(\rho,\beta,\Theta,P_o) = 0 \tag{3.70}$$

The functions A,B and C in equation (3.70) can be represented in terms of previously defined functions F, G, etc. as follows:

$$\begin{aligned} A(\rho,\beta) &= 2(G^2 + R^2 + N^2 - G*R - R*N - N*G) \\ B(\rho,\beta,\Theta,P_o) &= 4(F*G + H*R + M*N) - 2(F*R + F*N + \\ &\quad H*G + H*N + M*R + M*G) \\ C(\rho,\beta,\Theta,P_o) &= 2(F^2 + H^2 + M^2 - F*H - H*M - M*F - \sigma_0^2) \end{aligned}$$

Variables ρ, β, Θ, P_i and P_o are related in equation (3.70). Any combination of these variables which satisfy equation (3.70) can produce the critical condition for plastic yielding. Numerical results of the critical pressures using this equation as well as the experimental results obtained for the critical pressures are discussed later in Chapter 6. If internal pressure is increased beyond the critical value calculated from equation (3.70), then plastic flow will progress in the cylinder wall. If the load is released, then the cylinder will develop residual stresses across the thickness.

So far in the analysis of time-independent plastic and residual stress distributions of thick-walled cylinders the effect of time-dependent material deformation has been

ignored. As long as the temperature is below $0.3T_m$ (where T_m is the absolute melting temperature) the time-dependent deformations are negligible (Fessler and Hyde (1978)). However, at temperatures above the creep threshold, deformation of the cylinder is dominated by the time-dependent process of creep.

3.3 Creep Stress and Damage Analysis

3.3.1 Introduction

With a full understanding of the non-linear plastic (time-independent) deformation of thick-walled cylinders and because of the strong need and demand of the power generating industries to an accurate prediction of the creep stress and damage histories of high energy piping components, which is necessary for their safety and reliability, it was attempted in this investigation to complete the analysis of thick-walled cylinders in both time-dependent and time-independent aspects.

The pressure containing high-temperature components of power plants, are mainly deteriorated by creep mechanism. Creep is due to time-dependent deterioration of material under constant service condition. According to the current understanding of damage to high-pressure and high-temperature components, creep is the most frequently observed damage mechanism which should be carefully investigated (Tolksdorf (1995)). In analysis of creep stress and damage histories the creep strains which are

time, temperature and stress dependent must be considered. Considering the creep strains in the stress-strain relationships makes the non-linear analysis of thick-walled tubes much more difficult. Because, it is not only non-linear but also the deformation is a time-dependent process as well. The rate of deformation in creep regime depends on the stress level and temperature. In a thick-walled tube, loaded with an internal pressure and a thermal gradient, a variable stress and a distributed temperature field are encountered throughout the tube wall which must be considered in the non-linear time-dependent analysis.

3.3.2 Formulation of the Creep Deformation of Thick-Walled Tubes

Thick-walled tubes are the main elements of all high-pressure and high-temperature apparatus and pipeworks employed in power generating industries. Therefore, in this section the time-dependent creep deformation of thick-walled tubes is formulated.

A long thick-walled tube loaded with an internal pressure and a thermal gradient similar to the practical situation during the normal operation of a power plant has been considered. The equilibrium of forces and compatibility of deformations must always be satisfied for all the tube elements at all the times. So the equilibrium and compatibility equations which are the same as previous time-independent analysis are

rewritten here for the time-dependent creep analysis as follows:

$$\frac{d\sigma_r}{dr} + \frac{\sigma_r - \sigma_\theta}{r} = 0 \tag{3.71}$$

$$\frac{d\varepsilon_\theta}{dr} + \frac{\varepsilon_\theta - \varepsilon_r}{r} = 0 \tag{3.72}$$

In this case, the stress strain relationships contain the time-dependent creep strains as follows:

$$\begin{aligned} \varepsilon_r &= \frac{1}{E}[\sigma_r - \nu(\sigma_\theta + \sigma_z)] + \varepsilon_r^c + \alpha T \\ \varepsilon_\theta &= \frac{1}{E}[\sigma_\theta - \nu(\sigma_z + \sigma_r)] + \varepsilon_\theta^c + \alpha T \\ \varepsilon_z &= \frac{1}{E}[\sigma_z - \nu(\sigma_r + \sigma_\theta)] + \varepsilon_z^c + \alpha T \end{aligned} \tag{3.73}$$

where ε_r^c, ε_θ^c and ε_z^c are total creep strains. These total creep strains are time, temperature and stress dependent (path dependent) and are accumulated incrementally during the life of the tube.

The boundary conditions for a thick-walled tube loaded with an internal pressure P_a and no external pressure are written as:

$$\begin{aligned} \sigma_r &= -P_a \qquad at \;\; r = a \\ \sigma_r &= 0 \qquad\;\; at \;\; r = b \end{aligned} \tag{3.74}$$

where a and b are the inner and outer radii of the tube and the minus sign stands for the compressive stress due to the pressure P_a on the internal surface of the tube.

The condition of an open end tube can be mathematically expressed as follows:

$$\int_a^b \sigma_z r dr = 0 \tag{3.75}$$

In which the integration of the axial stress across the thickness of the tube is set to zero to satisfy the open end condition.

The temperature distribution for the steady state outward flow of heat in a tube with an internal temperature T_a and an external temperature of T_b is rewritten as follows:

$$T = ln\frac{a}{b}(T_a ln\frac{b}{r} - T_b ln\frac{a}{r}) \tag{3.76}$$

Stresses and strains must satisfy the equations of equilibrium, compatibility and stress-strain relationships as well as the boundary and end conditions. The stress-strain relationship contains the total accumulated creep strains which are path dependent. A numerical procedure for the computation of total accumulated creep strains in a variable stress and a distributed temperature field of a thick-walled tube has been developed by using an improved long-term material creep constitutive model known as theta projection. However derivation of functional relationships between stresses and the total accumulated creep strains will facilitate computation of the creep stress and damage histories as well as the remaining life estimation of the tube.

3.3.3 Derivation of Creep Stresses

In a similar manner to that of the time-independent stress analysis, the set of equations of equilibrium, compatibility and stress-strain are solved simultaneously for the stresses. Using the above boundary and end condition and the temperature distribution the following functional relationships are obtained for the creep stresses.

$$\begin{aligned}
\sigma_r^c &= \frac{E\alpha(T_a - T_b)}{2(1-\nu)(b^2-a^2)ln\frac{b}{a}}[\frac{a^2b^2}{r^2}ln\frac{b}{a} + b^2 ln\frac{r}{b} - a^2 ln\frac{r}{a}] \\
&\quad -\frac{E}{2(1-\nu^2)r^2}[(1-2\nu)(\int_a^r r\varepsilon_\theta^c dr + \int_a^r r\varepsilon_r^c dr) + r^2(\int_a^r \frac{\varepsilon_\theta^c - \varepsilon_r^c}{r}dr] \\
&\quad +\frac{E}{2(1-\nu^2)(b^2-a^2)}[(1-2\nu)\int_a^b(\varepsilon_\theta^c + \varepsilon_r^c)rdr + b^2\int_a^b \frac{\varepsilon_\theta^c - \varepsilon_r^c}{r}dr](1-\frac{a^2}{r^2}) \\
&\quad +\frac{P_a a^2}{b^2-a^2}(1-\frac{b^2}{r^2}) \qquad (3.77) \\
\sigma_\theta^c &= \frac{E\alpha(T_a - T_b)}{2(1-\nu)(b^2-a^2)ln\frac{b}{a}}[-\frac{a^2b^2}{r^2}ln\frac{b}{a} + b^2 ln\frac{r}{b} - a^2 ln\frac{r}{a} + (b^2-a^2)] \\
&\quad +\frac{E}{2(1-\nu^2)r^2}y[(1-2\nu)\int_a^r r(\varepsilon_\theta^c + \varepsilon_r^c)dr - r^2\int_a^r \frac{\varepsilon_\theta^c - \varepsilon_r^c}{r}dr - \\
&\quad 2r^2((1-\nu)\varepsilon_\theta^c - \nu\varepsilon_r^c)] + \frac{E}{2(1-\nu^2)(b^2-a^2)}[(1-2\nu)\int_a^b(\varepsilon_\theta^c + \varepsilon_r^c)rdr \\
&\quad +b^2\int_a^b \frac{\varepsilon_\theta^c - \varepsilon_r^c}{r}dr](1+\frac{a^2}{r^2}) + \frac{P_a a^2}{b^2-a^2}(1+\frac{b^2}{r^2}) \qquad (3.78) \\
\sigma_z^c &= \frac{E\alpha(T_a - T_b)}{2(1-\nu)(b^2-a^2)ln\frac{b}{a}}[2b^2 ln\frac{r}{b} - 2a^2 ln\frac{r}{a} + (b^2-a^2)] \\
&\quad -\frac{\nu E}{1-\nu^2}[(1-\nu)\varepsilon_\theta^c - \nu\varepsilon_r^c + \int_a^r \frac{\varepsilon_\theta^c - \varepsilon_r^c}{r}dr] + \frac{\nu E}{(1-\nu^2)(b^2-a^2)}[\\
&\quad (1-2\nu)\int_a^b(\varepsilon_\theta^c + \varepsilon_r^c)rdr + b^2\int_a^b \frac{\varepsilon_\theta^c - \varepsilon_r^c}{r}dr] - \frac{2E}{b^2-a^2}\int_a^b(\varepsilon_\theta^c + \varepsilon_r^c)rdr \\
&\quad -\frac{E}{b^2-a^2}[2\int_a^b(\varepsilon_\theta^c + \varepsilon_r^c)rdr - (b^2-a^2)(\varepsilon_\theta^c + \varepsilon_r^c)] \qquad (3.79)
\end{aligned}$$

where σ_r^c, σ_θ^c and σ_z^c are creep stresses and ε_r^c, ε_θ^c and ε_z^c are total creep strains.

Creep stresses may be represented in terms of mechanical, thermal and history dependent stresses in the following form:

$$\begin{aligned}
\sigma_r^c &= U'(r, \varepsilon_r^c, \varepsilon_\theta^c) + F'(r, \Delta T) + G'(r, P_a) \\
\sigma_\theta^c &= V'(r, \varepsilon_r^c, \varepsilon_\theta^c) + H'(r, \Delta T) + R'(r, P_a) \\
\sigma_z^c &= W'(r, \varepsilon_r^c, \varepsilon_\theta^c) + M'(r, \Delta T) \qquad (3.80)
\end{aligned}$$

where functions U', V', W', F', H', M', G' and R' are defined below.

1- History-dependent functions:

$$
\begin{aligned}
U'(r,\varepsilon_r^c,\varepsilon_\theta^c) &= -\frac{E}{2(1-\nu^2)r^2}[(1-2\nu)(\int_a^r r\varepsilon_\theta^c dr+\int_a^r r\varepsilon_r^c dr)+r^2(\int_a^r \frac{\varepsilon_\theta^c-\varepsilon_r^c}{r}dr]+\\
&\frac{E}{2(1-\nu^2)(b^2-a^2)}[(1-2\nu)\int_a^b(\varepsilon_\theta^c+\varepsilon_r^c)rdr+b^2\int_a^b\frac{\varepsilon_\theta^c-\varepsilon_r^c}{r}dr](1-\frac{a^2}{r^2})\\
V'(r,\varepsilon_r^c,\varepsilon_\theta^c) &= \frac{E}{2(1-\nu^2)r^2}[(1-2\nu)\int_a^r r(\varepsilon_\theta^c+\varepsilon_r^c)dr-r^2\int_a^r\frac{\varepsilon_\theta^c-\varepsilon_r^c}{r}dr-\\
&2r^2((1-\nu)\varepsilon_\theta^c-\nu\varepsilon_r^c)]+\frac{E}{2(1-\nu^2)(b^2-a^2)}[(1-2\nu)\int_a^b(\varepsilon_\theta^c+\varepsilon_r^c)rdr\\
&+b^2\int_a^b\frac{\varepsilon_\theta^c-\varepsilon_r^c}{r}dr](1+\frac{a^2}{r^2})\\
W'(r,\varepsilon_r^c,\varepsilon_\theta^c) &= -\frac{\nu E}{1-\nu^2}[(1-\nu)\varepsilon_\theta^c-\nu\varepsilon_r^c+\int_a^r\frac{\varepsilon_\theta^c-\varepsilon_r^c}{r}dr]+\frac{\nu E}{(1-\nu^2)(b^2-a^2)}[\\
&(1-2\nu)\int_a^b(\varepsilon_\theta^c+\varepsilon_r^c)rdr+b^2\int_a^b\frac{\varepsilon_\theta^c-\varepsilon_r^c}{r}dr]-\frac{2E}{b^2-a^2}\int_a^b(\varepsilon_\theta^c+\varepsilon_r^c)rdr\\
&-\frac{E}{b^2-a^2}[2\int_a^b(\varepsilon_\theta^c+\varepsilon_r^c)rdr-(b^2-a^2)(\varepsilon_\theta^c+\varepsilon_r^c)]
\end{aligned}
$$

2- Thermal stress functions:

$$
\begin{aligned}
F'(r,\Delta T) &= \frac{E\alpha(T_a-T_b)}{2(1-\nu)(b^2-a^2)ln\frac{b}{a}}[\frac{a^2b^2}{r^2}ln\frac{b}{a}+b^2ln\frac{r}{b}-a^2ln\frac{r}{a}]\\
H'(r,\Delta T) &= \frac{E\alpha(T_a-T_b)}{2(1-\nu)(b^2-a^2)ln\frac{b}{a}}[-\frac{a^2b^2}{r^2}ln\frac{b}{a}+b^2ln\frac{r}{b}-a^2ln\frac{r}{a}+(b^2-a^2)]\\
M'(r,\Delta T) &= \frac{E\alpha(T_a-T_b)}{2(1-\nu)(b^2-a^2)ln\frac{b}{a}}[2b^2ln\frac{r}{b}-2a^2ln\frac{r}{a}+(b^2-a^2)]
\end{aligned}
$$

3- Mechanical stress functions:

$$
\begin{aligned}
G'(r,P_a) &= \frac{P_a a^2}{b^2-a^2}(1-\frac{b^2}{r^2})\\
R'(r,P_a) &= \frac{P_a a^2}{b^2-a^2}(1+\frac{b^2}{r^2})
\end{aligned}
$$

Functions U', V' and W' are containing the creep strains. These total accumulated creep strains can be calculated by integration or summation of creep strain increments throughout the loading history during the life of the tube. To determine the creep strain increments, the non-linear time-independent incremental stress-strain relationship must be modified to include the material's time-dependency. Thus non-linear time-dependent stress-strain relationship or the creep flow rule is introduced here.

3.3.4 Creep Flow Rule

Creep stresses are functions of total creep strains defined by equations (3.80). Creep strains are time, temperature and stress dependent. In an incremental approach the total accumulated creep strains can be calculated by integration or summation of the creep strain increments over the loading path during the life of the tube. If variation of radial, tangential and axial creep strains during a short increment of time (Δt) are defined as $\Delta\varepsilon_r^c$, $\Delta\varepsilon_\theta^c$ and $\Delta\varepsilon_z^c$, then the incremental stress-strain relationship may be written as follows:

$$\begin{aligned} \Delta\varepsilon_r^c &= \frac{\Delta\varepsilon_e^c}{\sigma_e}[\sigma_r - \frac{1}{2}(\sigma_\theta + \sigma_z)] \\ \Delta\varepsilon_\theta^c &= \frac{\Delta\varepsilon_e^c}{\sigma_e}[\sigma_\theta - \frac{1}{2}(\sigma_z + \sigma_r)] \end{aligned} \tag{3.81}$$

where σ_e and $\Delta\varepsilon_e^c$ are the effective stress and the effective creep strain increment. Dividing both sides of the above equation by Δt will result in the non-linear stress-

strain relationship in the rate form as follows:

$$\begin{aligned} \dot{\varepsilon}_r^c &= \frac{\dot{\varepsilon}_e^c}{\sigma_e}[\sigma_r - \frac{1}{2}(\sigma_\theta + \sigma_z)] \\ \dot{\varepsilon}_\theta^c &= \frac{\dot{\varepsilon}_e^c}{\sigma_e}[\sigma_\theta - \frac{1}{2}(\sigma_z + \sigma_r)] \end{aligned} \tag{3.82}$$

where $\dot{\varepsilon}_r^c$ and $\dot{\varepsilon}_\theta^c$ are radial and tangential creep strain rates and $\dot{\varepsilon}_e^c$ and σ_e are effective creep strain rate and effective stress. The fraction term $(\dot{\varepsilon}_e^c/\sigma_e)$ in the above equation is the path-dependent (history dependent) part of the non-linear time-dependent stress-strain relationship. The creep strain rate in axial direction can be obtained by using the incompressibility condition in creep regime. Therefore it can be written in the rate form as follows:

$$\dot{\varepsilon}_z^c = -(\dot{\varepsilon}_r^c + \dot{\varepsilon}_\theta^c) \tag{3.83}$$

The effective stress (σ_e) and the effective creep strain rate $(\dot{\varepsilon}_e^c)$ in equation (3.82) are defined as follows:

$$\sigma_e = \frac{1}{\sqrt{2}}[(\sigma_r - \sigma_\theta)^2 + (\sigma_\theta - \sigma_z)^2 + (\sigma_z - \sigma_r)^2]^{\frac{1}{2}} \tag{3.84}$$

$$\dot{\varepsilon}_e^c = \frac{\sqrt{2}}{3}[(\dot{\varepsilon}_r^c - \dot{\varepsilon}_\theta^c)^2 + (\dot{\varepsilon}_\theta^c - \dot{\varepsilon}_z^c)^2 + (\dot{\varepsilon}_z^c - \dot{\varepsilon}_r^c)^2]^{\frac{1}{2}}. \tag{3.85}$$

The material uniaxial creep curves represent the effective stress and the effective creep strain relationship. Mathematical representation of this relationship is the material creep constitutive equation. In this case, the material creep constitutive equations are rewritten from Chapter 1 as follows:

$$\varepsilon = \Theta_1(1 - e^{-\Theta_2 t}) + \Theta_3(e^{\Theta_4 t} - 1) \tag{3.86}$$

$$\dot{\varepsilon} = \Theta_1\Theta_2 e^{-\Theta_2 t} + \Theta_3\Theta_4 e^{\Theta_4 t} \tag{3.87}$$

where

$$Log_{10}\Theta_i = a_i + b_i T + c_i \sigma + d_i \sigma T \qquad i = 1, 2, 3, 4 \tag{3.88}$$

coefficients a_i, b_i, c_i and d_i are material constants which have been introduced in Chapter 1 (Table 1.1).

Creep stresses are obtained as functions of total creep strains, the creep strain rates are related to the stresses and the loading history by the incremental stress-strain relationship and the material creep properties. It is necessary to introduce a damage model and the material's creep rupture properties in order to obtain the damage history and the remaining life of the tube.

3.3.5 Creep Damage Model

The life time of components operating at elevated temperature is limited by creep mechanism. Creep damage which is a time-dependent process depends on the history of stresses and temperature applied to the component. Many damage models using either mechanical or micro-structural constitutive relations have been proposed in the past. The mechanical models are based on stress, strain, strain rate, time and temperature whereas the micro-structural models are based on surface energy, grain size, dislocation movement, cavity formation and spacing, crack initiation and growth. In this study the Robinson's creep damage model known as the Robinson's life fraction rule has been adopted for creep damage accumulation and this has also been adopted in the ASME

Code Case N47. In a variable stress and temperature field, similar to the case of a tube subjected to an internal pressure and a thermal gradient, validity of the Robinson's life fraction rule is justified experimentally by Viswanathan et al. (1994). The Robinson's life fraction rule states that

$$D = \sum_{i=1}^{n} \frac{\Delta t_i}{t_{ri}} \tag{3.89}$$

where D is the creep damage, Δt_i is the time spent at any given stress and temperature and t_{ri} is the rupture time under those conditions. When the damage fractions under different sets of stress-temperature conditions add up to unity failure will occur. Based on the above definition the remaining life is then given by the following equation

$$RL = (1 - D)t_{rf} \tag{3.90}$$

where RL is the remaining life and t_{rf} is the creep-rupture life at expected future operating temperature and stress.

The rupture life is the time taken to reach the failure strain and can be obtained by the numerical solution of the following equation:

$$\Theta_1(1 - e^{-\Theta_2 t_r}) + \Theta_3(e^{\Theta_4 t_r} - 1) - \varepsilon_f = 0 \tag{3.91}$$

where t_r is the rupture time and ε_f is the fracture strain. The fracture strain is a function of stress and temperature as follows:

$$\varepsilon_f = a_i + b_i T + c_i \sigma + d_i \sigma T \qquad i = 5 \tag{3.92}$$

The coefficients in this equation are already introduced in Chapter 1 (Table 1.2). The above damage model in conjunction with the material's creep rupture properties has

been incorporated in a non-linear time-dependent stress analysis to predict the creep stress and damage histories as well as the remaining life of thick-walled tubes. Before introducing the procedure a summary of the governing equations involved in the procedure are introduced below.

3.3.6 Summary of the creep Governing Equations

Stresses:

$$\begin{aligned} \sigma_r^c &= U'(r, \varepsilon_r^c, \varepsilon_\theta^c) + F'(r, \Delta T) + G'(r, P_a) \\ \sigma_\theta^c &= V'(r, \varepsilon_r^c, \varepsilon_\theta^c) + H'(r, \Delta T) + R'(r, P_a) \\ \sigma_z^c &= W'(r, \varepsilon_r^c, \varepsilon_\theta^c) + M'(r, \Delta T) \end{aligned} \tag{3.93}$$

Non-linear stress-strain relationship in the rate form:

$$\begin{aligned} \dot{\varepsilon}_r^c &= \frac{\dot{\varepsilon}_e^c}{\sigma_e}[\sigma_r - \frac{1}{2}(\sigma_\theta + \sigma_z)] \\ \dot{\varepsilon}_\theta^c &= \frac{\dot{\varepsilon}_e^c}{\sigma_e}[\sigma_\theta - \frac{1}{2}(\sigma_z + \sigma_r)] \end{aligned} \tag{3.94}$$

Incompressibility:

$$\dot{\varepsilon}_z^c = -(\dot{\varepsilon}_r^c + \dot{\varepsilon}_\theta^c) \tag{3.95}$$

Effective stress and the effective creep strain rate:

$$\sigma_e = \frac{1}{\sqrt{2}}[(\sigma_r - \sigma_\theta)^2 + (\sigma_\theta - \sigma_z)^2 + (\sigma_z - \sigma_r)^2]^{\frac{1}{2}} \tag{3.96}$$

$$\dot{\varepsilon}_e^c = \frac{\sqrt{2}}{3}[(\dot{\varepsilon}_r^c - \dot{\varepsilon}_\theta^c)^2 + (\dot{\varepsilon}_\theta^c - \dot{\varepsilon}_z^c)^2 + (\dot{\varepsilon}_z^c - \dot{\varepsilon}_r^c)^2]^{\frac{1}{2}}. \tag{3.97}$$

Material constitutive model:

$$\varepsilon = \Theta_1(1 - e^{-\Theta_2 t}) + \Theta_3(e^{\Theta_4 t} - 1) \tag{3.98}$$

$$\dot{\varepsilon} = \Theta_1\Theta_2 e^{-\Theta_2 t} + \Theta_3\Theta_4 e^{\Theta_4 t} \tag{3.99}$$

Damage model:

$$D = \sum_{i=1}^{n} \frac{\Delta t_i}{t_{ri}} \tag{3.100}$$

Remaining life:

$$RL = (1 - D)t_{rf} \tag{3.101}$$

Material creep rupture properties:

$$\Theta_1(1 - e^{-\Theta_2 t_r}) + \Theta_3(e^{\Theta_4 t_r} - 1) - \varepsilon_f = 0 \tag{3.102}$$

$$\varepsilon_f = a_i + b_i T + c_i \sigma + d_i \sigma T \qquad i = 5 \tag{3.103}$$

Based on the above governing equations a numerical procedure has been developed which gives the stress and damage histories and the remaining life of the tube.

In this method a time increment Δt is selected and a distribution is assumed for the creep strain increments $\Delta\varepsilon_r^c$ and $\Delta\varepsilon_\theta^c$ at the end of this time increment. Total creep strains at this stage are equal to the initial estimated values of creep strain increments. Integrals of total creep strains in equation (3.93) are evaluated and a first estimate of stresses σ_r, σ_θ and σ_z are obtained. The effective stresses are then obtained using equation (3.96). These values of effective stresses and the temperature distribution in conjunction with the material creep constitutive model (equation (3.99)) are used to

obtain the effective creep strain rates. Creep strain rates are then calculated using equation (3.94). New values are obtained for the creep strain increments using the creep strain rates and the time increment. Using these new values of creep strain increments a second and presumably better approximation is obtained for the stresses and total creep strains. The process is continued until the differences between two successive sets of strain increments are less than the convergence criterion. Having the converged stresses at the end of this time increment and the temperature distribution, creep rupture strains and the time to ruptures are calculated using equations (3.102) and (3.103). Using the Robinson's life fraction rule the damages are calculated from equation (3.100) for this time increment. The remaining life can then be calculated using equation (3.101). Therefore, the solution is obtained for the first time increment. Time is increased incrementally and in a similar manner the complete stress, strain and damage histories as well as the remaining life are calculated during the life of the tube. A block diagram of the proposed numerical procedure is shown in Figure 3.7.

Numerical models of the calculation of plastic and creep strains which were introduced here will be completely expanded in next Chapter which is devoted to numerical procedures.

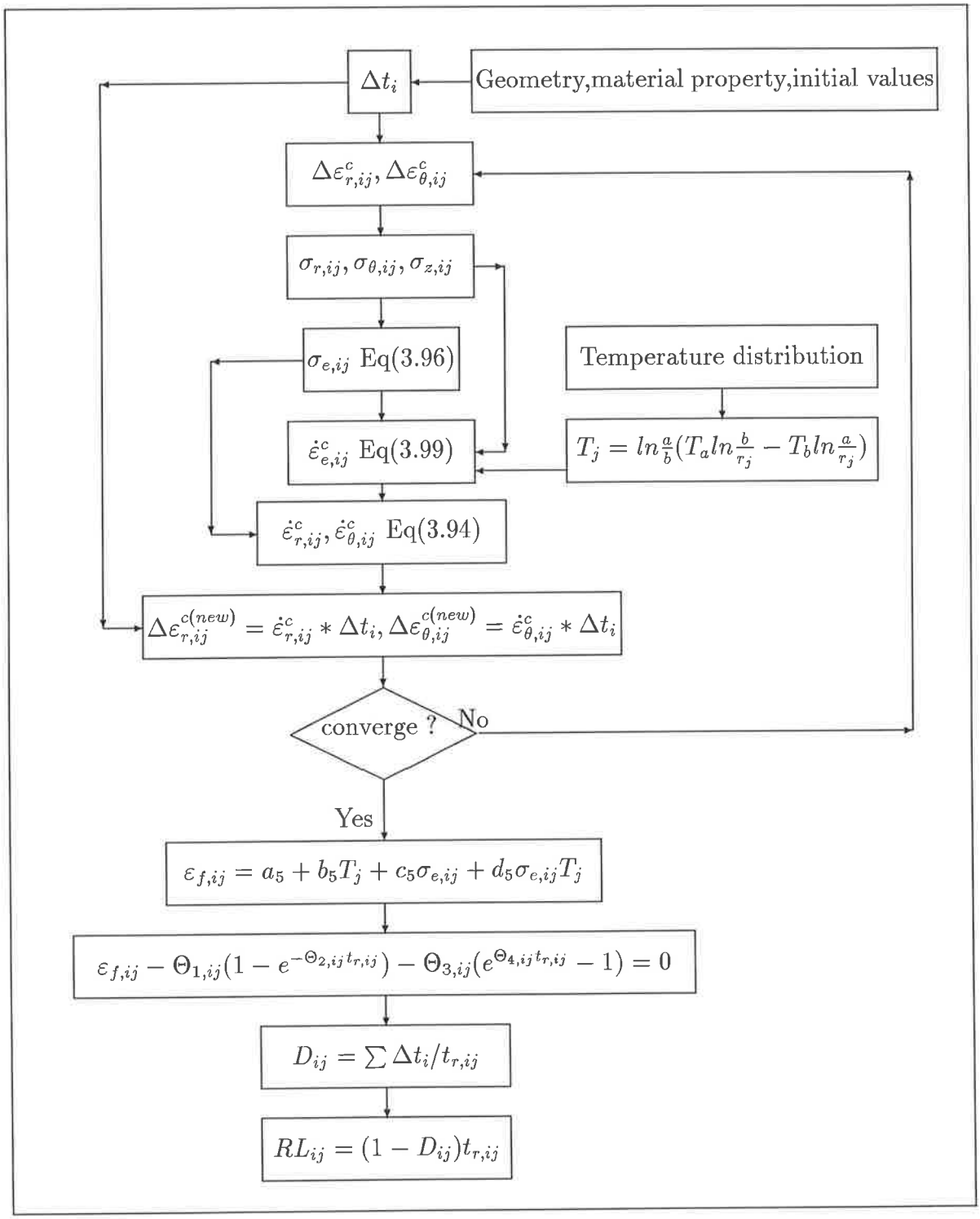

Figure 3.7: Flow diagram for the computation of creep stress and damage histories

Chapter 4

NUMERICAL PROCEDURE

In previous chapter numerical procedures for computation of thermoelastoplastic and residual stresses as well as the creep stress and damage histories were introduced briefly. Details of the procedures are discussed in this Chapter.

4.1 Numerical Procedure for the Computation of Thermoelastoplastic and Residual Stresses

In this section step-by-step procedure for the computation of plastic stresses resulted from an internal pressure and a thermal gradient and the subsequent residual stresses as well as the progress of elastic-plastic boundary is discussed as follows:

1. For a fixed temperature gradient the critical pressure (P_{crit}) and the radius at which plastic yielding begins are calculated from the equation of critical condition

rewritten here as follows:

$$A(\rho,\beta)P_i^2 + B(\rho,\beta,\Theta,P_o)P_i + C(\rho,\beta,\Theta,P_o) = 0 \tag{4.1}$$

If the applied pressure is less than the critical pressure the cylinder remains elastic. However, for pressures more than the critical pressure plastic flow will take place in the cylinder wall.

2. A final pressure of P_f which is more than the critical inner pressure of the cylinder has been considered. The pressure beyond the critical pressure is applied incrementally such that the pressure increment Δp is

$$\Delta p = \frac{P_f - P_{crit}}{N} \tag{4.2}$$

where P_{crit} is the critical pressure and N is the number of loading steps. Therefore, the internal pressure at the ith loading step is given by

$$P_{i,i} = P_{crit} + i * \Delta p \tag{4.3}$$

3. Initial values are assumed for radial and tangential plastic strain increments $\Delta\epsilon^p_{r,ij}$ and $\Delta\epsilon^p_{\theta,ij}$ and are added to the accumulated plastic strains obtained from the previous loading steps at all divisions of radius in the plastic zone. In the initial loading step, the accumulated plastic strains are zero. The plastic strain distribution at the ith loading step can be written in dimensionless form as:

$$\begin{aligned} \epsilon^p_{r,ij} &= \sum_{k=1}^{i-1} \Delta\epsilon^p_{r,kj} + \Delta\epsilon^p_{r,ij} \\ \epsilon^p_{\theta,ij} &= \sum_{k=1}^{i-1} \Delta\epsilon^p_{\theta,kj} + \Delta\epsilon^p_{\theta,ij} \end{aligned} \tag{4.4}$$

where the subscripts i and j refer to the loading step and the layer along the radius respectively.

The plastic strain increment in the axial direction is obtained from the incompressibility condition in plastic regime which can be written as follows:

$$\Delta\epsilon^p_{z,ij} = -(\Delta\epsilon^p_{r,ij} + \Delta\epsilon^p_{\theta,ij}) \tag{4.5}$$

In this study, the initial values of -0.00003 and +0.00004 are assumed for the radial and tangential plastic strain increments, respectively.

4. The effective plastic strain increments for all divisions of radius in the plastic zone are then computed as follows:

$$\Delta\epsilon_{p,ij} = \frac{\sqrt{2}}{3}[(\Delta\epsilon^p_{r,ij} - \Delta\epsilon^p_{\theta,ij})^2 + (\Delta\epsilon^p_{\theta,ij} - \Delta\epsilon^p_{z,ij})^2 + (\Delta\epsilon^p_{z,ij} - \Delta\epsilon^p_{r,ij})^2]^{\frac{1}{2}} \tag{4.6}$$

5. The effective stresses are obtained for all divisions of radius in the plastic zone using the material's constitutive model. The procedure is shown in Figure 4.1.

The material's constitutive model in a dimensionless form is mathematically represented as follows:

$$S_{e,ij} = 1 + H(\epsilon_{p,ij})^{\gamma} \tag{4.7}$$

where H and γ are temperature dependent constants. The constitutive model at room temperature which is obtained experimentally is written in the following form.

$$S_{e,ij} = 1 + 2.92(\epsilon_p)^{0.21842186} \tag{4.8}$$

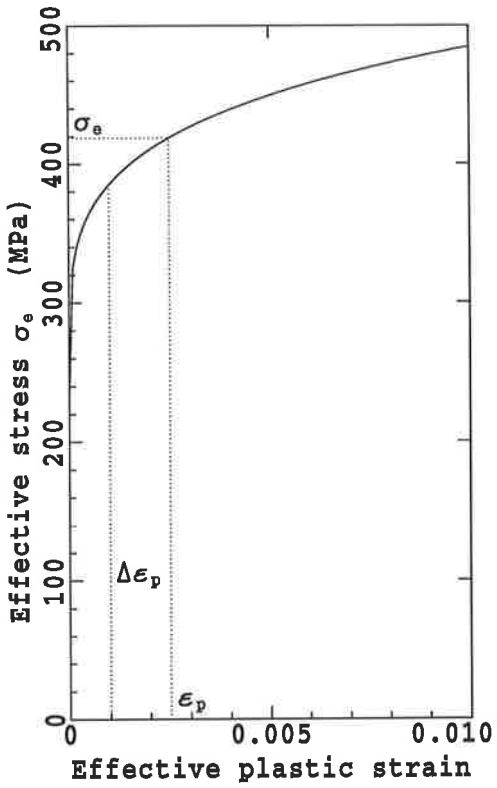

Figure 4.1: Determination of effective stress from the effective plastic strain.

in which $\epsilon_{p,ij} = \sum \Delta\epsilon_{p,ij}$. High-temperature material constants are selected from the experimental results of Niitsu and Ikegami (1990).

6. The radius of the elastic-plastic boundary at the ith loading step, ρ_{ci} is found by setting the boundary conditions at this radius. At the plastic zone boundary the von Mises condition must be satisfied. If yielding starts from the inside radius, then the radial stress at elastic-plastic boundary is equal to the critical pressure of the outer elastic cylinder. In this case equation (4.1) can be written in the

following form:

$$A[\rho_{ci},\beta]S_r^2(\rho_{ci}) + B[\rho_{ci},\beta,\Theta,P_o]S_r(\rho_{ci}) + C[\rho_{ci},\beta,\Theta,P_o] = 0 \qquad (4.9)$$

For the case in which yielding starts from the outer surface, equation (4.1) takes the form:

$$A(\rho_{ci},\beta)P_i^2 + B[\rho_{ci},\beta,\Theta,S_r(\rho_{ci})]P_i + C[\rho_{ci},\beta,\Theta,S_r(\rho_{ci})] = 0 \qquad (4.10)$$

Solving equations (4.9) or (4.10) will give the radius of elastic-plastic boundary at the ith loading step (ρ_{ci}).

7. With ρ_{ci} known, the integrals of plastic strains in equations (3.60), (3.61) and (3.62) can now be evaluated numerically and plastic stresses S_r^p, S_θ^p and S_z^p can be calculated.

8. Having calculated the stresses from step 7, and the effective plastic strain and effective stress from steps 4 and 5, a new and better approximation is obtained for the latest increment of the plastic strains by employing the incremental stress-strain relationship (Prandtl-Reuss equations) as follows:

$$\begin{aligned}
\Delta\epsilon_{r,ij}^{p(new)} &= \frac{\Delta\epsilon_{p,ij}}{S_{e,ij}}(2S_{r,ij}^p - S_{\theta,ij}^p - S_{z,ij}^p) \\
\Delta\epsilon_{\theta,ij}^{p(new)} &= \frac{\Delta\epsilon_{p,ij}}{S_{e,ij}}(2S_{\theta,ij}^p - S_{r,ij}^p - S_{z,ij}^p)
\end{aligned} \qquad (4.11)$$

9. New values of axial plastic strain increments are obtained using incompressibility condition in plastic regime as follows:

$$\Delta\epsilon_{z,ij}^{p(new)} = -(\Delta\epsilon_{r,ij}^{p(new)} + \Delta\epsilon_{\theta,ij}^{p(new)}) \qquad (4.12)$$

10. The solution is iterated from step 4 until it converges for the ith loading step.

11. If the internal pressure and the thermal gradient are removed at the ith loading step, then residual stresses will be distributed throughout the cylinder wall which can be calculated as follows:

$$\begin{aligned} S^r_{r,ij} &= S^p_{r,ij} - S^e_{r,ij} \\ S^r_{\theta,ij} &= S^p_{\theta,ij} - S^e_{\theta,ij} \\ S^r_{z,ij} &= S^p_{z,ij} - S^e_{z,ij} \end{aligned} \tag{4.13}$$

where $S^r_{r,ij}$, $S^r_{\theta,ij}$ and $S^r_{z,ij}$ are residual stresses, $S^p_{r,ij}$, $S^p_{\theta,ij}$ and $S^p_{z,ij}$ represent the current plastic stresses and $S^e_{r,ij}$, $S^e_{\theta,ij}$ and $S^e_{z,ij}$ are an elastic stress system due to pressure (P_i) and temperature gradient (ΔT) which can be written as

$$\begin{aligned} S^e_{r,ij} &= F(\rho_{ij}, \beta, \Theta, P_o) + G(\rho_{ij}, \beta) * P_i \\ S^e_{\theta,ij} &= H(\rho_{ij}, \beta, \Theta, P_o) + R(\rho_{ij}, \beta) * P_i \\ S^e_{z,ij} &= M(\rho_{ij}, \beta, \Theta) + N(\beta) * P_i \end{aligned} \tag{4.14}$$

12. Reverse yielding is predicted by the von Mises yield condition including the Bauschinger effect factor as follows:

$$(S^r_{r,ij} - S^r_{\theta,ij})^2 + (S^r_{\theta,ij} - S^r_{z,ij})^2 + (S^r_{z,ij} - S^r_{r,ij})^2 = 2(BEF_{ij})^2 \tag{4.15}$$

in which the Bauschinger effect factor BEF_{ij} is obtained experimentally and represented mathematically as follows:

$$\begin{aligned} BEF_{ij} &= 1.0170029 + 0.36592732(\%\varepsilon_{p,ij}) - 0.0025343135(\%\varepsilon_{p,ij})^3 - \\ &\quad 0.97738304(\%\varepsilon_{p,ij})^{0.5} \end{aligned} \tag{4.16}$$

where $\%\varepsilon_{p,ij}$ is the percent overstrain.

13. The loading step is advanced one increment (to $i+1$) and the numerical procedure for calculation of plastic stresses and the residual stresses is repeated until the full load is applied ($P_{i,i} = P_f$).

The above numerical method is validated experimentally the procedure of which is discussed in the next Chapter. A block diagram of the above developed procedure is shown in Figure 4.2.

In the next section, details of the procedure developed for the computation of creep stress and damage histories as well as the remaining life of the thick-walled tubes are discussed.

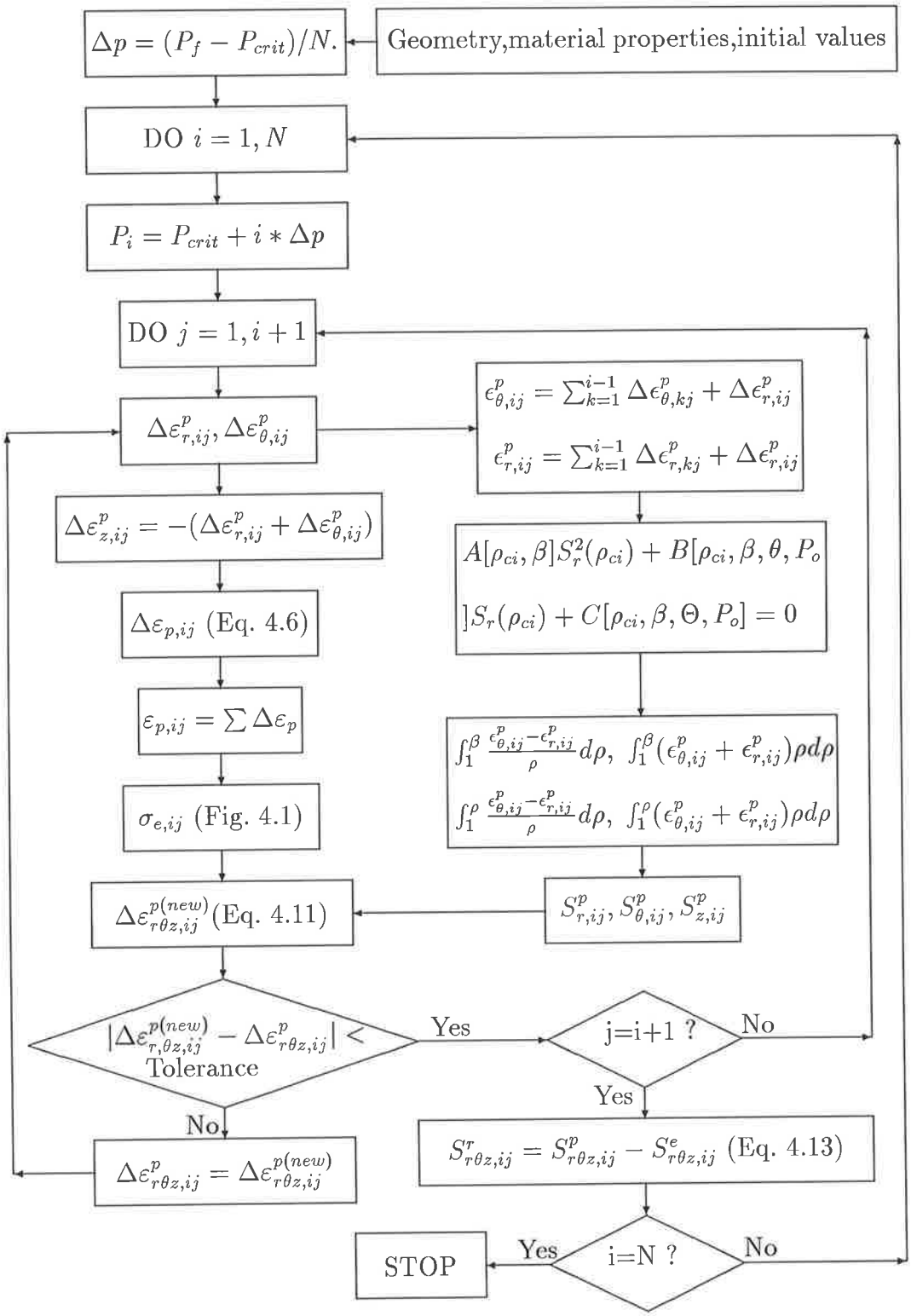

Figure 4.2: Block diagram for calculation of plastic and residual stresses

4.2 Numerical Procedure for Computation of Creep Stresses and Creep Damages

A numerical procedure for the computation of creep stress and damage histories as well as the remaining life evaluation of thick-walled tubes was briefly introduced in previous Chapter. A full description of the procedure has been considered for this section. Step by step procedure is explained as follows:

1. For a fixed temperature gradient of 7^oC which is selected according to the operating condition of a boiler header tube of a fossil fueled power plants, the critical pressure (P_{crit}) is calculated from equation (4.1).

2. Initial elastic stress distribution throughout the wall of the tube is calculated using the operating pressure and operating temperature of the tube. Operating pressure is usually lower than the above calculated critical pressure. In this study the internal pressure of the header is 20 MPa and the inner temperature of the header is 557^oC in the presence of a 7^oC thermal gradient. This initial elastic stress distribution varies with time.

3. An appropriate time increment is selected. The total time is the sum of time increments as the creep process is progressing.

$$t_i = \sum_{k=1}^{i-1} \Delta t_k + \Delta t_i \tag{4.17}$$

where i is the timing step.

The time increment selection depends on the creep strain rate. Considering the

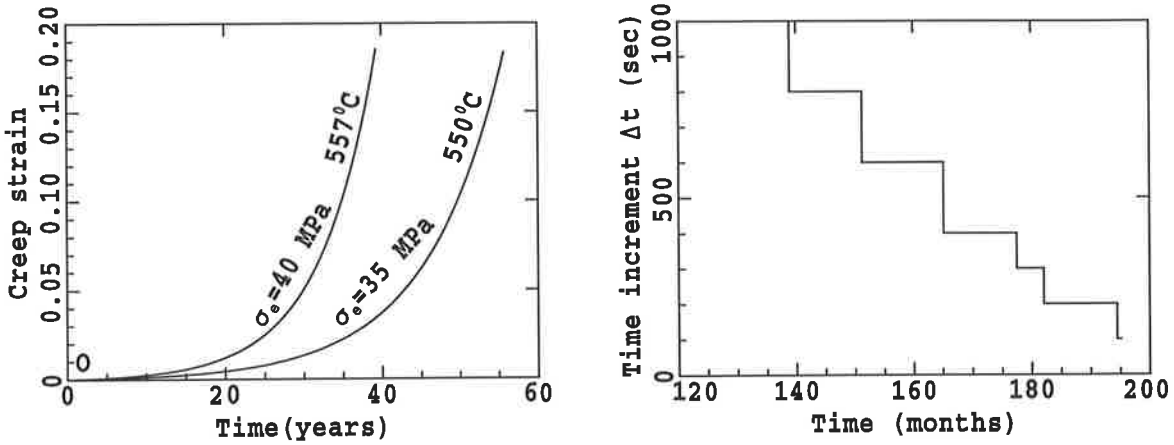

(a) (b)

Figure 4.3: (a) Creep curves predicted by the Θ projection for the $\frac{1}{2}Cr, \frac{1}{2}Mo, \frac{1}{4}V$ ferritic steel; (b) Time incrementation pattern at later stages of creep process.

strain-time behaviour of the material in Figure 4.3(a), at early stages of the creep in which the creep strain rate is small the numerical procedure converges with large steps of time increment for example 10,000 sec (2.77 hours) , because large steps of time are followed by small changes in the creep strain (curve is flat). But later in the tube life when there is a sharp rise in the creep strain rate near the rupture time (where small steps of time are followed by significant rise of creep strain) the time increment should be very small for convergence of the procedure (even less than 20 sec). A pattern of time incrementation which is variable during the life of the tube due to variations in creep strain rate is illustrated in Figure 4.3(b)

4. Initial values of -0.00001 and 0.00001 are assumed for radial and tangential creep strain increments $\Delta\varepsilon^c_{r,ij}$ and $\Delta\varepsilon^c_{\Theta,ij}$ and are added to the accumulated creep strains obtained from the previous timing step at all division points throughout the tube wall. In the initial timing step the accumulated creep strains are zero. The radial and tangential creep strains at the ith timing step are

$$\begin{aligned} \varepsilon^c_{r,ij} &= \sum_{k=1}^{i-1} \Delta\varepsilon^c_{r,kj} + \Delta\varepsilon^c_{r,ij} \\ \varepsilon^c_{\Theta,ij} &= \sum_{k=1}^{i-1} \Delta\varepsilon^c_{\Theta,kj} + \Delta\varepsilon^c_{\Theta,ij} \end{aligned} \tag{4.18}$$

The subscripts i and j refer to the timing step and the division point across the thickness respectively. The creep strain increment in axial direction is obtained from the incompressibility condition in creep regime which is

$$\Delta\varepsilon^c_{z,ij} = -(\Delta\varepsilon^c_{r,ij} + \Delta\varepsilon^c_{\Theta,ij}) \tag{4.19}$$

5. With the assumed creep strain distribution the integrals in equations (3.80) are evaluated. Therefore initial esimates of creep stresses are calculated.

6. Effective stresses at all division points along the radius is then calculated as follows:

$$\sigma_{e,ij} = \frac{1}{\sqrt{2}}[(\sigma_{r,ij} - \sigma_{\Theta,ij})^2 + (\sigma_{\Theta,ij} - \sigma_{z,ij})^2 + (\sigma_{z,ij} - \sigma_{r,ij})^2]^{\frac{1}{2}} \tag{4.20}$$

7. Temperature distributions at all division points along the tube radius are calculated as follows:

$$T_j = ln\frac{a}{b}(T_a ln\frac{b}{r_j} - T_b ln\frac{a}{r_j}) \tag{4.21}$$

8. with the above temperature and effective stress distributions the effective creep strain rates at all the division points are obtained using the material's creep constitutive equation as follows:

$$\dot{\varepsilon}^{c}_{e,ij} = \Theta_{1,ij}\Theta_{2,ij}e^{-\Theta_{2,ij}t_i} + \Theta_{3,ij}\Theta_{4,ij}e^{\Theta_{4,ij}t_i} \tag{4.22}$$

where Θ_1, Θ_2, Θ_3 and Θ_4, are written as follows:

$$Log_{10}\Theta_{k,ij} = a_k + b_kT_j + c_k\sigma_{e,ij} + d_k\sigma_{e,ij}T_j \qquad k = 1,2,3,4 \tag{4.23}$$

9. Radial and tangential creep strain rates are obtained using the incremental stress-strain relationship (Prandtl-Reuss) in the rate form as follows:

$$\begin{aligned} \dot{\varepsilon}^{c}_{r,ij} &= \frac{\dot{\varepsilon}^{c}_{e,ij}}{\sigma_{e,ij}}[\sigma_{r,ij} - \frac{1}{2}(\sigma_{\Theta,ij} + \sigma_{z,ij})] \\ \dot{\varepsilon}^{c}_{\Theta,ij} &= \frac{\dot{\varepsilon}^{c}_{e,ij}}{\sigma_{e,ij}}[\sigma_{\Theta,ij} - \frac{1}{2}(\sigma_{z,ij} + \sigma_{r,ij})] \end{aligned} \tag{4.24}$$

10. Axial creep strain rates are calculated by using the incompressibility condition as follows:

$$\dot{\varepsilon}^{c}_{z,ij} = -(\dot{\varepsilon}^{c}_{r,ij} + \dot{\varepsilon}^{c}_{\Theta,ij}) \tag{4.25}$$

11. Having the strain rates, new and better approximations are obtained for the latest creep strain increments at all division points along the tube radius.

$$\begin{aligned} \Delta\varepsilon^{c(new)}_{r,ij} &= \dot{\varepsilon}^{c}_{r,ij} * \Delta t_i \\ \Delta\varepsilon^{c(new)}_{\Theta,ij} &= \dot{\varepsilon}^{c}_{\Theta,ij} * \Delta t_i \\ \Delta\varepsilon^{c(new)}_{z,ij} &= \dot{\varepsilon}^{c}_{z,ij} * \Delta t_i \end{aligned} \tag{4.26}$$

12. The method is iterated from step 4 until it converges for ith timing step.

13. Creep-fracture strains at all divisions throughout the tube wall are calculated using the material's creep rupture properties, temperature distribution and the effective stress histories as follows:

$$\varepsilon_{f,ij} = a_5 + b_5 T_j + c_5 \sigma_{e,ij} + d_5 \sigma_{e,ij} T_j \tag{4.27}$$

14. Creep-fracture times $t_{r,ij}$ are then calculated numerically using the material creep constitutive model in the following form

$$\varepsilon_{f,ij} - \Theta_{1,ij}(1 - e^{-\Theta_{2,ij} t_{r,ij}}) - \Theta_{3,ij}(e^{\Theta_{4,ij} t_{r,ij}} - 1) = 0 \tag{4.28}$$

15. Having the creep rupture times for all the division points along the radius the damages are calculated and summed throughout the life of the tube using the Robinson's life fraction damage rule as follows:

$$D_{ij} = \sum \frac{\Delta t_i}{t_{r,ij}} \tag{4.29}$$

16. The remaining life is then computed for all divisions across the tube thickness using equation (3.101) as follows:

$$RL_{ij} = (1 - D_{ij}) t_{r,ij} \tag{4.30}$$

Material creep rupture properties:

17. The time is advanced one increment (to $i+1$) and the numerical procedure is repeated and the stress and damage and the remaining life are recorded.

A block diagram of the numerical procedure is shown in Figure 4.4.

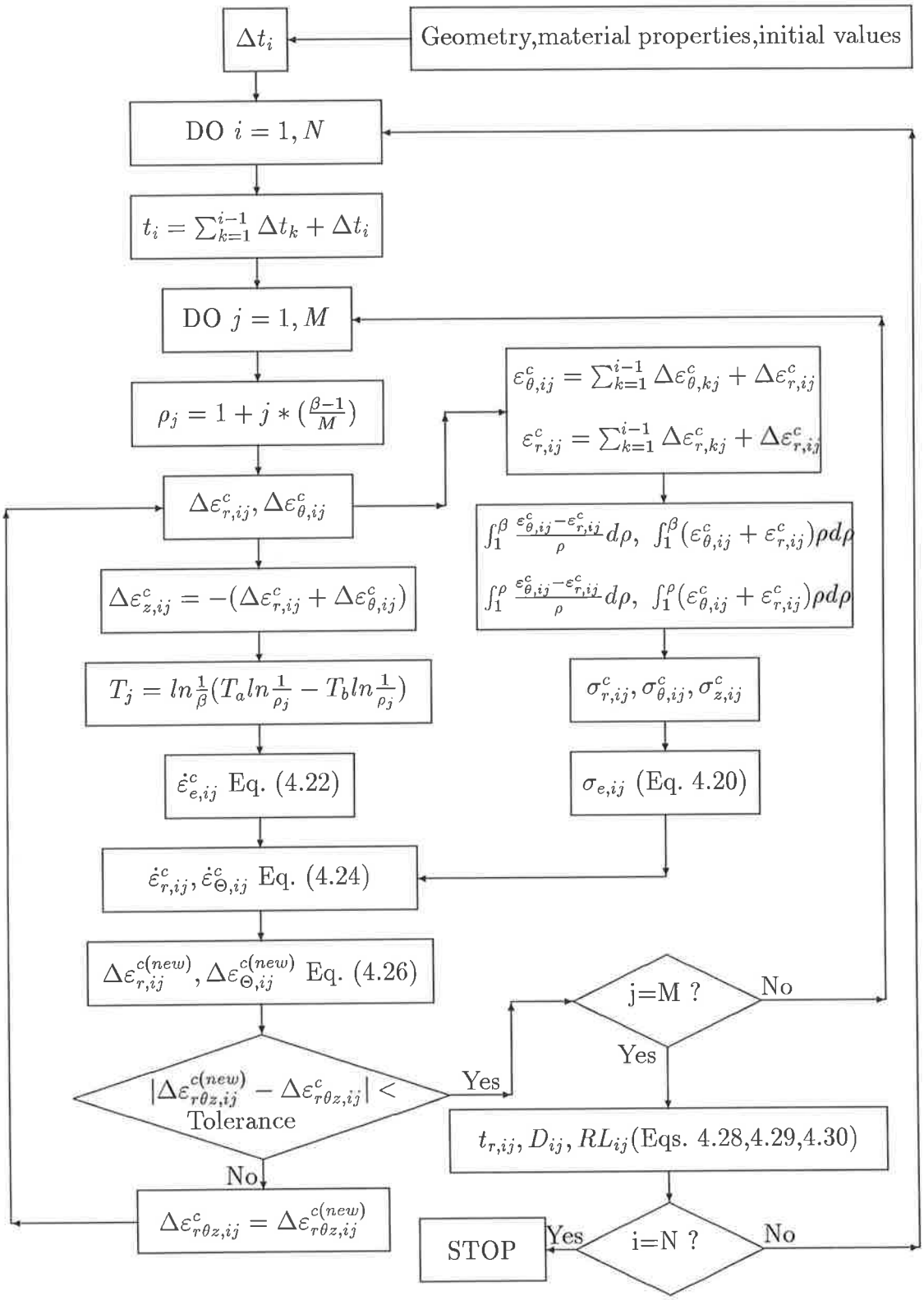

Figure 4.4: Block diagram for calculation of creep stress and damage histories

Chapter 5

EXPERIMENTAL INVESTIGATION

5.1 Introduction

The analytical-numerical models developed in previous Chapters for the critical inner pressure and the spread of plastic yielding as well as the subsequent residual stress distributions in thick-walled cylinders are validated experimentally. A high pressure (284 MPa, 2800 bar) hand pump designed for laboratory high pressure tests is used to produce high pressures required in this investigation. A digital pressure transducer (model EPXH-M10JIW-1400G) with sensitivity of 0.0854 mV/bar is used to provide the internal pressure measurements. The maximum permissible pressure is limited to 172.37 MPa (1700 bar) which is the maximum range of the pressure transducer. Rosette strain gauges are mounted at the axial center of the test specimens and are oriented

such that the two legs measure strains in axial and tangential directions.Specifications of test specimens and experimental setup and procedures are described in this Chapter. However, since the material's model is one of the important ingredients of the proposed analytical-numerical model, experimental investigations for the material constitutive model and the Bauschinger effect factor are also described here in this Chapter.

5.2 Material's Constitutive Model Tests

In the proposed analytical-numerical model the material loading and unloading functions are used as the relationship between the effective stress and the effective plastic strain in a multi-axial stress-strain situation. Moreover, the model also considers the effect of Bauschinger phenomenon on the residual stress distributions and the reverse yielding predictions of thick-walled cylinders. Therefore the material's model plays a significant role in this non-linear stress analysis. Test specimens for loading-unloading tests are produced from the as received stainless steel SUS 304 with the following composition and mechanical properties specified by the manufacturer.

Table 5.1: Chemical composition of testing material % basis

C	Mn	Ni	Cr
0.06	1.7	9.5	18

Table 5.2: Mechanical properties of testing material

σ_0 (MPa)	U.T.S. (MPa)	%EL	Hardness (HB)
230	590	50	170

5.2.1 Specifications of Test Specimens

The test specimens for loading-unloading tests are designed with a smaller gauge length than the standard tension test specimens. Based on the manufacturer specified mechanical properties the critical buckling load for an ASTM E-8M-89b (1989) standard round (d=12.5 mm) test specimen of this material, with 10 centimeter length of the reduced section, is about 750 kN. This critical load is computed by using Euler's buckling equation which is recommended by the ASTM (1989) standard compression test method as follows:

$$P_{cr} = n\frac{\pi^2 EI}{L^2} \tag{5.1}$$

where P_{cr} is the critical buckling load, E is Young's modulus, I is the moment of inertia of the cross section about centroidal axis, L is the column length and n is the end-fixity coefficient which is 4 for both ends fixed condition. The critical buckling load for a similar test specimen with 8 centimeter length of the reduced section designed for this experiment is about 1171 kN which is 36% more than the critical buckling load of the standard test specimen. The critical buckling stress for the standard and the designed test specimens are 6107 MPa and 9543 MPa respectively. Since the buckling stress

is greater than the proportional limit of the material (230 MPa) the critical inelastic buckling load must be calculated using the modified Euler equation. According to the ASTM (1989) suggestion the modified Euler equation is represented as follows:

$$P_{cr} = n\frac{\pi^2 E_t I}{L^2} \tag{5.2}$$

where E_t is tangent modulus at buckling stress ($S_{cr} = P_{cr}/Area$). The tangent modulus of the material at compressive yield point is approximately 63.3 GPa. The critical inelastic buckling load is then calculated as 468 kN for the designed test specimens and 300 kN for the standard test specimen. These are obtained by using equation (5.2). Taking into account that the machine load has never exceeded 60 kN during all the tests it is concluded that the experimental magnitudes of the Bauschinger effect factor are not influenced by the buckling. Buckling was not observed during all tests. A schematic of the designed test specimen is shown in Figure 5.1. These test specimens are designed

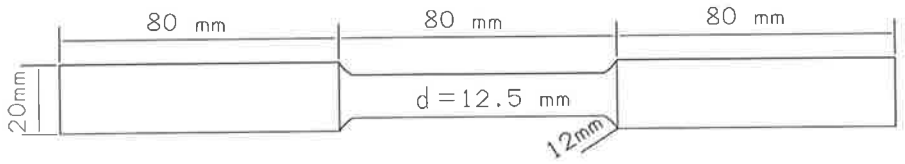

Figure 5.1: Loading-Unloading Round test specimen for material property

for material's loading-unloading property and the Bauschinger effect factor.

5.2.2 Material Loading-Unloading Tests

A series of 10 test specimens with the above specification are tested using a computer controlled uniaxial testing machine. The machine configuration menu is set up such that the test specimens were overstrained to prescribed values of 0.1%, 0.25%, 0.50%, 0.75%, 1.0%, 1.5%, 2.0%, 3.0%, 4.0% and 5.0% and then reverse loaded until the zero strain is reached. The straining speed is 0.1 mm/sec during each second of which 20 series of data are recorded in the data file. Each series of data are composed of time (sec), length (mm), load (kN) and strain (mm/mm). A sample of data recorded during half a second of a test is rewritten from the data file into table 5.5 located at the end of this Chapter. The experimental stress-strain curve of 0.75% overstrained condition obtained from the corresponding data file is shown in Figure 5.2. The material's constitutive model and the Bauschinger effect factors are obtained from these experiments. A summary of the material's experimental properties obtained from these tests are written in table 5.3.

In this table, σ_0 is the yield stress and σ_A and σ_D are the direct and reverse yield point based on 0.1% offset method as are shown in Figure 5.2. The Bauschinger effect factor (BEF) written in table 5.3 is calculated based on the modified formula introduced in Chapter 1 and rewritten here as follows:

$$BEF = \frac{\sigma_D}{\sigma_B} \tag{5.3}$$

Elastic strains have been subtracted from the total overstrains to give the plastic strains. To find the best mathematical function representing the variation of BEF

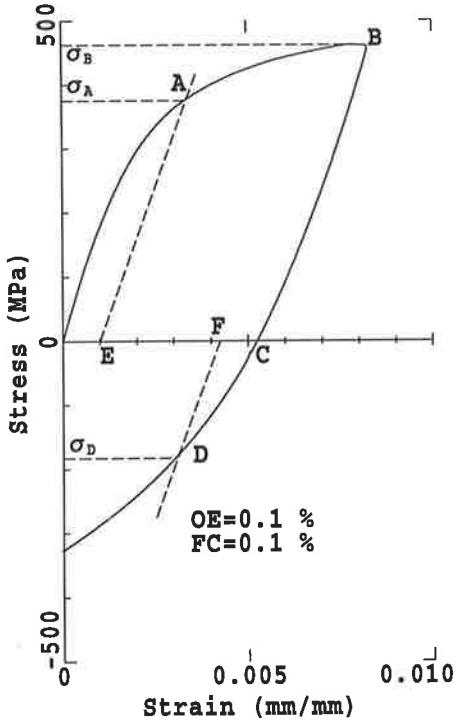

Figure 5.2: Experimental loading-unloading stress-strain curve obtained for SUS 304

with respect to the percentage amount of plastic overstrain, a curve fitting software has been employed (The Jandel Scientific Table Curve version 3.03 (1991)). The variation of BEF can be best represented as a continuous function of the amount of plastic overstrain by the following function:

$$BEF = 1.0170029 + 0.36592732(\varepsilon_p\%) - 0.0025343135(\varepsilon_p\%)^3 - 0.97738304(\varepsilon_p\%)^{0.5} \tag{5.4}$$

In a similar manner the material's data files are modified by subtracting the elastic strains from the total strains to give the plastic strains. By using the same software the

Table 5.3: Material constants calculated from the materials data file

Test case	E (MPa)	σ_0 (MPa)	σ_A (MPa)	σ_D (MPa)	BEF
0.1%	157824.17	236	358	286	0.798
0.25%	156147.09	235	350	210	0.600
0.50%	159390.63	237	366	175	0.478
0.75%	164100.45	234	363	159	0.438
1.0%	152162.06	236	370	148	0.400
1.50%	159162.67	240	369	136	0.370
2%	159557.59	237	366	131	0.358
3%	160341.32	233	365	129	0.353
4%	158879.63	235	368	128	0.347
5%	159692.13	236	364	127	0.349
Average	158725.81	236	363.8	-	-

strain-hardening is mathematically represented by the following constitutive equation:

$$\sigma_e = 232.68187 + 689.01541(\varepsilon_p)^{0.21842186} \tag{5.5}$$

The above actual material model and the Bauschinger effect factor have been incorporated in the analytical-numerical procedure for an accurate prediction of the non-linear response of thick-walled cylinders. Experimental verification of the procedure is discussed below.

5.3 Thick-Walled Cylinder Tests

5.3.1 Introduction

In order to verify the results of the analytical-numerical method developed in this study for the prediction of critical pressures as well as the elastic-plastic stress distributions and the subsequent residual stresses, several experiments are carried out on thick-walled cylindrical test specimens. These experiments are critical pressure tests and the pressure expansion tests as well as the residual stress distribution tests. All the manufactured test specimens have the same total length of 140 mm, gauge length of 60 mm, identical end geometry and bore diameter of 6 mm (Figure 5.3).

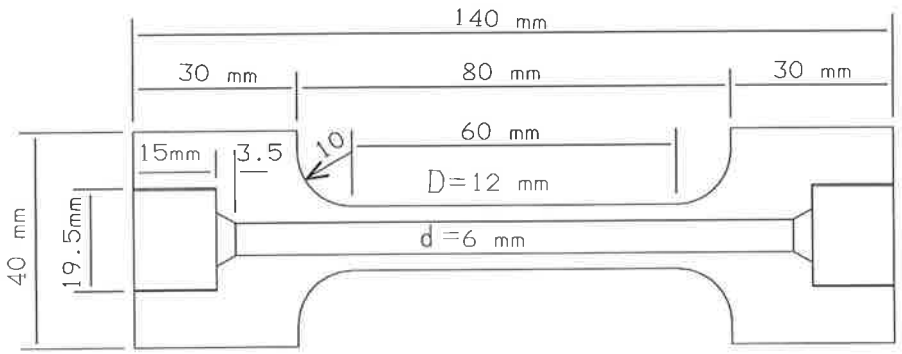

Figure 5.3: Thick-walled cylindrical test specimen

However, they have different outer diameters which cover a wide range of radii ratios. Roark (1975) suggests that the hollow cylinders with radii ratio greater than 1.105 must be considered as a thick-walled component. Therefore the outer diameter of the

designed cylindrical test specimens starts from 7.2 mm and ended with 12 mm which gives a scatter of radii ratios from 1.2 (7.2/6) up to 2 (12/6). Specifications of the test specimens are introduced here before discussing procedures of each individual experiment.

5.3.2 Specifications of specimens

Cylindrical test specimens of the same material, stainless steel SUS 304, with different wall thicknesses are produced in order to investigate the effect of radii ratio on the critical pressure and progress of plastic zone and the consequent residual stresses. In order to produce an accurate and constant wall thickness, the cylinder bore is machined into the 40 *mm* bar first. Then the cylinder is machined down to its final outer dimension using the two ends of the bore as the turning axis. The test specimens are designed such that the gauge length are at least equal to 5 times as their diameters. This is because early studies (Crossland et al. (1958)) have shown that the end effect is negligible in thick-walled cylinders having a length-to-diameter ratio of 4. In order to prevent leakage of fluid from the specimen under the high applied internal pressure, female cone and thread fittings are machined into the end of the cylinder. High pressure hydraulic systems, above 71.4 MPa (700 bar), require special fittings and tubing. These fittings and accessories are designed by the hydraulic pump manufacturer to be used with the high pressure hand pump. These high pressure fittings seal on a cone surface and do not require pipe sealer. Female cones and threads of the machined test

specimens are consistent with the manufacturer supplied fittings. Figure 5.3 shows a drawing of the thick-walled test specimens which are designed for this experimental investigation. These test specimens are used in critical pressure, pressure expansion and the residual stress tests which are discussed here.

5.3.3 Critical Pressure Tests

When internal hydraulic pressure of a cylinder is increased, then the cylinder will respond it by deformation. If the internal pressure is less than the critical pressure, then the cylinder deformation is elastic and it will return back to its original configuration upon the release of internal pressure. However, if the internal pressure is greater than the vessel critical pressure, then plastic strains will be developed in the cylinder wall which are irreversible. It means, the cylinder will not return back to its original configuration after releasing such an internal pressure. This physical phenomenon has been considered for the critical pressure investigations. It is difficult to obtain the critical pressures by measurements of the inside surface deformations of the cylinder because of the sealing problem under such a high internal pressures. Therefore, the critical pressure of the cylinder is investigated by loading-unloading tests of the cylinder, while the outer surface deformations are carefully measured by the strain gauges.

Experimental Procedure

A series of nine thick-walled cylindrical test specimens within the range of the most commonly used radii ratios of 1.2, 1.3, 1.4, 1.5, 1.6, 1.7, 1.8, 1.9 and 2.0 are tested in this experiment. Specification of each test specimen is shown in table 5.4. Other

Table 5.4: Specification of test specimen used in critical pressure tests

Specimen	1	2	3	4	5	6	7	8	9
gauge length mm	60	60	60	60	60	60	60	60	60
Inner diameter mm	6	6	6	6	6	6	6	6	6
Outer diameter mm	7.2	7.8	8.4	9	9.6	10.2	10.8	11.4	12
Radii ratio	1.2	1.3	1.4	1.5	1.6	1.7	1.8	1.9	2

specifications are exactly the same as shown in Figure 5.3. These specimens are connected to the hydraulic pump supply tube such that the both ends of the specimens are supported on the levelled bearings as shown in Figure 5.4. After the specimens are connected to the supply tube, the air is evacuated from the piping system and the specimen using full strokes several times as necessary to purge air from the system and cylinder while the end of test specimen is not yet closed tightly. Care was taken to evacuate the air completely from the system because the air is compressive and the failure can be followed by throwing the fragments of the failed specimen.

To prevent any possible residual stress development during the air evacuation and tightening of the specimen's end cap, the cylinder is clamped to the bearings and base

plate during this period of time. However, after the air evacuation, the cylinder is free to expand in axial direction similar to the generalized plane strain assumption which has been made in the theoretical analysis of this investigation. A schematic diagram of the experimental setup is shown in Figure 5.4

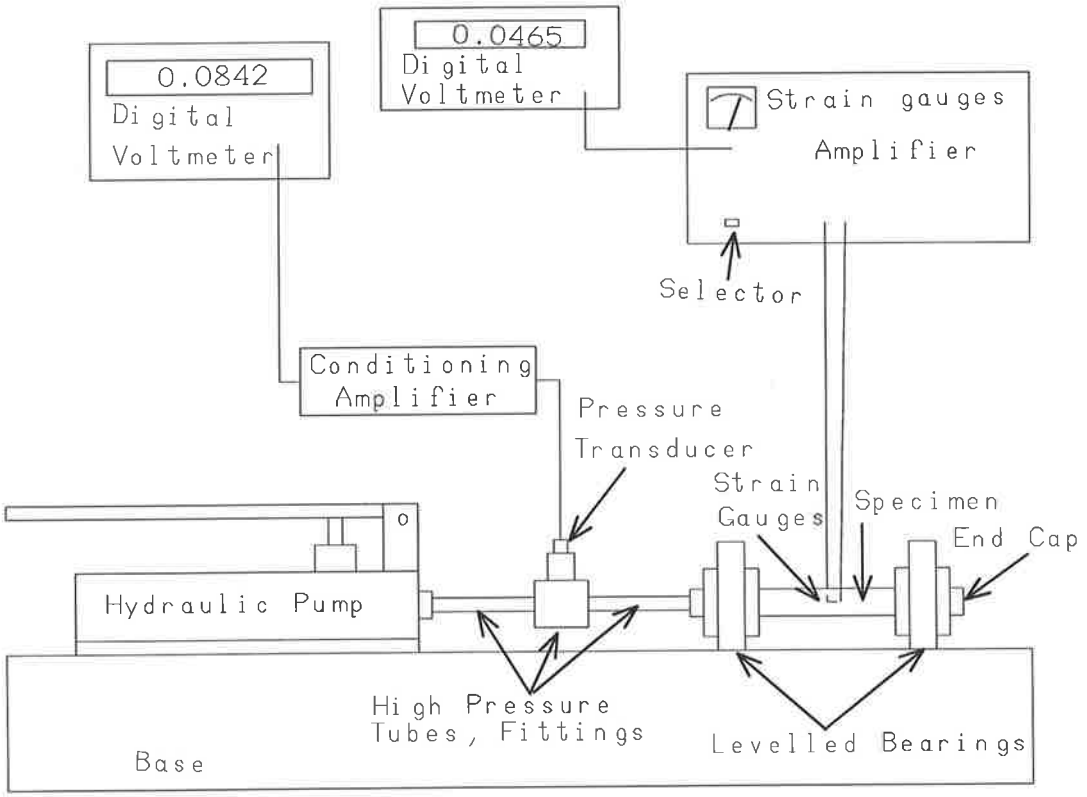

Figure 5.4: Schematic diagram of the experimental setup for critical pressure tests

After the air evacuation from the system, it is ready for the test. Taking into account that the pressure transducer sensitivity is 0.0854 mV/bar (0.8422 mV/MPa) and the maximum permissible range of pressure transducer is 1700 bar (172.37 MPa), then the

maximum permissible output voltage is 145.18 mV or 0.14518 V which should never be exceeded.

Internal pressure is increased step-by-step and released when the pressure transducer's output voltage is stabilized. The outer surface tangential strain is recorded after the pressure is released and the stabilized value of strain is monitored by the digital voltmeter connected to the strain gauge amplifier. A sample of experimental data obtained for the third test specimen (b/a=1.4) is written in table 5.6 located at the end of this Chapter.

As long as the internal pressure is not high enough to yield the cylinder, then the outer surface tangential strain will be zero after the pressure is released. The tabulated data shows that the tangential strain is zero for the first seven steps of loading-unloading tests. Variation of internal pressure versus residual tangential strain is shown in Figure 5.5.

The procedure for critical pressure evaluation is illustrated in this figure. In this manner, critical pressures of all nine test specimens are obtained. The results are compared with the numerical model predictions to be discussed in the next Chapter. After the critical pressures are obtained the progress of plastic zone is investigated by pressure-expansion tests.

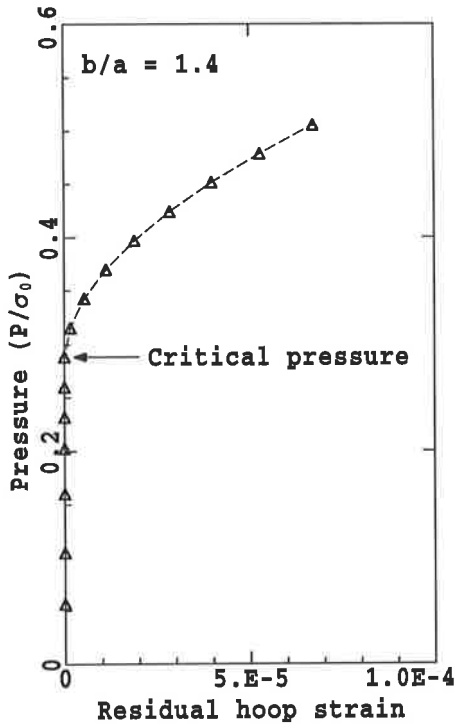

Figure 5.5: Internal pressure and its subsequent residual tangential strain at the outer surface of the cylinder.

5.3.4 Pressure Expansion Tests

In order to verify the numerical procedure for the prediction of non-linear deformation of the cylinder, a series of three test specimens with radii ratios of 1.2, 1.3 and 1.4 are selected. These are exactly the same as the first three test specimens described in table 5.4. The lower radii ratios are selected for this experiment because the maximum permissible pressure of the pressure transducer is 172.37 MPa (1700 bar, 0.73 σ_0). With this maximum pressure limit, it is impossible to create significant amount of plastic strains at the cylinders with higher radii ratios.

The specimens are connected to the hydraulic pump, in the same way as the previous critical pressure tests, and step by step, their internal hydraulic pressure is increased. The axial and tangential strains are recorded for the outer surface of the specimens. A photograph of the experimental setup is shown in Figure 5.6

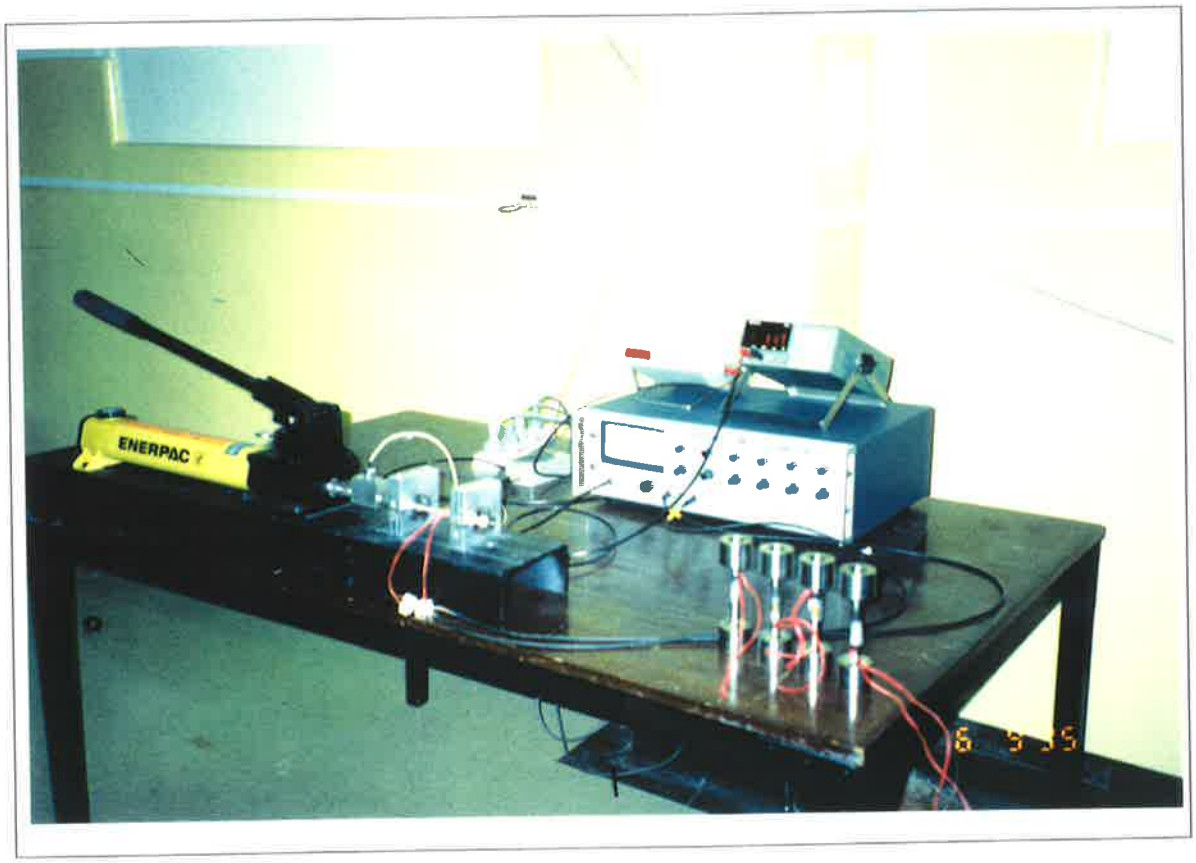

Figure 5.6: Photograph of the experimental setup for cylinder critical pressure tests

A sample of the experimental data obtained for the third test specimen (b/a=1.4) is written in table 5.7 located at the end of this Chapter.

In this way, pressure-expansion of the cylinders are obtained experimentally. These experimental results are compared with the numerical predictions of the outer surface

deformation in Figure 5.7. The numerical procedure accurately predicts the non-linear

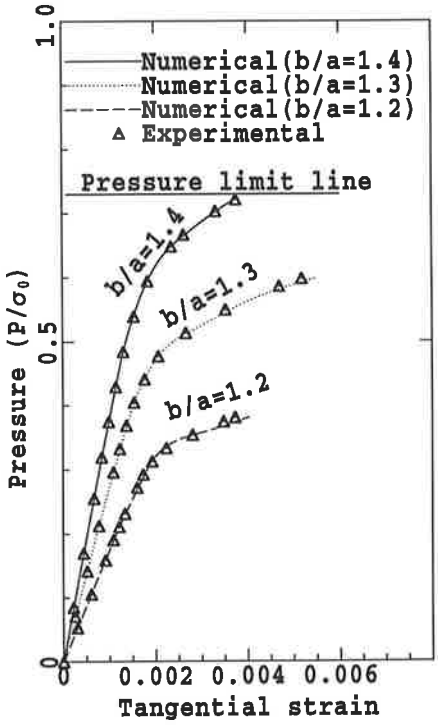

Figure 5.7: Internal pressure versus outer surface total tangential strains

deformation of the cylinder. Therefore the results of the numerical procedure can be used with confidence. The numerical procedure has also been developed to predict the subsequent residual stresses generated in the cylinder wall upon the release of internal pressure. Experimental verification of which is considered below.

5.3.5 Residual Stress Tests

If at any stages of plastic flow in the cylinder, the internal pressure is released, then there will be a distribution of residual stresses throughout the thickness of the vessel. In fact, the action of the elastic region to return back to its original configuration is

counteracted by the plastic region which has developed irreversible plastic strains. On the other hand, the plastic region will be compressed by the elastic region until a self-equilibrium condition is obtained throughout the cylinder thickness. For any particular internal pressure, beyond the critical pressure of the cylinder, a corresponding distribution is predicted for the residual stress-strain throughout the cylinder wall by the proposed analytical-numerical model. The numerical predicted values of the residual axial and tangential strains at the outer surface of the cylinder will be compared with the experimentally measured values of these two components in order to validate the proposed analytical-numerical model for the prediction of residual stress and strain. Similar to the previous pressure-expansion test, a series of 3 test specimens with radii ratios of 1.2, 1.3 and 1.4 are selected. Again, the lower radii ratios are selected due to the limited maximum permissible pressure of the pressure transducer which is 1700 bar (172.37 MPa, 0.73 σ_0). However, with this pressure limit, it will be possible to create significant amount of plastic deformation at these three low radii ratio test specimens. Therefore, the subsequent residual strains can be easily measured by the strain gauges located at the outer surface of the test specimens. The specimens are connected to the hydraulic pump, in the same way as the previous tests, and their internal hydraulic pressure are increased. In these experiments, the internal pressure is released several times and the residual strains are measured by strain gauges. The unloading path and the subsequent residual strains at a particular loading condition for the second and third test specimens are shown in Figure 5.8.

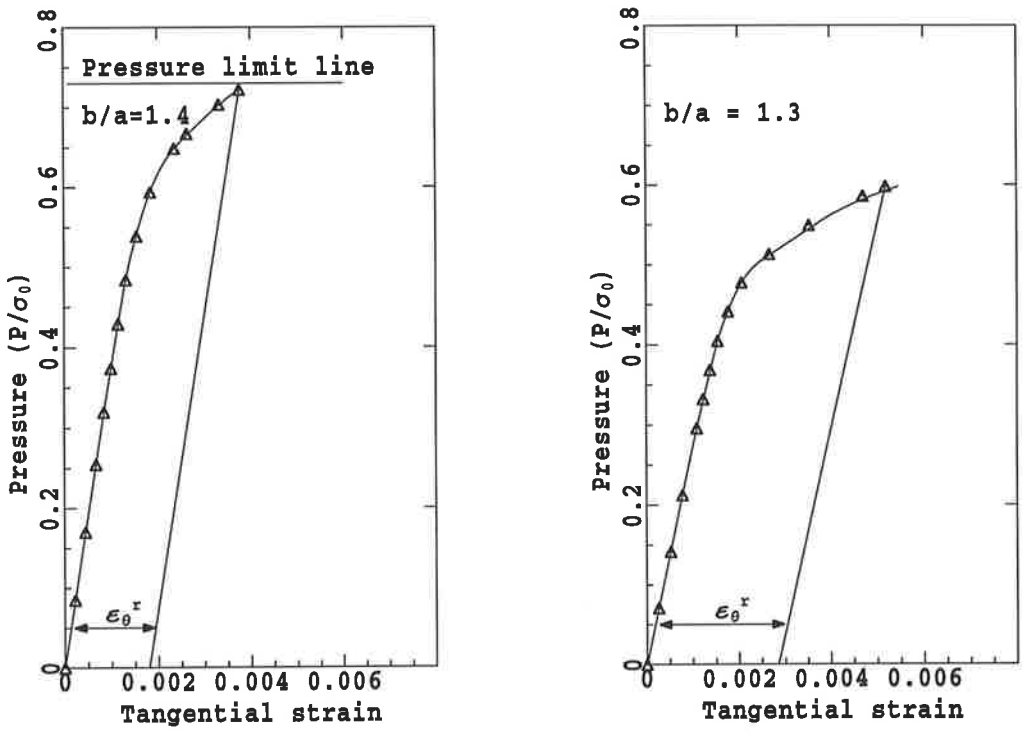

(a) (b)

Figure 5.8: Residual tangential strains resulted from unloading of two different test specimens

It is necessary to point out that the residual strains are not recorded immediately after releasing the internal pressure as it takes at least 5 minutes for the strain gauges to monitor a stabilized value of axial and tangential strains. Only stabilized values are considered for the analysis. Experimental values of the residual tangential and axial strains are recorded in table 5.8 located at the end of this Chapter. These results are compared with the predicted values of the axial and tangential strains by the proposed numerical procedure in Figure 5.9 (a) and (b). which shows good agreement between

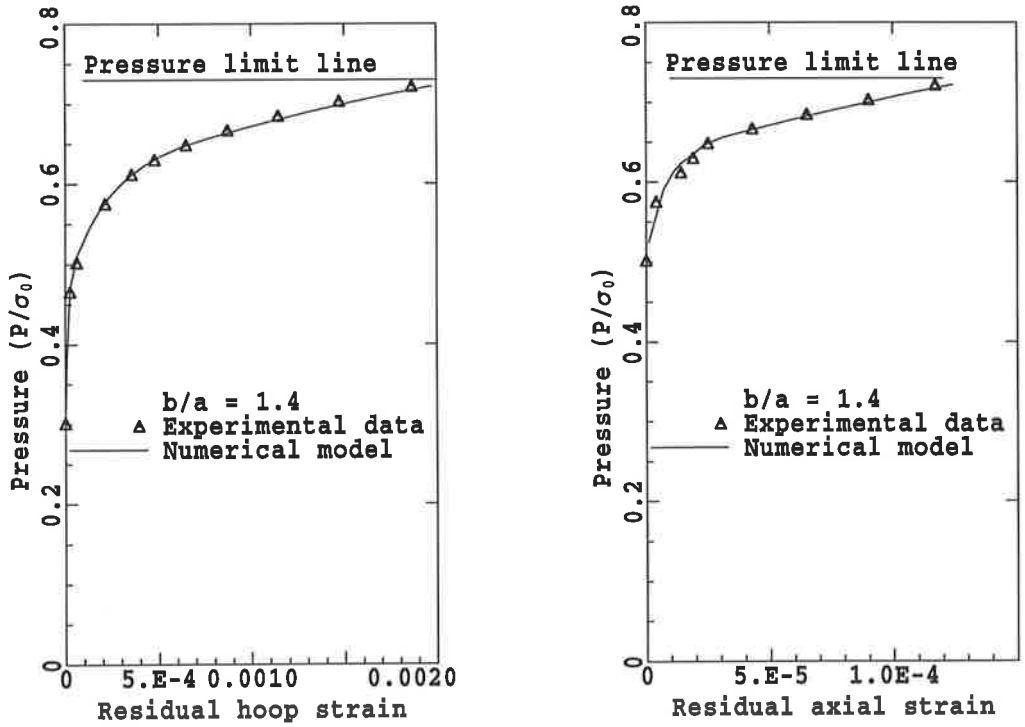

(a) (b)

Figure 5.9: (a) Variation of the internal pressure versus residual tangential strain; (b) Variation of the internal pressure versus residual axial strain

the experimental and numerical results. The proposed numerical procedure which is justified experimentally has been used to predict the thermoelastoplastic and residual stress distribution of thick walled cylinders the result of which is fully discussed in the next Chapter.

Table 5.5: Sample data obtained during half a second of loading-unloading test

Time (sec)	Length (mm)	Load (kN)	Strain (mm/mm)
0.52259994	0.000446614	0.353802145	0.0000034522
0.57259995	0.005617315	0.745849431	0.0000241369
0.62259996	0.005617315	1.000033975	0.0000327555
0.67259997	0.008202666	1.538560390	0.0000568876
0.72239995	0.015958721	2.003847122	0.0000724011
0.77259994	0.023714775	2.555298090	0.0000965333
0.82259995	0.023714775	3.063667059	0.0001206654
0.87259996	0.028885478	3.610810041	0.0001361789
0.92259997	0.034056179	4.110562801	0.0001672060
0.97259992	0.039226882	4.623239994	0.0001827195
1.02259994	0.044397585	5.101451397	0.0002016805

Table 5.6: Data obtained for the critical pressure investigation

P (V)	P (MPa)	P/σ_0	ε_θ^r (V)	ε_θ^r (mm/mm)
0.0112	13.298	0.0563	0.0000	0.000000000
0.0208	24.697	0.1046	0.0000	0.000000000
0.0318	37.758	0.1599	0.0000	0.000000000
0.0403	47.850	0.2027	0.0000	0.000000000
0.0461	54.737	0.2319	0.0000	0.000000000
0.0517	61.386	0.2601	0.0000	0.000000000
0.0573	68.0183	0.2882	0.0000	0.000000000
0.0627	74.4251	0.3154	0.0027	0.000001661
0.0681	80.8318	0.3425	0.0088	0.000005457
0.0735	87.2386	0.3697	0.0183	0.000011295
0.0789	93.6453	0.3968	0.0310	0.000019051
0.0843	100.0521	0.4239	0.0465	0.000028614
0.0897	106.4588	0.4511	0.0649	0.000039884
0.0951	112.8656	0.4782	0.0858	0.000052768
0.1005	119.2723	0.5054	0.1093	0.000067187

Table 5.7: Data obtained for pressure-expansion test of the third specimen

P (V)	P (MPa)	P/σ_0	ε_θ (V)	ε_θ (mm/mm)	ε_z (V)	ε_z (mm/mm)
0.0000	0.000	0.0000	0.0000	0.000000	0.0000	0.000000
0.0168	20.021	0.0848	0.0364	0.000224	0.0101	0.000053
0.0337	40.042	0.1697	0.0728	0.000448	0.0202	0.000105
0.0506	60.063	0.2545	1.0927	0.000671	0.0303	0.000158
0.0635	75.368	0.3194	1.3725	0.000843	0.0381	0.000198
0.0744	88.315	0.3742	1.6147	0.000992	0.0448	0.000233
0.0853	101.262	0.4291	1.8615	0.001144	0.0517	0.000269
0.0962	114.209	0.4839	2.1438	0.001317	0.0596	0.000310
0.1072	127.156	0.5388	2.5182	0.001547	0.0647	0.000336
0.1181	140.103	0.5937	2.9948	0.001840	0.0719	0.000374
0.1290	153.050	0.6485	3.8382	0.002358	0.0796	0.000414
0.1326	157.366	0.6668	4.2775	0.002628	0.0823	0.000428
0.1399	165.997	0.7034	5.4108	0.003324	0.0880	0.000458
0.1435	170.313	0.7217	6.1262	0.003764	0.0909	0.000473

Table 5.8: Data obtained for the residual tangential and axial strains

P (V)	P (MPa)	P/σ_0	ε_θ (V)	ε_θ (mm/mm)	ε_z (V)	ε_z (mm/mm)
0.0599	71.053	0.3011	0.0004	0.000000	0.0001	0.000000
0.0927	109.894	0.4657	0.0400	0.000025	0.0005	0.000000
0.0999	118.525	0.5022	0.0992	0.000061	0.0011	0.000000
0.1145	135.787	0.5754	0.3486	0.000214	0.0089	0.000004
0.1218	144.419	0.6119	0.5815	0.000357	0.0308	0.000014
0.1254	148.734	0.6302	0.7786	0.000478	0.0392	0.000019
0.1290	153.050	0.6485	1.0544	0.000648	0.0477	0.000025
0.1327	157.366	0.6668	1.4159	0.000870	0.0822	0.000043
0.1363	161.681	0.6851	1.8612	0.001144	0.1244	0.000065
0.1400	165.997	0.7034	2.3955	0.001472	0.1724	0.000090
0.1436	170.313	0.7217	3.0355	0.001865	0.2241	0.000117

Chapter 6

RESULTS AND DISCUSSIONS

6.1 Introduction

Results of the proposed analytical-numerical methods developed for the prediction of critical condition and the non-linear time-dependent and time-independent deformation of thick-walled cylinders are discussed in this Chapter.

Effect of variables such as radii ratio and temperature gradients on the critical pressure are investigated and the results are discussed. Progress of plastic zone with and without the effect of temperature gradient is investigated and the results of stress redistributions during plastic flow are discussed and interpreted in terms of physical nature of the problem. Results of residual stress distributions with and without the Bauschinger effect factor are compared and the effect of Bauschinger phenomenon on the predictions of reverse yielding is investigated and discussed.

Results obtained for the time-dependent creep stress and damage as well as the remain-

ing life evaluations of thick-walled tubes are also discussed in this Chapter. However, for a better understanding of the critical condition and the effect of plastic flow on the stress distributions of thick-walled cylinders, a brief discussion of the results obtained for the elastic stress distributions is considered here.

6.2 Elastic Stress Distribution

Elastic stress distributions of thick-walled cylinders are investigated using equations of elastic stresses (derived in Chapter 3) rewritten here as follows:

$$\begin{aligned} S_r^e &= F(\rho,\beta,\Theta) + G(\rho,\beta)P_i \\ S_\theta^e &= H(\rho,\beta,\Theta) + R(\rho,\beta)P_i \\ S_z^e &= M(\rho,\beta,\Theta) + N(\beta)P_i \end{aligned} \tag{6.1}$$

where S_r^e, S_θ^e and S_z^e are radial, tangential and axial stresses respectively. Taking into account that P_i is the dimensionless internal pressure and Θ is the non-dimensional temperature gradient, then the elastic stresses are the sum of a mechanical and a thermal stress component. If functions containing Θ are ignored in the above equation then the results are only mechanical stresses due to P_i written in the following form:

$$\begin{aligned} S_r^e &= G(\rho,\beta)P_i \\ S_\theta^e &= R(\rho,\beta)P_i \\ S_z^e &= N(\beta)P_i \end{aligned} \tag{6.2}$$

If the terms containing P_i are neglected in equation (6.1) then the remaining is only thermal stresses represented by the following equation:

$$\begin{aligned} S_r^e &= F(\rho, \beta, \Theta) \\ S_\theta^e &= H(\rho, \beta, \Theta) \\ S_z^e &= M(\rho, \beta, \Theta) \end{aligned} \tag{6.3}$$

In this study mechanical stresses resulted from the critical inner pressure and thermal stresses resulted from a thermal gradient of $\Delta T = 60^0 C$ as well as the combined effect of internal pressure and thermal gradient on the elastic stress distributions of thick-walled cylinders are considered. Critical pressure determines the maximum possible elastic stresses in the cylinder which will be compared with plastic stresses. A temperature gradient of $60^0 C$ can produce significant amount of thermal stresses and it will be shown that this can cause plastic yielding to start from the outside surface of the cylinder.

6.2.1 Mechanical Elastic Stress Distribution

Purely mechanical elastic stress distribution across the thickness of two different thick-walled cylinders due to their critical inner pressures are calculated from equation (6.2) and shown in Figures 6.1 (a) and (b). Radii ratio of these two cylinders are $\beta = 1.2$ (b/a=1.2) and $\beta = 2$ (b/a=2) which are the minimum and maximum radii ratio of test specimens used in experimental investigations. The critical inner pressure of these two cylinders are 0.176 σ_0 and 0.433 σ_0 respectively. It is evident from Figures 6.1

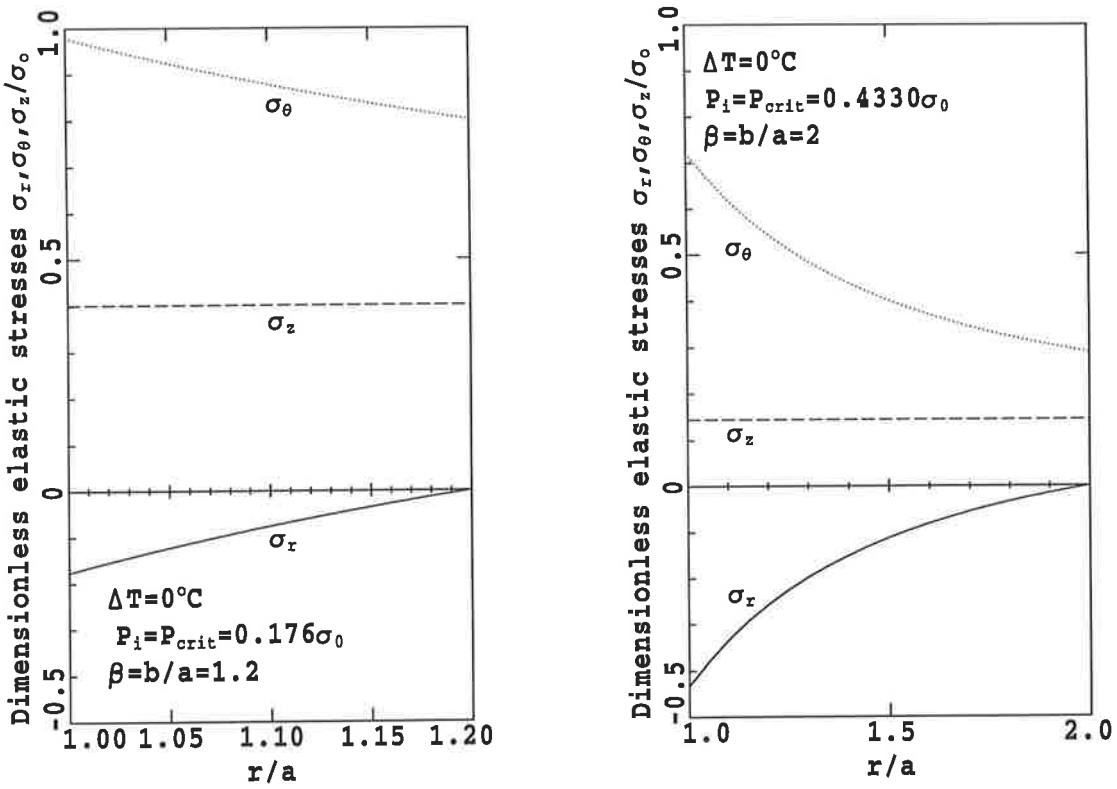

Figure 6.1: (a) Elastic stress distribution in thick-walled cylinders of radii ratio of $\beta = 1.2$ and; (b) $\beta = 2$.

(a) and (b) that the maximum tensile tangential stresses (σ_θ) and the maximum compressive radial stresses (σ_r) are located at the inside surface of the cylinders (r/a=1). The maximum compressive radial stresses at the inside surface of both cylinders are equal to their respective internal pressure which is expected from the boundary condition. Taking into account that the radial, tangential and axial stresses in a cylinder are the three principal stress components, then the maximum shear stress, which is

$(\sigma_\theta - \sigma_r)/2$, is also located at the inside wall of the cylinder (r/a=1). Therefore, in the absence of thermal gradient, it is expected that plastic yielding will start at the inside surface of the cylinder if internal pressure goes beyond the critical pressure. It is also evident from the Figures 6.1 (a) and (b) that the axial stress (σ_z) is the average of the radial and tangential stress components. If the stress distribution across the thickness of both cylinders are compared, a significant variation in radial and tangential stresses are observed for the cylinder of $\beta = 2$ while the other cylinder ($\beta = 1.2$) does not exhibit any significant variation. In fact, the cylinder of $\beta = 1.2$ is close to the margin of thin cylinders ($\beta = 1.105$, Roark (1975)) in which a uniform stress distribution have been recommended by Roark (1975) for design purposes.

6.2.2 Thermal Elastic Stress Distribution

Thermal elastic stresses resulted from a 60^0C thermal gradient due to an outward flow of heat in the same thick-walled cylinders are illustrated in Figures 6.2 (a) and (b). In the case of a pure thermal load, there is no tension or compression on the inside and outside surfaces of the cylinders. Therefore, the radial stresses (σ_r) are zero on the boundary surfaces which satisfy this condition. It is evident that the thermal tangential (σ_θ) and axial (σ_z) stresses are equal and compressive at the inside surface of the cylinders and are equal and tensile at the outer surface of the vessels. To describe this distribution, the cylinder can be considered as combination of a large number of thin cylindrical shells. The interior layers of the cylinder which are located at higher

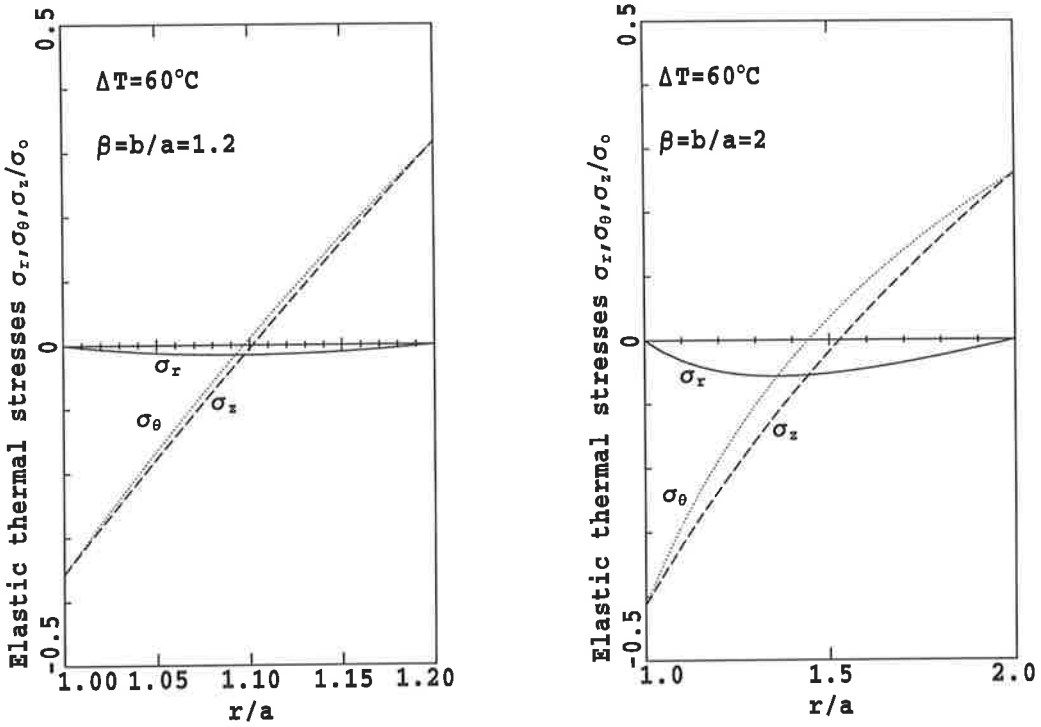

(a) (b)

Figure 6.2: (a) Elastic thermal stress distribution in thick-walled cylinders of $\beta = 1.2$ and; (b) $\beta = 2$.

temperatures than the outer layers would have more expansion due to their higher temperature if there was no constraint. However, the geometrical constraints imply that the surfaces normal to the axial and tangential directions must remain plane. It means, the higher expansion of the inside layers in axial and tangential directions are counteracted by the less expansion of the outer layers located at lower temperatures forcing the inner layers in compression while leaving the outer layers in tension until a self-equilibrium condition is reached. The boundary at both inside and outside sur-

faces is free of any external tension or compression and therefore, the expansion will be equal in both axial and tangential directions which will produce equal tangential and axial thermal stresses on both inside and outside surfaces. Finally, expansion in radial direction is dominated by the contractions induced by the Poisson's ratio due to the net expansions in axial and tangential directions, thereby leaving a small compressive radial stress throughout the cylinder wall.

6.2.3 Combined Mechanical and Thermal Elastic stresses

Combined effect of mechanical stresses due to the critical inner pressure and thermal stresses due to a 60^0C temperature gradient in the same thick-walled cylinders are shown in Figures 6.3 (a) and (b).

To understand these stress distributions one can superpose the pure mechanical stresses shown in Figures 6.1 on the pure thermal stresses shown in Figures 6.2 to obtain the combined effect of mechanical and thermal stresses. Highly compressive axial and tangential thermal stresses at the inside surface of the cylinders have decreased the effect of high tensile tangential mechanical stresses at these surfaces. Effects of thermal stresses at the outside surface of the cylinders are to increase the magnitudes of the tensile axial and tangential stress components. It is clear from Figures 6.3 (a) that, in this loading combination, the maximum shear stress $((\sigma_\theta - \sigma_r)/2)$ is located at the outside surface of the thinner cylinder ($\beta = 1.2$) which means plastic flow is more likely to start at the

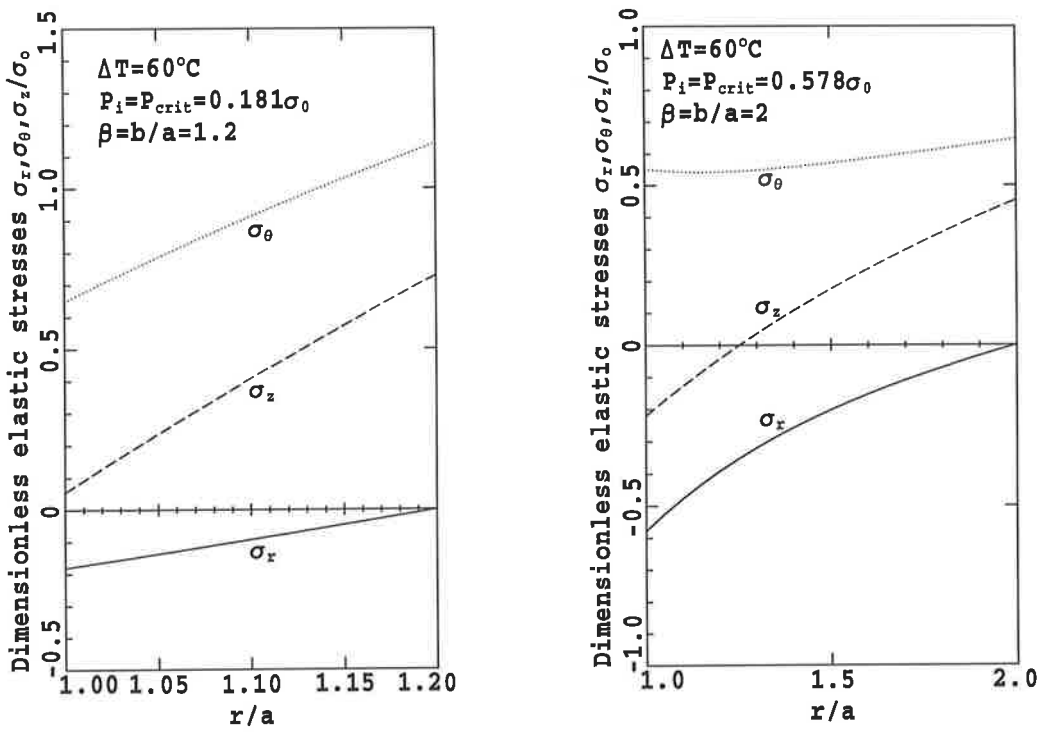

(a) (b)

Figure 6.3: (a) Elastic thermal stress distribution, (b) Elastic stress distribution in the presence of a thermal gradient

outside surface of this cylinder. This is not the case for the thicker cylinder ($\beta = 2$) as Figures 6.3 (b) indicates that the maximum shear stress is located at the inside surface of this cylinder.

The elastic stress distribution of thick-walled cylinders with and without the effect of thermal stresses is helpful in understanding the critical conditions. Critical conditions of thick-walled cylinders are investigated for a wide range of thermal gradients and

radii ratios which are important for practical applications and are discussed below.

6.3 Results from Critical Condition

The critical condition for many practical loading combinations and radii ratios is investigated using the critical condition equation rewritten here (discussed earlier in chapter 3) as follows:

$$A(\rho,\beta)P_i^2 + B(\rho,\beta,\Theta,P_o)P_i + C(\rho,\beta,\Theta,P_o) = 0 \tag{6.4}$$

Many variables such as ρ (dimensionless radius), β (radii ratio), Θ (dimensionless temperature gradient), P_o (dimensionless outer pressure) and P_i (dimensionless inner pressure) are involved in this equation. In general, any combination of these variables which satisfies the above equation can cause the critical condition for plastic yielding to occur anywhere in the cylinder wall thickness. In practice, most of the thick-walled cylinders are used as a pressure vessel component containing high internal pressure without any external pressure. For this reason, the effect of external pressure on the critical condition is not considered in this investigation. Therefore, there are four variables: P_i, ρ, β and Θ involved in the equation (6.4). Since the values of Θ, dimensionless temperature gradient does not indicate the magnitudes of temperature gradients, it was decided to use the specific values of temperature gradients in ^{0}C on all graphs and discussions rather than its non-dimensional representation Θ.

In a thick-walled cylinder with a uniform outward flow of heat Θ and β are constant and P_i and ρ are variables in equation (6.4). Then the minimum value of the inter-

nal pressure (P_i) satisfying the equation (6.4) is called the critical pressure and the value of ρ in which this minimum condition occurs is the starting surface of plastic yielding. For a better understanding of the critical pressure, the variable internal pressure (P_i), which satisfies equation (6.4), is plotted against ρ (dimensionless radius) at various constant temperature gradients from 0^0C to 100^0C and a constant radii ratio of $\beta = 1.2$ (Figure 6.4 (a)). This figure shows that at lower temperature gradients

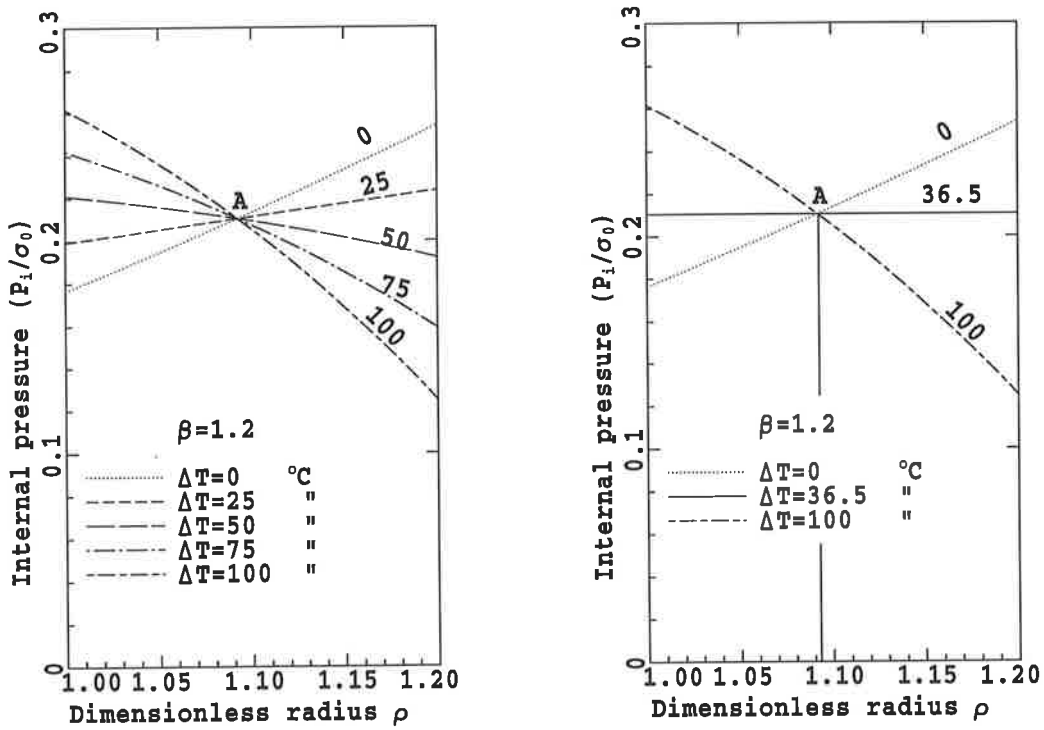

(a) (b)

Figure 6.4: (a) Internal pressure satisfying von Mises condition at various temperature gradients; (b) Critical condition for simultaneously yielding ($\rho = 1$ represents the inner surface and $\rho = 1.2$ represents outer surface of the cylinder).

minimum values of the internal pressure which satisfy the critical condition are located

at $\rho = 1$ which means yielding starts at the inner surface of this cylinder in these loading conditions. It can be interpreted that, in these loading conditions the combined effect of thermal and mechanical stresses is such that the Mises effective stress at the inside surface of the cylinder is greater than or equal to the material uniaxial yield stress and therefore, yielding starts at the inside surface of the cylinder. However, at higher temperature gradients, the minimum values of the internal pressure are located at $\rho = 1.2$ and therefore yielding starts at the outer surface of the cylinder for higher thermal gradients. In fact, the resultant effect of thermal and mechanical stresses is an effective stress which is greater than or equal to the yield stress at the outer surface of the cylinder in these loading conditions and therefore yielding starts at the outer surface of the vessel. These results are also consistent with the results of the elastic stress distribution already shown in Figure 6.1 (a) and 6.3 (a). It is also concluded from Figure 6.4 (a) that there is a loading condition in which the whole thickness of the cylinder will yield simultaneously. This loading condition is shown in Figure 6.4 (b) in which an internal pressure of $0.2105\sigma_0$ and a temperature gradient of 36.5 ^oC will cause the whole thickness to yield simultaneously. In this case, the combined effect of thermal and mechanical stresses is such that the effective Mises stress is uniform across the thickness and its magnitude is greater than or equal to the yield stress. A reference pressure($0.2105\sigma_0$), independent of temperature, has been identified in Figure 6.4 (a) and (b) which represents the critical pressure for the condition in which the whole thickness will yield simultaneously.

A similar plot of the internal pressure satisfying equation (6.4) for a cylinder of $\beta = 2$ is shown in Figure 6.5. The temperature gradients are the same as those selected for

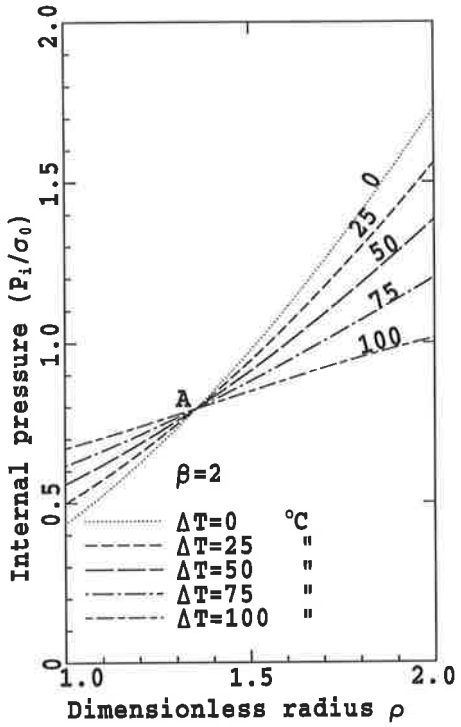

Figure 6.5: Internal pressure satisfying von Mises condition at the same temperature gradients in thick-walled cylinder of $\beta = 2$

Figure 6.4(a). The reference pressure can also be identified as the pressure of point "A" which indicates the critical pressure at which the whole thickness of the cylinder will yield simultaneously. Furthermore, the figure shows that, for the case of $\beta = 2$, yielding starts at the inner surface of the cylinder for all selected temperature gradients, because all minimum values of the internal pressure are located at $\rho = 1$ for the selected temperature gradients. This is also consistent with the results of the elastic stress distribution already shown in Figure 6.1 (b) and Figure 6.3 (b).

A computer program has been developed in this investigation to calculate the critical pressures for a wide range of practical temperature gradients and radii ratios (Appendix A). In order to show the effect of radii ratio on the critical pressure, the critical inner pressures at various temperature gradients, obtained from the computer program, are plotted against radii ratios in Figure 6.6. This figure shows that, except for a small

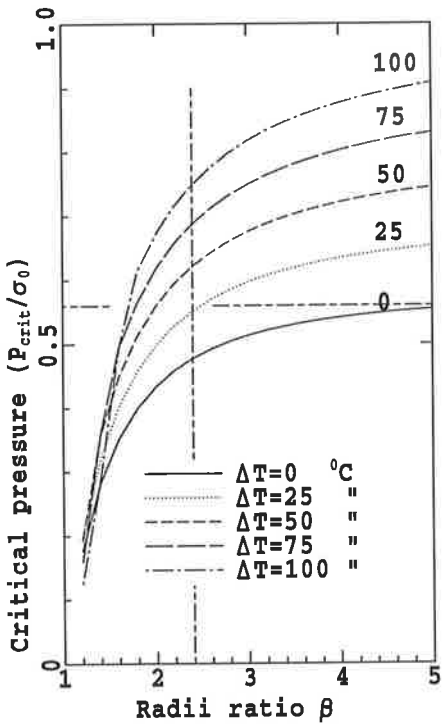

Figure 6.6: Critical pressures versus radii ratio for various temperature gradients

range of low radii ratios, higher temperature gradients tend to increase the critical pressure. An important and identical characteristic among all the above curves is that the changing rate of the critical pressure with respect to radii ratio substantially decreases with increasing radii ratio and finally approaches to zero where the curves approach to

a constant value. In the case of zero temperature gradient this constant value is shown in Figure 6.6 and is about 56% of the yield stress. It means that, if inner pressure is 56% of the yield stress, yielding is definitely to take place in the cylinder, no matter what the wall thickness of the cylinder is. In cylinders of lower radii ratios (ranging from 1.2 to 2.4), in which the changing rate of critical pressure is high, increasing the radii ratios of the cylinders significantly increases their critical pressures and improves their performances. While in cylinders of high radii ratios increasing the radii ratios of the cylinders do not substantially improve their performances.

As an example, let us consider a cylinder with an inner radius of 10 cm and an outer radius of 12 cm, the radii ratio of which becomes 1.2. The critical pressure of this cylinder in the absence of a thermal gradient is $0.1764\sigma_o$ (calculated from equation (6.4)). To improve the critical pressure of the vessel if we consider a cylinder with the same inner radius of 10 cm and an outer radius of 24 cm, the radii ratio of which is 2.4, twice of the previous vessel, then the critical pressure of the new improved vessel in the absence of thermal gradient is $0.4771\sigma_o$. Therefore, the critical pressure is improved to 2.7 times of the previous vessel which means a 170% increase in the critical pressure. However, if a cylinder with the same inner radius of 10 cm and the outer radius of 48 cm, twice of the second cylinder, is considered, then the critical pressure of the third cylinder is $0.5523\sigma_0$ which is just 15% more than the critical pressure of the second vessel. Therefore, increasing the radii ratio of the cylinder in this case does not substantially improves the critical pressure.

Effect of temperature gradient on the critical condition is also investigated and illustrated in Figure 6.7. In this figure critical pressures are plotted against temperature

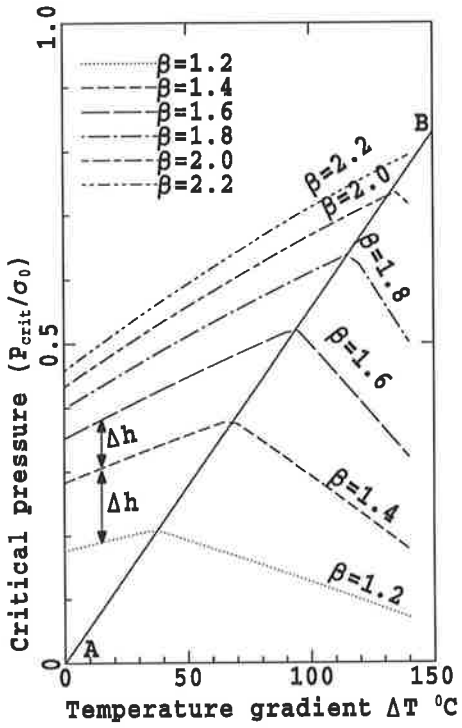

Figure 6.7: Critical pressures versus temperature gradient for a wide range of radii ratios.

gradients for a commonly used range of radii ratios. All the curves exhibit a maximum critical pressure which is, in fact, the previously identified reference pressure and belongs to the condition in which the whole thicknesses yield simultaneously. The locus of these maximum critical pressures is a straight line (AB) which divides the graph into two distinct regions. All points to the left of this straight line, AB (left region) represent conditions in which yielding starts at the inner surface of the cylinder. In

these loading conditions the combined effect of compressive thermal stresses and the mechanical stresses at the inside surface of the cylinder is such that the resultant Mises effective stress is greater than the yield stress in this region. Therefore, yielding starts at the inner surface. All points to the right of the dividing line (i.e, right region) belong to conditions in which yielding starts at the outer surface of the cylinder. It means, in these loading conditions the combined effect of thermal and mechanical stresses at the outer surface of the cylinder is such that the resultant Mises effective stress is greater than yield stress and therefore yielding starts at the outer surface of the cylinder. Along this border line between the regions the whole thickness yields simultaneously. This means, the resultant of thermal and mechanical stresses is a uniform effective stress across the thickness which is greater than or equal to yield stress and therefore the whole thickness yield simultaneously. Furthermore, it is evident from Figure 6.7 that the normal distances (Δh) between the lines of critical pressures for various radii ratios are decreasing with increasing radii ratio, while in general, critical pressure is increasing with increasing radii ratio. It has already been shown (in the example discussed earlier) that increasing the radii ratio at lower levels substantially increases the critical pressure of the cylinder, while this rate is low at higher radii ratios. Therefore, the higher normal distance Δh between the lines of critical pressures at lower radii ratios can be best described by the changing rate of critical pressure with respect to radii ratio (Figure 6.6). Critical pressures for a wide range of radii ratios from $\beta = 1.2$ to $\beta = 2$ are investigated experimentally and the method of experimentation has already been discussed in previous Chapter 5. The results are compared with the theoretical

values obtained from equation (6.4) as shown below in Figure 6.8. Experimental results are in good agreement with the theoretical values predicted by equation (6.4).

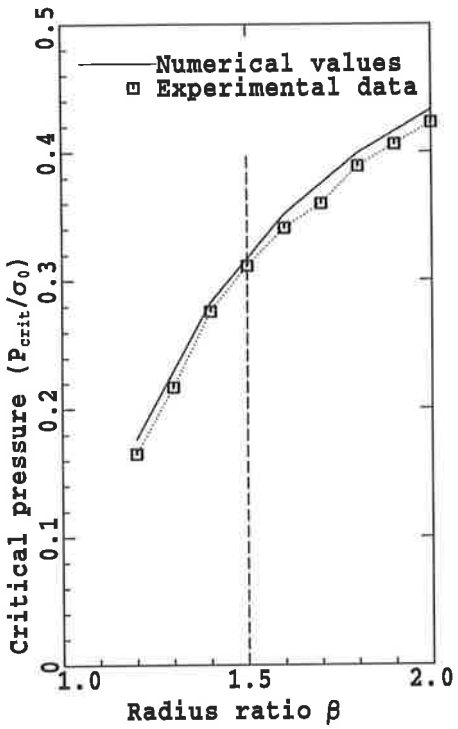

Figure 6.8: Comparison of the experimental critical pressures and numerical values

However, as the figure shows, for the cylinders of lower radii ratios the accuracy of the results is higher than the vessels with higher radii ratios. To describe this, a plot of the axial and tangential total strains (ε_z and ε_θ) of the minimum and maximum experimented radii ratios of $\beta = 1.2$ and $\beta = 2$ are shown in Figure 6.9. If the outer surface strains at points A and B in Figures 6.9 (a) and (b) are compared , the value of axial and tangential strains of the thinner cylinder ($\beta = 1.2$) are three times greater than the thicker one ($\beta = 2$), both of which are at the onset of yielding from their inside

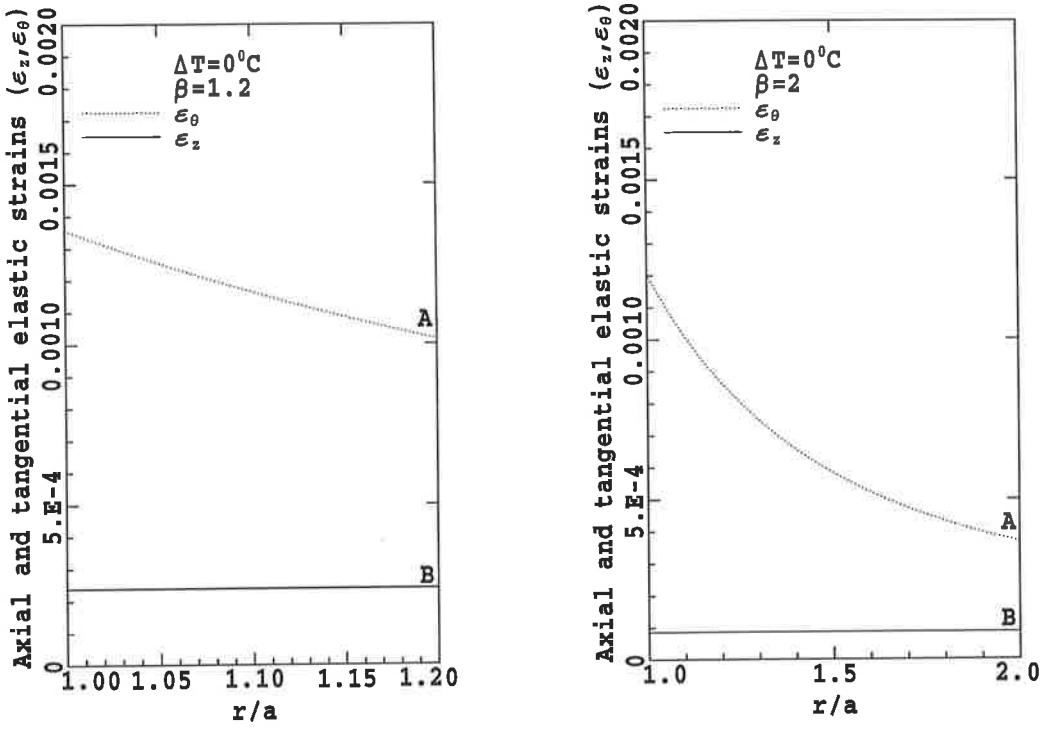

(a) (b)

Figure 6.9: (a) Axial and tangential elastic strain distribution across the thickness of the cylinders with $\beta = 1.2$ and; (b) $\beta = 2$

surfaces. Therefore, the measurements of strains at the outer surface of the thinner cylinderaremuch more accurate than the thicker one. So we must expect less accurate results for the critical pressure of thicker cylinders, because the prediction of critical pressure is based on the outer surface strain measurements.

If internal pressure greater than the critical pressure is applied to the cylinder, then plastic flow will occur in the cylinder wall. Numerical procedure for the computation

of plastic stresses and the subsequent residual stresses have lready been verified experimentally and the results obtained from this procedure are discussed in the next two sections. The result of plastic flow and the residual stresses can be obtained for any radii ratio, temperature gradient and internal pressure. However, the results reported in the next section is mainly discussed for a special radii ratio of $\beta = 2$ which is similar to a gun barrel. Then the results can particularly be used for the autofrettage of gun barrels since the real material properties including the Bauschinger effect phenomenon have been used to predict the elastoplastic and residual stress distributions as well as the onset of reverse yielding in this particular cylinder.

6.4 Plastic Stress Distribution

Results of the analytical-numerical method developed for the prediction of plastic stress and strains as well as the residual stress distribution are discussed in this section. It is difficult to verify the plastic stress and strain distribution throughout the wall thickness of the cylinder by direct measurements. Measurements of the internal surface deformation of the cylinder are also difficult because of the high applied internal pressure and the problems of cylinder sealing. The only way to verify the results of the proposed procedure is by measurements of the outer surface deformation of the cylinder while internal pressure is increasing monotonically. In this way experimental values of axial and tangential strains at the outer surface of the cylinder are measured by the strain gauges while the internal pressure is measured by a digital pressure transducer. Experi-

mental results of the pressure-expansion tests are compared with those values predicted by the numerical model. There is a good agreement between the experimental results and the numerical results predicted by the proposed procedure as it has already been shown in Figure 5.8 (a) and (b) in the previous Chapter. It is also justified to assume that the axial plastic strain is not zero as it has been assumed by all the previous investigators. It is true that the axial strain is small while comparing with the tangential plastic strain component; however, the experimental results show that it is not zero (Figure 5.8 (b)). Therefore the numerical model based on the generalized plane strain case, developed in this investigation, can be best satisfied by the experimental results. Elastoplastic stress distribution across the thickness of the cylinder is shown in Figure 6.10 (a). In order to compare the results of elastic-plastic and elastic cylinder, the elastic stress distribution of the same cylinder at the onset of plastic yielding is replotted with the same scale in Figure 6.10 (b). Let's first consider the effect of plastic flow on the stress distribution of the plastic region of the elastic-plastic cylinder. To justify this distribution, suppose the cylinder is made up of a large number of thin co-axial cylinders and the internal hydraulic pressure is increasing step by step using a high-pressure hydraulic pump (similar to the way we carried out the experiments). As a result of high internal pressure, which is more than critical pressure, a number of inside layers of the cylinder are in plastic regime, while the bulk of the cylinder material is still in elastic regime. Therefore, there is an elastic and a plastic region at the same time in the cylinder both of which have a different rate of deformation. Apart from the irreversibility of plastic strains in plastic regime, another important distinc-

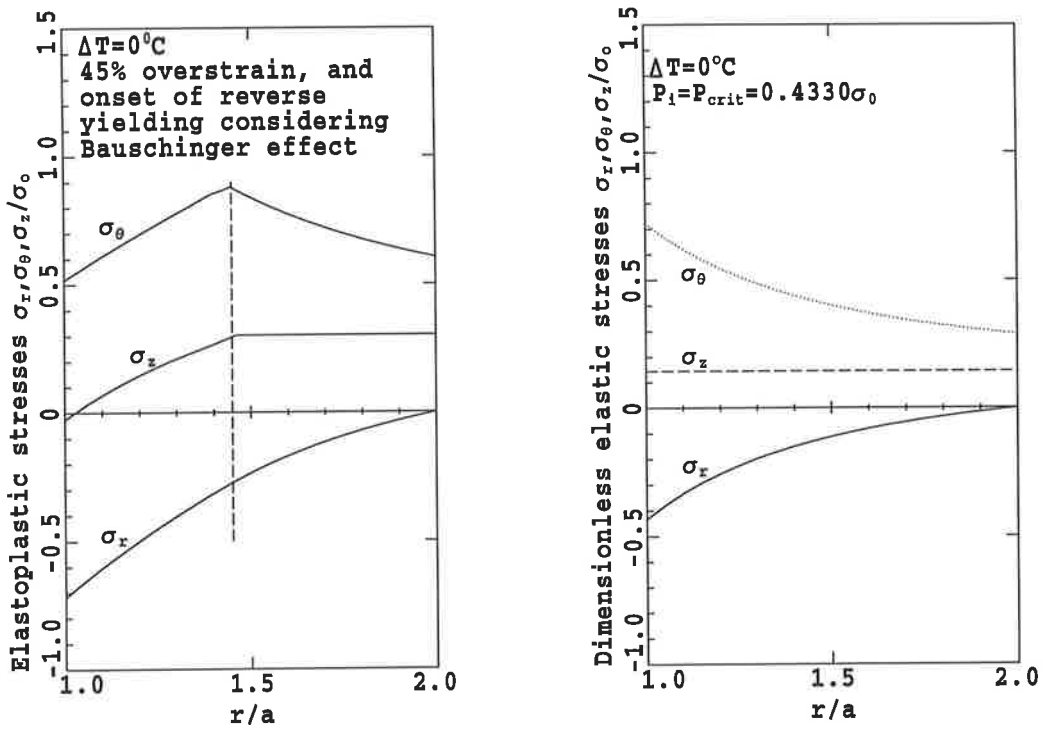

(a) (b)

Figure 6.10: (a) Elastoplastic stress distribution across the thickness of a 45% overstrained cylinder; (b) Elastic stress distribution of the same cylinder

tion between plasticity and elasticity is that the rate of deformation is much higher in the plastic regime than the elastic regime because the tangent modulus (slope of the stress-strain curve beyond the elastic limit) is less than the modulus of elasticity. It means, the inside layers of the cylinder must experience more deformation, in the tangential and axial direction, than if they would be in the elastic situation. This is not consistent with the elastic part of the cylinder. Deformations in the plastic and elastic region are not consistent, while the geometrical constraint imply that the planes

normal to the axial and tangential directions must remain plane. Therefore the plastic region, with higher rate of deformation will be pressed down by the dominant elastic region, decreasing its tensile stresses, while the elastic region itself will be stretched by the reaction force until a balance is reached and the geometrical constraint is satisfied. This can be clearly seen by comparing Figures 6.10 (a) and (b). At early stages of the plastic flow, when the bulk of the cylinder material is in elastic regime, then the elastic region will significantly hamper the higher deformation rate of the small plastic region at the inside layers. , thus decreasing the axial and tangential stresses significantly. That is why the tangential and axial stresses are decreasing at the inside layers. However, when the plastic region progresses more and more then the higher plastic deformation will dominate the lower elastic deformation. So stretching up the elastic layers and progressing toward the outer surface of the cylinder can be seen

Let's now consider the contribution of radial stresses in the elastic-plastic deformation of the cylinder. Obviously the radial compressive stress at the inside surface of the cylinder must always be equal to the internal hydraulic pressure and at the outer surface must be zero because there is no external pressure acting on the outer surface of the cylinder and is distributed throughout the wall between these two extremes. Therefore increasing internal hydraulic pressure beyond the critical values will increase the magnitude of the compressive radial stress at the inside surface of the cylinder. More compression in radial direction from the inside surface will give more lateral extension in the other two principal directions, axial and tangential, and giving more potential

for plastic flow to progress through the cylinder wall. Another important point here is that the lateral extension resulted from the radial compression is 72.4% higher in the plastic region than the elastic region. This may be more clear by comparing the non-linear incremental stress-strain relationship used to obtain the above solution and the elastic stress-strain relationship in the following form:

(a) **non-linear incremental stress-strain relationship:**

$$\begin{aligned} d\varepsilon_r^p &= \frac{d\varepsilon_p}{\sigma_e}[\sigma_r - \frac{1}{2}(\sigma_\theta + \sigma_z)] \\ d\varepsilon_\theta^p &= \frac{d\varepsilon_p}{\sigma_e}[\sigma_\theta - \frac{1}{2}(\sigma_z + \sigma_r)] \\ d\varepsilon_z^p &= \frac{d\varepsilon_p}{\sigma_e}[\sigma_z - \frac{1}{2}(\sigma_r + \sigma_\theta)] \end{aligned} \tag{6.5}$$

(b) **elastic stress-strain relationship:**

$$\begin{aligned} \varepsilon_r &= \frac{1}{E}[\sigma_r - \nu(\sigma_\theta + \sigma_z)] \\ \varepsilon_\theta &= \frac{1}{E}[\sigma_\theta - \nu(\sigma_z + \sigma_r)] \\ \varepsilon_z &= \frac{1}{E}[\sigma_z - \nu(\sigma_r + \sigma_\theta)] \end{aligned} \tag{6.6}$$

In equation (6.6), the Poisson's ratio ν defines the contribution of deformation in one principal direction to the deformation of the other two principal directions. The Poisson's ratio of the cylinder material is $\nu = 0.29$. Comparing with the above non-linear incremental stress-strain relationship (equation (6.5)), one can realize that, in plastic regime, the contribution of deformation in one direction to the lateral directions is given by the fraction $\frac{1}{2}$ or 0.5 instead of ν, which is 72.4% ($\frac{0.5-0.29}{0.29}$) higher than

elastic situation. Now it is clear that increasing the internal pressure of the cylinder will increase the compressive radial stress. More compression in radial direction will give more lateral extension to the axial and tangential directions thus giving further potential to plastic region to overrun the elastic region.

Elastic-plastic boundary can be easily identified in Figure 6.10 (a) as shown with a vertical dashed line. On the elastic-plastic boundary, the material is at the verge of yielding, the condition which has been used to locate the elastic-plastic interface. Elastic stress distribution in the elastic region of the elastic-plastic cylinder (Figure 6.10 (a)) is similar to the elastic stresses of an elastic cylinder (Figure 6.10 (b)). An important conclusion can be made here from the stress distribution pattern in the plastic region of the cylinder. Taking into account that the radial, tangential and axial stresses (σ_r, σ_θ and σ_z) are three principal stress components, then it can be concluded from the Figure 6.10 (a) that the maximum shear stress ($(\sigma_\theta - \sigma_r)/2$) is uniformly distributed throughout the plastic region of the cylinder.

For the case of a fully plastic cylinder (the stress distribution of which is shown in Figure 6.11) this uniform shear stress is distributed throughout the wall thickness of the cylinder. The initial elastic stress distributions shown in Figure 6.10 (b) are compared with the fully plastic stress distributions shown in Figure 6.11. As a result of plastic flow, the maximum tensile tangential and axial stresses are shifted from the inside surface of the cylinder to the outer surface of the vessel. The maximum compressive radial

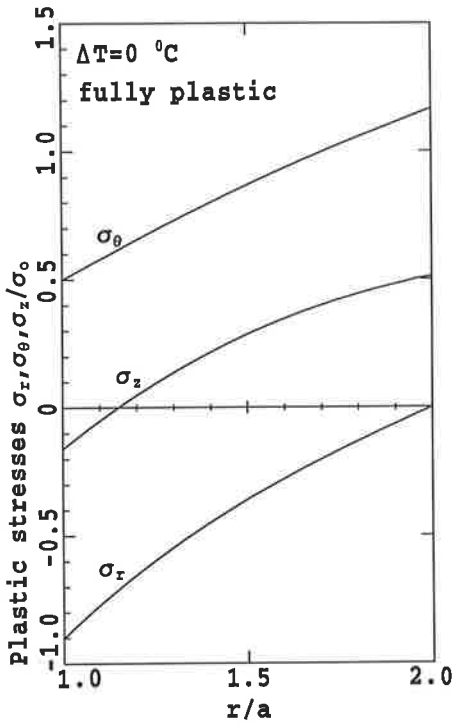

Figure 6.11: Fully plastic stress distribution across the thickness of the cylinder.

stress is always located at the inner surface of the cylinder and is equal to the internal pressure of the cylinder regardless of elastic or plastic condition. The axial stress is nearly the average of radial and tangential stress components in both elastoplastic and fully plastic condition of the cylinder.

To show the effect of plastic flow on each individual stress component, the tangential stress distributions at four subsequent loading steps from the initial elastic to fully plastic condition are plotted across the thickness of the cylinder (Figure 6.12). As a result of plastic flow in the cylinder, the tangential stress component at the inside

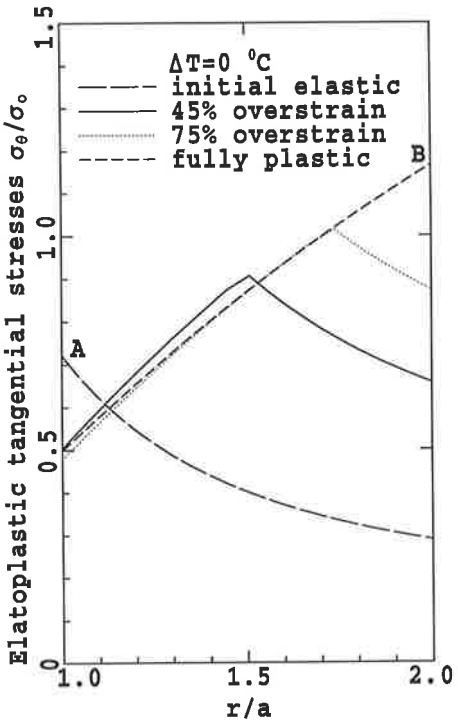

Figure 6.12: Elastoplastic tangential stress distributions across the thickness of the cylinder at four subsequent loading steps

surface of the cylinder is decreased comparing with its initial elastic situation. This has already been interpreted as the effect of geometrical constraint which imposes a balance between the higher plastic deformation rate of the internal layers and the lower elastic deformation rate of the outer layers. , and, pushing down the plastic layers, while stretching up the elastic layers. It is also interesting to compare the elastic tangential stresses in the elastic region of the elastic-plastic cylinder with their initial elastic distribution (Figure 6.12). Because of the higher deformation rate in plastic region and the effect of geometrical constraint, the elastic layers of the elastic-plastic

cylinder are stretched up and therefore the elastic tangential stresses in elastic-plastic vessel are higher than the initial elastic situation and ready to yield. The maximum tangential stress is located at the inside surface of the initial elastic cylinder (point A in Figure 6.12) while in the fully plastic condition it is located at the outer surface of the cylinder (point B in Figure 6.12). The maximum tangential stress at the outer surface of the fully plastic cylinder is very high in magnitude. It is almost four times of its initial elastic value and nearly twice of the initial maximum elastic tangential stress and 1.2 times of its material yield stress. Therefore, it is clear that any longitudinal crack at the outer surface of a fully plastic cylinder, normal to the tangential direction, can be quickly propagated throughout the thickness of the cylinder because of very high tensile tangential stress at the outer surface of the cylinder as well as its high tensile magnitude throughout the whole thickness.

Variations of radial stresses across the thickness of the cylinder during the process of plastic flow are shown in Figure 6.13. Radial stress must satisfy the boundary condition at the inner and outer surfaces, therefore it must be zero at the outer surface of the cylinder and must be equal to the internal pressure at the inner surface. It is distributed in compression between these two extremes. This distribution can be justified in two ways. First of all, there is a significant rise in magnitude of the radial stress component ($\Delta\sigma_r$ in Figure 6.13) as the plastic flow progresses from the initial elastic situation to a 45% overstrained condition. While this rise in radial stress is much less when plastic flow progresses from the 45% overstrained condition to the fully plastic

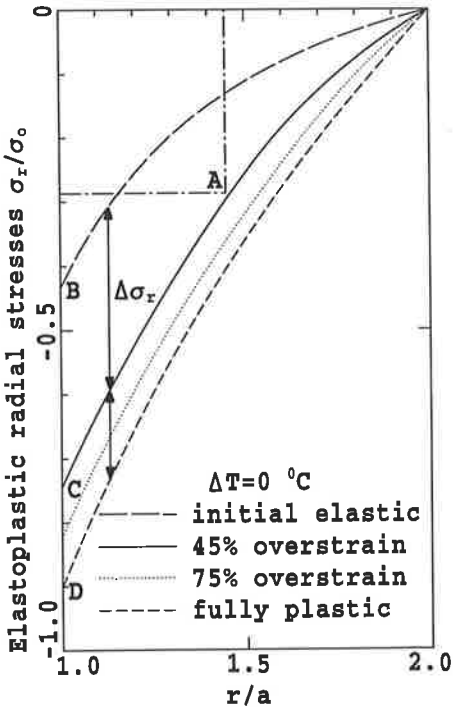

Figure 6.13: Elastoplastic radial stress distributions across the thickness of the cylinder during plastic flow

situation (Figure 6.13). It is because, at early stages of plastic flow in the cylinder, deformation is controlled by the dominated elastic region which is larger than the plastic region and therefore strongly hampers the progress of plastic zone. On the other hand, at early stages of plastic flow, the rate of pressure rise must be higher to overcome the elastic domination. Therefore, the radial stresses at the inner surface of tube shows a higher increase at early stages of plastic deformation. However, at later stages of plastic flow when deformation is controlled by the dominated plastic region, small increase of the internal pressure can have a significant progress of plastic zone. Furthermore

Figure 6.13 shows that a 32% increase in internal pressure from $0.42\sigma_0$ at point B to $0.74\sigma_0$ at point C (0.74-042=0.32), will cause 45% of the cylinder to deform plastically. But the remaining 55% elastic region will collapse to plastic regime just by a 16% rise in internal pressure from $0.74\sigma_0$ at point C to $0.9\sigma_0$ at point D (0.9-0.74=0.16), which is half of the previous growth in internal pressure. This can also be interpreted by the decreasing rate of internal pressure with progress of elastic-plastic boundary shown in Figure 6.14. The progress of plastic zone can be justified by considering point A in

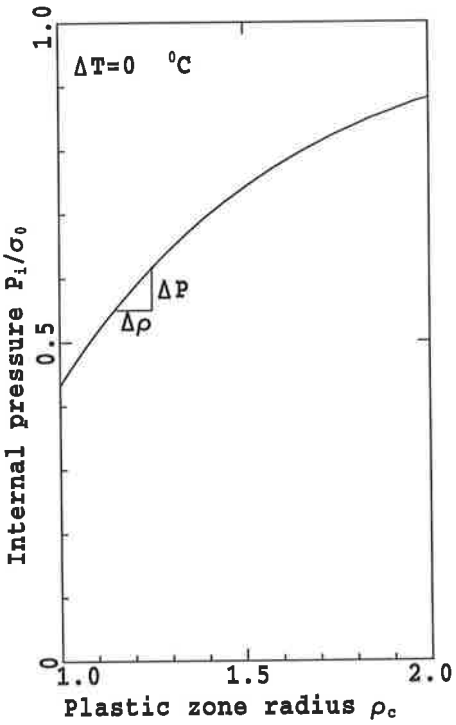

Figure 6.14: Variation of internal pressure versus elastic-plastic boundary

Figure 6.13 representing the elastic-plastic boundary of 45% overstrained cylinder. If 45% of the cylinder is yielded, the remaining 55% is in elastic condition. If we consider the remaining elastic cylinder as a new elastic cylinder with a radii ratio of 1.38

(2/1.45=1.38), then the critical inner pressure of this new cylinder is calculated from equation (6.1) and is equal to $0.28\sigma_0$. The radial stress at the elastic-plastic boundary (the value of radial stress at point A) must be equal to the critical pressure of this new elastic cylinder. And this is the case, because the radial stress at point A is also equal to $0.28\sigma_0$. Therefore, the radial stress distribution and the progress of plastic zone are justified.

Variation of elastic and fully plastic axial stresses across the cylinder thickness are compared in Figure 6.15. As a result of plastic flow, the axial stress component has

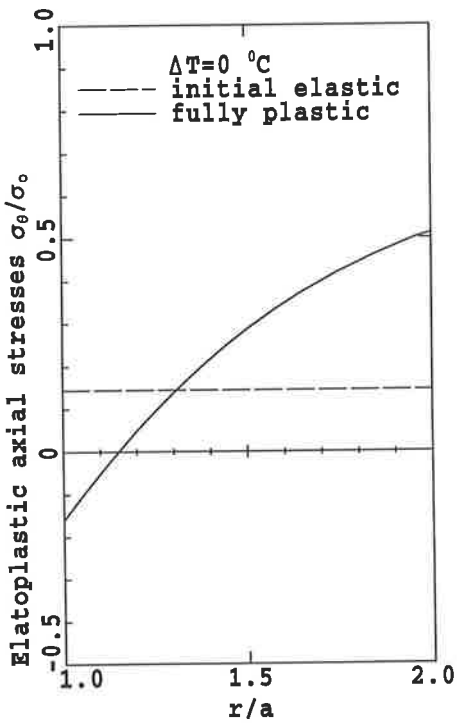

Figure 6.15: Elastic and fully plastic axial stress distributions across the thickness

been increased at the outer surface while its magnitude has been decreased at the inner

surface of the cylinder. The reason has already been discussed and will not be repeated here again.

Effects of temperature gradient on the plastic flow of thick-walled cylinders are discussed in the next section.

6.4.1 Effect of Temperature Gradient on Plastic Stresses

Effect of temperature gradient on the elastic stress distribution of thick-walled cylinders has already been discussed by superposing a pure thermal stress on the mechanical stress distribution resulted from an internal pressure. For understanding the result of plastic flow in the cylinders subjected to an internal pressure and a thermal gradient, one should consider the combined effect of thermal stresses and the mechanical stresses. Thermal stresses are resulted from an outward flow of heat with a 60^0C temperature gradient. It is clear that the inner layers of the cylinder which are located at higher temperatures should have a higher deformation than the outer layers of the cylinder, thus helping the inside plastic layers to progress much quicker. To show this, variation of internal pressure with progress of plastic zone across the thickness of the cylinder with and without the effect of a thermal gradient are compared in Figure 6.16. In the presence of a temperature gradient smaller pressure differential is needed for an equal progress of plastic zone. On the other hand, with an equal increase of internal pressure the cylinder with temperature gradient will develop a larger plastic zone than the cylinder without thermal gradients. Thermal stresses increase the critical pressure of

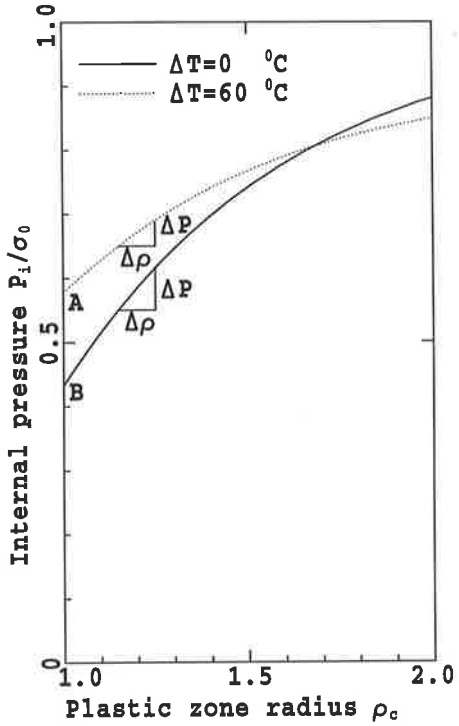

Figure 6.16: Progress of plastic zone across the thickness of the cylinder with and without the presence of a thermal gradient

the cylinder, as Figure 6.16 shows the critical pressure of the above cylinder is $0.578\sigma_0$ (point A) with the effect of thermal stresses and is $0.433\sigma_0$ (point B) without the effect of it. However, thermal stresses will facilitate the progress of plastic zone. To show the effect of thermal stresses on the plastic stress distribution of thick-walled cylinders, elastoplastic and fully plastic stress distributions of the same cylinder in the presence of a thermal gradient are shown in Figure 6.17 (a) and (b).

Let's first consider the case of a 45% overstrained condition shown in Figure 6.17 (a).

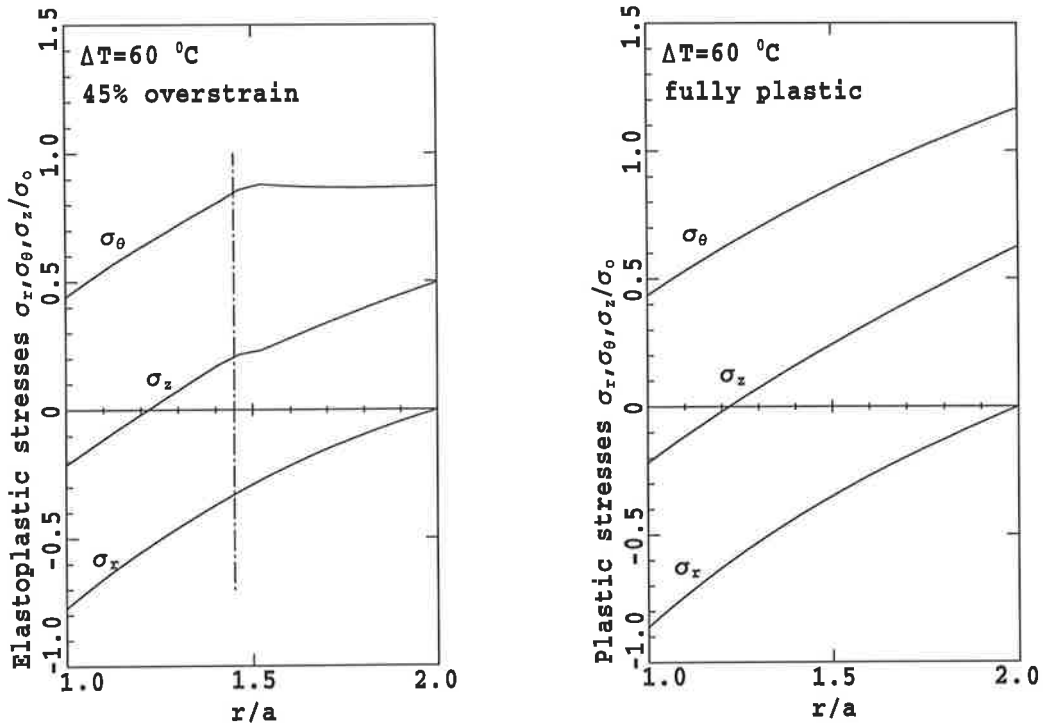

(a) (b)

Figure 6.17: (a) Thermoelastoplastic stress distribution across the thickness of a 45% overstrained cylinder; (b) Fully thermoplastic stress distribution across the thickness.

For a physical interpretation of the elastic-plastic stress distribution of this case, it is assumed that the cylinder is made up of a large number of thin cylinders free of constraint. Then the inner layers of the cylinder which are subjected to higher temperatures should have more expansion than the outer surface layers located at lower temperatures. Furthermore, yielding also starts at the inner layer of the cylinder in this loading condition as it has already been discussed. So the inside layers would have again more deformation than the outside elastic layers due to the higher deformation of

the plastic region. However, the geometrical constraint implies that the surface normal to the axial and tangential directions must remain plane. Thus the elastic region will be more stretched up while the plastic region will be more compressed down until a balance is obtained and the geometrical constraint is satisfied. Comparing this case, with the similar case in which there is no thermal stresses, Figure 6.10 (a), one can find that the axial and tangential plastic stresses with the effect of a thermal gradient are lower at the inside surface of the cylinder due to more constrainted compression on this region. It is pointed out that the combined effect of higher thermal expansion and higher plastic deformation at the inside layers of the cylinder will give a higher potential for plastic flow to progress toward the outer surface of the cylinder as it has already been discussed and shown in Figure 6.16. However, the plastic flow has the same effect of uniform maximum shear stress distribution throughout the plastic region of the cylinder. In the case of a fully plastic vessel the maximum shear stress is uniform throughout the thickness of the cylinder (Figure 6.17 (b)). Stress distribution in the elastic region of the elastoplastic cylinder is similar to an elastic cylinder with the combined effect of thermal and mechanical stresses which has already been discussed and shown in Figure 6.3 (b).

To show the effect of plastic flow on each individual stress component in the presence of a thermal gradient, radial and tangential stress distributions of four loading steps (from the initial elastic to fully plastic condition) are plotted across the thickness of the cylinder in Figure 6.18 (a) and (b). As the result of plastic flow, maximum tangential

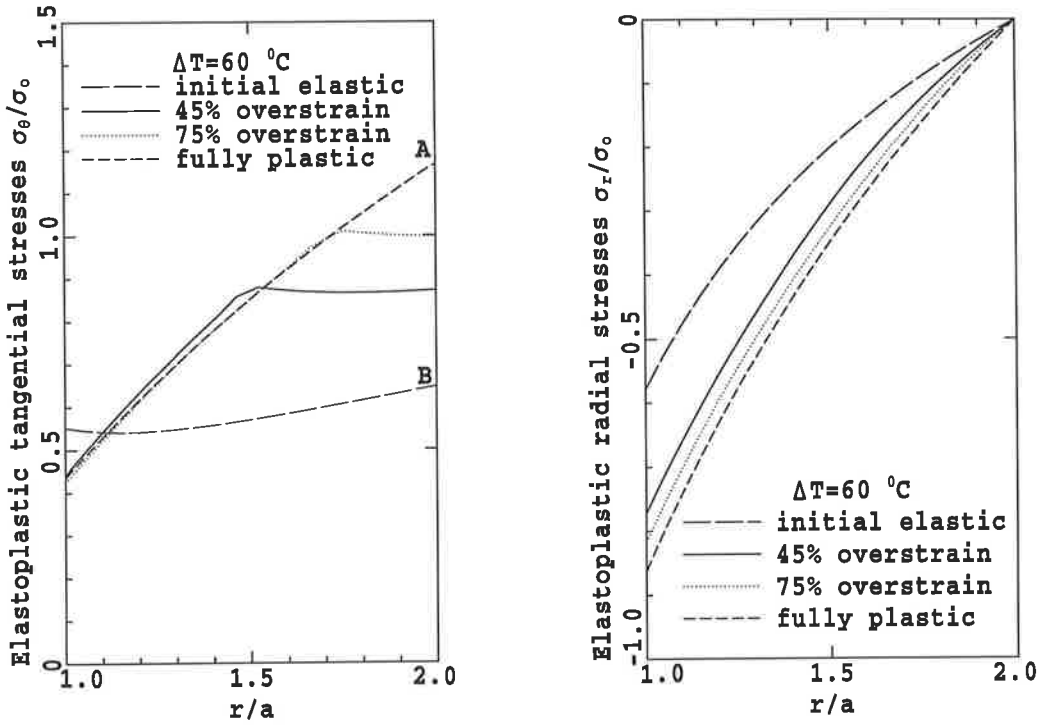

(a) (b)

Figure 6.18: (a) Thermoelastoplastic tangential stress distributions across the thickness; (b) Thermoelastoplastic radial stress distributions across the thickness.

stress at the outside surface of the fully plastic cylinder (point A)is almost twice of its initial elastic value (point B). Although there is a significant increase in the tangential stress component at the outer surface of the cylinder, but a small reduction of this component has occurred at the inside surface of the cylinder (Figure 6.18 (a)). However, the designers of pressure vessel must consider the existence of such a high tensile tangential stress which is distributed throughout the wall thickness of the cylinder, and the maximum of which is located at the outer surface.

Radial stress is equal to the internal pressure at the inside surface of the cylinder and is equal to zero at the outer surface of the cylinder which satisfies the boundary condition. In this case also, there is a substantial rise in magnitude of the radial stress component as the plastic flow progresses from the elastic situation to a 45% overstrained condition. While this is much less when plastic flow progresses from the 45% overstrained to the fully plastic condition. This can also be interpreted as the domination of elasticity at early stages of plastic flow and the plastic domination at later stages of plastic flow. However, in this case the growth in magnitude of the radial stresses between the subsequent loading steps is less than the case of zero thermal gradient shown in Figure 6.13. This is because, progress of plastic zone with the presence of thermal gradients is higher, as it has already been discussed and shown in Figure 6.16.
The residual stresses resulted from the subsequent unloading of the elastoplastic cylinders are considered in the next section.

6.4.2 Residual Stresses and the Bauschinger Phenomenon

If at any stages of plastic flow in a cylinder, the internal pressure is released, then there will be a distribution of residual stresses throughout the thickness of the vessel. In fact, the action of the elastic region to return back to its original configuration is counteracted by the plastic region which has developed irreversible plastic strains. On the other hand, the plastic region will be compressed by the elastic region until a

self-equilibrium condition is obtained throughout the cylinder thickness. Introducing a compressive region at the inside wall of a cylinder which is the location of a high tensile tangential stress resulted from an internal pressure (Figure 6.1 (b)) is beneficial to the life extension and durability of the cylinder. It is not only the compressive region at the inside wall of the cylinder which is beneficial, but also the higher elastic limit of the inside material which has taken advantage of the material's strain-hardening effect is another important privilege of the residual stresses. This can be more clear by comparing the initial yield stress at point A and the subsequent yield stress at points B and C of the material behaviour shown in Figure 6.19. The advantage of the compressive

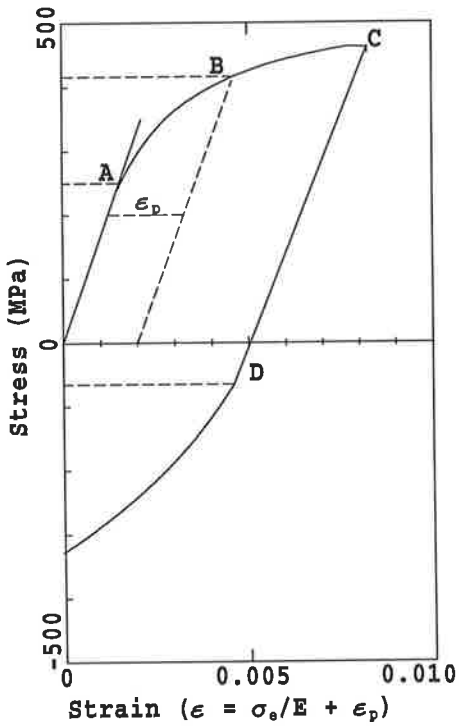

Figure 6.19: Initial and subsequent yield stress of the material

residual stresses will be decreased if reverse yielding occurs in the cylinder, as it has

been shown by Chen (1986). An important parameter which should be considered in reverse yielding predictions is the Bauschinger effect factor (BEF). The material's BEF is obtained experimentally as it has already been discussed in previous Chapter. To show the significant effect of the Bauschinger phenomenon on the residual stress distribution, residual stresses with and without the effect of Bauschinger phenomenon are compared in several figures in this section.

Residual stress distributions resulted from unloading of a 45% overstrained cylinder as well as the fully plastic vessel are shown in Figure 6.20 (a) and (b). Let's first consider the residual stress distribution shown in Figure 6.20 (a). Distribution of residual stresses can be clearly distinguished in the plastic and elastic regions of the elastic-plastic cylinder by the vertical dotted line shown on this figure. The residual tangential and axial stresses are highly compressive at the inner surface of the cylinder. This can be interpreted by the irreversibility of plastic strains in the plastic region of the cylinder. Suppose the cylinder is made up of a large number of thin cylinders free of constraint. When the load (internal pressure) is released in an elastic-plastic situation, the outer layers of the cylinder which are still in an elastic condition would return back to their original configuration while the inner layers of the cylinder which have developed plastic strains would not be able to return back to their original configuration. However, this incompatibility of deformation can not be tolerated by the geometrical constraint. The constraint imply that the planes normal to the axial and tangential directions must remain plane. On the other hand, the plastic region with larger deformation will be compressed down by the elastic region, while the elastic

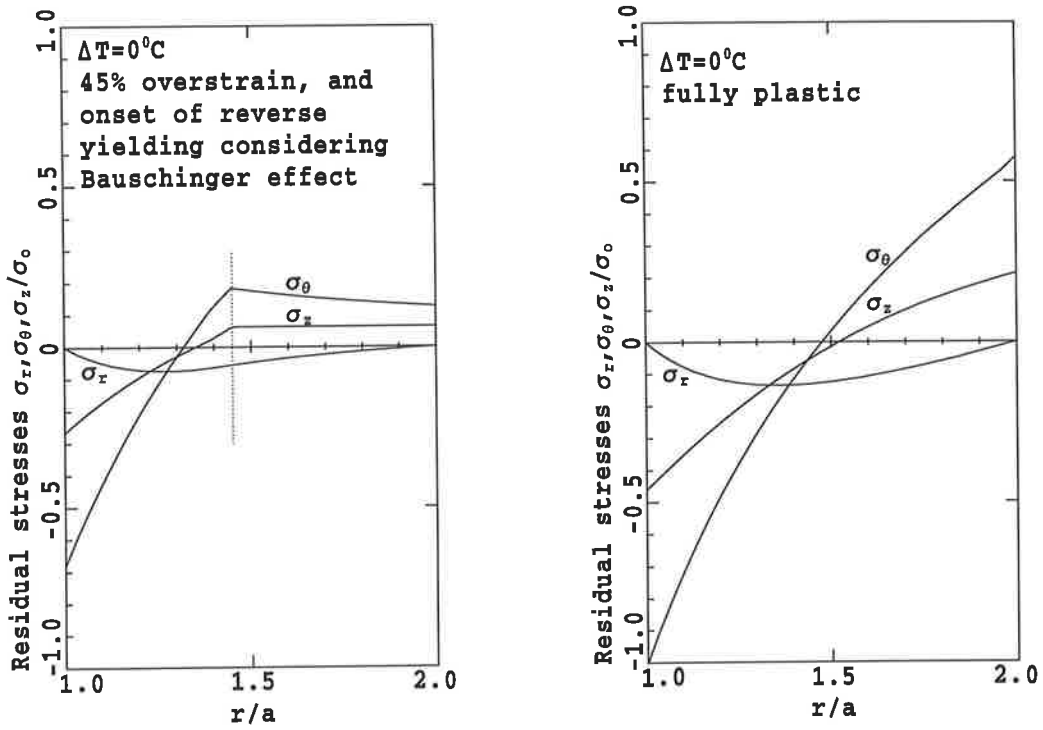

Figure 6.20: (a) Residual stress distribution at the onset of reverse yielding with the consideration of the Bauschinger effect factor; (b) Residual stress distribution by ignoring the Bauschinger effect factor.

region will be stretched up by the reaction force until a self-equilibrium condition is reached. For this reason, the inner layers of the cylinder which have developed more plastic strains during elastic-plastic deformation, will be highly compressive as shown in Figure 6.20 (a). Residual stress distributions in the elastic region of the cylinder is similar to the distribution of elastic stresses in an elastic cylinder.

The residual radial stress must satisfy the boundary condition of an unloaded vessel. There is no internal and external pressure on the inner and outer surfaces of an unloaded cylinder and therefore the radial stress will be zero on both surfaces. It is compressive throughout the thickness the reason of which will be discussed later in this section.

In the light of such a residual stress distribution, it is clear that the inner surface of the cylinder is more likely to yield because the maximum value of shear stress $((\sigma_r - \sigma_\theta)/2)$ is located at this surface. If the effective Mises stress at the inner surface of the cylinder becomes equal to the reverse yielding stress of the material then the inner surface of the cylinder is at the onset of reverse yielding. The reverse yielding stress depends on the BEF. The BEF depends on the amount of effective plastic strain in the plastic region of the cylinder as it has already been formulated in Chapter 1 and represented by the following continuous function.

$$BEF = 1.0170029 + 0.36592732(\varepsilon_p\%) - 0.0025343135(\varepsilon_p\%)^3 - 0.97738304(\varepsilon_p\%)^{0.5} \tag{6.7}$$

The BEF is variable during loading history of the cylinder, because the amount of effective plastic strain is variable for the plastic region of the cylinder during loading. Variation of BEF at the inner surface of the cylinder during progress of plastic zone is shown in Figure 6.21. For the particular case of 45% overstrained condition the magnitude of BEF at the inner surface of the cylinder is represented by its value at point E in this figure. Variation of the BEF at the inner surface of the cylinder has been calculated during the loading history and the reverse yielding has been investigated

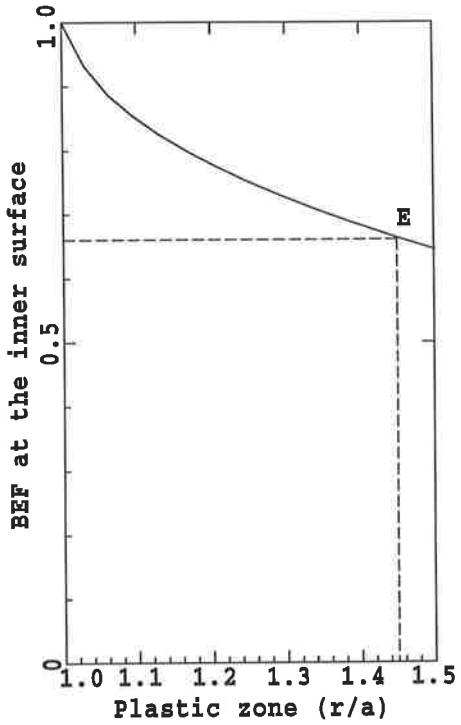

Figure 6.21: Variation of the Bauschinger effect factor at the inside layer of the cylinder versus the location of elastic-plastic boundary

using the von Mises criterion as follows:

$$(S_r^r - S_\theta^r)^2 + (S_\theta^r - S_z^r)^2 + (S_z^r - S_r^r)^2 = 2(BEF)^2 \tag{6.8}$$

This equation has been satisfied for the residual stresses obtained from 45% overstrained condition. Therefore, it is concluded that the residual stress distribution obtained from 45% overstrained condition (Figure 6.20 (a)) is at the onset of reverse yielding at the inside surface of the cylinder.

If the Bauschinger effect factor is ignored, even residual stresses obtained from the fully

plastic cylinder (Figure 6.20 (b)) are not at the onset of reverse yielding with all the same that their magnitudes are nearly twice of the 45% overstrained condition.

Variations of residual tangential stresses obtained from three different overstrained conditions are shown in Figure 6.22 (a) and (b). Figure 6.22 (a) representing progress of

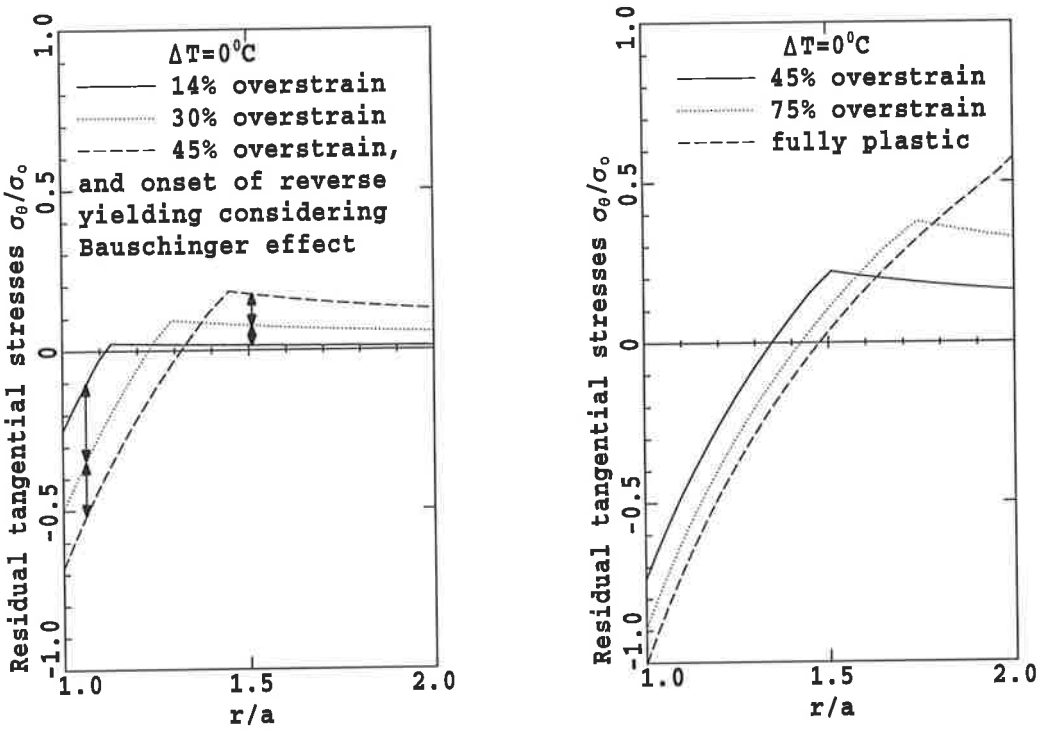

(a) (b)

Figure 6.22: (a) Residual tangential stress distribution at the onset of reverse yielding with the consideration of the Bauschinger effect factor; (b) Residual tangential stress distribution by ignoring the Bauschinger effect factor.

residual tangential stresses with considering the Bauschinger effect factor. In this case the maximum permissible tangential component of residual stresses at the onset of re-

verse yielding, which belongs to a 45% overstrained condition, is shown with a dashed line in this figure. As it is expected, when the plastic region progresses more and more during loading, then the subsequent residual stresses will also be more compressive at the inside layers of the cylinder and will be more tensile at the outer layers. This is because, there will be more incompatibility of deformation between the inner plastic region and the outer elastic region which implies more constraint compression on the inside layers and thus more stretching of the outer layers of the cylinder. However, if the normal distances between the two subsequent residual stress distribution shown in Figure 6.22 (a) are considered, then it can be concluded that the growing rate of compressive tangential stresses at the inside layers of the cylinder is decreasing, while it is increasing in the elastic region with progress of plastic zone. This can be interpreted as the domination of plastic deformation at later stages of plastic flow in the cylinder and thus a decreasing rate of deformation incompatibility between the inside and outside layers. The elastoplastic interface is clearly distinguishable in these figures where the slope of the curves change significantly. Residual stress distribution in the elastic region is similar to an elastic cylinder stress distribution. If the Bauschinger effect factor is ignored then the elastic residual tangential stresses at higher overstrained conditions are shown in Figure 6.22 (b). In this case the subsequent residual stresses of a fully plastic cylinder are not at the onset of reverse yielding as it has already been discussed. Therefore, there will be a great mistake in the residual stress distributions if the Bauschinger effect factor is ignored.

Residual radial stresses of the same overstrained conditions are compared in Figure 6.23 (a) and (b). Residual radial stresses are zero at the inside and outside surfaces of the

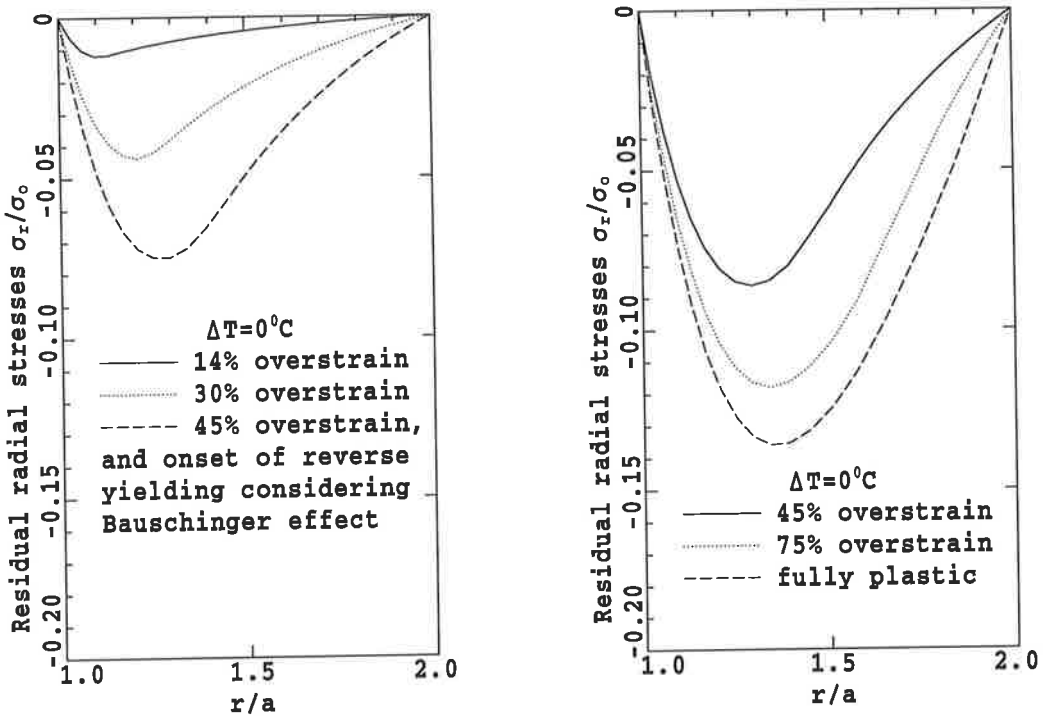

(a) (b)

Figure 6.23: (a) Residual radial stress distribution at the onset of reverse yielding with the consideration of the Bauschinger effect factor; (b) Residual radial stress distribution by ignoring the Bauschinger effect factor.

cylinder because there is no internal or external pressure on the cylinder surfaces, after the load is released. These residual radial stresses are all compressive throughout the cylinder thickness. These compressive stresses can be described in the following way. When an elastic-plastic cylinder is unloaded, it will never return back to its original configuration because of the irreversible plastic strains. Therefore, the net deforma-

tion is extension in axial and tangential directions. Extension in these two directions will cause contraction on the lateral radial direction proportional to the Poisson's ratio. Therefore the resultant residual radial stresses will be compressive throughout the whole thickness of the cylinder for all unloading stages.

The maximum permissible elastic residual radial stress with the Bauschinger effect is shown in Figure 6.23 (a) with a dashed line. This relatively small magnitude of residual radial stress belongs to a condition which is at the onset of reverse yielding because of the Bauschinger effect factor. While, higher magnitudes of residual radial stresses (Figure 6.23 (b)) are not even at the verge of reverse yielding because of ignoring the Bauschinger effect factor. Therefore, Bauschinger effect factor has a significant effect on the prediction of reverse yielding in thick-walled cylinders. A plot of critical pressures for direct and reverse yielding with the effect of Bauschinger phenomenon for prediction of reverse yielding in the most commonly used radii ratios is shown in Figure 6.24. The normal distance between these two extreme lines of direct and reverse critical pressures (ΔP_{max} in Figure 6.24) is the maximum permissible range of pressure growth beyond which reverse yielding will take place in the cylinder wall.

In the next section the results obtained for the time-dependent creep stresses and the subsequent creep damages as well as the remaining life evaluations are discussed.

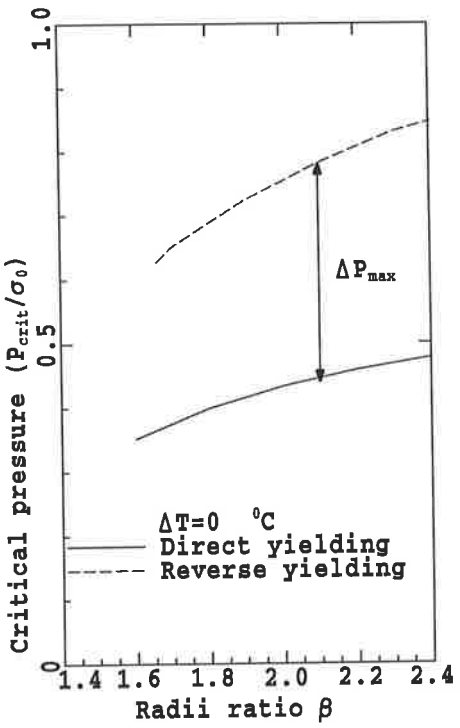

Figure 6.24: Critical pressures for direct and reverse yielding

6.5 Results of Creep Stress and Damage Analysis

6.5.1 Introduction

Thick-walled tubes are often used to withstand the high operating pressures and high temperatures of power stations. In such an environment deformation of the tube is dominated by the time-dependent process of creep. During normal operation of the plant the temperature between the inner and outer surfaces of the tube reach a steady state condition similar to the assumption which has been made in the formulation of the creep problem in this investigation. Results of the proposed analytical-numerical

model which has been developed in this investigation for the computation of creep stress and damage histories are discussed in this section. The history of creep stresses and creep damages of thick-walled tubes are important in the life assessment and for the routine inspection of high-temperature high-pressure tubes to avoid unexpected failures.

6.5.2 Creep Stress Redistributions

Results of the creep stress redistributions are presented for a boiler header tube with a radii ratio of $\beta = 1.65$ (inside diameter is 508 mm and outside diameter is 304.8mm, $\beta = 508/304{=}1.65$). Internal pressure is 20 MPa which is the design pressure of this component (operating pressure is 17.24 Mpa (Ripley (1995)). Internal and external temperatures are 557^0C and 550^0C respectively. Through-thickness variation of initial elastic and distribution of stresses after 317 months (26.4 years) are shown in Figure 6.25 (a). It is evident that the variation of radial and axial stresses with time are not significant, while the major stress redistribution occurs for the tangential stress component. It is clear from the Figure 6.25 (a) that the creep process is directed toward the generation of a uniform maximum shear stress distribution across the thickness of the tube. Redistributions of tangential creep stress across the thickness of the tube at two progressive steps of creep process are shown in Figure 6.25 (b). The tangential stress component at the inner surface of the tube has decreased while its magnitude at the outer surface of the tube has increased substantially during the process of time-

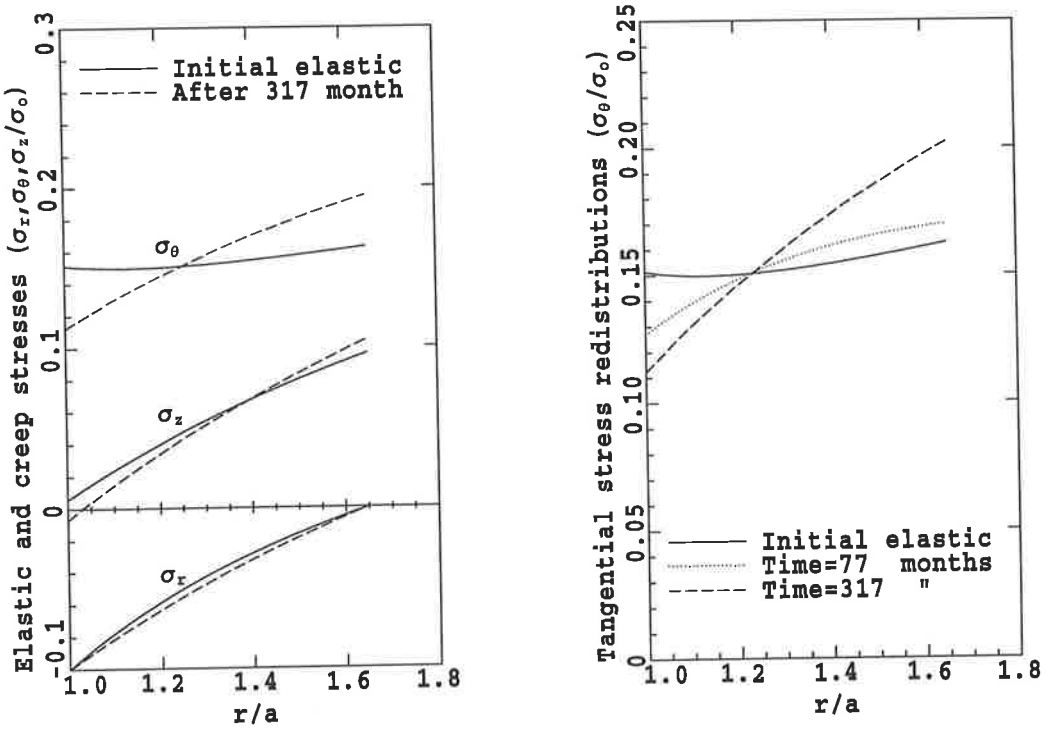

(a) (b)

Figure 6.25: (a) Initial elastic and distribution of creep stresses after 317 months; (b) Tangential creep stress redistributions

dependent creep deformation. This is because, the maximum effective stress (to be discussed later in this section) and the maximum temperature are both located at the inside surface of the tube and therefore the inside layers of the tube have a higher deformation rate. This higher deformation rate is not consistent with the lower rate of deformation at the outer layers of the tube. However, since planes normal to the tangential direction remain plane during deformation it can be concluded that the inner

layers will be pressed down while outer layers will be stretched up resulting the above stress redistribution. The maximum tangential stress at the outer surface of tube is nearly twice of its minimum value located at the inside surface of the tube. Through-thickness variation of radial and axial stresses at some stages of creep progress are shown in Figure 6.26 (a) and (b). Radial stress at the inner and outer surfaces remains

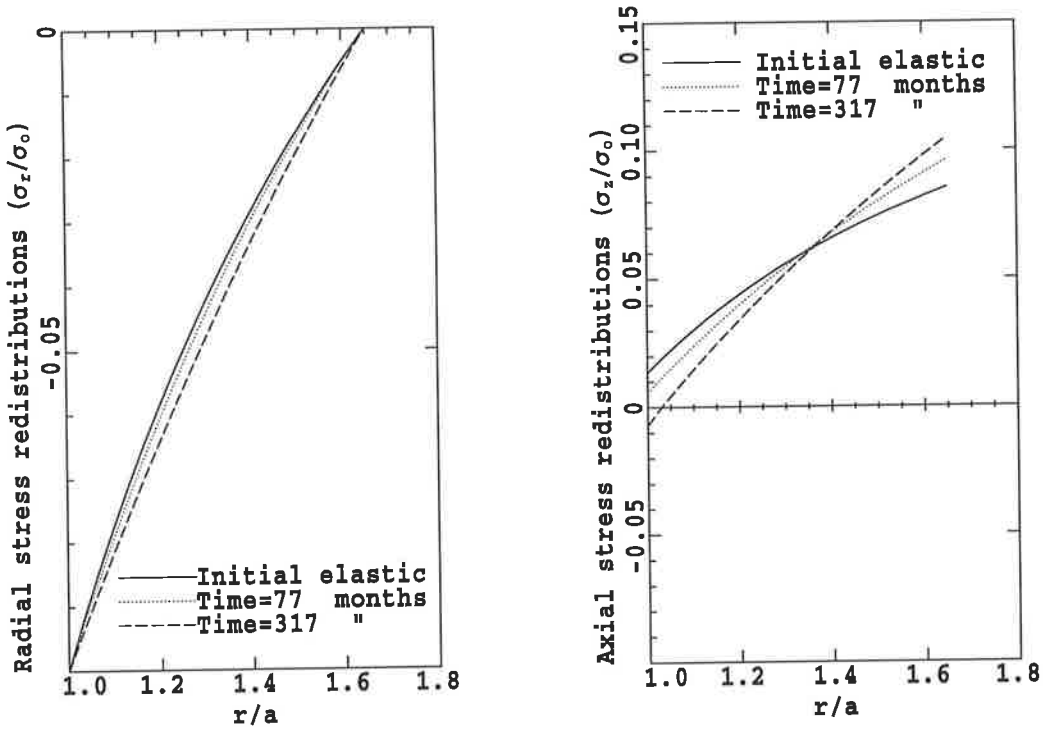

(a) (b)

Figure 6.26: (a) Radial stress redistributions; (b) Axial stress redistributions.

unchanged due to the constancy of the pressure on the boundary surfaces while its curvature throughout the thickness decreases and approaches to a linear distribution due to the multi-axial creep deformation of the tube. The axial stress redistribution is not also significant and its redistribution can be interpreted with the higher deformation

rate of the inside layers of the tube and the geometrical constraint.

6.5.3 Effective Stress Histories

One of the major problems in the tube life assessment is that the stresses are changing with time throughout the thickness of the tube. If the thick-walled tube is subdivided into a large number of thin cylindrical layers, then any layer of the tube continuously experiences a variable stress field with time. On the other hand, each layer of the tube is at a different stage of creep which depends on its temperature and stress level. A variable multi-axial state of stress exists at each layer of the tube, while the material's creep data are obtained from the uniaxial creep tests. Therefore it is necessary to select an effective stress in this multi-axial stress state to identify the creep situation of each layer of the tube. In this study, the Mises effective stress is selected which is also adopted by the ASME Code Case N47. Variations of effective stresses through the thickness of the cylinder during progressive steps of redistributions are shown in Figure 6.27. at some progressive steps of redistributions is shown in Figure 6.27.

Effective stress histories for all layers of the tube are computed using the history of stresses as the creep process is progressing with time. Effective stress histories of the inner, middle and outer layers of the tube are shown in Figure 6.28. At initial stage of the creep process, maximum effective stress is located at inner surface of the tube while its minimum value is located at the outer surface of the tube. As a result of stress redistribution, maximum effective stress at the inner surface of the tube is decreasing and the minimum effective stress at the outer surface of tube is increasing with time. Consequently a reference time has been identified in which the effective stresses at the

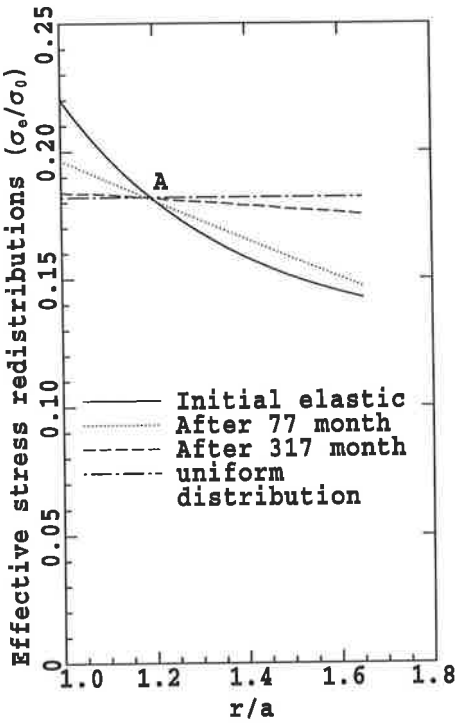

Figure 6.27: Effective stress redistribution from the initial elastic to stationary creep

inner, middle and outer layers of the tube are identical (point "A" in Figure 6.28 (a) and (b)). On the other hand, at this reference time the effective stress is uniform throughout the tube wall as it has already been shown in Figure 6.27. At this reference time the radial, axial and hoop stress distributions become parallel throughout the tube wall thickness. It means that the maximum shear stress distribution also becomes uniform throughout the thickness. After this reference time the maximum effective stress will be located at the outer surface of the tube. Therefore, this reference time is a turning point in creep stress redistributions. The reference time depends on the internal pressure and temperature gradient. It has been found in this investigation

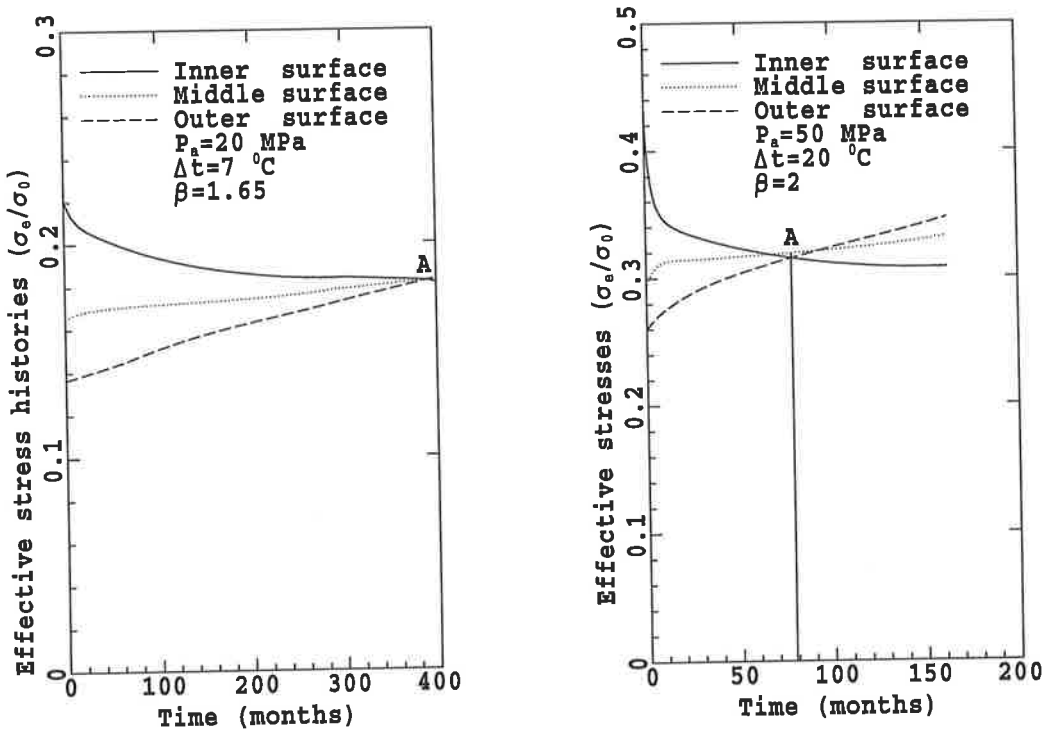

(a) (b)

Figure 6.28: Inner, middle and outer surface effective stress histories for two different tubes and loading conditions.

that this reference time existed for all different loading conditions and radii ratios (two different cases of which are shown in Figure 6.28). Effect of internal pressure on the reference time is investigated and the results are shown in Figure 6.29. The reference time significantly decreases with increasing internal pressure. When the tube is loaded with the critical inner pressure, the reference time is less than four months (116 days), while its magnitude is about 132 months (11 years) when internal pressure is reduced to 40% of the critical pressure (Figure 6.29).

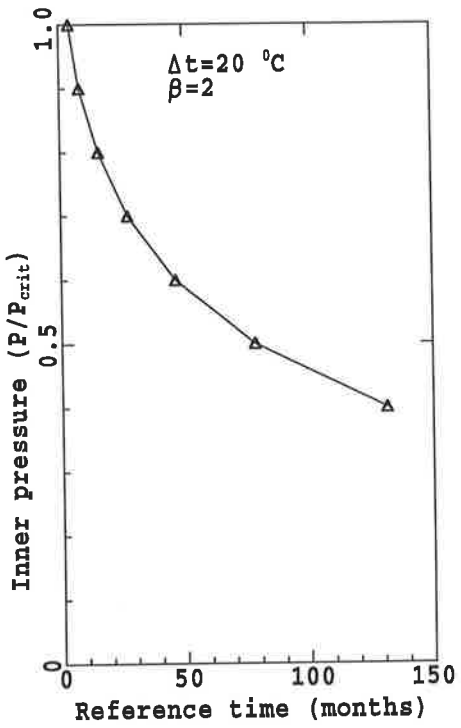

Figure 6.29: Internal pressure versus reference time

6.5.4 Damage Histories and Remaining Life Evaluation

Since the effective stress histories are established, then the damage histories and damage distribution across the tube wall can be calculated. It is assumed that the effective stress distribution across the thickness of the tube remains unchanged during a short increment of time, Δt_i. Then the rupture times, $t_{r,ij}$, can be calculated for all cylindrical layers using the effective stress and temperature distributions in conjunction with the material's creep-rupture properties as it has already been shown in numerical analysis. Having the rupture times of all cylindrical layers at those effective stress levels and temperatures and the short increment of time as a duration time for all the layers,

then the increments of damage, $\Delta D_{ij} = \Delta t_i / t_{r,ij}$, are calculated and the remaining life of the layers are evaluated. These increments of damage are accumulated to give the total accumulated damage of each cylindrical shell during the life of the tube as the life is exhausting. When the total accumulated damage at a cylindrical layer approaches to one, then all the life of that layer is exhausted. Results of this investigation for the damage histories as well as the remaining life variation with damage are shown in Figure. 6.30 (a) and (b).

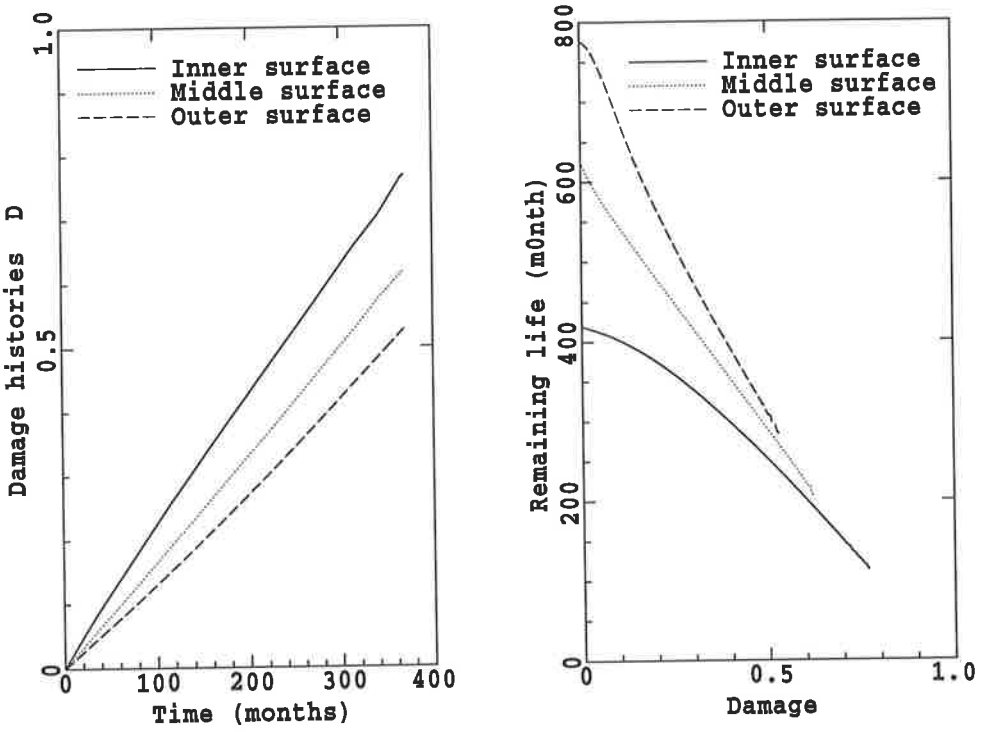

(a) (b)

Figure 6.30: (a) Variation of damage at inner, middle and outer surfaces of the tube with time; (b) Remaining life of inner, middle and outer layers of the tube.

The results show that the inner layer of the tube is the mostly damaged layer and the outer cylindrical layer is carrying the minimum damages at this loading condition (Figure. 6.30 (a)). The life exhaustion rate at the outer surface of the tube is much higher than the inside surface of the tube because its effective stress is increasing with time. However, later in the tube life, when the effective stress becomes uniform across the thickness the rate of life exhaustion becomes constant and the remaining life curves linearly approach to one as shown in Figure. 6.30 (b).

Through-thickness variation of damages with time are shown in Figure. 6.31. This

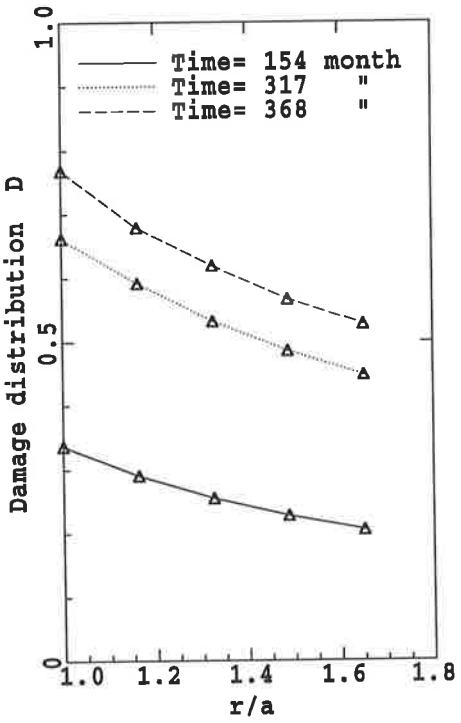

Figure 6.31: Through-thickness variation of damage at different times

figure also shows that the maximum damaged layer is located at the inner surface of

the tube for this loading condition. It is because the temperature at the inner surface is higher than outer surface and the maximum effective stress is also located at the inner surface of the tube during a long period of the tube life (Figure 6.28 (a)). Due to changes in the creep strain rate (slope of the creep curves) a variable time incrementation has been employed for rapid convergence of the numerical procedure. The time increment history is shown in Figure 6.32 (a).

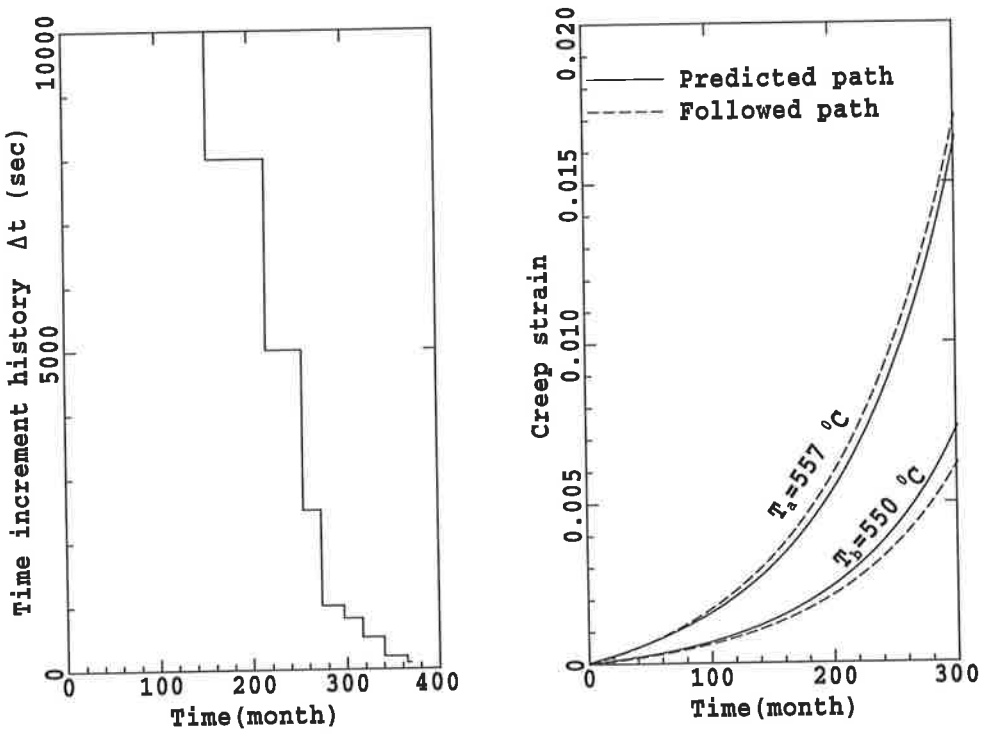

(a) (b)

Figure 6.32: (a) The time increment history; (b) The Θ predicted path and the numerically followed curves.

At early stages of the creep progress, the numerical procedure converged with a $\Delta t =$

10,000 seconds. While later in the tube life, when the creep strain rates are high, the procedure converged with a 20 seconds time increment. However, after such a low time increment it was decided to stop the solution although the procedure could go ahead with lower time increments. The numerical procedure converged for all situations regardless of the size of the tube, loading condition and material's creep stages. The creep strain rates (slope of the creep curves) have a major effect on the convergence of the numerical solution. The creep strain rates are variable along the creep curves. Therefore, an appropriate time increment should be selected for any stress level and timing step. The accuracy of the numerical solution has been examined by plotting the Θ predicted path and the numerically followed path at the inner and outer surfaces Fig. 6.32 (b). Temperatures of $557^{o}C$ and $550^{o}C$ belong to the inner and outer surfaces respectively. In fact a family of curves between these two extremes have been followed for each individual point along the tube wall thickness. A good consistency exists between the Θ predicted path and the numerically followed path which means that the results of this numerical solution are reliable.

Chapter 7

SUMMARY, CONCLUSIONS AND FUTURE WORK

7.1 Summary and Conclusions

Time-independent thermoelastoplastic and residual stress analysis of thick-walled cylinders as well as the time-dependent creep stress and damage analysis of thick-walled tubes have been investigated using incremental theory of plasticity in conjunction with the improved material elastoplastic and creep constitutive models. The results are validated experimentally and numerically.

A cylindrical element at the middle section of the cylinder has been considered. The equations of equilibrium, compatibility and stress-strain are written in cylindrical coordinates for this element. The stress-strain relationships are containing the irreversible

total plastic and creep strains. These irreversible total strains are assumed to be the accumulation of plastic and creep strain increments during the loading history and the life of the cylinder. To calculate these total irreversible strains, the incremental stress-strain relationships are employed. Increments of plastic and creep strains are related to the stresses and the loading history in these non-linear incremental stress-strain relationships. Numerical procedures have been proposed in which the material loading-unloading and time-dependent constitutive models represent the history dependent parts of the incremental stress-strain relationships in the plastic and creep regimes. The numerical models are simplified by derivation of functional relationships between stresses and the total plastic and creep strains. In fact, a direct relationship between stresses and the total irreversible plastic and creep strains have been established by simultaneously solution of the equilibrium, compatibility and stress-strain equations for the stresses. Expressions for the elastic stresses are obtained by neglecting the functions containing the plastic and creep strains. Critical condition of the cylinder has been investigated using this elastic solution in conjunction with the von Mises yield criterion.

For time-independent thermoelastoplastic and residual stress analysis, thick-walled cylinders of stainless steel SUS 304 have been selected. The material's loading and unloading properties including the Bauschinger effect factor (BEF) are obtained experimentally. A large number of loading-unloading test specimens have been specifically designed and manufactured in order to reduce the effect of buckling on material prop-

erties during reverse loading. These test specimens have been loaded up to a specific strain beyond the elastic limit and then reverse loaded down to zero strain by using a computer controlled testing machine. The machine configuration menu was set up such that 20 series of data were recorded at each second of the test into the material data file. Using these data files in a scientific table-curve software (The Jandel Scientific Table Curve version 3.03 (1991)) the material strain-hardening and the Bauschinger effect factor are mathematically represented by continuous functions of effective plastic strain. This realistic material's model including the BEF have been incorporated in the analytical-numerical model to predict the cylinders non-linear and residual stresses and the critical pressures of direct and reverse yielding. The material high-temperature properties and constitutive models are selected from the experimental results of Niitsu and Ikegami (1990).

The analytical-numerical models for the prediction of critical inner pressure, plastic stress distributions and the subsequent residual stresses of thick-walled cylinders are validated experimentally. A high pressure hydraulic hand pump has been employed to produce high pressures required in this investigation. A digital pressure transducer is used to provide the internal pressure measurements. Rosette strain gauges are mounted at the axial center of the specifically designed test specimens and are oriented to measure strains in axial and tangential directions. Several experiments are carried out on thick-walled cylindrical test specimens in which the internal hydraulic pressure has been increased and the outer surface deformations are measured by the strain gauges.

Subsequently the load has been released and the residual strains are again measured at the outer surface of the cylinder. These experimentally measured values are compared with the predicted values of the analytical-numerical model and in most cases the model predictions are accurate as it has been shown in Chapter 5.

For time-dependent creep stress and damage analysis, thick-walled tubes of ferritic steel $\frac{1}{2}Cr, \frac{1}{2}Mo, \frac{1}{4}V$ have been considered as this composition is often used in high temperature components of fossil fueled power stations. Improved material creep and creep rupture properties are obtained from the literature. The material long-term creep properties up to rupture and the creep rupture data are defined by the Θ projection concept. For time-dependent creep stress and damage analysis, a numerical model has been developed for the computation of creep stresses and strains and the creep damages in a thick-walled tube subjected to an internal pressure and a thermal gradient. The model predicts the history of stresses and strains and the changes in the creep damage rates during the life of the tube due to variation in stresses with time and through-thickness variations. The creep damage accumulation is based on the Robinson's linear life fraction damage rule which has also been adopted by the ASME code (case N47) which governs the design of high-temperature nuclear components. The Robinson's rule has been incorporated in this non-linear time-dependent stress analysis. Following the stress histories, the damages are calculated and cumulatively summed during the life of the tube. Furthermore, from the effective stress histories a reference time has been identified when the effective stress distributions become uniform throughout the

tube wall. Effect of internal pressure on this reference time is investigated. The accuracy of the results has been examined by comparing the theoretically predicted creep curves and the numerically followed curves. Deviation of the followed paths from the predicted paths is small.

Important conclusions of this investigation are itemized as follows:

- It is concluded from the experimental results of Chapter 5 that the analytical-numerical model developed in this investigation considering the generalized plane strain and the improved material model can accurately predict the non-linear response of thick-walled cylinders to loading and unloading.

- Graphs of critical condition are provided such that the critical pressure of the cylinders can be obtained for the most practical radii ratios and loading combinations. It is concluded from these graphs that the higher temperature gradients tend to increase the critical pressure of the cylinders except for a small range of low radii ratios.

- It is also concluded that the critical pressure of thick-walled cylinders of low radii ratios can be significantly improved by increasing their radii ratio. However, this is not significant for high radii ratio cylinders.

- A loading combination has been identified in which the whole thickness of the cylinder yields simultaneously.

- Effect of plastic flow on thick-walled cylinders is such that the maximum shear

stress distribution becomes uniform across the wall of the fully plastic vessel.

- Progresses of plastic zones with and without the effect of temperature gradient are compared and it is concluded that the temperature gradient facilitates the progress of plastic zone. On the other hand, in the presence of a temperature gradient smaller pressure differential is needed for an equal progress of plastic zone.

- Residual stresses with and without the effect of Bauschinger phenomenon are obtained and compared. In the case study of a specific cylinder, it has been concluded that the residual stresses subsequent to a 45% overstrained condition are at the onset of reverse yielding when BEF is considered. However, residual stresses resulted from unloading of the same cylinder at a fully plastic overstrained condition are not at the onset of reverse yielding when BEF is neglected.

- The nature of creep deformation in thick-walled tubes is such that the maximum shear stress distribution becomes uniform throughout the tube thickness and is similar to the plastic deformation of the tube in this respect.

- A reference time has been identified in which the effective stress distribution becomes uniform across the tube wall. This reference time depends on the internal pressure and the temperature gradient.

- The maximum tensile tangential stress is located at the inside surface of the tube at early stage of the tube life. However, it will be located at the outer surface of the tube later in the tube life as a result of stress redistribution.

- In the damage analysis of a tube subjected to an internal pressure and a thermal gradient, it has been concluded that the maximum damage is located at the inner surface of the tube while the outer surface of the tube is carrying minimum damages.

7.2 Recommendations for Future Work

The work presented in this thesis has succeeded in incorporating a realistic material model including the Bauschinger effect factor in the non-linear time-independent stress distribution analysis of thick-walled cylinders. The experimental results proved that the analytical-numerical model developed in this investigation can accurately predict the non-linear response of thick-walled cylinders to loading and unloading.

Furthermore, a long-term creep constitutive model known as the " Theta (Θ) projection " has been successfully employed in a non-linear time-dependent analysis for the prediction of creep damages of a thick-walled tube. The creep damages have been used to evaluate the remaining life of the tube. A significant body of work exists in this research work on the effective stress and damage histories and the remaining life evaluation of thick-walled tubes which needs to be extended.

Results of the remaining life evaluations using the long-term creep constitutive model defined by the Theta projection concept can be validated as follows. Using the current methodology, the accelerated post-exposure creep rupture tests are to be carried out

at the service stress (iso-stress accelerated tests) but at higher temperatures so that extrapolation to the service temperature gives an estimate of the remaining useful creep life as shown in Figure 7.1

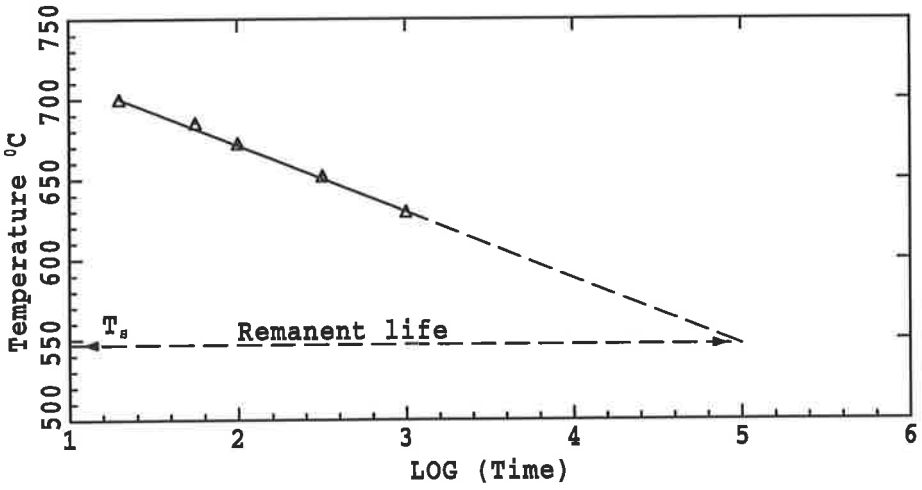

Figure 7.1: Accelerated post-exposure stress-rupture test datas at higher temperatures and the service stress are extrapolated to the service temperature to obtain an estimate of the remaining life.

Meanwhile, the above post-exposure test datas in conjunction with the "Theta (Θ) projection" concept can also be used to obtain an estimate of the remaining life of the tube as shown in Figure 7.2 (Evans et al.(1992)) and explained below.

Since the material's constitutive model defined by the "Theta (Θ) projection" is known, then the full creep curves up to rupture for the service condition (curve OC in Figure 7.2) and for the accelerated test condition (curve OB) can be constructed. The creep data recorded in a post-exposure test for a sample taken from the tube (cure

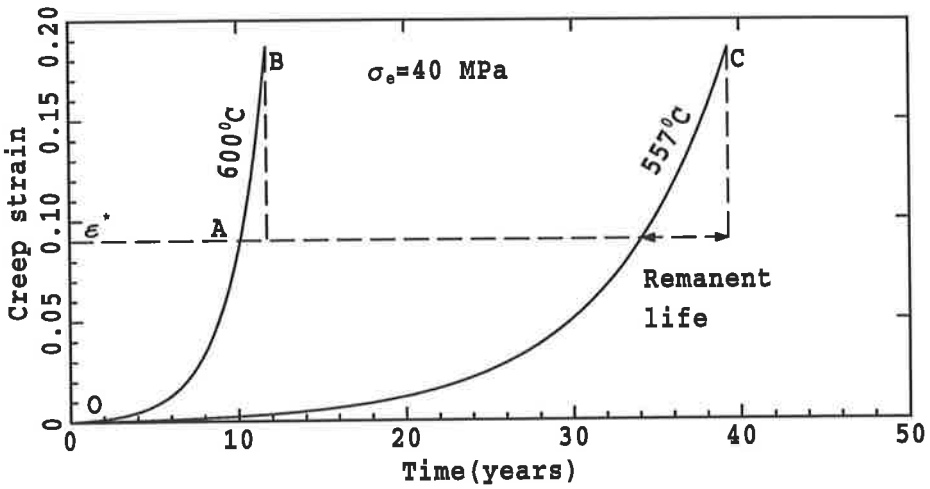

Figure 7.2: Iso-stress creep curves of $\frac{1}{2}Cr, \frac{1}{2}Mo, \frac{1}{4}V$ ferritic steel at service temperature of 557 ^{0}C and accelerated test temperature of 600 ^{0}C

AB) corresponds to the final portion of the full creep curve expected for non-exposed material at the accelerated test condition. The post-exposure test therefore identifies the creep strain (ε^* at position A) accumulated under the service conditions which can be used to obtain the remaining life of the tube as shown in Figure 7.2. The remanent life estimates obtained using Θ analysis can then be compared with those derived from the above method to validate the remaining life estimations.

The reference time which has been identified in this investigation (from the effective stress histories) needs to be investigated for a wide range of operating temperatures. Effect of internal pressure on this reference time has already been investigated in this research work. Then a family of curves similar to Figure 6.29 can be generated for a

wide range of internal pressures and operating temperatures. These family of curves can be used by the designers to obtain an estimate of the time during which the major stress redistribution occurs for the tube. It is necessary to point out that the effective stress at the reference time is uniformly distributed across the thickness of the tube and in fact is the stationary effective stress.

Appendix A

The computer programs which have been developed in this investigation for the computation of critical pressures and the spread of plastic yielding as well as the subsequent residual stress distributions of thick-walled cylinders are introduced in this appendix.

```
C     ****************************************************************
C     This program has been developed for the computation of critical   *
C     inner pressures for a wide range of radii ratios. The method is   *
C     based on the computation of the minimum value of internal pressure*
C     satisfying equation (4.1)  *                                      *
C     ****************************************************************
      PROGRAM pcrit
      DIMENSION PCR(51),RC(51),FF(51),FH(51),FG(51),FR(51),FM(51),
     $FN(51)
C     ****************************************************************
C     INPUT DATA: Elastic modulus, yield stress, coefficient of linear *
C                 expansion, Poisson's ratio, radii ratio, temperature *
C                 gradient, number of divisions along radius, outer    *
C                 pressure.                                            *
C     ****************************************************************
      DATA E,SO,ALPHA,PR,BE,DT,N,PO /671.3,1.0,0.0000117,0.29,1.0,
     $0.0,50,0.0/
C     ****************************************************************
C     In the following loop the temperature will be changed in 20       *
C     step from 0 to 100 degree centigrade                              *
C     ****************************************************************
      DO 30 J=1,20
      THETA=(E*ALPHA*DT)/((1-PR)*SO)
      WRITE(20,1)DT,THETA
1     FORMAT(F6.2,5X,F8.4,5X,30(1H-))
C     ****************************************************************
C     In the following loop Radii ratio will be increased in 20 step    *
C     and then critical inner pressure will be computed for each radii  *
C     ratio for the specified  temperature gradient.                    *
C     ****************************************************************
      DO 37 I=1,20
      BE=BE+0.2
      DR=(BE-1)/N
      NP=N+1
C     ****************************************************************
C     The cylinder thickness is divided into N number of division and   *
C     the functions F, G, H, R, M and N are evaluated at all division   *
C     points (N+1) across the thickness.                                *
C     ****************************************************************
      DO 40 K=1,NP
      RC(K)=1+(K-1)*DR
      FG(K)=((1/(BE**2-1))*(1-(BE**2/RC(K)**2)))
      FR(K)=((1/(BE**2-1))*(1+(BE**2/RC(K)**2)))
      FN(K)=1/(BE**2-1)
      FF(K)=((E*ALPHA*DT)/(2*(1-PR)*(BE**2-1)*ALOG(BE)))*(((
     $BE**2*ALOG(BE))/RC(K)**2)+(BE**2*ALOG(RC(K)/BE))-ALOG(
     $RC(K)))-(PO**2*BE**2/(BE**2-1))*(1-1/RC(K)**2)
      FH(K)=((E*ALPHA*DT)/(2*(1-PR)*(BE**2-1)*ALOG(BE)))*(((-
     $BE**2*ALOG(BE))/RC(K)**2)+(BE**2*ALOG(RC(K)/BE))-ALOG(
     $RC(K))+(BE**2-1))-(PO**2*BE**2/(BE**2-1))*(1+1/RC(K)**2)
      FM(K)=((E*ALPHA*DT)/(2*(1-PR)*(BE**2-1)*ALOG(BE)))*(2*BE**2
     $*ALOG(RC(K)/BE)-2*ALOG(RC(K))+(BE**2-1))
```

```
C     ****************************************************************
C      A, B and C are the coefficients of the critical condition  in    *
C      equation (4.1) which are function of the history-independent     *
C      functions of F, G, H, R, M and N and therefore can be evaluated  *
C      for all division points across the thickness of the tube         *
C     ****************************************************************
       A=2*(FG(K)**2+FR(K)**2+FN(K)**2-FG(K)*FR(K)-FR(K)*FN(K)-FN(K)*FG(K
      $))
       B=4*(FF(K)*FG(K)+FH(K)*FR(K)+FM(K)*FN(K))-2*(FF(K)*FR(K)+FH(K)*FG(
      $K)+FH(K)*FN(K)+FM(K)*FR(K)+FM(K)*FG(K)+FF(K)*FN(K))
       C=2*(FF(K)**2+FH(K)**2+FM(K)**2-FF(K)*FH(K)-FH(K)*FM(K)-FM(K)*FF(K
      $)-SO**2)
C     ****************************************************************
C      The pressure satisfying equation (4.1) is calculated for all     *
C      division points across the thickness the minimum of which is the *
C      critical pressure and its location is the place in which yielding*
C      will first start to progress. Therefore the critical pressure for*
C      the specified radii ratio and temperature gradient is calculated *
C     ****************************************************************
       IF(B**2-4*A*C)44,60,60
60     P1=(-B+SQRT(B**2-4*A*C))/(2*A)
       P2=(-B-SQRT(B**2-4*A*C))/(2*A)
       IF(P1.LT.0..AND.P2.LT.0.)GO TO 44
       IF(P1.LT.0..AND.P2.GT.0.)GO TO 150
       IF(P2.LT.0..AND.P1.GT.0.)GO TO 140
       IF(P1-P2)140,140,150
140    PCR(K)=P1
       GO TO 40
150    PCR(K)=P2
       GO TO 40
44     WRITE(30,82)RC(K)
82     FORMAT(12X,F6.4,5X,'NEGATIVE OR IMAGINARY')
       STOP
40     CONTINUE
       PCMIN=PCR(1)
       RCC=RC(1)
       PCRA=PCR(1)
       PCRB=PCR(NP)
       DO 51 IK=2,NP
       IF(PCMIN-PCR(IK))51,51,17
17     PCMIN=PCR(IK)
       RCC=RC(IK)
51     CONTINUE
       WRITE(20,182)BE,PCMIN
182    FORMAT(F8.4,5X,F8.4)
37     CONTINUE
       BE=1
       DT=DT+5
30     CONTINUE
       STOP
       END
```

```
C     ****************************************************************
C     * This computer Program has been developed for the computation of *
C     * thermoelastoplastic and residual stress distribution of thick-  *
C     * walled cylinders based on the block diagram of Figure 4.2.      *
C     * It contains five subprograms which will be introduced after the *
C     * main program.                                                   *
C     *                                                                 *
C     * Definition of arrays:                                           *
C     * 1- FF(51),FH(51),FG(51),FR(51),FM(51),FN(51): In these arrays   *
C     *    magnitudes of non-history dependent functions of F, H, G, R, *
C     *    M and N defined in Equation (3.62) at all 51 division points *
C     *    across the thickness are stored.                             *
C     * 2- PCR(51): This array representing the magnitudes of internal  *
C     *    pressure satisfying Equation (3.69) at all division points   *
C     * 3- R(51): Representing magnitudes of radius at all divisions    *
C     * 4- SRE(51),STE(51),SZE(51):Radial, tangential and axial elastic *
C     *    stresses                                                     *
C     * 5- SR(50,51),ST(50,51),SZ(50,51):Radial, tangential and axial   *
C     *    elastic stresses in the elastic region of elastic-plastic    *
C     *    cylinder                                                     *
C     * 6- SRP(50,51),STP(50,51),SZP(50,51): Radial, tangential and     *
C     *    axial plastic stresses.                                      *
C     * 7- EPR(50,51),EPT(50,51),EPZ(50,51): Radial, tangential and     *
C     *    axial plastic strains.                                       *
C     * 8- DEPR(50,51),DEPT(50,51),DEPZ(50,51):  Radial, tangential and *
C     *    axial plastic strain increments.                             *
C     * 9- DEPRN(50,51),DEPTN(50,51),DEPZN(50,51): New obtained values  *
C     *    Radial, tangential and axial plastic strain increments.      *
C     * 10- RSR(50,51),RST(50,51),RSZ(50,51): Radial, tangential and    *
C     *     axial residual stresses in the plastic region of the vessel *
C     * 11- SRR(50,51),STR(50,51),SZR(50,51):Radial, tangential and     *
C     *     axial residual stresses in the elastic region of the vessel *
C     * 12- ER(50,51),ET(50,51),EZ(50,51): Radial, tangential and axial *
C     *     total strains                                               *
C     * 13- DEP(50,51),EP(50,51): Effective plastic strain increment    *
C     *     the total accumulated plastic strain.                       *
C     * 14- PEREP(50,51),BEF(50,51): Percentage overstrain and the      *
C     *     Bauschinger effect factor                                   *
C     * 15- SEF(50,51): Effective stress                                *
C     * 16- YF(50,51):  Yield function                                  *
C     * 17_ TTC1(50,51),TTC2(50,51),TRC1(50,51),TRC2(50,51): Integrals  *
C     *     of radial and tangential total plastic strains              *
C     * ****************************************************************
C     ****************************************************************
      PROGRAM plastic
      DIMENSION FF(51),FH(51),FG(51),FR(51),FM(51),FN(51),PCR(51),R(51),
     $SRE(51),STE(51),SZE(51),SR(50,51),ST(50,51),SZ(50,51),RE(50,51),
     $EPR(50,51),DEPRN(50,51),EPT(50,51),DEPTN(50,51),P(51),SRP(50,51),
     $STP(50,51),SZP(50,51),SEF(50,51),RC(51),TTC1(50,51),YF(50,51),
     $TTC2(50,51),TRC1(50,51),TRC2(50,51),DEP(50,51),EP(50,51),
     $DEPZN(50,51),DEPR(50,51),DEPT(50,51),DEPZ(50,51),EPZ(50,51)
     $,RSR(50,51),RST(50,51),RSZ(50,51),SRR(50,51),STR(50,51),SZR(50,51)
     $,ER(50,51),ET(50,51),EZ(50,51),PEREP(50,51),BEF(50,51)
```

```
C     ****************************************************************
C      INPUT DATA:Elastic modulus, yield stress, coefficient of linear  *
C                 expansion, Poisson's ratio, inner radius, outer radius*
c                 number of load step, number of divisions along radius,*
c                 initial value of radial and tangential plastic strain *
c                 increment, convergence criteria, Inner and outer      *
c                 temperature                                           *
c     ****************************************************************

      DATA E,SO,ALPHA,PR,RA,RB,M1,N1,EPRI,EPTI,Q,TA,TB/671.3,1.0,
     $ 0.0000117,0.3,1.0,2.0,50,50,-0.000035,0.000045,0.1E-5,60.0,0.0/
C     ****************************************************************
C     * THE RESULTS WILL BE WRITTEN INTO THE FOLLOWING OUTPUT FILES.    *
C     * elstrs.dat: Elastic stress distribution                         *
c     * prc.dat:    Pressure versus elastoplastic boundary              *
c     * befr.dat:   Bauschinger effect factor in the plastic region     *
c     * plstra.dat: Plastic strain distribution                         *
c     * plstrs.dat: Plastic stress distribution                         *
c     * rpstrs.dat: Residual stress distribution in the plastic region  *
c     * elestrs.dat:Elastic stress distribution in the elastic region   *
c     * restrs.dat: Residual stress distribution in the elastic region  *
c     ****************************************************************
      OPEN(UNIT=10,FILE='elstrs.dat',STATUS='old')
      OPEN(UNIT=11,FILE='prc.dat',STATUS='OLD')
      OPEN(UNIT=12,FILE='befr.dat',STATUS='old')
      OPEN(UNIT=13,FILE='plstra.dat',STATUS='old')
      OPEN(UNIT=14,FILE='plstrs.dat',STATUS='old')
      OPEN(UNIT=15,FILE='rpstrs.dat',STATUS='old')
      OPEN(UNIT=16,FILE='elestrs.dat',STATUS='old')
      OPEN(UNIT=17,FILE='restrs.dat',STATUS='old')
C     ****************************************************************
c     *                 ELASTIC SOLOUTION                             *
C     ****************************************************************
      DT=TA-TB
C     ****************************************************************
C     The critical pressure will be computed in PCRIT  subprogram and  *
C     the maximum elastic stress distribution will be computed.        *
C     ****************************************************************
      CALL PCRIT(FF,FG,FH,FR,FM,FN,R,PCMIN,RCMIN,PCMAX,RMAX,PCR,DT,E,
     $SO,ALPHA,PR,RA,RB,N)
      NP=N+1
      DO 10 I=1,NP
      SRE(I)=FF(I)+FG(I)*PCMIN
      STE(I)=FH(I)+FR(I)*PCMIN
      SZE(I)=FM(I)+FN(I)*PCMIN
      WRITE(10,15)R(I),SRE(I),STE(I),SZE(I)
15    FORMAT(12X,F8.6,5X,F14.12,3X,F14.12,3X,F14.12)
10    CONTINUE
c     ****************************************************************
c     *              ELASTOPLASTIC SOLOUTION                          *
c     ****************************************************************
c     Define the final pressure (PF) and the pressure increment (PD)   *
c     and apply the load in a large number of loading step (M1)        *
c     ****************************************************************
```

```
      PF=PCMAX
      PD=(PCMAX-PCMIN)/M1
      IF(RCMIN.EQ.RA)THEN
            RC(1)=RA
         ELSE
            RC(1)=RB
      ENDIF
c     ********************************************************************
c     The load will be applied in  M1 number of loading step and the   *
c     outer pressure is zero according to the boundary condition       *
c     ********************************************************************
      DO 100 I=1,M1
      P(I)=PCMIN+I*PD
      PI=P(I)
      PO=0.0
      IM=I+1
c     ********************************************************************
c     Initial values are assumed for the plastic strain increment      *
c     ********************************************************************
      DO 143 K=1,I
      IF(I .EQ. 1 .OR. K .EQ. I) THEN
            DEPR(I,K)=EPRI
            DEPT(I,K)=EPTI
            DEPZ(I,K)=-(DEPR(I,K)+DEPT(I,K))
        ELSE
            DEPR(I,K)=DEPR(I-1,K)
            DEPT(I,K)=DEPT(I-1,K)
            DEPZ(I,K)=-(DEPR(I,K)+DEPT(I,K))
      ENDIF
143   CONTINUE
      DEPR(I,IM)=0
      DEPT(I,IM)=0
      DEPZ(I,IM)=-(DEPR(I,IM)+DEPT(I,IM))
c     ********************************************************************
c     The plastic strain increments will be added to the previously    *
c     converged value of plastic strains in EPSPL subprogram and the   *
c     the integral of total plastic strains will be computed in AREA   *
c     subprogram. The elastioplastic interface will be obtaind in the  *
c     BISEC1 or BISEC2 subprogram. Then an estimate of stresses within *
c     the  plastic region of the vessel will be obtained and a new     *
c     value for plastic strain increments will be compouted by using   *
c     the incremental stress-strain relatioship. The new value will    *
c     be compared with its previous value for the convergence.         *
c     ********************************************************************
      DO 101 J=1,IM
9     CALL  EPSPL(I,EPR,EPT,EPZ,DEPR,DEPT)
      CALL  AREA(I,TRB1,TRB2,TTB1,TTB2,TTC1,TTC2,TRC1,TRC2,EPR,EPT,RC)
      IF(RCMIN.EQ.RB)GO TO 191
      CALL  BISEC1(I,RA,RB,RCC,SO,E,ALPHA,DT,PR,RCMIN,PI,PO,TA,TB,RC(I)
     $,EPR(I,I),EPT(I,I),TRC1(I,I),TRC2(I,I),TTC1(I,I),TTC2(I,I),
     $TTB1,TTB2,TRB1,TRB2)
      GO TO 193
```

```
      CALL  BISEC1(I,RA,RB,RCC,SO,E,ALPHA,DT,PR,RCMIN,PI,PO,TA,TB,RC(I)
     $,EPR(I,I),EPT(I,I),TRC1(I,I),TRC2(I,I),TTC1(I,I),TTC2(I,I),
     $TTB1,TTB2,TRB1,TRB2)
      GO TO 193
191   CALL  BISEC2(I,RA,RB,RCC,SO,E,ALPHA,DT,PR,RCMIN,PI,PO,TA,TB,RC(I))
193   RC(IM)=RCC
      TRC1(I,IM)=TRC1(I,I)+0.5*(EPR(I,I)*RC(I))*ABS(RC(IM)-RC(I))
      TTC1(I,IM)=TTC1(I,I)+0.5*(EPT(I,I)*RC(I))*ABS(RC(IM)-RC(I))
      TRC2(I,IM)=TRC2(I,I)+0.5*(EPR(I,I)/RC(I))*ABS(RC(IM)-RC(I))
      TTC2(I,IM)=TTC2(I,I)+0.5*(EPT(I,I)/RC(I))*ABS(RC(IM)-RC(I))
      TRB1=TRC1(I,IM)
      TRB2=TRC2(I,IM)
      TTB1=TTC1(I,IM)
      TTB2=TTC2(I,IM)
      IF(RCMIN.EQ.RB)THEN
         TRC1(I,J)=TRB1-TRC1(I,J)
         TRC2(I,J)=TRB2-TRC2(I,J)
         TTC1(I,J)=TTB1-TTC1(I,J)
         TTC2(I,J)=TTB2-TTC2(I,J)
      ENDIF
C     ****************************************************************
C     Plastic stresses within the plastic region are calculated       *
C     ****************************************************************
      SRP(I,J)=((E*ALPHA*DT)/(2*(1-PR)*(RB**2-RA**2)*ALOG(RB/RA)))*(((
     $RA**2*RB**2*ALOG(RB/RA))/RC(J)**2)+(RB**2*ALOG(RC(J)/RB))-(RA**2*
     $ALOG(RC(J)/RA)))+(PI*RA**2-PO*RB**2)/(RB**2-RA**2)+RA**2*RB**2*(
     $PO-PI)/((RB**2-RA**2)*RC(J)**2)+(E/(2*(1-PR**2)*(RB**2-RA**2)))*
     $((1-2*PR)*TTB1+(1-2*PR)*TRB1+RB**2*TTB2-RB**2*TRB2)*(1-RA**2/RC(J
     $)**2)-(E/(2*(1-PR**2)*RC(J)**2))*(+(1-2*PR)*TTC1(I,J)+(1-2*PR)*
     $TRC1(I,J)+RC(J)**2*(TTC2(I,J)-TRC2(I,J)))
      STP(I,J)=((E*ALPHA*DT)/(2*(1-PR)*(RB**2-RA**2)*ALOG(RB/RA)))*(((-
     $RA**2*RB**2*ALOG(RB/RA))/RC(J)**2)+(RB**2*ALOG(RC(J)/RB))-(RA**2*
     $ALOG(RC(J)/RA))+(RB**2-RA**2))+(PI*RA**2-PO*RB**2)/(RB**2-RA**2)
     $-RA**2*RB**2*(PO-PI)/((RB**2-RA**2)*RC(J)**2)+(E/(2*(1-PR**2)*(
     $RB**2-RA**2)))*((1-2*PR)*TTB1+(1-2*PR)*TRB1+RB**2*TTB2-RB**2*TRB2
     $)*(1+RA**2/RC(J)**2)+(E/(2*(1-PR**2)*RC(J)**2))*(+(1-2*PR)*TTC1(I
     $,J)+(1-2*PR)*TRC1(I,J)-RC(J)**2*(TTC2(I,J)-TRC2(I,J))-2*RC(J)**2*
     $((1-PR)*EPT(I,J)-PR*EPR(I,J)))
      SZP(I,J)=((E*ALPHA*DT)/(2*(1-PR)*(RB**2-RA**2)*ALOG(RB/RA)))*(2*
     $RB**2*ALOG(RC(J)/RB)-2*RA**2*ALOG(RC(J)/RA)+(RB**2-RA**2))+PI*RA
     $**2/(RB**2-RA**2)+(E*PR/((RB**2-RA**2)*(1-PR**2)))*((1-2*PR)*TTB1
     $+(1-2*PR)*TRB1+RB**2*TTB2-RB**2*TRB2)-(E/(1-PR**2))*PR*((TTC2(I,J
     $)-TRC2(I,J))+(1-PR)*EPT(I,J)-PR*EPR(I,J))-(E/(RB**2-RA**2))*(2*
     $TRB1+2*TTB1-(RB**2-RA**2)*(EPR(I,J)+EPT(I,J)))
      DEP(I,J)=(2**0.5/3)*(SQRT((DEPR(I,J)-DEPT(I,J))**2+(DEPT(I,J)-
     $DEPZ(I,J))**2+(DEPZ(I,J)-DEPR(I,J))**2))
C     ****************************************************************
C     Effective plastic strain increments are accumulated to give the  *
C     the total effective plastic strain                               *
C     ****************************************************************
      IF(I .EQ. 1) THEN
            EP(I,J)=DEP(I,J)
         ELSE
            EP(I,J)=EP(I-1,J)+DEP(I,J)
      ENDIF
```

```
C     ***************************************************************
C      Material's constitutive model and the Bauschinger effect factor  *
C      are incorporated in analysis .                                    *
C     ***************************************************************
C       BET=0.78
C       H=36.5/93.3
C       SEF(I,J)=1+H*(EP(I,J)**BET)
       SEF(I,J)=1+2.9612*(EP(I,J)**0.21842186)
       PEREP(I,J)=100*EP(I,J)
       BEF(I,J)=1.0170029+0.36592732*(PEREP(I,J))-0.0025343135*(
      $PEREP(I,J))**3-0.97738304*(PEREP(I,J))**0.5
C     ***************************************************************
C      New values are estimated for the plastic strain increments        *
C     ***************************************************************
       DEPRN(I,J)=(DEP(I,J)/(2*SEF(I,J)))*(2*SRP(I,J)-STP(I,J)-SZP(I,J))
       DEPTN(I,J)=(DEP(I,J)/(2*SEF(I,J)))*(2*STP(I,J)-SRP(I,J)-SZP(I,J))
       DEPZN(I,J)=-(DEPRN(I,J)+DEPTN(I,J))
       DELR=ABS(DEPRN(I,J)-DEPR(I,J))
       DELT=ABS(DEPTN(I,J)-DEPT(I,J))
C     ***************************************************************
C      Convergence of the procedure is controlled.                       *
C     ***************************************************************
       IF(DELR.LT.Q.AND.DELT.LT.Q)GO TO 209
       DEPR(I,J)=DEPRN(I,J)
       DEPT(I,J)=DEPTN(I,J)
       DEPZ(I,J)=DEPZN(I,J)
       GO TO 9
C     ***************************************************************
C      Residual stresses are computed for each converged loading step    *
C     ***************************************************************
209    RSR(I,J)=SRP(I,J)-((P(I)*RA**2)/(RB**2-RA**2))*(1-RB**2/RC(J)**2)
      $+((E*ALPHA*(-DT))/(2*(1-PR)*(RB**2-RA**2)*ALOG(RB/RA)))*(((
      $RA**2*RB**2*ALOG(RB/RA))/RC(J)**2)+(RB**2*ALOG(RC(J)/RB))-(RA**2*
      $ALOG(RC(J)/RA)))
       RST(I,J)=STP(I,J)-((P(I)*RA**2)/(RB**2-RA**2))*(1+RB**2/RC(J)**2)
      $+((E*ALPHA*(-DT))/(2*(1-PR)*(RB**2-RA**2)*ALOG(RB/RA)))*(((-
      $RA**2*RB**2*ALOG(RB/RA))/RC(J)**2)+(RB**2*ALOG(RC(J)/RB))-(RA**2*
      $ALOG(RC(J)/RA))+(RB**2-RA**2))
       RSZ(I,J)=SZP(I,J)-((P(I)*RA**2)/(RB**2-RA**2))+
      $((E*ALPHA*(-DT))/(2*(1-PR)*(RB**2-RA**2)*ALOG(RB/RA)))*(2*
      $RB**2*ALOG(RC(J)/RB)-2*RA**2*ALOG(RC(J)/RA)+(RB**2-RA**2))
C     ***************************************************************
C      Effective Mises stress is computed for the residual stresses      *
C      across the thickness for the prediction of reverse yielding       *
C     ***************************************************************
       YF(I,J)=0.5*((RSR(I,J)-RST(I,J))**2+(RST(I,J)-RSZ(I,J))**2+
      $(RSZ(I,J)-RSR(I,J))**2)
101    CONTINUE
C     ***************************************************************
C      Results are written into the appropriate files after the          *
C      convergence is reached for each loading increment                 *
C     ***************************************************************
       WRITE(11,9101)RC(IM),P(I)
       WRITE(12,208)RC(IM),BEF(I,1),YF(I,1),PEREP(I,1)
```

```
9101  FORMAT(2(F14.12,2X))
      WRITE(13,2031)I
2031  FORMAT('PLASTIC STRAINS',10X,'STEP OF LOAD INCREMENT=',I3/
     $'RC/RA',8X,'EPR',5X,'EPT',4X,'EPZ'/60(1H_))
      DO 207 JJ=1,IM
      WRITE(13,208)RC(JJ),EPR(I,JJ),EPT(I,JJ),EPZ(I,JJ)
208   FORMAT(F8.6,5X,F14.12,5X,F14.12,5X,F14.12)
      WRITE(14,201)RC(JJ),SRP(I,JJ),STP(I,JJ),SZP(I,JJ)
201   FORMAT(F8.6,3X,F7.4,3X,F7.4,3X,F7.4)
      WRITE(15,205)RC(JJ),RSR(I,JJ),RST(I,JJ),RSZ(I,JJ)
205   FORMAT(F8.6,3X,F7.4,3X,F7.4,3X,F7.4)
207   CONTINUE
      IF(YF(I,1) .GE. BEF(I,1)**2) STOP
      ENDIF
      IF(ABS(RC(IM)-RB) .LT. 0.0001)STOP
      IT=M1-I
      IF(I.EQ.M1)STOP
C     ********************************************************************
C     Elastic and residual stresses in the remaining elastic region    *
C     are computed and written into the appropriate files              *
C     ********************************************************************
      IF(RCMIN.EQ.RA)THEN
            DR=(RB-RC(IM))/IT
        ELSE
            DR=(RC(IM)-RA)/IT
      ENDIF
      DO 73 KK=1,IT
      T=(TA*ALOG(RB)-TB*ALOG(RA))/ALOG(RB/RA)+((TB-TA)*ALOG(RC(IM))
     $)/ALOG(RB/RA)
      IF(RCMIN.EQ.RA)THEN
           RE(I,KK)=RC(IM)+KK*DR
           TD=T-TB
           PII=ABS(SRP(I,IM))
           POO=0.0
           AR=RC(IM)
           BR=RB
        ELSE
           RE(I,KK)=RC(IM)-KK*DR
           TD=TA-T
           POO=ABS(SRP(I,IM))
           PII=P(I)
           BR=RC(IM)
           AR=RA
      ENDIF
C     ********************************************************************
C     Residual stresses within the elastic region are computed.        *
C     ********************************************************************
           SRR(I,KK)=-((P(I)*RA**2)/(RB**2-RA**2))*(1-RB**2/RE(I,KK)**2)
     $     +((E*ALPHA*(-DT))/(2*(1-PR)*(RB**2-RA**2)*ALOG(RB/RA)))*(((
     $     RA**2*RB**2*ALOG(RB/RA))/RE(I,KK)**2)+(RB**2*ALOG(RE(I,KK)/RB
     $     ))-(RA**2*ALOG(RE(I,KK)/RA)))
```

```
      STR(I,KK)=-((P(I)*RA**2)/(RB**2-RA**2))*(1+RB**2/RE(I,KK)**2)
     $ +((E*ALPHA*(-DT))/(2*(1-PR)*(RB**2-RA**2)*ALOG(RB/RA)))*(((-
     $ RA**2*RB**2*ALOG(RB/RA))/RE(I,KK)**2)+(RB**2*ALOG(RE(I,KK)/RB
     $ ))-(RA**2*ALOG(RE(I,KK)/RA))+(RB**2-RA**2))
      SZR(I,KK)=-((P(I)*RA**2)/(RB**2-RA**2))+
     $ ((E*ALPHA*(-DT))/(2*(1-PR)*(RB**2-RA**2)*ALOG(RB/RA)))*(2*RB*
     $ *2*ALOG(RE(I,KK)/RB)-2*RA**2*ALOG(RE(I,KK)/RA)+(RB**2-RA**2))
C    ***************************************************************
C    Elastic stresses in the elastic region are computed            *
C    ***************************************************************
76    SR(I,KK)=((E*ALPHA*TD)/(2*(1-PR)*(BR**2-AR**2)*ALOG(BR/AR)))*(((
     $AR**2*BR**2*ALOG(BR/AR))/RE(I,KK)**2)+(BR**2*ALOG(RE(I,KK)/BR))-
     $(AR**2*ALOG(RE(I,KK)/AR)))+(PII*AR**2-POO*BR**2)/(BR**2-AR**2)+(
     $AR**2*BR**2*(POO-PII))/((BR**2-AR**2)*RE(I,KK)**2)
      ST(I,KK)=((E*ALPHA*TD)/(2*(1-PR)*(BR**2-AR**2)*ALOG(BR/AR)))*(((-
     $AR**2*BR**2*ALOG(BR/AR))/RE(I,KK)**2)+(BR**2*ALOG(RE(I,KK)/BR))-
     $(AR**2*ALOG(RE(I,KK)/AR))+(BR**2-AR**2))+(PII*AR**2-POO*BR**2)/(
     $BR**2-AR**2)-(AR**2*BR**2*(POO-PII))/((BR**2-AR**2)*RE(I,KK)**2)
      SZ(I,KK)=((E*ALPHA*TD)/(2*(1-PR)*(BR**2-AR**2)*ALOG(BR/AR)))*(
     $2*BR**2*ALOG(RE(I,KK)/BR)-2*AR**2*ALOG(RE(I,KK)/AR)+(BR**2-AR**2))
     $+(PII*AR**2-POO*BR**2)/(BR**2-AR**2)
      SRR(I,KK)=SRR(I,KK)+SR(I,KK)
      STR(I,KK)=STR(I,KK)+ST(I,KK)
      SZR(I,KK)=SZR(I,KK)+SZ(I,KK)
C    ***************************************************************
C     Elastic and residual stresses in the elastic region of the     *
C     cylinder are written into the appropriate files.               *
C    ***************************************************************
      WRITE(16,77)RE(I,KK),SR(I,KK),ST(I,KK),SZ(I,KK)
77    FORMAT(F8.6,3X,F7.4,3X,F7.4,3X,F7.4)
      WRITE(17,771)RE(I,KK),SRR(I,KK),STR(I,KK),SZR(I,KK)
771   FORMAT(F8.6,3X,F7.4,3X,F7.4,3X,F7.4)
73    CONTINUE
100   CONTINUE
      STOP
      END
```

```
C     ******************************************************************
C     This subprogram has been developed to calculate the critical inner*
C     pressure of the cylinder beyond which the plastic flow will take  *
C     place in the cylinder  wall. The method is based on finding the   *
C     minimum value of internal pressure which satisfies equation (4.1) *
C     ******************************************************************
      SUBROUTINE PCRIT(FF,FG,FH,FR,FM,FN,RC,PCMIN,RCC,PCMAX,RMAX,PCR,DT,
     $E,SO,ALPHA,PR,RA,RB,N1)
      DIMENSION FF(51),FG(51),FH(51),FR(51),FM(51),FN(51),PCR(51),RC(51)
C     ******************************************************************
C     The cylinder thickness is divided into N1 number of division and *
C     the functions F, G, H, R, M and N are evaluated at all division   *
C     points across the thickness.                                      *
C     ******************************************************************
      NP=N+1
      DR=(RB-RA)/N
      DO 40 K=1,NP
      RC(K)=RA+(K-1)*DR
      IF(K.EQ.NP)RC(K)=RB
      FG(K)=((RA**2/(RB**2-RA**2))*(1-(RB**2/RC(K)**2)))
      FR(K)=((RA**2/(RB**2-RA**2))*(1+(RB**2/RC(K)**2)))
      FN(K)=RA**2/(RB**2-RA**2)
      FF(K)=((E*ALPHA*DT)/(2*(1-PR)*(RB**2-RA**2)*ALOG(RB/RA)))*(((RA**2
     $*RB**2*ALOG(RB/RA))/RC(K)**2)+(RB**2*ALOG(RC(K)/RB))-(RA**2*ALOG(
     $RC(K)/RA)))
      FH(K)=((E*ALPHA*DT)/(2*(1-PR)*(RB**2-RA**2)*ALOG(RB/RA)))*(((-RA**
     $2*RB**2*ALOG(RB/RA))/RC(K)**2)+(RB**2*ALOG(RC(K)/RB))-(RA**2*ALOG(
     $RC(K)/RA))+(RB**2-RA**2))
      FM(K)=((E*ALPHA*DT)/(2*(1-PR)*(RB**2-RA**2)*ALOG(RB/RA)))*(2*RB**2
     $*ALOG(RC(K)/RB)-2*RA**2*ALOG(RC(K)/RA)+(RB**2-RA**2))
C     ******************************************************************
C     A, B and C are the coefficients of the critical condition         *
C     equation (4.1) which are function of the history-independent      *
C     functions of F, G, H, R, M and N and therefore can be evaluated   *
C     for all division points across the thickness of the tube          *
C     ******************************************************************
      A=2*(FG(K)**2+FR(K)**2+FN(K)**2-FG(K)*FR(K)-FR(K)*FN(K)-FN(K)*FG(K
     $))
      B=4*(FF(K)*FG(K)+FH(K)*FR(K)+FM(K)*FN(K))-2*(FF(K)*FR(K)+FH(K)*FG(
     $K)+FH(K)*FN(K)+FM(K)*FR(K)+FM(K)*FG(K)+FF(K)*FN(K))
      C=2*(FF(K)**2+FH(K)**2+FM(K)**2-FF(K)*FH(K)-FH(K)*FM(K)-FM(K)*FF(K
     $)-SO**2)
C     ******************************************************************
C     The pressure satisfying equation (4.1) is calculated for all      *
C     division points across the thickness the minimum of which is the  *
C     critical pressure and its location is the place in which yielding*
C     will first start to progress.                                     *
C     ******************************************************************
      IF(B**2-4*A*C)44,60,60
60    P1=(-B+SQRT(B**2-4*A*C))/(2*A)
      P2=(-B-SQRT(B**2-4*A*C))/(2*A)
      IF(P1.LT.0..AND.P2.LT.0.)GO TO 44
```

```
      IF(P1.LT.0..AND.P2.GT.0.)GO TO 150
      IF(P2.LT.0..AND.P1.GT.0.)GO TO 140
      IF(P1-P2)140,140,150
140   PCR(K)=P1
      GO TO 40
150   PCR(K)=P2
      GO TO 40
44    PCR(K)=0.0
40    CONTINUE
      DO 61 KK=1,NP
      IF(PCR(KK).EQ.0.)RETURN
61    CONTINUE
      PCMIN=PCR(1)
      RCC=RC(1)
      DO 51 IK=2,NP
      IF(PCMIN-PCR(IK))51,51,17
17    PCMIN=PCR(IK)
      RCC=RC(IK)
51    CONTINUE
      PCMAX=PCR(1)
      RMAX=RC(1)
      DO 50 IT=2,NP
      IF(PCMAX-PCR(IT))1,50,50
1     PCMAX=PCR(IT)
      RMAX=RC(IT)
50    CONTINUE
      RETURN
      END
```

```
c     ************************************************************
c     This subprogram calculates the plastic strain distribution *
c     within the plastic region of the elastoplastic vessel by   *
c     adding the converged value of plastic strain increments to *
c     the previously accumulated plastic strains.                *
c     ************************************************************
      SUBROUTINE  EPSPL(I,EPR,EPT,EPZ,DEPR,DEPT)
      REAL EPR(50,51),EPT(50,51),EPZ(50,51),DEPR(50,51),DEPT(50,51)
      IM=I+1
      DO 3 J=1,IM
      IF(I.EQ.1)GO TO 1
      IF(J.EQ.IM)GO TO 2
      EPR(I,J)=EPR(I-1,J)+DEPR(I,J)
      EPT(I,J)=EPT(I-1,J)+DEPT(I,J)
      EPZ(I,J)=-(EPT(I,J)+EPR(I,J))
3     CONTINUE
1     EPR(I,J)=DEPR(I,J)
      EPT(I,J)=DEPT(I,J)
      EPZ(I,J)=-(EPT(I,J)+EPR(I,J))
2     EPT(I,IM)=0.
      EPR(I,IM)=0.
      EPZ(I,IM)=0.
      RETURN
      END
```

```
c     ****************************************************************
c     This subprogram has been developed for the computation of the    *
c     integrals of total plastic strains. Plastic strain distributions *
c     calculated in EPSPL subprogram are used to evaluate the integral *
c     of plastic strains. The procedure is based on trapezoid method.  *
c     ****************************************************************
      SUBROUTINE AREA(I,TRB1,TRB2,TTB1,TTB2,TTC1,TTC2,TRC1,TRC2,EPR,EPT,
     $RC)
      REAL  EPR(50,51),EPT(50,51),RC(51),TTC1(50,51),TTC2(50,51),TRC1(50
     $,51),TRC2(50,51)
      DO 20 J=1,I
      IF(J.EQ.1) THEN
          TRC1(I,J)=0.
          TRC2(I,J)=0.
          TTC1(I,J)=0.
          TTC2(I,J)=0.
        ELSE
          TRC1(I,J)=TRC1(I,J-1)+0.5*(EPR(I,J-1)*RC(J-1)+EPR(I,J)*RC(J))*
     $    ABS(RC(J)-RC(J-1))
          TTC1(I,J)=TTC1(I,J-1)+0.5*(EPT(I,J-1)*RC(J-1)+EPT(I,J)*RC(J))*
     $    ABS(RC(J)-RC(J-1))
          TRC2(I,J)=TRC2(I,J-1)+0.5*(EPR(I,J-1)/RC(J-1)+EPR(I,J)/RC(J))*
     $    ABS(RC(J)-RC(J-1))
          TTC2(I,J)=TTC2(I,J-1)+0.5*(EPT(I,J-1)/RC(J-1)+EPT(I,J)/RC(J))*
     $    ABS(RC(J)-RC(J-1))
      ENDIF
20    CONTINUE
      TRB1=TRC1(I,I)
      TRB2=TRC2(I,I)
      TTB1=TTC1(I,I)
      TTB2=TTC2(I,I)
      RETURN
      END
```

```
C     ****************************************************************
C     This subprogram has been developed for the computation of the   *
C     elastoplastic interface by using the boundary condition at this *
C     surface. At this boundary the von Mises yield condition must be *
C     satisfied. The procedure is based on the bisection method to    *
C     find the radius which satisfies the Mises equation.             *
C     ****************************************************************
      SUBROUTINE  BISEC1(I,RA,RB,RCC,SO,E,ALPHA,DT,PR,RCMIN,PI,PO,TA
     $,TB,RC,EPR,EPT,TRC1,TRC2,TTC1,TTC2,TTB1,TTB2,TRB1,TRB2)
      FG(R)=((R**2/(RB**2-R**2))*(1-(RB**2/R**2)))
      FR(R)=((R**2/(RB**2-R**2))*(1+(RB**2/R**2)))
      FN(R)=R**2/(RB**2-R**2)
      FH(R)=((E*ALPHA*((TA*ALOG(RB)-TB*ALOG(RA))/ALOG(RB/RA)-((TA-TB)/
     $ALOG(RB/RA))*ALOG(R)-TB))/(2*(1-PR)*(RB**2-R**2)*ALOG(RB/R)))*
     $(-2*RB**2*ALOG(RB/R)+RB**2-R**2)
      FM(R)=((E*ALPHA*((TA*ALOG(RB)-TB*ALOG(RA))/ALOG(RB/RA)-((TA-TB)/
     $ALOG(RB/RA))*ALOG(R)-TB))/(2*(1-PR)*(RB**2-R**2)*ALOG(RB/R)))*
     $(-2*RB**2*ALOG(RB/R)+RB**2-R**2)
      SR(R)=((E*ALPHA*DT)/(2*(1-PR)*(RB**2-RA**2)*ALOG(RB/RA)))*(((
     $RA**2*RB**2*ALOG(RB/RA))/R**2)+(RB**2*ALOG(R/RB))-(RA**2*
     $ALOG(R/RA)))+(PI*RA**2-PO*RB**2)/(RB**2-RA**2)+RA**2*RB**2*(
     $PO-PI)/((RB**2-RA**2)*R**2)+(E/(2*(1-PR**2)*(RB**2-RA**2)))*
     $((1-2*PR)*(TTB1+0.5*(EPT*RC)*(R-RC))+(1-2*PR)*(TRB1+0.5*(EPR*RC)*
     $(R-RC))+RB**2*(TTB2+0.5*(EPT/RC)*(R-RC))-RB**2*(TRB2+0.5*(EPR/RC)
     $*(R-RC)))*(1-RA**2/R**2)-(E/(2*(1-PR**2)*R**2))*((1-2*PR)*
     $(TTC1+0.5*(EPT*RC)*(R-RC))+(1-2*PR)*(TRC1+0.5*(EPR*RC)*(R-RC))+
     $R**2*(TTC2+0.5*(EPT/RC)*(R-RC)-TRC2-0.5*(EPR/RC)*(R-RC)))
      IF(RC .GE. RB)STOP
      R2=RC+0.1
      R1=RC
      DO 108 K=1,50
      R3=(R1+R2)/2.
      IF(ABS(R1-R2).LT.0.0001)GO TO 109
      A1=2*(FG(R1)**2+FR(R1)**2+FN(R1)**2-FG(R1)*FR(R1)
     $-FR(R1)*FN(R1)-FN(R1)*FG(R1))
      A2=2*(FG(R2)**2+FR(R2)**2+FN(R2)**2-FG(R2)*FR(R2)
     $-FR(R2)*FN(R2)-FN(R2)*FG(R2))
      A3=2*(FG(R3)**2+FR(R3)**2+FN(R3)**2-FG(R3)*FR(R3)
     $-FR(R3)*FN(R3)-FN(R3)*FG(R3))
      B1=4*(FH(R1)*FR(R1)+FM(R1)*FN(R1))-2*(FH(R1)*FG(R1)
     $+FH(R1)*FN(R1)+FM(R1)*FR(R1)+FM(R1)*FG(R1))
      B2=4*(FH(R2)*FR(R2)+FM(R2)*FN(R2))-2*(FH(R2)*FG(R2)
     $+FH(R2)*FN(R2)+FM(R2)*FR(R2)+FM(R2)*FG(R2))
      B3=4*(FH(R3)*FR(R3)+FM(R3)*FN(R3))-2*(FH(R3)*FG(R3)
     $+FH(R3)*FN(R3)+FM(R3)*FR(R3)+FM(R3)*FG(R3))
      C1=2*(FH(R1)**2+FM(R1)**2-FH(R1)*FM(R1)-SO**2)
      C2=2*(FH(R2)**2+FM(R2)**2-FH(R2)*FM(R2)-SO**2)
      C3=2*(FH(R3)**2+FM(R3)**2-FH(R3)*FM(R3)-SO**2)
      Y1=A1*SR(R1)**2+B1*ABS(SR(R1))+C1
      Y2=A2*SR(R2)**2+B2*ABS(SR(R2))+C2
      IF((Y1*Y2).GT.0.)GO TO 11
      Y3=A3*SR(R3)**2+B3*ABS(SR(R3))+C3
```

```
      IF((Y1*Y3).GT.0.)GO TO 104
      R2=R3
      GO TO 108
104   R1=R3
108   CONTINUE
109   RCC=R3
      IF(RCC .GE. RB)RCC=RB
      RETURN
11    WRITE(30,12)
12    FORMAT(2X,'INITIAL VALUE ARE NOT TRUE')
      STOP
      END
```

```
C     ****************************************************************
C     This subprogram has been developed for the computation of the   *
C     elastoplastic interface for the case in which yielding starts   *
C     from the outside surface of the cylinder by using the boundary  *
C     condition at the elastic-plastic boundary                       *
C     At this boundary the von Mises yield condition must be          *
C     satisfied. The procedure is based on the bisection method to    *
C     find the radius which satisfies the Mises equation.             *
C     ****************************************************************
      SUBROUTINE  BISEC2(I,RA,RB,RCC,SO,E,ALPHA,DT,PR,RCMIN,PI,PO,TA
     $,TB,RC)
      FR(R)=(RA**2/(R**2-RA**2))*2
      FN(R)=RA**2/(R**2-RA**2)
      FF(R)=-((R**2/(R**2-RA**2))*(1-RA**2/R**2))*ABS((
     $((E*ALPHA*DT)/(2*(1-PR)*(RB**2-RA**2)*ALOG(RB/RA)))*(((
     $RA**2*RB**2*ALOG(RB/RA))/R**2)+(RB**2*ALOG(R/RB))-(RA**2*
     $ALOG(R/RA)))+(PI*RA**2-PO*RB**2)/(RB**2-RA**2)+RA**2*RB**2*(
     $PO-PI)/((RB**2-RA**2)*R**2)))
      FH(R)=((E*ALPHA*(TA-(TA*ALOG(RB)-TB*ALOG(RA))/ALOG(RB/RA)+((TA-TB)
     $/ALOG(RB/RA))*ALOG(R)))/(2*(1-PR)*(R**2-RA**2)*ALOG(R/RA)))*
     $(-2*RA**2*ALOG(R/RA)+R**2-RA**2)-((R**2/(R**2-RA**2))*(1+RA**2/R**
     $2))*ABS(((E*ALPHA*DT)/(2*(1-PR)*(RB**2-RA**2)*ALOG(RB/RA)))*(((
     $RA**2*RB**2*ALOG(RB/RA))/R**2)+(RB**2*ALOG(R/RB))-(RA**2*
     $ALOG(R/RA)))+(PI*RA**2-PO*RB**2)/(RB**2-RA**2)+RA**2*RB**2*(
     $PO-PI)/((RB**2-RA**2)*R**2)))
      FM(R)=((E*ALPHA*(TA-(TA*ALOG(RB)-TB*ALOG(RA))/ALOG(RB/RA)+((TA-TB)
     $/ALOG(RB/RA))*ALOG(R)))/(2*(1-PR)*(R**2-RA**2)*ALOG(R/RA)))*(-2*
     $RA**2*ALOG(R/RA)+R**2-RA**2)
      R1=RC-0.03
      R2=RB
      DO 108 K=1,50
      R3=(R1+R2)/2.
      IF(ABS(R1-R2).LT.0.0001)GO TO 109
      A1=2*(FR(R1)**2+FN(R1)**2-FR(R1)*FN(R1))
      A2=2*(FR(R2)**2+FN(R2)**2-FR(R2)*FN(R2))
      A3=2*(FR(R3)**2+FN(R3)**2-FR(R3)*FN(R3))
      B1=4*(FH(R1)*FR(R1)+FM(R1)*FN(R1))-2*(FF(R1)*FR(R1)
     $+FH(R1)*FN(R1)+FM(R1)*FR(R1)+FF(R1)*FN(R1))
      B2=4*(FH(R2)*FR(R2)+FM(R2)*FN(R2))-2*(FF(R2)*FR(R2)
     $+FH(R2)*FN(R2)+FM(R2)*FR(R2)+FF(R2)*FN(R2))
      B3=4*(FH(R3)*FR(R3)+FM(R3)*FN(R3))-2*(FF(R3)*FR(R3)
     $+FH(R3)*FN(R3)+FM(R3)*FR(R3)+FF(R3)*FN(R3))
      C1=2*(FF(R1)**2+FH(R1)**2+FM(R1)**2-FF(R1)*FH(R1)-FH(R1)*FM(R1)
     $-FM(R1)*FF(R1)-SO**2)
      C2=2*(FF(R2)**2+FH(R2)**2+FM(R2)**2-FF(R2)*FH(R2)-FH(R2)*FM(R2)
     $-FM(R2)*FF(R2)-SO**2)
      C3=2*(FF(R3)**2+FH(R3)**2+FM(R3)**2-FF(R3)*FH(R3)-FH(R3)*FM(R3)
     $-FM(R3)*FF(R3)-SO**2)
      Y1=A1*PI**2+B1*PI+C1
      Y2=A2*PI**2+B2*PI+C2
      IF((Y1*Y2).GT.0.)GO TO 11
      Y3=A3*PI**2+B3*PI+C3
```

```
      IF((Y1*Y3).GT.0.)GO TO 104
      R2=R3
      GO TO 108
104   R1=R3
108   CONTINUE
109   RCC=R3
      IF(ÀBS(RCC-RA) .LT. 0.001)RCC=RA
      RETURN
11    WRITE(30,12)
12    FORMAT(2X,'INITIAL VALUE ARE NOT SUITABLE')
      STOP
      END
```

Appendix B

The computer program which has been developed for the computation of creep stress and damage histories as well as the remaining life evaluation of thick-walled tubes subjected to an internal pressure and a thermal gradient is introduced in this appendix.

```
C     ****************************************************************
C     * This computer Program has been developed for the computation of *
C     * creep stress and damage histories as well as the remaining life *
C     * evaluations of thick-walled tubes subjected to an internal      *
C     * pressure and a thermal gradient.                                *
C     * The program is written based on the block diagram of Figure 4.4.*
C     * It contains four subprograms which will be introduced after the *
C     * main program.                                                   *
C     ****************************************************************
C     * Definition of arrays:                                           *
C     * 1- FF(51),FH(51),FG(51),FR(51),FM(51):These arrays representing *
C     *    magnitudes of non-history dependent functions of F', H', G', *
C     *    R' and M' defined in Equation (3.80) at all 51 division      *
C     *    points across the thickness of the tube.                     *
C     * 2- PCR(51): This array representing the magnitudes of internal  *
C     *    pressure satisfying Equation (3.70) at all division points   *
C     * 3- R(51): Representing magnitudes of radius at all divisions    *
C     * 4- SRE(51),STE(51),SZE(51):Radial, tangential and axial elastic *
C     *    stresses                                                     *
C     * 5- T(51): Temperature distribution                              *
C     * 6- SRC(20001,51),STC(20001,51),SZC(20001,51):Radial, tangential *
C     *    and axial creep stresses.                                    *
C     * 7- ECR(20001,51),ECT(20001,51),ECZ(20001,51): Radial, tangential*
C     *    and axial total creep  strains.                              *
C     * 8- DECR(20001,51),DECT(20001,51),DECZ(20001,51):  Radial,       *
C     *    tangential and axial creep strain increments.                *
C     * 9- DECRN(20001,51),DECTN(20001,51),DECZN(20001,51):New obtained *
C     *    values of Radial,tangential and axial creep strain increments*
C     * 10- ECDR(20001,51),ECDT(20001,51): Radial and tangential creep  *
C     *     strain rate                                                 *
C     * 11- TET1(20001,51),TET2(20001,51),TET3(20001,51),TET4(20001,51):*
C     *     representing functions defined by the theta projection.     *
C     * 12- ITME(20001): increment of time                              *
C     * 13- TMON(20001): Time (month)                                   *
C     * 14- DEC(20001,51),EC(20001,51): Effective creep strain          *
C     *     increment and the total accumulated effective creep strain. *
C     * 15- SEF(20001,51): Effective stress                             *
C     * 16- EPF(20001,51): Creep rupture strain                         *
C     * 17_ TTC1(20001,51),TTC2(20001,51),TRC1(20001,51),TRC2(20001,51):*
C     *     Integrals of radial and tangential total creep strains      *
C     * 18- DM(20001,51),RL(20001,51): Creep damage and remaining life  *
C     * ****************************************************************
C     ****************************************************************
      PROGRAM creep
      DIMENSION FF(51),FH(51),FG(51),FR(51),FM(51),PCR(51),R(51)
     $,SRE(51),STE(51),SZE(51),T(51),RC(51),ITME(20001),ECE(20001,51),
     $ECR(20001,51),DECRN(20001,51),ECT(20001,51),DECTN(20001,51),
     $SRC(20001,51),STC(20001,51),SZC(20001,51),SEF(20001,51),TTC1(20001
     $,51),TTC2(20001,51),TRC1(20001,51),TRC2(20001,51),DEC(20001,51)
     $,DECZN(20001,51),DECR(20001,51),DECT(20001,51),DECZ(20001,51)
     $,TET1(20001,51),TET2(20001,51),TET3(20001,51),TET4(20001,51)
     $,ECDT(20001,51),ECDR(20001,51),EC(20001,51),ECZ(20001,51)
     $,EPF(20001,51),SF(51),DM(20001,51),RL(20001,51),TMON(20001)
```

```
C     ***************************************************************
C      INPUT DATA: Dimensionless elastic modulus, dimensionless yield   *
C                  stress, coefficient of linear thermal expansion,      *
C                  Poisson's ratio, inner radius, outer radius, number   *
C                  of timing step, number of divisions along radius,     *
C                  initial value of radial and tangential creep strain   *
C                  increments, convergence criteria, Inner and outer     *
C                  temperature, time increment, constant coefficient of  *
C                  material creep properties as; A1,A2,A3,A4,A5,B1,B2,   *
C                  B3,B4,B5,C1,C2,C3,C4,C5,D1,D2,D3,D4,D5.               *
C     ***************************************************************
C
      DATA E,SO,ALPHA,PR,RA,RB,M1,N1,ECRI,ECTI,Q,
     $TA,TB,IDTIME,A1,A2,A3,A4,A5,B1,B2,B3,B4,B5,C1,C2,C3,C4,C5,D1,D2
     $,D3,D4,D5/702,1.0,0.0000117,0.3,1.0,1.65,50,20001,-0.00001,
     $0.00001,0.1E-10,557,550,10000,
     $-8.736,-0.002346,-1.869,-16.43,-1.123,0.004604,0.02225,-0.002034,
     $0.009149,0.001517,-0.04489,0.02195,-0.05497,-0.04723,0.0005473,
     $0.00006814,-0.00001951,0.00007990,0.00007139,-0.0000004721/
C     ***************************************************************
C     * OUTPUT DATA WILL BE WRITTEN INTO THE FOLLOWING OUTPUT FILES.    *
C     * elstrs.dat: Elastic stress distribution                         *
C     * cstrs.dat:  Creep stress distribution                           *
C     * esd.dat:    Effective stress distribution                       *
C     * csd.dat:    Creep strain distribution                           *
C     * esh.dat:    Effective stress histories                          *
C     * ecsh.dat:   Effective Creep strain histories                    *
C     * dh.dat:     Damage histories                                    *
C     * dd.dat:     Damage distribution                                 *
C     * fdd.dat:    Final damage distribution                           *
C     * rlh.dat:    Remaining life histories                            *
C     * fcsd.dat:   Final creep strain distribution                     *
C     ***************************************************************
      OPEN(UNIT=10,FILE='elstrs.dat',STATUS='OLD')
      OPEN(UNIT=20,FILE='cstrs.dat',STATUS='OLD')
      OPEN(UNIT=25,FILE='esd.dat',STATUS='OLD')
      OPEN(UNIT=30,FILE='csd.dat',STATUS='OLD')
      OPEN(UNIT=40,FILE='esh.dat',STATUS='OLD')
      OPEN(UNIT=50,FILE='ecsh.dat',STATUS='OLD')
      OPEN(UNIT=60,FILE='dh.dat',STATUS='OLD')
      OPEN(UNIT=65,FILE='dd.dat',STATUS='OLD')
      OPEN(UNIT=70,FILE='fdd.dat',STATUS='OLD')
      OPEN(UNIT=75,FILE='rlh.dat',STATUS='OLD')
      OPEN(UNIT=80,FILE='fcsd.dat',STATUS='OLD')
C     ***************************************************************
C     *                  ELASTIC SOLUTION                             *
C     ***************************************************************
C      Critical pressure of the tube will be calculated in subprogram  *
C      PCRIT and the elastic stress distribution will be calculated    *
C     ***************************************************************
      DT=TA-TB
```

```
      CALL PCRIT(FF,FG,FH,FR,FM,RC,PCMIN,RCMIN,PCMAX,RMAX,PCR,DT,E,
     $SO,ALPHA,PR,RA,RB,M1)
      NP=M1+1
      DO 11 I=1,NP
c      PI=PCMIN
      PI=0.5*PCMIN
      SRE(I)=FF(I)+FG(I)*PI
      STE(I)=FH(I)+FR(I)*PI
      SZE(I)=FM(I)+FN(I)*PI
      SF(I)=((1/(2**0.5))*(SQRT((SRE(I)-STE(I))**2+(STE(I)-
     $SZE(I))**2+(SZE(I)-SRE(I))**2)))
      WRITE(10,15)RC(I),SRE(I),STE(I),SZE(I),SF(I),PI
15    FORMAT(F8.6,3X,F7.4,3X,F7.4,3X,F7.4,3X,F7.4,X,F7.4)
11    CONTINUE
c     ***************************************************************
c                          CREEP SOLUTION                             *
c     ***************************************************************
c     The above elastic stress distribution has been considered as the *
c     stress distribution which will be changed with time. A short     *
c     time increment (IDTIME) will be selected and a variation of      *
c     stresses and strains will be computed for this time increment    *
c     ***************************************************************
      DO 100 I=1,N1
      ITER=0
      IF(I .EQ. 1) THEN
            ITME(I)=IDTIME
          ELSE
            ITME(I)=ITME(I-1)+IDTIME
      ENDIF
      TMON(I)=ITME(I)/2592000.0
      TIME=ITME(I)
      DR=(RB-RA)/M1
      IM=M1+1
c     ***************************************************************
c     Initial values are estimated for the creep strain increments     *
c     ***************************************************************
      IF(I .EQ. 1) THEN
          DO 420 K=1,IM
          DECT(I,K)=EPTI
          DECR(I,K)=EPRI
          DECZ(I,K)=-(DECR(I,K)+DECT(I,K))
420       CONTINUE
        ELSE
          DO 402 K=1,IM
          DECR(I,K)=DECR(I-1,K)
          DECT(I,K)=DECT(I-1,K)
          DECZ(I,K)=-(DECR(I,K)+DECT(I,K))
402       CONTINUE
      ENDIF
```

```
C     ****************************************************************
C     The creep strain increments will be added to the previously      *
C     converged values of creep strains in ECSPL subprogram and the    *
C     integral of total creep strains will be computed in the AREACR   *
C     subprogram. Then an estimate of stresses will be obtained        *
C     ****************************************************************
      DO 101 J=1,IM
      R(J)=RA+(J-1)*DR
9     CALL  ECSPL(I,M1,ECR,ECT,ECZ,DECR,DECT)
      CALL AREACR(I,M1,TRB1,TRB2,TTB1,TTB2,TTC1,TTC2,TRC1,TRC2,ECR,ECT,
     $R,DR,RA)
      IF(ITER .GT. 20) STOP
      SRC(I,J)=SRE(J)+(E/(2*(1-PR**2)*(RB**2-RA**2)))*
     $((1-2*PR)*(TTB1+TRB1)+RB**2*(TTB2-TRB2))*(1-RA**2/R(J
     $)**2)-(E/(2*(1-PR**2)*R(J)**2))*(+(1-2*PR)*(TTC1(I,J)+TRC1(I,J))
     $+R(J)**2*(TTC2(I,J)-TRC2(I,J)))
      STC(I,J)=STE(J)+(E/(2*(1-PR**2)*(
     $RB**2-RA**2)))*((1-2*PR)*(TTB1+TRB1)+RB**2*(TTB2-TRB2)
     $)*(1+RA**2/R(J)**2)+(E/(2*(1-PR**2)*R(J)**2))*(+(1-2*PR)*(TTC1(I
     $,J)+TRC1(I,J))-R(J)**2*(TTC2(I,J)-TRC2(I,J))-2*R(J)**2*
     $((1-PR)*ECT(I,J)-PR*ECR(I,J)))
      SZC(I,J)=SZE(J)+(E*PR/((RB**2-RA**2)*(1-PR**2)))*((1-2*PR)*(TTB1
     $+TRB1)+RB**2*(TTB2-TRB2))-(E/(1-PR**2))*PR*((TTC2(I,J
     $)-TRC2(I,J))+(1-PR)*ECT(I,J)-PR*ECR(I,J))-(E/(RB**2-RA**2))*(2*
     $TRB1+2*TTB1-(RB**2-RA**2)*(ECR(I,J)+ECT(I,J)))
      SEF(I,J)=((1/(2**0.5))*(SQRT((SRC(I,J)-STC(I,J))**2+(STC(I,J)-
     $SZC(I,J))**2+(SZC(I,J)-SRC(I,J))**2)))
C     ****************************************************************
C     Temperature distribution and the effective stresses will be      *
C     computed across the thickness and the effective creep strain     *
C     will be calculated from the material constitutive model.         *
C     ****************************************************************
      T(J)=(TA*LOG10(RB)-TB*LOG10(RA))/LOG10(RB/RA)+(((TB-TA)*
     $LOG10(R(J)))/LOG10(RB/RA))+273.15
      SE=SEF(I,J)*200
      TET1(I,J)=10.0**(A1+B1*T(J)+C1*SE+D1*SE*T(J))
      TET2(I,J)=10.0**(A2+B2*T(J)+C2*SE+D2*SE*T(J))
      TET3(I,J)=10.0**(A3+B3*T(J)+C3*SE+D3*SE*T(J))
      TET4(I,J)=10.0**(A4+B4*T(J)+C4*SE+D4*SE*T(J))
      EPF(I,J)=A5+B5*T(J)+C5*SE+D5*SE*T(J)
      ECE(I,J)=TET1(I,J)*(1-EXP(-TET2(I,J)*(TIME)))+
     $TET3(I,J)*(-1+EXP(TET4(I,J)*(TIME)))
C     ****************************************************************
C      Creep strain rate in radial and tangential directions will be   *
C      computed and new values will be calculated for the previously   *
C      estimated creep strain increments and will inspected  for the   *
C      convergence.                                                    *
C     ****************************************************************
      ECDR(I,J)=((TET1(I,J)*TET2(I,J)*EXP(-TET2(I,J)*(TIME+IDTIME/2)))+(
     $TET3(I,J)*TET4(I,J)*EXP(TET4(I,J)*(TIME+IDTIME/2))))*(2*SRC(I,J)-
     $STC(I,J)-SZC(I,J))/(2*SEF(I,J))
      ECDT(I,J)=((TET1(I,J)*TET2(I,J)*EXP(-TET2(I,J)*(TIME+IDTIME/2)))+(
     $TET3(I,J)*TET4(I,J)*EXP(TET4(I,J)*(TIME+IDTIME/2))))*(2*STC(I,J)-
     $SRC(I,J)-SZC(I,J))/(2*SEF(I,J))
```

```
      DECRN(I,J)=ECDR(I,J)*IDTIME
      DECTN(I,J)=ECDT(I,J)*IDTIME
      DECZN(I,J)=-(DECRN(I,J)+DECTN(I,J))
      DEC(I,J)=((2**0.5)/3)*(SQRT((DECRN(I,J)-DECTN(I,J))**2+
     $(DECTN(I,J)-DECZN(I,J))**2+(DECZN(I,J)-DECRN(I,J))**2))
      IF(I .GT. 1)THEN
           EC(I,J)=EC(I-1,J)+DEC(I,J)
      ENDIF
      DELR=ABS(DECRN(I,J)-DECR(I,J))
      DELT=ABS(DECTN(I,J)-DECT(I,J))
      IF(DELR.LT.Q.AND.DELT.LT.Q) THEN
            ITER=0
            GO TO 101
         ELSE
            DECR(I,J)=DECRN(I,J)
            DECT(I,J)=DECTN(I,J)
            DECZ(I,J)=DECZN(I,J)
            ITER=ITER+1
            GO TO  9
      ENDIF
101   CONTINUE
c     ***************************************************************
c     After the convergence the effective stress histories will be used*
c     in DAMAGE subprogram and the damage history and the remaining    *
c     life of the tube will be obtained and the results will be written*
c     into the output files.                                           *
c     ***************************************************************
      CALL DAMAGE(I,DM,EPF,TET1,TET2,TET3,TET4,TIME,SEF,IDTIME,RL)
100   CONTINUE
      DO 189 K=1,N1,2000
      WRITE(40,158)TMON(K),SEF(K,1),SEF(K,26),SEF(K,51),STC(K,1),STC(K,
     $51)
158   FORMAT(F12.6,2X,5(E10.4,2X))
      WRITE(50,158)TMON(K),ECE(K,1),ECE(K,26),ECE(K,51),EC(K,1),
     $EC(K,51)
      WRITE(60,158)TMON(K),EPF(K,1),EPF(K,51),DM(K,1),DM(K,26),DM(K,51)
      WRITE(65,58)DM(K,1),RL(K,1),DM(K,26),RL(K,26),DM(K,51),RL(K,51)
      WRITE(75,158)TMON(K),EPF(K,1),EPF(K,51),RL(K,1),RL(K,26),RL(K,51)
58    FORMAT(3(E10.4,2X,F10.4,2X))
189   CONTINUE
      DO 139 I=N1,N1
      DO 207 JJ=1,IM
      IF(I .EQ. N1)THEN
              WRITE(80,311)ECR(I,JJ),ECT(I,JJ),EC(I,JJ),ITME(I)
311           FORMAT(3(2X,E15.8),2X,I12)
          IF(JJ .EQ. IM) THEN
                DO 2020 JK=1,IM,5
2020            WRITE(70,104)R(JK),DM(I,JK),ITME(I)
104             FORMAT(E12.5,2X,E20.14,2X,I12)
          ENDIF
      ENDIF
207   WRITE(30,208)R(JJ),ECR(I,JJ),ECT(I,JJ),ECZ(I,JJ),EC(I,JJ)
```

```
208   FORMAT(5(E13.6,X))
      DO 202 JJ=1,IM
      WRITE(25,204)R(JJ),SEF(I,JJ),TMON(I)
204   FORMAT(E12.5,2X,E12.5,2X,F12.6)
202   WRITE(20,201)R(JJ),SRC(I,JJ),STC(I,JJ),SZC(I,JJ),TMON(I)
201   FORMAT(E12.5,2X,E12.5,2X,E12.5,2X,E12.5,2X,F12.6)
139   CONTINUE
      STOP
      END
```

```
C     ****************************************************************
C     This subprogram has been developed to calculate the critical inner*
C     pressure of the tube and is similar to  subroutine PCRIT already  *
C     discussed in Appendix A  and therefore no further comment will be *
C     written on this subprogram.                                       *
C     ****************************************************************
      SUBROUTINE PCRIT(FF,FG,FH,FR,FM,RC,PCMIN,RCC,PCMAX,RMAX,PCR,DT,
     $E,SO,ALPHA,PR,RA,RB,M1)
       DIMENSION FF(51),FG(51),FH(51),FR(51),FM(51),PCR(51),RC(51)
       NP=M1+1
       DR=(RB-RA)/M1
       DO 40 K=1,NP
       RC(K)=RA+(K-1)*DR
       IF(K.EQ.NP)RC(K)=RB
       FG(K)=((RA**2/(RB**2-RA**2))*(1-(RB**2/RC(K)**2)))
       FR(K)=((RA**2/(RB**2-RA**2))*(1+(RB**2/RC(K)**2)))
       FF(K)=((E*ALPHA*DT)/(2*(1-PR)*(RB**2-RA**2)*ALOG(RB/RA)))*(((RA**2
     $*RB**2*ALOG(RB/RA))/RC(K)**2)+(RB**2*ALOG(RC(K)/RB))-(RA**2*ALOG(
     $RC(K)/RA)))
       FH(K)=((E*ALPHA*DT)/(2*(1-PR)*(RB**2-RA**2)*ALOG(RB/RA)))*(((-RA**
     $2*RB**2*ALOG(RB/RA))/RC(K)**2)+(RB**2*ALOG(RC(K)/RB))-(RA**2*ALOG(
     $RC(K)/RA))+(RB**2-RA**2))
       FM(K)=((E*ALPHA*DT)/(2*(1-PR)*(RB**2-RA**2)*ALOG(RB/RA)))*(2*RB**2
     $*ALOG(RC(K)/RB)-2*RA**2*ALOG(RC(K)/RA)+(RB**2-RA**2))
       A=2*(FG(K)**2+FR(K)**2-FG(K)*FR(K))
       B=4*(FF(K)*FG(K)+FH(K)*FR(K))-2*(FF(K)*FR(K)+FH(K)*FG(
     $K)+FM(K)*FR(K)+FM(K)*FG(K))
       C=2*(FF(K)**2+FH(K)**2+FM(K)**2-FF(K)*FH(K)-FH(K)*FM(K)-FM(K)*FF(K
     $)-SO**2)
       IF(B**2-4*A*C)44,60,60
60     P1=(-B+SQRT(B**2-4*A*C))/(2*A)
       P2=(-B-SQRT(B**2-4*A*C))/(2*A)
       IF(P1.LT.0..AND.P2.LT.0.)GO TO 44
       IF(P1.LT.0..AND.P2.GT.0.)GO TO 150
       IF(P2.LT.0..AND.P1.GT.0.)GO TO 140
       IF(P1-P2)140,140,150
140    PCR(K)=P1
       GO TO 40
150    PCR(K)=P2
       GO TO 40
44     PCR(K)=0.0
40     CONTINUE
       DO 61 KK=1,NP
       IF(PCR(KK).EQ.0.)RETURN
61     CONTINUE
       PCMIN=PCR(1)
       RCC=RC(1)
       DO 51 IK=2,NP
       IF(PCMIN-PCR(IK))51,51,17
17     PCMIN=PCR(IK)
       RCC=RC(IK)
51     CONTINUE
```

```
      PCMAX=PCR(1)
      RMAX=RC(1)
      DO 50 IT=2,NP
      IF(PCMAX-PCR(IT))1,50,50
1     PCMAX=PCR(IT)
      RMAX=RC(IT)
50    CONTINUE
      RETURN
      END
```

```
C     ************************************************************
C     This subprogram calculates the creep strain distribution   *
C     across the thickness of the tube by adding the converged   *
C     value of creep strain increment to the previously          *
C     accumulated creep strains.                                 *
C     ************************************************************
      SUBROUTINE   ECSPL(I,M1,ECR,ECT,ECZ,DECR,DECT)
      DIMENSION ECR(20001,51),ECT(20001,51),ECZ(20001,51),
     $DECR(20001,51),DECT(20001,51)
      IM=M1+1
      DO 3 J=1,IM
      IF(I .EQ. 1) THEN
            ECZ(I,J)=-(ECT(I,J)+ECR(I,J))
         ELSE
            ECR(I,J)=ECR(I-1,J)+DECR(I,J)
            ECT(I,J)=ECT(I-1,J)+DECT(I,J)
            ECZ(I,J)=-(ECT(I,J)+ECR(I,J))
      ENDIF
3     CONTINUE
      RETURN
      END
```

```
c     ****************************************************************
c     This subprogram has been developed for the computation of the    *
c     integrals of total creep strains. Creep strain distributions     *
c     calculated in ECSPL subprogram are used to evaluate the integral *
c     of creep strains. The procedure is based on the trapezoid method.*
c     ****************************************************************
      SUBROUTINE AREACR(I,M1,TRB1,TRB2,TTB1,TTB2,TTC1,TTC2,TRC1,TRC2,
     $ECR,ECT,R,DR,RA)
      DIMENSION  ECR(20001,51),ECT(20001,51),TTC1(20001,51),
     $TTC2(20001,51),TRC1(20001,51),TRC2(20001,51),R(51)
      IM=M1+1
      DO 20 J=1,IM
      IF(J.EQ.1) THEN
          TRC1(I,J)=0.
          TRC2(I,J)=0.
          TTC1(I,J)=0.
          TTC2(I,J)=0.
        ELSE
          R(J)=RA+(J-1)*DR
          TRC1(I,J)=TRC1(I,J-1)+0.5*(ECR(I,J-1)*R(J-1)+ECR(I,J)*R(J))*DR)
          TTC1(I,J)=TTC1(I,J-1)+0.5*(ECT(I,J-1)*R(J-1)+ECT(I,J)*R(J))*DR)
          TRC2(I,J)=TRC2(I,J-1)+0.5*(ECR(I,J-1)/R(J-1)+ECR(I,J)/R(J))*DR)
          TTC2(I,J)=TTC2(I,J-1)+0.5*(ECT(I,J-1)/R(J-1)+ECT(I,J)/R(J))*DR)
      ENDIF
20    CONTINUE
      TRB1=TRC1(I,IM)
      TRB2=TRC2(I,IM)
      TTB1=TTC1(I,IM)
      TTB2=TTC2(I,IM)
      RETURN
      END
```

```
C     ****************************************************************
C     This subprogram has been developed for the computation of creep  *
C     damages and the remaining life evaluations thick-walled tubes    *
C     by using the effective stress histories and the materials creep  *
C     constitutive model and rupture properties.                       *
C     ****************************************************************
      SUBROUTINE DAMAGE(I,DM,EPF,TET1,TET2,TET3,TET4,TIME,SEF,IDTIME
     $,RL)
      DIMENSION TET1(20001,51),TET2(20001,51),TET3(20001,51),RL(20001,
     $51),TET4(20001,51),EPF(20001,51),Y0(20001,51),DM(20001,51),
     $Y1(20001,51),Y2(20001,51),SEF(20001,51),DDM(20001,51)
      ITER=60
      DO 35 K=1,51,5
C     ****************************************************************
C     Time to rupture has been  computed by numerical solution of      *
C     equation(4.28) and the increments of damage are calculated using *
C     the time increment and the rupture time in conjunction with the  *
C     Robinson's damage rule. The damage increments are then           *
C     accumulated to give the total damages. Furthermore, remaining    *
C     life of the tube are calculated using the damage and the rupture *
C     times.                                                           *
C     ****************************************************************
C     TES1 and TES2 are initial values for a bisection method to find  *
C     the rupture times across the thickness.                          *
C     ****************************************************************
      TES1=0.1E+06
      TES2=0.1E+12
      DO 102 M=1,ITER
      Y0(I,K)=-EPF(I,K)+TET1(I,K)*(1-EXP(-TET2(I,K)*(TES1)))+
     $TET3(I,K)*(-1+EXP(TET4(I,K)*(TES1)))
      Y1(I,K)=-EPF(I,K)+TET1(I,K)*(1-EXP(-TET2(I,K)*(TES2)))+
     $TET3(I,K)*(-1+EXP(TET4(I,K)*(TES2)))
      IF((Y0(I,K)*Y1(I,K)) .GT. 0.0) THEN
            WRITE(10,321)
321         FORMAT(5X,'STARTING VALUE UNSUITABLE')
            STOP
         ELSE
            TNEW=(TES1+TES2)/2.0
            Y2(I,K)=-EPF(I,K)+TET1(I,K)*(1-EXP(-TET2(I,K)*(TNEW)))+
     $      TET3(I,K)*(-1+EXP(TET4(I,K)*(TNEW)))
      ENDIF
C     ****************************************************************
C     Convergence of the  method for the rupture time is controlled    *
C     ****************************************************************
      DEF=ABS(TES2-TES1)
      IF(DEF .LT. 150)THEN
                DDM(I,K)=IDTIME/TNEW
           IF(I .EQ. 1)THEN
                DM(I,K)=DM(1,K)+DDM(I,K)
                RL(I,K)=(1-DM(I,K))*(TNEW/2592000.0)
              ELSE
                DM(I,K)=DM(I-1,K)+DDM(I,K)
                RL(I,K)=(1-DM(I,K))*(TNEW/2592000.0)
              ENDIF
```

```
                GO TO 35
      ENDIF
      IF((Y0(I,K)*Y2(I,K)) .GT. 0.0)THEN
          TES1=TNEW
        ELSE
           TES2=TNEW
      ENDIF
102   CONTINUE
35    CONTINUE
      RETURN
      END
```

Chapter 8

REFERENCES

- Allen, D. N. de G. and Sopwith, D. G. (1951), "The Stresses and Strains in a Partly Plastic Thick Tube Under Internal Pressure and End-Load," Proceedings of the Royal Society of London, A205, pp. 69-83.

- ANSYS 5.0 (1992), ANSYS User's Manual for Revision 5.0, Vol. 4, Theory, Swanson Analysis Systems, Inc. Houston, USA.

- API (1978), Recommended Practice for calculation of Heater Tube Thickness in Petroleum Refineries, API Recommended practice, vol. 530, 1978.

- ASME Boiler and Pressure Vessel Code (1981), Class 1 Component in Elevated Temperature Service, Section III, Division 1, Case Interpretations, Code Case N-47-20.

- ASTM (1989), "Standard Test Method of Compression Testing of Metallic Material at Room Temperature, Designation: E 9-89a, pp. 161-168

- Bailey, R. W. (1929), Transaction of the World Power Conference, Tokyo, pp. 1089-1097.

- Bailey, R. W. (1951a), "Creep Relationship and Their Application to Pipes, tubes, and Cylindrical Parts Under Internal Pressure," Proceedings of The Institution of Mechanical Engineers, vol. 164, pp. 425-431.

- Bailey, R. W. (1951b), "Steam Piping for High Pressures and High Temperatures," Proceedings of The Institution of Mechanical Engineers, vol. 164, pp. 324-335.

- Bailey, R. W. (1935), "The Utilization of Creep Test Data In Engineering Design," Proceedings of The Institution of Mechanical Engineers, vol. 131, pp. 131-349.

- Bland, D. R. (1956), "Elastoplastic Thick-Walled Tubes of Work-Hardening Material Subject to Internal and External Pressure and to Temperature Gradients," J. Mech. Phys. Solids, vol. 4, pp. 209-229.

- Bree, J. (1967), "Elastic-Plastic Behaviour of Thin Tubes Subjected to Internal Pressure and Intermittent High-Heat Fluxes With Application to Fast-Nuclear-Reactor Fuel Elements," Journal of Strain Analysis, vol. 2, No. 3, pp. 226-238.

- Brown, R.J., Lonsdale, D. and Flewitt, P.E.J. (1982), "Multiaxial Stress Rupture Testing and Compendium of Data for Creep Resisting Steels," ASME Journal of Engineering Materials and Technology, vol. 104, pp. 291-300.

- Chen, P.C.T. (1986), "The Bauschinger and Hardening Effect on Residual Stresses in an Autofrettaged Thick-Walled Cylinder," ASME Journal of Pressure Vessel Technology , vol. 108, pp. 108-112.

- Coffin, L. F., Shepler, P. R. and Cherniak, G. S. (1949), "Primary Creep in the Design of Internal-Pressure Vessels," Journal of Applied Mechanics, vol. 16, pp. 229-241.

- Cohn, M. J. (1990), "Remaining Life of High-Energy Piping Systems Using Equivalent Stress," ASME Journal of Pressure Vessel Technology, vol. 112, pp 260-265.

- Cook, G. (1934), "The Stresses in Thick-Walled Cylinders of Mild Steel Over-strained by Internal Pressure," Proceedings of The Institution of Mechanical Engineers, vol. 126, pp. 407-455.

- Crossland, B. and Bones, J. A. (1955), "The Ultimate Strength of Thick-Walled Cylinders Subjected To Internal Pressure," Engineering, vol. 179, pp. 80-83 and pp. 114-117.

- Crossland, B. and Bones, J. A. (1958), "Behaviour of Thick-Walled Cylinders Subjected To Internal Pressure," Proceedings of The Institution of Mechanical Engineers, vol. 172, pp. 777-804.

- Crossland, B., Jorgensen S. M. and Bones, J. A. (1959), "The Strength of Thick-Walled Cylinders," Journal of Engineering for Industry, vol. 81, pp. 95-114.

- Derington, M. G. (1962), "The Onset of Yield in a Thick Cylinder Subjected to Uniform Internal or External Pressure and Steady State Heat Flow," Int. J. Mech. Sci. Pergamon Press Ltd., vol. 4, pp. 83-103.

- Evans, R. W., Parker, J. D. and Wilshire, B. (1982), "Recent Advances in Creep and Fracture of Engineering Materials and Structures," Pineridge Press, Swansea, pp. 135-148.

- Evans, R. W., Beden, I. and Wilshire, B. (1984), "Proc. 2nd Int. Conf. on Creep and Fracture of Engineering Materials and Structures," Pineridge Press, Swansea, pp. 1277-1238.

- Evans, R. W. and Wilshire, B. (1985), Creep of Metals and Alloys, Inst. of Metals, London.

- Evans, R. W., Parker, J. D. and Wilshire, B. (1992), "The Θ Projection Concept A Model-Based Approach to Design and Life Extension of Engineering Plant," Int. J. Pres. Ves. & Piping , vol. 50, pp. 147-160.

- Fessler, H. and Hyde, T.H. (1978), "Creep Deformation of Metals," Creep of Engineering Materials, A Journal of Strain Analysis Monograph, Editted by Pomeroy, C. D. pp. 85-110

- Findley, W. N. and Reed, R. M. (1983), "Fatigue of Autofrettage Thick Tubes: Closed and Open Ended," ASME Journal of Engineering Materials and Technology, vol. 105, pp. 195-201.

- Franklin, G. J. and Morrison, J. L. M. (1960), "Autofrettage of Cylinders: Prediction of Pressure/External Expansion Curves and Calculation of Residual Stresses," Proceedings of the Institute of Mechanical Engineers, vol. 174, pp. 947-974.

- Hayhurst, D.R. (1972), " Creep Under Multiaxial State of Stress," Journal of Mechanics and Physics of Solids, vol. 20, pp. 381-390

- Hencky, H. (1933), "The New Theory of Plasticity, Strain Hardening, and Creep, and the Testing of the Inelastic behaviour of Metals," Transactions of the ASME, vol. 55, pp. 151-155.

- Hill, R. (1950), The Mathematical Theory of Plasticity, Oxford Univ. Press, London.

- Hill, R., Lee E. H. and Tupper S. J. (1947), "The Theory of Combined Plastic and Elastic Deformation with Particular Reference to a Thick Tube Under Internal Pressure," Proc. Roy. Soc. London, A, 191, pp. 278-303.

- Hoff, N. J. (1954), "Approximate Analysis of Structures in the Presence of Moderately Large Creep Deformation," Q. Appl. Math., vol. 12, pp. 49-55

- Hodge, P. G. and White, G. N. (1950), "A Quantitative Comparison of Flow and Deformation Theories of Plasticity," Journal of Applied Mechanics, vol. 17, pp. 180-184.

- Huddlestone, R.L. (1985), "An Improved Multiaxial Creep-Rupture Strength Criterion," ASME Journal Of Pressure Vessel Technology, vol. 107, pp. 421-429.

- Hussain M.A., Pu S.L., Vasilkis J.D. and O'Hara P. (1980), "Simulation of Partial Autofrettage by Thermal Loads, ASME Journal of Pressure Vessel Technology , vol. 102 ,pp. 314-318.

- Ibarra and Konet (1995), "Life Assessment of $1\frac{1}{4}Cr - \frac{1}{2}Mo$ Steel Catalytic Reformer Furnace Tubes Using the MPC Omega Method," ASME Journal Pressure Vessel Technology, vol. 117, pp. 19-23.

- Jaske, C.E. and Begley, J.A. (1978), "An Approach to The Assessing Creep/Fatigue Crack Growth, Ductility and Toughness Considerations in Elevated Temperature Service," MPC-8, The ASME Engineers, New york, N.Y., p 391.

- Jaske, C.E. (1990), "Life Assessment of Hot Reheat Steam Pipe," ASME Journal of Pressure Vessel Technology, vol. 112, pp 20-27.

- Jaske, C.E. (1995), "Life Prediction in High-Temperature Structural Materials," ASME Journal of Pressure Vessel Technology, vol. 117, pp. 1-6.

- Koh, S. K. and Stephens, R. I. (1991), "Stress analysis of an autofrettaged thick-walled pressure vessel containing dn external groove," International Journal of pressure vessels and piping, vol. 46, pp. 95-111.

- Koiter, W. T. (1953), "On Partially Plastic Thick-Walled Tubes," Biezeno Anniversary volume in Applied Mechanics, N. V. De Technische Uitgeverij Stam, Haarlem, pp. 232-251.

- Kraus, H. (1980), Creep Analysis, John Wiley& Sons, New york.

- Larson, F. R. and Miller, J. (1952), "A Time Temperature Relationship for Rupture and Creep Stresses," Transactions of The ASME, vol. 174.

- Mackenzie, A. C. (1968), "On the Use of a Single Uniaxial Test to Estimate Deformation Rates in Some Structures Undergoing Creep," International Journal of Mechanical science, Pergamon Press, vol. 10, pp. 441-453.

- Manning, W.R.D. (1945), "The Overstrain of Tubes by Internal Pressure," Engineering, vol. 159, pp. 101-183.

- Manson, S. S. and Haferd, A. M. (1953), "A linear Time-Temperature Relation for Extrapolation of Creep and Stress Rupture Data," NACA, TN 2890.

- Manson, S. S. (1963), "Design Considerations for Long Life at Elevated Temperatures," ASME/ASTM/IME joint International Conference on Creep, New York and London.

- Marriott, D. L. and Leckie, F. A. (1964), "Some Observations on the Deflection of Structures During Creep," Proceedings of The Institution of Mechanical Engineers, vol. 178, pp. 115-125

- Marriott, D. L. (1970), "A Review of Reference Stress Methods for Estimating Creep Deformation," Proceedings of IUTAM Symposium on Creep of Structures, Gothenburg, pp. 137-152.

- Maruyama, K., Tanaka, C. and Oikawa, H. (1990), "Long-Term Creep Curve Prediction Based on the Modified Θ Projection Concept," ASME Journal of

Pressure Vessel Technology, vol. 112, pp. 92-97.

- Maruyama, K. and Oikawa, H. (1987), "An Extrapolation Procedure of Creep Data For S_t Determination: With Special Reference to Cr-Mo-V Steel," ASME Journal of Pressure Vessel Technology, vol. 109, pp. 142-146.

- Mendelson A. (1968), Plasticity Theory and Application, The Macmillan Company, New York.

- Milligan, R.V. ,Koo W.H. and Davidson T.E. (1966), "The Bauschinger Effect in a High Strength Steel," ASME Journal of Basic Engineering, pp. 480-488.

- Nadai, A. (1931), Plasticity, Mc-Graw-Hill, New York.

- Nadai, A. (1963), Theory of Flow and Fracture of Solids, Mc-Graw-Hill, New York.

- , Niitsu, Y. and Ikegami, K. (1990), "Effect of Temperature variation on Cyclic Elastic-Plastic Behaviour of SUS 304 Stainless Steel," ASME Journal of Pressure Vessel Technology, vol. 112, pp. 152-157.

- , Niitsu, Y. and Ikegami, K. (1985), "Effect of Temperature variation on Plastic Behaviour of SUS 304 Stainless Steel," Buletin of JSME, vol. 28, pp. 2853-2858.

- Nogata, F. and Takahashi, H. (1995), "A Creep Damage Estimation Method for In-Service Fossil Fuel Boiler Superheater Tubes," ASME Journal of Pressure Vessel Technology, vol. 117, pp. 14-18.

- Norton, F. H. (1939), "Creep in Tubular Pressure Vessels," Transactions of the ASME, vol. 61, pp. 239-245.

- Norton, F. H. (1941), "Progress Report on Tubular Creep Tests," Transactions of the ASME, vol. 63, pp. 735-736.

- Norton, F. H. (1929), Creep of Steel at High Temperatures, McGraw-Hill, New York.

- Norton, F. H. and Soderberg, C. R. (1942), "Report on Tubular Creep Tests," Transactions of the ASME, vol. 63, pp. 769-777.

- Parker, A. P. and Andrasic, C. P. (1981), "Safe Life Design of Gun Tubes-some Numerical Methods and Results," Proceedings of the 1981 Army Numerical Analysis and Computer Conference, pp. 311-333.

- Parker, A. P., Underwood, J. H., Throop, J. F. and Andrasic, C. P. (1983), "Stress Intensity and Fatigue Crack Growth in a Pressurized Autofrettaged Thick Cylinder," Proceedings of the 14th National Symposium on Fracture Mechanics, ASTM STP 791, vol. 1, pp. 216-237.

- Parker, J. D. (1985), "Prediction of Creep Deformation and Failure for $\frac{1}{2}Cr, \frac{1}{2}Mo, \frac{1}{4}V$ and 2-$\frac{1}{4}Cr, 1Mo$ Steel," ASME Journal of Pressure Vessel Technology, vol. 107, pp. 279-284.

- Perl M. and Arone, R. (1994a), "An Axisymmetric Stress Release Method For Measuring The Autofrettage Level in Thick-Walled Cylinders-Part1: Basic Con-

cept and Numerical Simulation," ASME Journal of Pressure Vessel Technology, vol. 116, pp. 384-388.

- Perl M. and Arone, R. (1994b), "An Axisymmetric Stress Release Method For Measuring The Autofrettage Level in Thick-Walled Cylinders-Part1: Experimental Validation," ASME Journal of Pressure Vessel Technology, vol. 116, pp. 389-395.

- Pu, S. L. and Chen, P. C. T. (1983), "Stress Intensity Factors For Radial Cracks in a Pre-Stressed Thick-Walled Cylinder of Strain-Hardening Material," ASME Journal of Pressure Vessel Technology , vol. 105 , 1983, pp. 117-123.

- Pu, S. L. and Sha, G. T. (1987), "Bauschinger Effect of Reverse Yield Stress Reduction on Radial Crack Growth of a Cylindrical Pressure Vessel," Engineering Fracture Mechanics, vol. 26, pp. 519-525.

- Pu S. L. and Hussain M. A. (1981), "Residual Stress Redistribution caused by notches and Cracks in a Partially Autofrettage Tube," ASME Journal of Pressure Vessel Technology , vol. 103 , pp. 302-306.

- Rees D.W.A. (1987a), "A Theory of Autofrettage With Application to Creep and Fatigue," International Journal of Pressure Vessels and Piping ,vol 30 ,pp. 57-76.

- Rees, D. W. A. (1987b), "Application of Classical Plasticity Theory to Non-Radial Loading Paths," Proceedings of the Royal Society of London,Series A: Mathematical and Physical Science, vol. 410, pp. 443-472.

- Rees,D. W. A. (1991a), "Bounding Method for Predicting the Fatigue Life of Plain and Autofrettaged Thick-walled Cylinders," International Journal of Fatigue, vol. 13, pp. 59-65.

- Rees, D. W. A. (1991b), "Fatigue Life of Thick-Walled Autofrettaged Cylinders With Closed Ends," Fatigue and Fracture of Engineering Materials & Structures, vol. 14, pp. 51-58.

- Ripley, M. I., Humphries, S. R., Mitchel, D. R. G. and Small, R. F. (1995), "Remaining Creep Life Determination of Seam-Welded $2\frac{1}{4}Cr1Mo$ Steel Headers," An International Conference on Failures Repairs & Life Assessment of pressure Vessels and Pipework, Institute of Metals and Materials Australasia Ltd, Melbourne, pp. 105-109.

- Roach, D.P. and Priddy, T.G. (1994), "Effect of Material Properties on the Strain to Failure of Thick-Walled Cylinders Subjected to Internal Pressure," ASME Journal of Pressure Vessel Technology , vol. 116 , pp. 96-104.

- Roark, R.J. and Young, W.C. (1975), Formulas for Stress and Strain , New York.

- Robinson, E. L. and Schenectady, N. Y. (1952), "Effect of Temperature Variation on the Long-Time Rupture Strength of Steels," Transactions of the ASME, vol. 74, pp. 777-781.

- Schulte, C. A. (1960), "Predicting Creep Deflections of Plastic Beams," Proc. ASTM, vol. 60, pp. 895-904.

- Seshadri, R. (1988), " Design and Life Prediction of Fired Heater Tubes in the Creep Range," ASME Journal of Pressure Vessel Technology, vol. 110, pp. 322-328.

- Seshadri, R. (1994), "Residual Stress Estimation and Shakedown Evaluation Using Gloss Analysis," ASME Journal of Pressure Vessel Technology, vol. 116, pp. 290-294.

- Sidebottom, O. M. and Chu, S. C. (1975), "Bursting Pressure of Thick-Walled Cylinders Subjected to Internal and External Pressure , Axial load and Torsion," Experimental Mechanics, vol. 15 (6), 209-218.

- Sidebottom, O. M., Chu, S. C. and Lamba, H. S. (1976), "Unloading of Thick-Walled Cylinders That Have Been Plastically Deformed," Experimental Mechanics, vol. 16 (6), 454-460.

- Sim, R. G. (1970), "Reference Stress Concepts in the Analysis of Structures During Creep," International Journal of Mechanical Science, vol. 12, pp. 561-573.

- Sim, R. G. (1971), "Evaluation of Reference Stress Parameters for Structures Subject to Creep," Journal of Mechanical Engineering Science, vol. 13, pp. 47-70.

- Sim, R. G. and Penny (1971), "Plane Strain Creep behaviour of Thick-Walled Cylinders," International Journal of Mechanical Science, vol. 13, pp. 987-1009.

- Sim, R. G. (1973), "Reference Stresses and Temperatures for Cylinders and spheres Under Internal Pressure With a Steady Heat Flow in the Radial Direction," International Journal of Mechanical Science, vol. 15, pp. 211-220.

- Simonen, F. A. and Jaske, C. E. (1985), " A Computational Model For Predicting the Life of Tubes Used in Petrochemical Heater Service," ASME Journal of Pressure Vessel Technology, vol. 107, pp. 239-246.

- Soderberg, C. R. (1941), "Interpretation of Creep Tests on Tubes," Transactions of the ASME, vol. 63, pp. 737-748.

- Stacey, A. and Webster, G. A. (1988), Determination of Residual Stress Distribution In Autofrettaged Tubing," International Journal of pressure vessels and piping, vol. 31, pp. 205-220.

- Stacey, A., MacGillivary, H. J., Webster, G. A., Webster, P.,J., Ziebeck, K. R. A. (1985), "Measurement of Residual Stresses by Neutron Diffraction," Journal of Strain Analysis, vol 20, No 2, pp. 93-100.

- Steele, M. C. (1952), "Partially Plastic Thick-Walled Cylinder Theory," Journal of Applied Mechanics, vol. 19, pp. 133-140.

- Tolksdorf, Erich (1995), "Residual service life of creep exposed components and means of repair," 3rd. International Conference on Failures Repairs & Life Assessment of pressure Vessels and Pipework, Institute of Metals and Materials Australasia Ltd, Melbourne 29-30 March 1995, pp. 31-40.

- Throop, J. F. and Reemsnyder, H. S. (1982), "Residual Stress Effect in Fatigue," ASTM STP 776.

- Viswanathan, R., Paterson, S. R., Grunloh, H. and Gehl, S. (1994), "Life Assessment of Superheater Reheater Tubes in Fossil Boilers," ASME Journal of Pressure Vessel Technology, vol. 116, pp. 1-16.

- Whalley, E. (1956), "The Design of Pressure Vessels Subjected to Thermal Stresses," Canad. J. Tech. vol 34 ,p 291-303.

- Zamrik, S. Y. (1990), "An Interpretation of Axial Creep-Fatigue Damage Interaction in Type 316 Stainless Steel," ASME Journal of Pressure Vessel Technology, vol. 112, pp. 4-19.

Publications Originated From This Research

Papers Published and Accepted for Publication in the Refereed Journals

1. Loghman, A. and Wahab M. A. (1994), "Loading and Unloading of Thick-Walled Cylindrical Pressure Vessels of Strain Hardening Material," ASME Journal of Pressure Vessel Technology, vol. 116, pp. 105-109

2. Loghman, A. and Wahab, M.A. (1995), "Creep Damage Simulation of Thick-Walled Tubes Using the Theta Projection Concept," The International Journal of Pressure Vessels & Piping, accepted for publication.

Refereed National and International Conference Publications

1. Loghman, A. and Wahab, M.A. (1995), "Multiaxial Stress Redistributions of Thick-Walled Tubes Using a Long-Term Creep Constitutive Equation," Proceedings of the International Conference on the Mechanics of solids and Materials Engineering, Singapore, June 5-7, vol. C, pp. 790-795.

2. Loghman, A. and Wahab, M.A. (1995), "Creep Damage Simulation of Thick-Walled Tubes Using a Long-Term Creep Constitutive Equation," 3rd. International Conference on Failures Repairs & Life Assessment of pressure Vessels and Pipework, Institute of Metals and Materials Australasia Ltd, Melbourne 29-30 March 1995, pp. 133-138.

3. Loghman, A. and Wahab, M.A. (1993), "Thermoelastoplastic and Residual Stresses in Thick-Walled Cylindrical Pressure Vessels of Strain Hardening Material," Advances in Engineering Plasticity and its Application, Editor: W.B. Lee. Elsevier Science Publishers, Amsterdam, ISBN: 0-444-89991-X, pp 843-850.

4. Loghman, A. and Wahab, M.A. (1993), "The Onset and Spread of Yielding in Thick-Walled Cylinders Subjected to Internal Pressure and Thermal Loads," Thirteenth Australasian Conference on the Mechanics of Structures and Materials, Wollongong, July 5-7, pp. 525-532.

5. Loghman, A. and Wahab, M.A. (1993), "Thermoelastoplastic Stress Analysis of Thick-Walled Cylindrical Pressure Vessels of Strain Hardening Material," The Institution Of Engineers Australia, Conference On Dynamic Loading In Manufacturing And Service, Melbourne, February 9-11, pp. 137-142.

6. Loghman, A. and Wahab, M.A. (1992), "Thermoelastoplastic and Residual Stresses in Thick-Walled Cylindrical Pressure Vessels of Strain Hardening Material," proceedings of the Asia-Pacific Symposium on Advances in Engineering Plasticity And Its Application (AEPA'92), Abstract P176, Hong Kong, December 15-17.